Aus der Klinik für Chirurgie
Direktor: Prof. Dr. med. Dr. h. c. Tobias Keck
Sektion für Translationale Chirurgische Onkologie und Biomaterialbanken
Leiter: Prof. Dr. Dr. med. Jens K. Habermann
Universität zu Lübeck

Molecular characterization of breast cancer in patients aged 50 years and older with respect to prognostication, genomic instability, and tumor heterogeneity

Inauguraldissertation

zur Erlangung der Doktorwürde
der Universität zu Lübeck
- Aus der Sektion Medizin -

vorgelegt von
Anna-Sophie Liegmann
aus Lübeck

Lübeck 2025

1. Berichterstatter: Prof. Dr. Dr. med. Jens K. Habermann
Ko-Betreuer: Prof. Dr. med. Karl-Friedrich Klotz
2. Berichterstatter: Prof. Dr. med. Cyrus Khandanpour
Tag der mündlichen Prüfung: 10.02.2025
Zum Druck genehmigt. Lübeck, den 20.02.2025
-Promotionskommission der Sektion Medizin-

Meinen Eltern in Liebe und Dankbarkeit

TABLE OF CONTENTS

ABBREVIATIONS

AJCC	American Joint Committee on Cancer
ASCO	American Society of Clinical Oncology
av.	Average
BCS	breast-conserving surgery
BRCA1/BRCA2	Breast Cancer Gene 1/2
CCND1	Cyclin D1
CDH1	Cadherin 1
CEP4/CEP10	Centrosomal protein 4/10
CIN	Chromosomal instability
CNAs	Copy number alterations
COSMIC	Catalogue of Somatic Mutations in Cancer
COX2	Cyclooxygenase 2
DAPI	4´6-Diamidino-2-phenylindole
DBC2	Deleted in breast cancer 2 gene
DC	Ductal carcinoma
DNA	Deoxyribonucleic acid
ER	Estrogen receptor
ESMO	European Society for Medical Oncology
ExAC	Exome Aggregation Consortium
e.g.	For example (*exempli gratia*)
FISH	Fluorescence in situ hybridization
FFPE	Formalin-fixed paraffin-embedded
H&E	Haematoxylin and eosin
HER2	Human epidermal growth factor receptor 2
IGV	Integrative Genomics Viewer
ITGB2	Integrin Subunit Beta 2
ITH	Intratumor heterogeneity
IS	In situ carcinoma
Ki-67	Kiel-67
KMT2C	Lysine methyltransferase 2C
LC	Lobular carcinoma
MAP3K1	Mitogen-activated protein kinase kinase kinase 1
MAPQ	Mapping Quality

MEMo	Mutual Exclusivity Modules
miFISH	Multiplex fluorescence in situ hybridization
mRNA	Messenger ribonucleic acid
MYC	Proto-oncogene MYC (also called: c-MYC)
NCBI	National Center for Biotechnology Information
NCI	National Cancer Institute
ND	Not determined
NGS	Next-generation sequencing
NIH	National Institutes of Health
NP40	Nonidet P40
PBS	Phosphate buffered saline
Pfam	Protein family database from Wellcome Trust Sanger Institute
PIK3CA	Phosphatidylinositol-4,5-bisphosphate 3-kinase catalytic subunit alpha
PR	Progesteron receptor
SF3B1	Splicing factor 3b subunit 1
SNP	Single-nucleotide polymorphism
SSC	Saline sodium citrate (buffer)
TCGA	The Cancer Genome Atlas
TNM	Tumor-Node-Metastasis (Classification of Malignant Tumors)
TP53	Tumor protein 53
UICC	Union internationale contre le cancer
UKSH	University Hospital Schleswig-Holstein
USA	United States of America
vs	Versus
WGD	Whole genome duplication
WHO	World Health Organization
ZNF217	Zinc finger protein 217

1 INTRODUCTION

Over the last decades, there have been major improvements in diagnosis, prognostication, and treatment strategies in breast cancer patients. Nevertheless, breast cancer is the second leading cause of cancer-related mortality for women in the Western world[1]. Especially older women are affected with a median age of breast cancer death at 74 years in Germany[2]. An accurate diagnosis and prognostication, which is currently based on clinical and histological parameters as well as molecular features, is essential for an optimized treatment decision for breast cancer patients. One challenge of a successful therapy of breast cancer patients is the heterogeneity within one tumor (intra-tumor heterogeneity) but also between breast cancer of different individuals (inter-tumor heterogeneity). Tumor heterogeneity is a common phenomenon in breast cancer, leading to a large variability of clinical and histological parameters, tumor aggressiveness, and treatment response including treatment failure.
The aim of this doctoral thesis was to further elucidate the role of intra- and inter-tumor heterogeneity in breast cancer and assess additional molecular features. A better understanding of tumor heterogeneity and further molecular features of breast cancer can help to improve diagnosis and individualized prognostication and therefore choice of treatment, paving the way towards precision medicine. Furthermore, this doctoral thesis sets the focus on older patients (median age of the analyzed cohort: 67 years) as they are underrepresented in cancer research while comprising the largest group of patients with the highest cancer incidence and mortality.

1.1 Epidemiology and risk factors of breast cancer

Breast cancer is the most prevalent invasive cancer among women, with an estimated 70,450 new cases (69,700 women and 750 men) diagnosed in Germany in 2020[2]. In 2020, breast cancer caused 684,996 deaths worldwide[3], with 1,8401 women and 192 men in Germany[2]. The incidence of breast cancer shows a large variety around the world, with the highest incidence in more-developed and the lowest rates in less-developed countries[4]. In Germany, the lifetime risk of developing breast cancer for women is around 1:8 (13-14%). Being a rare condition, breast cancer can also occur in men[5,6], accounting for 1:125 (0.8%) of all breast cancer cases[7]. Epidemiologic studies have identified several risk factors for developing breast cancer, including gender, age, race, estrogen exposure (increased at early menarche, late or no childbearing, late menopause or postmenopausal hormone replacement therapy), obesity, alcohol, radiation exposure, higher breast density, previous breast cancer and familiar occurrence[8,9]. 5 - 10% of all breast cancer cases are caused by inherited mutations[8],

predominantly in the genes *BReast CAncer Gene 1* and *BReast CAncer Gene 2* (*BRCA1*[10] and *BRCA2*[11]).

1.2 The role of age in breast cancer patients

Advancing age has a major impact on the likelihood of developing breast cancer, with an average age at diagnosis of 64 years in Germany[12]. 82% of all women diagnosed with breast cancer in Germany are older than 50 years[12], with 74 being the median age of breast cancer death[2]. Since 2002, women in Germany between 50 and 69 years have been invited to mammography as a screening option every two years. This is the current standard breast screening technique[13,14] with costs fully covered by statutory health insurers[15]. A decrease in the incidence of late-stage breast cancer in the screening exposed age group could be shown[16]. Due to significant advancements in health care and public health, life expectancy has significantly increased in Germany. This leads to an increase in the population aged 67 and above from 10.4 million (13% of the population) since 1990 to 16.3 million (20% of the population) in 2020; it is projected to rise to 21 million (27% of the population) in 2060[17]. This demographic change towards an aging population is also observed in many other first-world countries[18]. For example, between 2010 and 2030, a 67% rise in the incidence of cancer among people 65 years of age and older is expected in the US[19]. However, there is evidence that older people are underrepresented in cancer research, demonstrated by several studies[20,21]. Therefore, the Institute of Medicine[20] and the American Society of Clinical Oncology[21] recommended intensified research efforts on particularly older cancer patients, for instance, examining the efficacy and side effects of therapy as well as the biochemical and genetic features of cancer in older people.

1.3 Classification and prognosis

In order to best possible predict the course of the disease, factors with prognostic significance based on the features of the breast cancer and the patient are established. The main prognostic markers currently determined within clinical routine are: the TNM-stage and UICC-status, histopathological features and grading, hormone receptor- and HER2-status, Ki67 proliferation index and the classification into molecular subtypes.

1.3.1 UICC- and TNM classification

The TNM classification is based on the anatomical extent of the malignant tumor (T0-4), regional lymph node involvement (N0-3), and the presence of distant metastases (M0-1)[22].

It is an internationally recognized standard and widely used in clinical practice as an indicator of prognosis and assistance of treatment allocation as well as in research[23,24].
Based on the T-, N- and M-stage, the UICC-TNM classification according to the Union for International Cancer Control can be made. Here, a distinction is made between tumor stages from 0 to IV, which are associated with different prognoses and, therefore, can imply different treatment strategies. For example, the relative 5-year survival rate for breast cancer in UICC stage I tumors in Germany were 100% in 2018, decreasing to only 29% for UICC stage IV cancer[20].

1.3.2 Histopathological classification and grading

Breast carcinomas can be separated by histological features into non-invasive carcinomas, limited to the epithelial component of the breast, and invasive malignancies, which have broken through the basement membrane and invaded the stroma[25]. Depending on the site of origin, invasive and non-invasive breast carcinomas can be further subclassified: lobular carcinomas originate from the lobules, and ductal carcinomas from the milk ducts of the breast[25].
The grading of a breast tumor is a morphological feature based on the degree of differentiation of the tissues shown in numerous studies[26,27]. Here, the formation of tubular structures, nuclear polymorphism, and mitotic activity are considered to define the tumor tissue in the three grades I-III. The higher the grade, the less the tumor cells resemble healthy breast tissue, associated with a worse prognosis[26,28].

1.3.3 Hormone receptor-status

In addition to the previously mentioned classification options for breast cancer, determining the estrogen receptor (ER) and progesterone receptor (PR) status serves as a further prognostic factor[29]. Around 70-75% of all breast carcinomas are hormone receptor-positive, the most common clinical subtype[30]. Supporting tumor progression by their growth-stimulating effect when docking on the hormone receptors on the cell surfaces, the hormones estrogen and progesterone are essential targets in breast cancer treatment[31].

1.3.4 HER2-status

The human epidermal growth factor receptor 2 (HER2) is membrane-bound and can be over-expressed in tumor cells[32]. HER2 can stimulate cell proliferation, inhibit apoptosis, and is involved in other diverse biological processes such as differentiation and migration[32]. Thus, overexpression of HER2 in breast carcinomas is a marker of a clinically aggressive disease

and poor prognosis[30,33,34]. Carcinomas expressing high levels of HER2 protein measured by immunohistochemistry or with a high amplification of the gene *HER2*, revealed by fluorescence *in situ* hybridization (FISH), are defined as HER2 positive[35]. In 25-30% of primary breast carcinomas, HER2 is amplified[36]. As a treatment option for HER2-positive breast cancer, a human monoclonal antibody, trastuzumab, was developed to be directed against the extracellular domain of HER2[37,38].

1.3.5 Ki67 proliferation index

Due to the strict association of the human Ki-67 protein and cell proliferation, the determination of Ki-67 expression by immunohistochemistry is established in routine pathological diagnostics. Ki-67 serves as a cell proliferation marker representing the growth fraction of a cell population[39]. Here, the growth fraction is defined as the number of dividing cells in relation to the total number of tumor cells and thus provides information about tumor growth[39]. The determination of Ki67 has a prognostic value as high Ki67-expression is associated with tumor recurrence and shorter overall survival, as shown by uni- and multivariate analysis[39,40].

1.3.6 Molecular subtypes

Beyond the conventional hormone receptor-positive and negative breast cancer classification (see 1.3.3), gene expression studies have identified a molecular classification consisting of four subtypes, termed luminal A (ER/PR+, HER2-, low proliferative), luminal B (ER/PR+, HER2+/-, high proliferative), HER2-enriched (HER2+, ER+/-) and basal-like (primary "triple-negative": ER-, PR-, HER2-)[30,41,42]. These subtypes are associated with different prognoses[42–44], also across several treatment settings, for example, in their response to preoperative chemotherapy[45]. The luminal subtype (luminal A and B) accounts for around 70% of invasive breast cancers and is associated with the best prognosis. As the luminal subtype presents a high expression of hormone receptors (ER/PR+), it benefits from endocrine therapy in general[41]. Due to an increased proliferation in luminal B compared to luminal A tumors, luminal B tumors correlate with a poorer prognosis[43]. The HER2-enriched and the basal-like subtypes account for 15% of all breast cancer types[41] and generally show a poor prognosis[41,46,47]. Basal-like subtypes reveal the worst overall and disease-free survival[46] and show a higher prevalence in patients with germline *BRCA1* mutations[42].

1.4 Treatment

The choice of treatment depends on several factors: besides the treatment preferences of the patient, the size and location of the primary tumor ("T-stage"), involvement of lymph nodes ("N-stage") and distant metastasis ("M-stage"), the tumor´s subtype, including hormone receptor status and HER2-status, the patient´s age, general health, menopausal status and the presence of mutations in genes related to breast cancer (e.g. *BRCA1* and *BRCA2*) is taken into account[48]. A treatment plan often combining different types of treatments such as surgery, chemotherapy, radiotherapy, biological or hormone therapy for each patient should be created by a multidisciplinary and specialized team consisting of oncologists, breast surgeons, radiation oncologists, breast radiologists, and pathologists[49,50]. Treatment options and recommendations are personalized.

1.4.1 Adverse effects of treatment

Treatment has several adverse effects varying from slight to fatal, life-threatening, or permanently affecting toxicities[51]. The most frequently reported adverse effects of adjuvant chemotherapy are nausea[52], vomiting[52], and oral and gastrointestinal mucositis[53]. Each of them potentially affects compliance and can lead to malabsorption, anorexia, weight loss, anemia, and peripheral neuropathy[54]. As older breast cancer patients, especially those with comorbidities, are more vulnerable to side effects of adjuvant chemotherapy, new "elderly-friendly" drugs with reduced toxicity have been developed[55,56]. Regarding radiotherapy, adverse effects frequently include acute skin reactions (radiation dermatitis) ranging from harmless itching or erythema to severe ulcerations and organ complications caused by incidental exposure to radiation[51,57]. Due to the adverse side effects, the role of radiotherapy after breast-conserving therapy in elderly patients has been questioned[56,58].

1.5 Prognostic limitations of conventional parameters and description of new approaches of breast cancer prognostication

As a result of regular mammography screening programs, the majority of breast cancer is diagnosed at an early, localized stage (63%) associated with a better prognosis (5-year relative survival of 98.9%[20]). In 30% of all diagnosed cases, the mamma carcinomas have already invaded regional lymph nodes with a 5-year relative survival of 86%[59]. A challenging task for clinicians is the choice of optimal adjuvant treatment, especially at an early, localized stage. At early stages of breast cancer, relapse rates after surgery are relatively low, and the risk of adverse effects and long-term consequences (see 1.4.1) of

anticancer treatment cannot always outweigh the benefits[51]. Thus, overtreatment of women with a low risk of recurrence should be avoided to prevent long-term toxic side effects. On the other hand, undertreatment can lead to disease relapse and metastasis[60]. Therefore, a precise prognostication and prediction of treatment response and recurrence risk is of prime importance to avoid both over- and undertreatment.

Until today, the TNM stage (1.3.1), histopathological type (1.3.2), the hormone- und HER2-receptor status (1.3.3 and 1.3.4), as well as the expression of Ki67 (1.3.5) are the most clinically relevant information for the selection of first-line therapy[61]. However, different molecular mechanisms can affect the proliferation of cancer cells even at an early tumor stage, resulting in disease progression, including metastasis. Consequently, the prognostic significance of the mentioned histopathological parameters is limited, demanding new approaches for personalized medicine: more precisely, analyzing the genetic and transcriptomic landscape of the individual breast cancer by using mRNA- and DNA-based biomarkers[62] and considering modifiable risk factors unique to each patient[63]. Thus, several techniques including expression profiling of multiple genes have been developed to guide therapeutic decisions[64–67]. Despite its potential benefit towards optimized prognostication, gene expression profiling is still performed to a limited extent in clinical routine due to higher costs and more complex procedures today[68]. Furthermore, for some of the novel biomarkers sufficient validation could not be reached[60] or have not shown significant superiority over routine tools[62]. Currently, different commercial tests are available based on multigene or protein expression signatures, for example, OncotypeDX (Genomic Health)[66], MammaPrint[64], or EndoPredict[64]. A minimum of four gene expression signatures have been implemented in official guidelines[69,70], for instance, the S3 Guideline in Germany[71] or American Society of Clinical Oncology (ASCO) Guidline[72].

Moreover, other possibilities for precise prognostication are subject to research. To give an example, the amount of circulating tumor cells in the blood of a cancer patient at diagnosis is described by Cristofanilli et al. as an “independent predictor of progression-free survival and overall survival in patients with metastatic breast cancer”[73].

1.6 Aneuploidy and genomic instability

Euploidy describes the presence of a complete single (haploid), double (diploid), or multiple complete (polyploid) set of chromosomes in a cell[74]. If a numerical chromosomal aberration occurs, the cell is considered aneuploid[74]. More specifically, these numerical chromosomal

aberrations can be deletions or duplications of individual chromosomes, chromosome pairs or larger chromosome pieces, and fusions between chromosomes.

For over 100 years, aneuploidy has been described as a common characteristic of cancer[75–78]. One theory published by Boveri in 1914 describes the origin of tumorigenesis due to "imbalances in the chromosomes"[77]. However, there has been a long debate about the role of aneuploidy as a cause or consequence of cancer[79–81]. Holand and Cleveland, on the one hand, confirmed that aneuploidy can increase the potential of cellular transformation. On the other hand, revisiting Boveri, they postulate that aneuploidy can also function as a tumor suppressor in a particular genetic context[82]. An association between aneuploidy and a higher recurrence rate and frequency of distant metastasis at diagnosis compared to diploid tumors was described in breast cancer[79,80,83]. It could be shown that highly aneuploid cancers are associated with more TP53 mutations[84,85] and overexpress genes controlling chromosomal segregation and mitosis[75,85]. In order to keep genomic stability, the prevention of chromosome mis-segregation during mitosis is pivotal[86]. Unequal chromosomal segregation can lead to apoptosis or malignant transformation[86]. Consequently, genomic instability was shown to be an integral characteristic in human cancers[87,88]. Genomic instability comprises an increase in small structural variations, for instance, base pair mutations, and ranges up to structural variation, including an increased rate of gains and losses of whole chromosomes or fractions of chromosomes, defined as chromosomal instability (CIN)[87,89,90]. Chromosomal instability is common in human cancers and is the predominant form of genomic instability[90]. It is associated with inferior prognosis in multiple cancer types, including breast cancer[67,91,92].

Mistakenly, the terms aneuploidy and chromosomal instability are used synonymously in some publications. An aneuploid tumor, irrespective of chromosomal instability, may originate within a single cell affected by chromosomal mis-segregation. In case of survival benefits, this aneuploid single cell can proliferate leading to clonal expansion. This origin of cancer development may result in aneuploid, "homogeneous" tumor cells forming a genomically stable tumor. In summary, aneuploidy only describes a state of numerical chromosomal aberration[93]. In contrast, elevated rates of chromosomal mis-segregation occur in cancers with chromosomal instability, leading to many different, heterogeneous karyotypes varying from one cell generation to the next[93].

Until today, the exact relationship between aneuploidy and chromosomal instability is not fully understood and has been controversially discussed for more than 20 years. Some authors have shown that aneuploidy can induce chromosome mis-segregation, leading to increased chromosomal instability, and therefore claim aneuploidy to be the primary cause

of chromosomal instability[94–96]. On the other hand, many authors describe aneuploidy as a consequence of chromosomal instability[91,97,98].

1.7 Inter- and intratumor heterogeneity in breast cancer

Tumor heterogeneity describes the difference of tumor cells regarding their phenotypic and morphological features comprising cellular morphology, motility, metabolism, gene expression, as well as the behavior of proliferation and formation of metastases[99]. Tumor heterogeneity can be classified as (i) inter-tumor heterogeneity, occurring between tumors of different patients, (ii) intersite heterogeneity, occurring between distinct tumors within the same patient, for instance, describing differences between the primary tumor and metastases and (iii) intratumor heterogeneity (ITH), characterizing differences between cancer cells or cellular populations within the same tumor[100].

In 1979, Peter Nowell published evolutionary principles in cancers, depicting that neoplasms arise from a progenitor cell forming clonal subpopulations while accumulating genetic alterations over time[101]. These genetic alterations comprise, among others, mutations based on defects in DNA damage repair, chromosomal rearrangements, and aneuploidy[101]. Thus, increased rates of genetic alterations due to CIN amplify ITH[101,102]. According to the Darwinian selection process, more aggressive clonal subpopulations are selected due to their higher fitness advantage[61]. Consequently, an individual tumor consists of a unique pattern of heterogenous clonal subpopulations leading to ITH. Supporting this theory, larger breast carcinomas express greater genotypic diversity[61]. Moreover, clonal subpopulations in distant regions of larger breast carcinomas feature more varying genetic alterations than neighbor subpopulations[61].

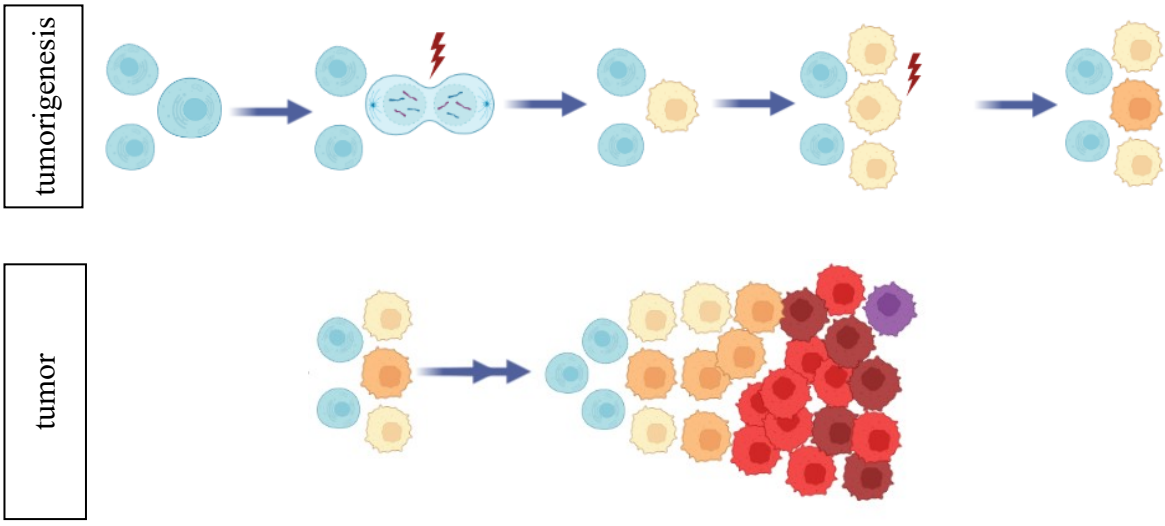

Figure 1: Visualization of the theory of tumorigenesis and progression over time according to Nowell et al. (1979)[101]. Tumorigenesis starts with a somatic mutation happening in a cell of origin (here colored in blue). Tumor progression is continued through stepwise, somatic mutations leading to multiple sub-clonal populations (colored in orange, red, dark-red, and purple) under selection pressure. Figure created with the biorender-software[103].

Multiplex interphase fluorescence *in situ* hybridization (miFISH) or single-cell sequencing were two of the molecular and cytological approaches used in various studies to analyze ITH, a prevalent occurrence in breast cancer[61,84,104–107]. In general, ITH is associated with therapeutic resistance, disease relapse, clinically aggressive progression, and poor prognosis[108–111]. This can be explained because breast carcinomas with a high degree of ITH consist of many different clonal subpopulations, resulting in a higher likelihood of the presence of cell clones resistant to treatment (so-called chemo-resistant cells). During treatment, chemo-sensitive cells can be eliminated, allowing chemo-resistant cells to proliferate and dominate the tumor due to the new environmental conditions and selective pressure[108]. Being a key challenge for treatment selection and cancer medicine in general, ITH is analyzed in many preclinical studies of breast cancer[61,102,112,113].

Next to ITH, inter-tumor heterogeneity in breast cancer has been known for several decades, first described in the first classification of breast carcinomas according to their histological types by Foote and Steward et al. in 1946[114]. Moreover, by analyzing the expression of estrogen receptors, inter-tumor heterogeneity became visible and guides treatment selection until today (see 1.3.3 and 1.4). One milestone regarding tumor heterogeneity in breast cancer was the identification of intrinsic molecular subtypes based on gene expression profiling, which again influences the choice of treatment (see 1.3.6)[115,116], pointing out the most significant study published by The Cancer Genome Atlas Network initiative (TCGA)[117].

1.8 Molecular alterations in cancer

As described in 1.6, genomic instability is a common phenomenon in most cancers[118], which can lead to an accumulation of structural abnormalities of chromosomes or parts thereof, including so-called copy number alterations (CNAs)[119]. These CNAs occur in somatic tissue, comprise deletions (copy number losses) and multiplications of chromosome regions (copy number gains) as well as decreasing or increasing copy numbers of specific genes. In general, copy number gains have a positive, respectively, copy number losses a negative correlation with the expression of genes within the altered chromosomal segments[120]. Interestingly, copy number gains can additionally influence the transcriptional levels of genes genome-wide[120]. However, there is no proportional correlation between CNAs and altered gene expression levels in some cases due to transcriptional adaptive mechanisms[119,121].

Regarding tumorigenesis, CNAs can promote tumor progression[119,120,122] by providing advantages for the mutated cell, for example, increased proliferation. Consequently, the tumor cell with beneficial CNAs could become the dominant cell clone within a tumor population under selection pressure. Cancerogenic properties of CNAs are caused by alterations involving oncogenes, often mutated or expressed at high levels in cancer cells, and tumor suppressor genes, frequently inhibited or lost in cancer cells.

On the one hand, genomic instability can lead to structural chromosomal aberrations and therefore CNAs. In turn, some CNAs can endanger genetic stability by accumulating oncogene-induced DNA damage made throughout the cell cycle's DNA replication, leading to aneuploidy and genomic instability[123].

1.9 Description of genes frequently subject to CNAs in breast cancer

CNAs built on cytogenetic evidence are commonly described[124–127]. In order to specify common regions of CNAs in breast carcinomas, comparative genomic hybridization served as a screening test as previously published[124–126]. In a study by Kallioniemi et al.[125], 15 breast cancer cell lines and 33 primary tumors were analyzed, revealing the chromosomal map of frequently altered regions shown in **Figure 2.**

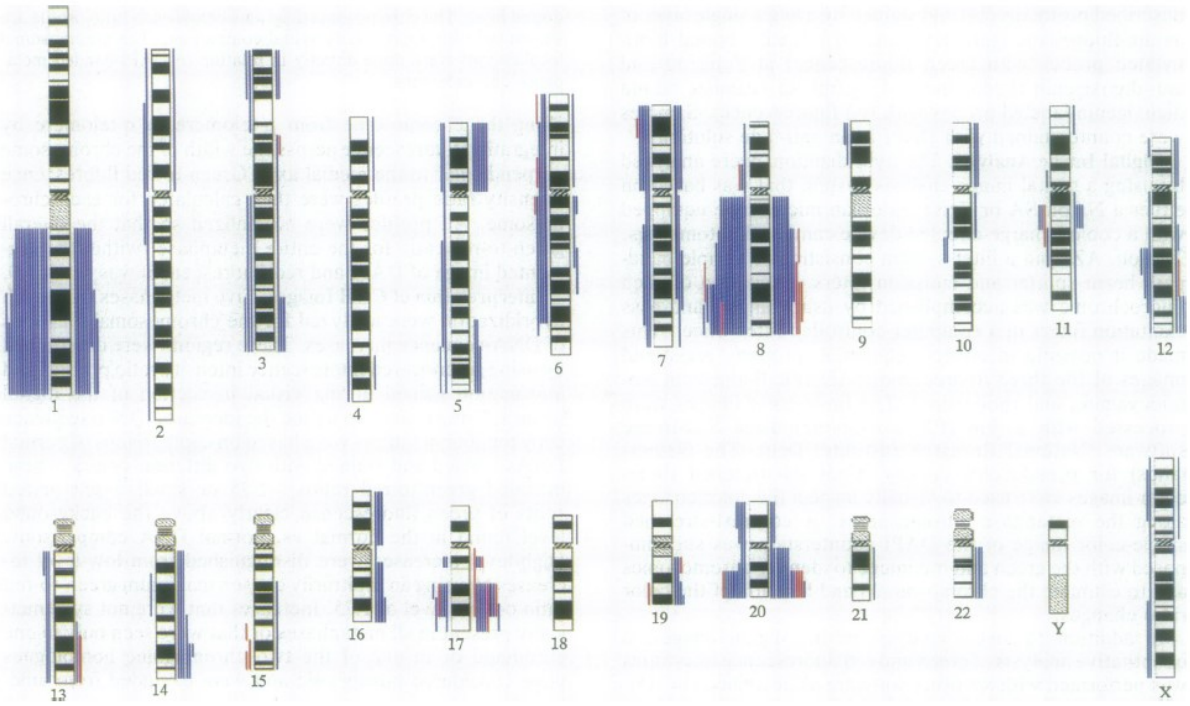

Figure 2: Visualization of copy number increases in breast cancer. 33 breast carcinomas are shown on the left side of the chromosome, and 15 breast cancer cell lines are presented on the right side of the chromosome[125]. In blue: low-level copy number increases; in red: high-level increases. Figure provided by courtesy of Dr. Kallioniemi and colleges and the journal PNAS[125]. Copyright (1994) National Academy of Sciences, U.S.A..

In accordance with the results of Kallioniemi et al.[125], Ried et al.[124] published a study based on comparative genomic hybridization and FISH revealing the regional high level of copy number increases on the chromosome bands (among others) 1q32, 8q24, 11q13, 17q11-12, and 20q11-13.2 as well as frequent DNA losses on chromosomes 17p and 22q.

One aim of this thesis was to analyze genes which often display CNAs in breast cancer to gain a better understanding of ITH and clonal tumorigenesis. Therefore, eight genes comprising the frequently altered chromosomal regions in breast cancer[124–126] (see **F**igure 2) were chosen as they were well investigated among others by studies conducted by Prof. Ried´s laboratory[84,104,128] and showed to be well suited for revealing CNAs in breast carcinomas. These selected genes consist of 5 oncogenes *COX2/PTGS2* (1q31.1), *MYC* (8q24.21), *CDH1* (16q22.1), *HER2/ERBB2* (17q12) and *ZNF217/ZABC1* (20q13.2) and three tumor suppressor genes *DBC2/RHOBTB2* (8p21.3), *CCND1/BCL1* (11q13.3) and *TP53/BCC7* (17p13.1). An overview about the primary function, location, and association with breast cancer prognosis of these eight genes is provided in **Table 1**. Each gene is described in more detail in 1.9.1-1.9.8.

Table 1: Overview of the tumor suppressor- and oncogenes selected for the miFISH analysis.

Gene	Function
Oncogenes	
COX2 (1q31.1)	Key enzyme for the synthesis of prostaglandins, which upregulates tumor growth, promotes metastasis and angiogenesis in breast cancer cells[129,130]. → Overexpression associated with poor prognosis[130–132].
MYC (8q24.21)	Multifunctional nuclear phosphoprotein, which regulates the transcription of various target genes, plays a role in tumorigenesis and promoting metastasis[133,134]. → Overexpression associated with poor prognosis[134,135].
CCND (11q13.3)	Holoenzyme's regulatory subunit that facilitates the G1-S phase transition and thus cell cycle progression by inactivating the Retinoblastoma (Rb) protein[136]. Intense controversy about prognostic value in breast cancer.
HER2 (17q12)	Tyrosine kinase receptor enhances activation of critical signaling pathways, including cell proliferation signals[137]. Prognostic marker of early recurrence and metastasis. → Overexpression associated with poor prognosis[72–74].
ZNF217 (20q13.2)	Krüppel-like zinc finger protein localizes in the nucleus playing a role in the transcription of several genes[138–140]. Overexpression stimulates cell survival and proliferation. → Overexpression indicates a poor prognosis[141,142].
Tumor suppressor genes	
DBC2 (8p21.3)	Rho GTPase plays a role in protein transport, cytoskeleton regulation, and inhibiting cell growth, proliferation, and development of metastasis[143]. → Loss of mRNA and protein level indicates a poor prognosis[144].
CDH1 (16q22.1)	Calcium ion-dependent cell adhesion molecule[145,146]. Reduction or loss of expression is associated with junctional disassembly, triggering cancer invasion and metastasis. → Loss of mRNA or protein level indicates a poor prognosis[147,148].
TP53 (17p13.1)	Transcription factor with a significant impact on cell cycle arrest, senescence, and apoptosis in response to diverse cellular stresses, suppressing cancer[149]. → Loss of mRNA or protein level can lead to tumorigenesis, tumor progression, genomic instability, and a poorer prognosis[84,150].

1.9.1 Cyclooxygenase 2 (COX2)

Located on 1q31.1, *COX2* encodes a key enzyme in catalyzing the conversion of arachidonic acid products to prostaglandin[129] and is also called *prostaglandin-endoperoxide synthase 2*. The expression of *COX2* inhibits apoptosis, stimulates cell proliferation and, thus, tumor growth and invasion when overexpressed. Moreover, *COX2* overexpression enhances cell motility, resulting in metastasis and angiogenesis in breast cancer[130]. Furthermore, *COX2*

expression correlates with established indicators of poor prognosis in breast cancer, such as higher grading and T- and N-status, age >50 years, as well as hormone receptor negativity[130–132]. There is a frequent overexpression of *COX2* in several human cancer types, including breast cancer[130,151]. Interestingly, enhanced levels of *COX2* expression are sufficient to cause mammary gland tumorigenesis[152,153]. Not surprisingly, selective *COX2* inhibitors effectively prevent and treat breast carcinomas in mouse models[152] and may potentially represent a chemo-preventive approach for developing human breast cancer[153–155].

1.9.2 Deleted in breast cancer 2 (DBC2)

The tumor suppressor gene *DBC2*, located on chromosome 8p21.3., is also called *RhoBTB2* as it encodes a Rho GTPase[143]. It inhibits cell growth, proliferation, and metastasis development in some breast cancers[143]. Yoshihara et al. showed that one essential step of its tumor suppressor function is the down-regulation of cyclin D1[156]. Furthermore, *DBC2* was found to be involved in protein transport and cytoskeleton regulation[157]. Mao et al. found a *DBC2*-loss of both mRNA and protein level in 60% of breast tumor samples with a correlation to older breast cancer patients (>50 years) and linked to a poorer prognosis[144].

1.9.3 MYC (c-MYC)

The proto-oncogene *MYC*, located on 8q24.21, encodes for a phosphoprotein, which can bind to the transcription factor MAX, regulating the transcription of various target genes. Reversely, many transforming oncogenes drive the expression of *MYC*, playing a role in cell survival, differentiation blockade, genetic instability, proliferation, and cell migration[133,134]. Hence, tumorigenesis and metastasis are promoted[133,134]. Interestingly, *MYC* strongly influences the survival of chemo-resistant cancer cells[135]. Moreover, *MYC* is amplified in numerous types of cancers and is associated with poor prognosis[134]. It is overexpressed in 30-50% of high-grade breast cancers[135,158].

1.9.4 CCND1

CCND1, also called *Cyclin D1*, *BCL1* or *PRAD1*, is located on 11q13.3. *CCND1* encodes a holoenzyme's regulatory subunit, which phosphorylates and inactivates the retinoblastoma protein (Rb) with its cell-cycle inhibiting function. This inactivation is an essential regulatory step for cell-cycle progression leading to DNA synthesis[136]. *CCND1* amplification or overexpression is predominantly associated with tumorigenesis in early-stage cancer and with the risk of tumor progression and cellular metastases in various human

cancers[136,159,160]. It is the second most frequently amplified oncogene in human cancer overall[161,162] and is amplified in up to 20% of breast carcinomas[162–164]. However, there is still a strong controversy about the prognostic value of *CCND1*. In a meta-analysis by Binabai et al. in 2020, a significant association between a high expression level of *CCND1* and poor overall survival could be shown for several cancers, however, excluding breast cancer[160]. While some studies provide evidence that *CCND1* overexpression has been linked to smaller carcinomas, good response to endocrine treatment, and prolonged survival[164–166], others conclude high level of *CCND1* expression is correlated with poorer prognosis and tamoxifen resistance[162,167,168].

1.9.5 CDH1

CDH1, also called *CADHERIN 1*, encodes a transmembrane-spanning adhesion glycoprotein[145]. This glycoprotein comprises five extracellular domains conferring homotypic interactions and a highly conserved tail on the cytoplasmic side that binds to several effectors, transducing biochemical and physical signals to the cell[145–147]. *CDH1* is located on chromosome 16q22.1[145]. *CDH1* mutations occur in different cancer types, including breast and ovarian malignancies[145]. Due to its important role in cell adhesion, the reduction or loss of *CDH1* expression is associated with junctional disassembly. Consequently, disease development and progression, as well as lymph node, and distant metastases can occur. Thus, reduced *CDH1* expression is associated with a poorer prognosis[147,148,169,170].

1.9.6 Human epidermal growth factor 2 (HER2)

The *HER2* oncogene is located on chromosome 17q12[137]. It is also named *NEU* or *ERBB2* and encodes for a receptor for the tyrosine kinase belonging to the epidermal growth factor (EGF) receptor family[137]. Due to its lack of a ligand binding domain, it cannot bind growth factors. However, it is able to build a heterodimer with further ligand bound EGF receptor family members. As a heterodimer, it increases signaling pathways regulated by kinases, such as those stimulating cell proliferation[137]. *HER2* was reported to be amplified and/ or overexpressed in a variety of cancers, among them breast and ovarian cancer[137]. Slamon et al.[171] reported that *HER2* was amplified from 2- to more than 20-fold in 30% of their analyzed breast carcinoma, leading to an increased expression of the protein gene product. *HER2* amplification was found to be an independent prognostic indicator of early recurrence (regardless of T-, N-, ER- and PR-status), reduced overall survival, and early tumor dissemination[171–173]. *HER*2 amplification identifies a subset of aggressive breast carcinomas

sensitive to growth inhibition and apoptosis which are, in general, therefore treated with anti-HER2 therapies[174].

1.9.7 Tumor protein 53 (TP53)

TP53, located on chromosome 17p13.1, encodes for a tumor suppressor protein regulating the transcription of several target genes[149]. Tp53 suppresses cancer by regulating several key processes including apoptosis and cell-cycle arrest and therefore has been described as a "guardian in the genome" by Strachand and Read[175]. The protein P53 contains a transcriptional activation, DNA binding, and oligomerization domain, as visualized in **9.3.1 Supplemental Figure** S1. *TP53* mutations and a loss of TP53 activity are associated with various human cancers. In breast carcinomas, *TP53* alterations are observed in 30%, being one of the most frequent genetic alterations[150]. Furthermore, TP53 can promote genomic stability, control tumor inflammation, and immune response, and repress metastasis[150]. *TP53* mutations are correlated with poor prognosis in breast cancer patients[84].

1.9.8 Zinc finger protein 217 (ZNF217)

ZNF217 encodes for a Krüppel-like zinc finger protein and is located on 20q13.2[141]. This is a chromosomal region frequently amplified in human cancers, including 20-30% of early-stage human breast carcinomas[141,176]. It is a transcription factor, localizes in the nucleus and interacts with histone-modifying proteins and co-repressors. Moreover, it intervenes in the process of transcriptional repression of various genes by binding specific DNA sequences[138–140]. The overexpression of *ZNF217* is associated with an aggressive phenotype and shortened survival in breast cancer patients as it promotes the survival and invasiveness of cancer cells[141,142]. Cowger et al. could demonstrate that *ZNF217* represses the promotor of E-cadherin, using a combination of small interfering RNA and transient transfections[139]. Furthermore, high levels of *ZNF217* expression can attenuate the apoptotic signal and therefore be involved in resistance to chemotherapy, e.g., paclitaxel[141,176]. In summary, overexpression of *ZNF217* in breast carcinomas indicates a poor prognosis. A recent study by Sharma et al. describes that dimethyl fumarate inhibits ZNF217 in a subset of breast cancer[177], potentially leading to a new pharmacological therapy.

2 SYNOPSIS AND RESEARCH GOALS

Worldwide, breast cancer is the most common invasive malignancy in women, causing 684,996[3] deaths in 2020. Especially older women are affected with a median age of breast cancer death at 74 years in Germany[2]. Despite 82% of all women diagnosed with breast cancer in Germany are older than 50 years[12], older women are underrepresented in cancer research while comprising the largest group of patients. Regarding treatment, one major problem is over- or undertreatment or even therapy failure, which can be caused by intra- and/or inter-tumor heterogeneity limiting the prognostic importance of conventional histopathological parameters. Further development for improved prognostication and thus more accurate treatment selection was achieved with stratified medicine. Through this, tests based on gene expression profiling, such as OncotypeDX (Genomic Health)[66], MammaPrint[65], EndoPredict[64] and others were added into clinical management[178]. In addition to these tests, an improved prognostication could be shown by quantitative measurement of the nuclear DNA in breast cancer cells as the status quo of nuclear DNA content (more precisely: diploid or aneuploid tumors) was associated with disease outcome[179,180]. Simplified, a higher malignancy in aneuploid tumors than diploid tumors were observed. Moreover, the variability of the DNA content within the breast cancer cell population, defined as the degree of genomic instability, was also correlated with prognosis[181]. Here, a significantly better prognosis could be shown for patients with genomically stable tumors compared to their instable counterparts[181]. However, further research is needed to fully understand the exact interactions of chromosomal ploidy, degree of genomic stability, intra-tumor heterogeneity, tumor progression and patient prognosis.

Consequently, this doctoral thesis was motivated by the desire to elucidate the role of tumor heterogeneity as well as analyze chromosomal aneuploidy and genomic instability for improved prognostication while focusing on older breast cancer patients due to their underrepresentation in cancer research.

To address the following objectives, a comprehensive genetic analysis of 39 breast cancer patients (median age of 67 years) divided into two groups with profoundly different survival time after diagnosis (long survival patients, median 19 years, versus short survival patients, median 2.4 years) was conducted: using Formalin-fixed, paraffin-embedded (FFPE) archival material, (i) tumor clonality and heterogeneity were investigated by assessing copy number alterations of eight breast cancer-associated genes for their potential as biomarkers using multiplex interphase fluorescence *in situ* hybridization (miFISH), (ii) the genomic instability

and tumor ploidy using miFISH and DNA image cytometry were determined, (iii) phylogenetic tree modeling was performed in order to elucidate the process of tumor development and progression regarding clonal evolution, and (iiii) the mutation status of 563 breast cancer-associated genes with targeted sequencing for a custom panel (OncoVar) using next-generation sequencing (NGS) were assessed.
There are five main objectives of this thesis regarding breast cancer of 39 patients aged 50 years and older:

1. Are there gains and/ or losses in the eight analyzed breast cancer-associated genes? Is there an association between specific gains and/ or losses with overall survival or ploidy status?

2. What is the degree of ITH in each tumor sample, and how is the inter-tumor heterogeneity within the cohort? Is there a correlation between the degree of ITH and a) the clinical features and b) overall survival in the breast cancer samples?

3. Which ploidy has each tumor sample? Is there a correlation between the ploidy and a) the clinical features and b) overall survival?

4. How could tumor development and progression -or in general the clonal evolution of the tumor- have taken place?

5. Are there mutations in the analyzed 563 cancer-related genes in the breast cancer samples? Is there an association between the overall mutation burden and a) overall survival, b) ploidy status, or c) the degree of ITH?

3 MATERIALS AND METHODS

3.1 Clinical samples

For this thesis, 39 out of 245 breast cancer samples with corresponding follow-up data of up to 21 years were selected. The samples were collected between 1989 and 1992 at the University Hospital Schleswig-Holstein (UKSH) in Lübeck within clinical routine diagnostics and stored as formalin-fixed, paraffin-embedded (FFPE) biopsy specimens. The selected breast cancer patients had a median age of 67 years (age range 50 – 85 years). This study, a comprehensive genetic analysis on formalin-fixed, paraffin-embedded (FFPE) biopsy specimens, was performed under the guidelines of the Declaration of Helsinki and approved by the ethics committee of the University of Lübeck (#08-012 and #20-507). Two groups of patients were formed, differing in overall survival but matched for age, estrogen receptor (ER)-, progesterone receptor (PR)-, HER2 receptor, Ki67-status, and metastasis. The median survival time after diagnosis in the long-survival group (n = 21) was 19 years (range 13.2 – 21.5 years), whereas the short survival group (n = 18) had a median survival of only 2.4 years (range 0.2 – 4.8 years). An overview about the clinical and clinicopathological features of each tumor sample and patient separated into the groups of long and short survival patients is provided in the supplement (**Supplemental Table 1**).

For the determination of the ER, PR, and HER2 receptor status, staining protocols established in the Institute of Pathology for analysis in clinical routine (Standard Operation Procedure VA-033, VA-050, VA-015) at the UKSH in Lübeck were used. The determination was carried out according to the standards of the breast cancer guidelines of the ASCO/College of American Pathologists[35,182]. The staining was performed at the Institute of Pathology at the University of Lübeck/UKSH. Regarding the HER2 receptor status, additional staining with FISH was carried out using a commercially purchased HER2/CEP17 probe. The assessment of Ki67-expression levels was also performed at the Institute of Pathology at the University of Lübeck/ UKSH by determining the percentage of positively stained tumor cells (cut-off value of 20%)[183]. Furthermore, intrinsic subtypes were assigned according to the European Society for Medical Oncology (ESMO) Clinical Practice Guidelines[184].

3.2 Materials

The lists of laboratory equipment, consumables, and reagents are presented in the supplement (**Supplemental Table 2, 3, 4**).

3.3 Methods

Major parts of this thesis, particularly the execution of miFISH and analysis of its results, were conducted during three stays, including one research semester, in the laboratory of Prof. Dr. Thomas Ried, in the Genetics Branch at the National Cancer Institute (NCI), National Institutes of Health (NIH) in Bethesda, Maryland, USA.
Sample selection, Feulgen staining, and cytometric measurements were performed at the Laboratory for Translational Surgical Oncology and Biobanking of Prof. Dr. Dr. Jens K. Habermann, at the University of Lübeck, Germany, under the supervision of Prof. Timo Gemoll and Prof. Jens K. Habermann. The statistical analysis was carried out along with Dr. Yue Hu of the NCI. The sequencing of the 39 tumor samples was conducted by the Frederick National Laboratory for Cancer Research, NCI, and DNA extraction by Dr. Wei-Dong Chen, NCI. Sequencing data processing was applied by Dr. Yue Hu, NCI. The data from next-generation sequencing were obtained for result compilation, statistical analysis, and interpretation as part of this thesis.

3.3.1 Multiplex interphase fluorescence *in situ* hybridization (miFISH)

3.3.1.1 Principle of Multiplex interphase fluorescence *in situ* hybridization (miFISH)

As described in 1.8, CNAs of specific genes, chromosome arms, or whole chromosomes can promote tumor progression or tumorigenesis[119,120]. Some genes are frequently subject to CNAs specifically in breast cancer (see 1.9), while others are gained or lost in multiple cancer types. An excellent method to quantify CNAs on a single cell level is FISH[185]. Probes are labeled with fluorescent reporter molecules and contain DNA sequences complementary to the gene sequence of interest. The accessibility of the DNA strands is achieved by denaturation so that the target sequence of the probe can anneal to the respective DNA sequence, which can be observed under fluorescence microscopy.
In this thesis, multiplex interphase FISH (miFISH) was performed to investigate interphase nuclei isolated from FFPE breast tissues by multiplexing FISH probes. MiFISH is a method which was previously developed in the laboratory of Prof. Ried at the NIH. It allows the determination of copy numbers for up to 20 gene loci using tumor-specific probe panels. Copy numbers of each analyzed gene are counted within each nucleus assessed, revealing a comprehensive overview of CNAs on a single-cell level. In this way, unprecedented new

insights into tumor clonality and ITH are possible. The principle of the miFISH method is visualized in **Figure 3**.

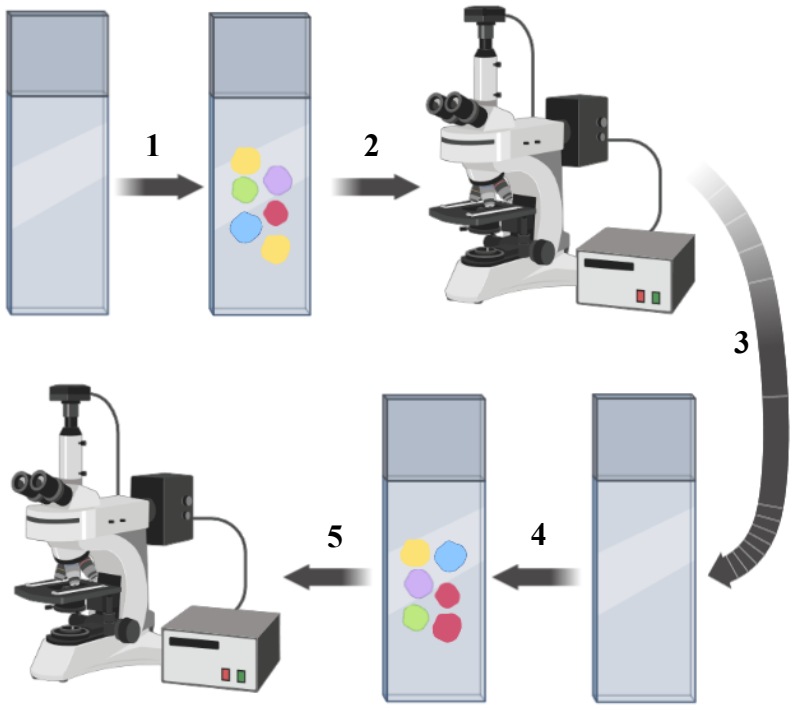

Figure 3. Sequential hybridization with a five-color FISH panel targeting breast cancer-specific genes. After hybridizing, the first five-color panel (1) nuclei are automatically imaged by a custom-designed Bioview software and scanner (2). After imaging, the first probe panel is washed off (3), followed by the rehybridization with the second five-color FISH panel (same slide) (4). After the rehybridization, each nucleus is automatically relocated for imaging by the software (5). This process can be repeated for up to four panels, allowing the enumeration of up to 20 genetic loci for each nucleus by the miFISH method. Figure created with the Biorender-software[103].

3.3.1.2 Preparation of single interphase nuclei cytospins from FFPE tissue

All analyses were performed on FFPE patient samples. Each specimen was cut in consecutive sections according to the protocol listed in **Table 2**. Then, a senior pathologist (Prof. Dr. med. Christoph Thorns) marked the tumor area on the second 4 µm Haematoxylin and Eosin (H&E) stained slide (Section 10 in the cutting scheme) according to histological evaluation as shown in **Figure 4.**

Table 2: Cutting protocol for analyses on FFPE-tissue.

Section	Thickness	Method
1	4 µm	HE
2 3 4 5 6	10 µm each	DNA/RNA-Extraction
7 8 9	10 µm each	Protein-Extraction
10	4 µm	HE
11 12	50 µm each	miFISH

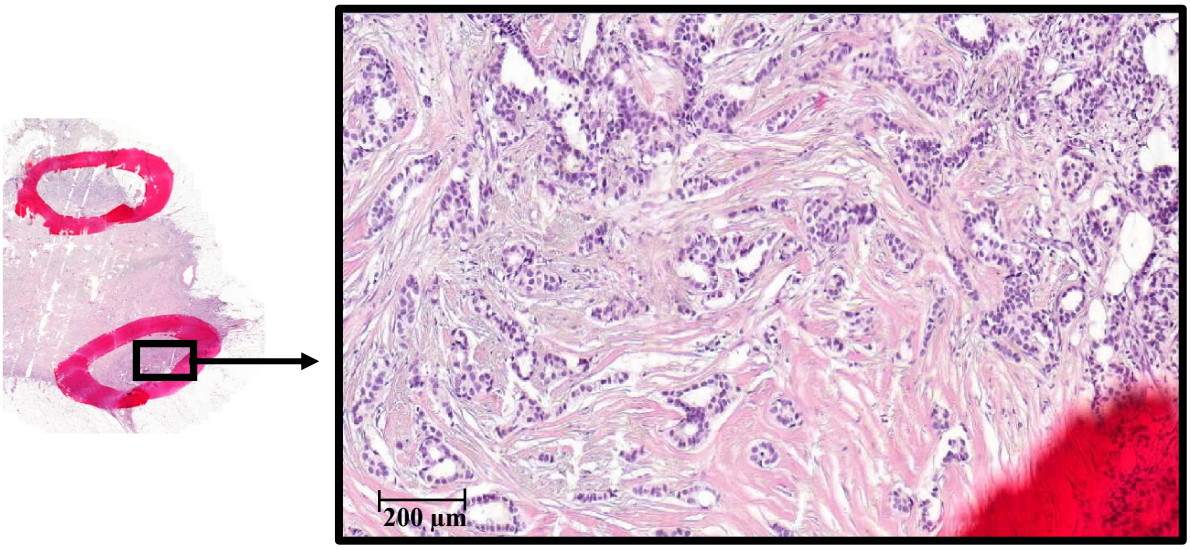

Figure 4: Breast cancer tissue on a slide. 4 µm HE-stained tissue on a slide with marked tumor area (in red).

The HE slide was used to mark the tumor area within the subsequent 50 µm unstained sections (Sections 11 and 12 in the cutting scheme), and the representative tumor material was removed with a scalpel (so-called macro-dissection). The tumor tissue was collected in a 1.5 ml Eppendorf safe lock tube. To prepare cytospin slides, a modified *Hedley* method[104] was used: The FFPE tumor tissue was macro-dissected, cut, and digested by protease to create a single-cell suspension as visualized in **Figure 5.** To achieve evenly spread-out single interphase nuclei on a slide, the single-cell solution was distributed by centrifuge (so-called "cytospin").

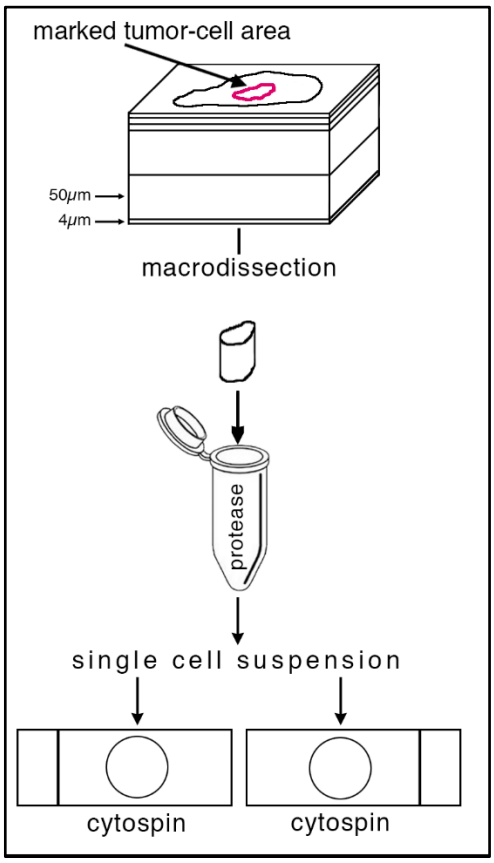

Figure 5: Workflow for the preparation of cytospins with archived FFPE patient samples. At first, the marked tumor-cell area (visualized in red) was macro-dissected and placed in an Eppendorf tube. Secondly, a single-cell suspension was produced by digesting the tumor tissue using protease. Afterwards, the single-cell suspension was distributed by a centrifuge within a circled area on a slide (so-called "cytospin"). Figure provided by courtesy of Dr. Kerstin Heselmeyer-Haddad.

Going more into detail in the process of preparing a cytospin, the 50 µm section of the tumor area of the FFPE tissue was placed in xylene for 3x10 minutes for deparaffinization and rehydrated in an ethanol series of 2x 100%, 90%, 70% for 5 minutes at room temperature, respectively. After each step, xylene and ethanol were removed by pipetting off and discarding the supernatant after the Eppendorf tube was centrifuged at 3,000 rpm for 3 minutes. The final step of the ethanol series was adding 1 ml of 50% ethanol (again leaving for 5 minutes at room temperature). To remove the ethanol, the Eppendorf tube was spun down at 4°C for 15 minutes at 14,000 rpm in a centrifuge, and the supernatant was discarded. After the removal of ethanol, 1 ml of sterile water was added and left at room temperature for 20 minutes. To remove the sterile water, the Eppendorf tube was spun down at 4°C for 15 minutes at 14,000 rpm, and the supernatant was discarded. 1 x phosphate buffered saline (PBS) was added for 10 minutes, the Eppendorf tube was centrifuged at 4°C for 15 minutes at 14,000 rpm and the supernatant was discarded. Again, 1 x PBS was added, and the sample was stored overnight at room temperature. The morning after, the Eppendorf tube was

centrifuged at 4°C for 15 minutes at 14,000 rpm to remove 1 x PBS, and the supernatant was carefully pipetted off. To start the digest, 10 U/ml bacterial protease type XXIV in 1 x PBS was added and the Eppendorf tube was put into a thermomixer at 950 rpm at 45°C for 30 - 90 minutes (tissue and sample specific). After 20 min of digestion, every 5 minutes, the level of tissue disintegration was monitored by placing 5 µl of supernatant stained with 5 µl of DAPI-Sulphorhodamine under a fluorescence microscope. In case of incomplete tissue disintegration, the digest was continued. Once the optimal level of disintegration was observed, the single nuclei suspension was removed into another Eppendorf tube, avoiding any remaining tissue pieces. The suspension was stored on ice to stop -respectively slow down- the digest. The remaining tissue pieces were further digested by adding fresh protease in 1 x PBS and repeating the steps described above (placing the Eppendorf tube in a thermomixer at 950 rpm at 37°C, again, rechecking every 5 minutes the level of tissue disintegration etc.). The digest was finished when no more tissue pieces were visible in the suspension or no more intact nuclei were released from any remaining tissue pieces when checking the digest level in the DAPI-stained supernatant under the fluorescence microscope. To preserve tumor heterogeneity, all single digests stored on ice were combined in an Eppendorf tube. Cytospins were generated by centrifuging 100 - 400 µl of the cell suspension for 5 minutes at 1,200 rpm onto microscope slides using single cytological funnels in a cytospin centrifuge. In case of very fragile nuclei, the speed of rotation was reduced, and the time of centrifuging was extended accordingly. The optimal cytospin slide has an even distribution of monolayered, non-overlapping intact nuclei with proximity to each other to achieve an optimal density for efficient scanning. The quality and density of nuclei on the cytospin were checked under the phase contrast microscope. If the density of nuclei was too high, resulting in several nuclei overlaying each other, a lower volume of the cell suspension was prepared to generate the next cytospin, and/or the suspension was diluted with 1 x PBS. Similarly, if the density of the nuclei was too sparse, the volume of the cell suspension used for the cytospin was corrected upwards accordingly. To fix the nuclei, obtained cytospin slides with single-layered intact nuclei were dehydrated in an ascending ethanol series (70 % and 90 % for 5 minutes and 100 % for 10 minutes). Afterwards, the slides were air-dried and stored at 4°C in the fridge until further use.

3.3.1.3 Hybridization

For the miFISH analysis, eight breast cancer-related genes were included (detailed description is provided in **Table 1** and 1.9): *COX2/PTGS2* (1q31.1), *DBC2/RHOBTB2* (8p21.3), *MYC* (8q24.21), *CCND1* (11q13.3), *CDH1* (16q22.1), *TP53* (17p13.1),

HER2/ERBB2 (17q12) and *ZNF217* (20q13.2). Furthermore, two centromere probes were selected as ploidy references (CCP4, 4p11.1-q11.1, and CCP10, 10p11.1-q11.1, targeting the centromeres of chromosome 4 and 10). To gain more information regarding the ploidy in one specific case (case 13S), additional hybridizations were carried out using 12 centromere and five locus-specific probes (CCP2, 3, 4, 6, 7, 9, 10, 11, 12, 15, 18, X and *CCNB1* (5q13.2), *RB1* (13q14.2), *CCNE1* (19q12), *DSCR8* (21q22.13) and *NF2* (22q12.2) as visualized in **Supplemental Figure S2**.

As shown in **Figure 3**, by separating the eight breast cancer-related genes plus the two centromere probes into two panels (panel 1: *HER2*, *CDH1*, *TP53*, *ZNF217*, *CCP10;* panel 2: *COX2*, *CCND1*, *DBC2*, *MYC*, *CEP4*), the hybridization was carried out consecutively onto the same cytospin slide. Additionally, for around 50% of the cases, a third panel with an individual probe-selection out of the eight breast cancer-related genes and centromeres of chromosomes 4 and 10 was consecutively hybridized onto the same cytospin slide for validation purposes. In this third panel, the probes were attached to fluorophores differently colored than in panel one respectively panel two.

For the hybridization, the probe panel was denatured at 73°C for 5 minutes. Covered with aluminum foil for light protection, the probe panel was pre-annealed for 60 minutes at 37°C, shaking in a thermomixer at 350 rpm. Meanwhile, the previously generated cytospins were equilibrated in a Coplin jar containing 2 x saline sodium citrate (SSC) for 5 minutes and afterwards in 1 x PBS for 2 minutes. It was necessary to pretreat each cytospin slide before hybridization by pipetting 120 µl of 10 U/ml bacterial protease type XXIV and placing it in a hybridization chamber inside an incubator at 37°C while frequently observing the nuclei under the light microscope using phase objectives until the nuclei appeared brighter. The time of protease treatment was dependent on the amount of cytoplasm: the more cytoplasm was observed, the longer the slides had to be pretreated with protease inside the incubator (between 15 seconds and several minutes) to digest the remaining cytoplasm. Afterwards, three washing steps in 1x PBS for 3 minutes each, followed by dehydration in an ethanol series starting with 70%, 90%, and 100% for 5 minutes, respectively, were performed. Afterwards, the slides were allowed to air-dry (~5 minutes). 150 µl 2 x SSC/ 70% formamide were applied on a 24 x 60 mm² coverslip. To denature the DNA, the cytospin slide was touched carefully to the coverslip by strictly avoiding the formation of air bubbles and was placed on a Thermobrite hot plate at 73°C for 30 - 45 seconds (length depending on the fragility of nuclei). After quickly and carefully removing the coverslip from the cytospin slides, the dehydration of the slides were carried out in an ice-cold ethanol series (70%, 90% and 100%) for 3 minutes each. Afterwards, they were left to air-dry. 2 µl of the probe panel

was applied on each cytospin slide, covered with a round coverslip (12 mm diameter) by strictly avoiding the formation of air bubbles. Then, the edges of the coverslip were completely glued using rubber cement. Hybridizations were performed 24 - 48 hours at 37°C in a humid, light-tight hybridization chamber.

3.3.1.4 Signal Detection of Hybridization

After hybridization for 24 - 48 hours, cytospin slides were removed from the hybridization chamber, and the rubber cement was gently removed from the top of the slide. All steps were carried out under avoidance of light. The cytospin slides were immersed in pre-warmed (48°C) 2 x SSC/ 0.3% NP40 buffer in a Coplin jar by gently sliding the coverslip to the side with a tweezer. Subsequently, a washing step in another Coplin jar with fresh, pre-warmed (48°C) 2 x SSC/ 0.3% NP40 solution for 2 minutes was performed under careful and periodical shakes. Washing steps were continued by transferring slides in 2 x SSC/ 0.1 NP40 at room temperature for 1 minute, 2 x SSC for 10 seconds, and 1 x PBS for 2 minutes. For DAPI staining, slides were transferred in a 2.5 µg/ml DAPI/ 1 x PBS solution for 30 seconds, followed by three washing steps in 2 x SSC for 2 minutes each while agitating gently. Cytospin slides were dehydrated in an increasing ethanol series of 70%, 90%, and 100% for 2 minutes, respectively, and left to air-dry. Finally, one drop of Vectashield fluorescence mounting medium was added onto the coverslip and touched onto the cytospin slide under avoidance of bubble formation.

3.3.1.5 Imaging of miFISH results

After detection, hybridized cytospin slides were examined under a fluorescence microscope to check the quality of the nuclei, the DAPI staining, and the signals of the hybridized fluorescent probes. If the quality of the hybridization was approved, the cytospin slide was prepared to be scanned by placing it onto the Bioview DUET scanning workstation comprising of an Olympus BX-63 fluorescence microscope equipped with custom optical filters, an Xcite metal halide light source and a 40x oil immersion objective. Before each scan, scanning parameters (focus, brightness, exposure time, intensity) had to be adjusted to obtain optimal probe signal intensity with no or slight background fluorescence. Therefore, representative areas of the slide were checked for all six filters (DAPI, Aqua, Green, Gold, Red, and Far Red) to find the optimal scanning parameters. On average, 12,000 nuclei were automatically imaged by a 2,448 x 2,048 monochrome digital camera within the DUET workstation.

For re-scanning a slide after re-hybridization with panel 2 or 3, respectively, scanning parameters had to be adjusted again. Furthermore, to relocate to the identical nuclei imaged

in the first scan, the program allows to match the nuclei positions of any subsequent scan to the positions of the same nuclei in the first scan. The automated relocation to the identical nuclei for the following probe panels allows the custom FISH-after-FISH software to provide a computerized image overlay. However, for all cases, the relocation to the same nucleus had to be reviewed and, in several cases, carried out manually to ensure accurate matching. Finally, images of all ten probes were visualized within the same nucleus in a custom gallery overview. In this way, signals of all probes within the same nucleus could be counted, as shown in **Figure 6.**

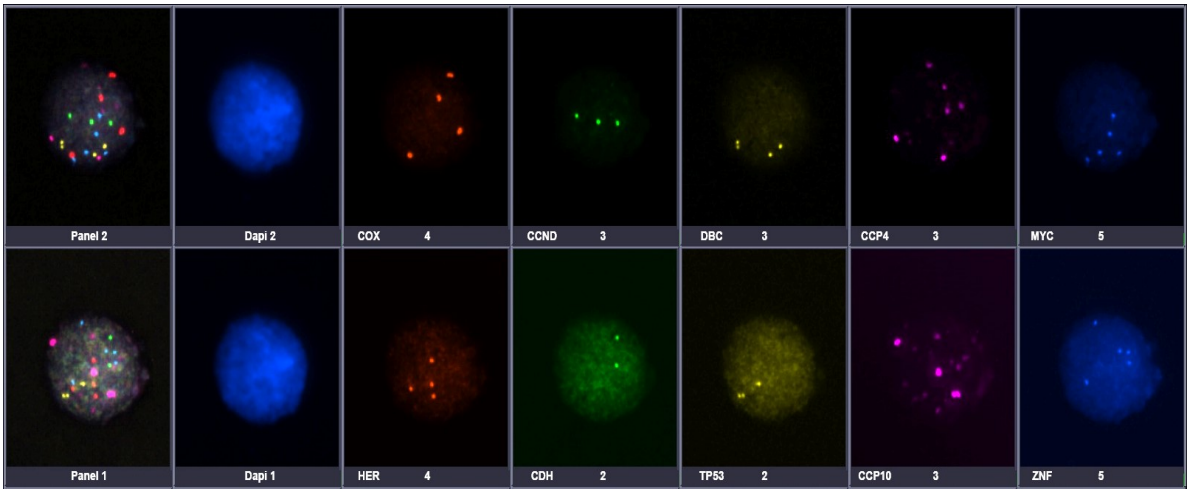

Figure 6: Images of a single breast cancer nucleus after the fluorescence *in situ* hybridization of the first (top row) and the second multicolor panel (bottom row). The cytospin has been consecutively hybridized with two five-color panels containing eight breast cancer-related genes and two centromere probes. Additionally, an overlay of all images was visualized on the left side, and pictures of the nucleus stained with DAPI are provided on the right side of the overlay image. The image was created using the DUET scanning imaging workstation and the Bioview software.

All signals of minimum 250 nuclei per case were counted. Exclusively undamaged nuclei not overlapping with other nuclei and with clearly visible signals for all ten probes were included. Enumeration was carried out manually in a consecutive manner, followed by a review process for improved accuracy.

3.3.1.6 Re-hybridization

To hybridize a second or third miFISH panel on the same slide (so-called consecutive re-hybridization), the probes of the previously hybridized slide had to be washed off after scanning and imaging had been completed. Therefore, the coverslip was carefully removed in 2 x SSC by sliding it to the side with a tweezer, followed by three washing steps in 2 x SSC in a Coplin jar for 2 minutes each. To remove the probes and denature the DNA on the

cytospin slide, it was immersed in 2 x SSC/ 70% formaldehyde in a water bath at 80°C for 10 seconds, followed by dehydration in a series of cold ethanol (70%, 90% and 100%) for 2 minutes each. Meanwhile, the denaturation of the miFISH probe panel was carried out at 73°C for 5 minutes, and the pre-annealing at 37°C for 60 minutes, shaking in a Thermomixer at 350 rpm, and covered with aluminum foil for light protection.
2 µl of the probe panel was added to the air-dried cytospin slides, which were covered with a round cover slip sealed with rubber cement and hybridized in a hybridization chamber at 37°C for 1-2 days. Signal detection and imaging were performed as described in 3.2.1.4 and 3.2.1.5.

3.3.1.7 Data assessment

The determination of clonal signal patterns, ploidy, as well as gain and loss patterns were carried out as described before[84]. The manual counts of all signals in each of the 250 nuclei per case were recorded by the Bioview software in an Excel spreadsheet, with every row representing the copy numbers for the ten probes within the respective nucleus (signal pattern). These raw data of analyzed nuclei were manually re-sorted for each case in Excel. The columns were ordered according to the chromosomal location of the probes in ascending order and the rows (signal patterns) in ascending signal numbers. The Excel file then displayed nuclei with the lowest signal counts on top and nuclei with high signal numbers at the bottom; nuclei with the same signal patterns were grouped to determine clonal signal patterns, and the number of nuclei with this signal pattern was specified in an extra column. The largest group of nuclei with the same signal pattern represents “the major clone” in the tumor population. Nuclei with two signals in every gene- and centromere probe were excluded as most likely representing diploid immune- or stroma instead of tumor cells.

3.3.1.8 Description of the instability index, ploidy, and gain-and-loss patterns

As a measurement of the degree of tumor heterogeneity quantified by the frequency of altered clone patterns, the instability index (I) of each case was determined as presented in the following formula[104]:

$$I = (N * 100)/n$$

N: number of signal patterns observed

n: number of nuclei analyzed

By calculating the average of all FISH gene probes and evaluating the signal counts for the centromere probes, the ploidy of each of the 250 nuclei was determined. Gene probes with

amplifications that biased the average were excluded. In the second step, the average ploidy value (decimal number) for each breast cancer sample was calculated based on the miFISH results by averaging the ploidy values of each nucleus.

Each of the 39 tumors within this study was assigned to the group "diploid" or "aneuploid" tumor according to their average ploidy (determined through miFISH): a value of 2.0 and 2.1 was classified as "diploid" and a value of 2.2 and above as "aneuploid". This cut-off value 2.2 was identified in an independent cohort of tumor samples previously published by Koçak et al., where both miFISH and DNA image cytometry had been carried out[128]. By comparing the miFISH and DNA image cytometry data in this independent cohort, the cut-off value of 2.2 for the average ploidy based on the miFISH results was revealed as the most accurate matching the ploidy-determination by quantitative measurement of the nuclear DNA. Further validation regarding the cut-off value was performed within the cohort of this study by additionally analyzing 20 cases (11 long survival and 9 short survival cases) with DNA image cytometry as described in 3.3.1.9.

For each of the 250 nuclei, a gain and loss pattern was identified in relation to the determined ploidy of the tumor sample. To visualize the gain and loss patterns of the 250 nuclei, a color chart for each breast cancer tissue was created (e.g. **Figure 8**, **Figure 9D,H** and **Figure 10D,H**). CNAs were considered for statistical analysis only when the corresponding aberration occurred in at least 15% of the cell population.

3.3.1.9 Quantitative measurement of the nuclear DNA by image cytometry

In preparation of performing image cytometry, cytospins were Feulgen-stained. For the Feulgen-staining, cytospin slides were incubated in 4.5 % formaldehyde for fixation at room temperature overnight in a fume hood under avoidance of light. Afterwards, cytospins were washed under running tap water (until the smell of formaldehyde was entirely removed). Cytospin slides were then incubated with 5 M hydrochloric acid for 60 minutes at room temperature under avoidance of light, followed by three washing steps with sterile purified water. For staining, cytospin slides were incubated in Schiff´s reagent for 120 minutes and covered with aluminum foil for light protection. Afterwards, cytospin slides were washed under running tap water, followed by three washing steps for 10 minutes, respectively, in freshly prepared sodium pyrosulfite washing solution: In the first step, 2.4g of sodium pyrosulfite was solved in 125 ml sterile purified water. Then, 10 ml of this solved pyrosulfite was added to 10 ml of 1 M hydrochloric acid and 180 ml of sterile purified water. For dehydration, cytospin slides were incubated in an increasing ethanol series of 1 x 70%, 2 x 96%, and 2 x 100% for 3 minutes, respectively. Slides were quickly immersed twice in xylol,

followed by a longer incubation step for 5 - 10 minutes. Finally, 2 drops of Entellan were added onto the slide, and a 24 x 60 mm coverslip was touched onto the cytospin slide under avoidance of bubble formation. In addition to the cytospins, a slide with tonsil tissue was Feulgen-stained as a control.

In the next step, the ICM imaging system was used for image cytometry. In the ICM gallery, particles were automatically detected and manually screened by excluding damaged or overlapping nuclei, with a mean of 6,700 nuclei (range 1,214 to 16,425) analyzed per evaluated case. To gain a reference value for the quantitative measurement of the DNA, each examined case was screened for numerous diploid nuclei such as granulocytes and lymphocytes for establishing the 2c value indicating a diploid DNA content. The tumor cells´ DNA values were then determined in relation to that 2c value. The Auer classification[179] was applied to categorize DNA histograms into diploid (Type I, III) and aneuploid (Type IV). Histograms showing next to the stem line at 2c/4c an additional stem line and/ or the corresponding cell population containing a minimum of 10 cells higher than 5c were defined as aneuploid.

3.3.1.10 Phylogenetic tree modeling

The software FISHtrees 3.2 in the ploidy less mode was used to run phylogenetic algorithms for the 39 cases to gain more information about the clonal evolution of each tumor[186]. In these phylogenetic trees, all observed signal patterns can be distinguished by the copy numbers of the analyzed gene probes[186]. The creation of these FISHtrees with the software was performed by Dr. Yue Hu, NCI, USA. Starting with a root node that indicates a physiological status (2, 2, 2, 2, 2, 2, 2), the software creates a phylogenetic tree by heuristically aiming to minimize the overall amount of CNAs throughout the tree. Thus, there is a modification in the copy number of one gene probe in every edge, leaving the root and proceeding to a new node. Whenever an upstream node cannot be linked to a downstream node, as the linking signal pattern was not observed in the tumor samples, the software algorithm predicts a transit signal pattern connecting these two nodes. The nodes containing such a predicted transit signal pattern are marked with a dashed circle line in the FISHtrees, whereas a solid circle line marks signal patterns observed in the tumor. Furthermore, the total number of events in the tree was computed, defined as the sum of events required to create all leaf nodes from the root node. The maximum tree depth was determined, defined as the maximum amount of edges from a leaf to the root node.

3.3.2 Targeted next-generation sequencing

For DNA extraction, macro-dissected FFPE-tissue sections were lysed in a mixture of proteinase K for digestion, mineral oil for removing the paraffin, plus ATL lysis buffer. Going more into detail, in the first step, a 50 µm tumor section was put into a 2.0 ml tube and 100 µl buffer ATL, 20 µl of Proteinase K, and 300 µl of mineral oil were added. The sample was mixed by inverting the tube 50 times, followed by an incubation step in a thermomixer at 65°C, 500 rpm for around 4 hours. Another 20 µl of Proteinase K was added and mixed by inverting 50 times before placing the tube into the thermomixer and incubated for 12-18 hours. Afterwards, a brief centrifugation step of the tube was carried out, and an additional 10 µl Proteinase K was added. Again, the sample was mixed by inverting it 50 times, followed by another overnight incubation in the thermomixer (65°C, 500 rpm). The next morning, the tube was quickly centrifuged, and the digest was assessed: in case of an incomplete digest, another 10 µl of Proteinase K was added, followed by an additional round of incubation in the thermomixer for a few hours more to ensure full digestion of the tissue. Afterwards, a spun of the tubes for one minute at 13,200 rpm was carried out, and 130 µl of the lysate was pipetted to a 1.5 ml Eppendorf tube. After the addition of 1.5 µl RNAse A, the tube was vortexed (5 seconds), centrifuged (10 seconds at 8,000 rpm), and kept at room temperature (5 minutes). Then, 10 µl of 3 M sodium acetate and 650 µl of buffer PM were added, followed by vortexing the tube (5 seconds). Next, pipetting the sample onto Quick spin columns was carried out. To collect the eluate, a centrifugation step at 5,000 rpm for 30 seconds took place. This step was repeated to assure all DNA was attached to the column. Afterwards, the collecting tubes were substituted. After adding 700 µl of buffer PE, a centrifugation step (30 seconds at 8,000 rpm) followed. Repeatedly, collection tubes were substituted, and 700 µl of 80% ethanol was added, followed by a centrifugation step (1 minute at 13,200 rpm). One more time, collection tubes were substituted, followed by another centrifugation step (5 minutes at 13,200 rpm). Afterwards, the tube was placed into the thermomixer at 65°C for 10 minutes. 1.5 ml Eppendorf tubes were filled with the filter columns together with 40 µL of 10% Buffer AE. Another incubation step in the thermomixer (5 minutes at 65°C) was carried out, followed by centrifuging the tube (1 minute at 13,200 rpm). Again, the initial elution was utilized at the same column, followed by an incubation step in the thermomixer (5 minutes at 65°C). Then, the sample was spun (1 minute at 13,200 rpm). Finally, an analysis of the yield and the purity of the DNA were conducted with a NanoDrop 1000 Spectrophotometer. The dsDNA High Sensitivity Assay Kit was used to

quantify the DNA on Qubit. Next, the DNA integrity was evaluated on a Bioanalyzer system. The DNA library preparation was performed using a DNA sample input of 200 ng.

Targeted NGS was carried out with OncoVar, a panel created to span coding exons of 563 cancer-related genes (gene list presented in **Supplemental Table 5**). The KAPA Hyper Prep Kits for Illumina were used for library construction. The produced libraries were then sequenced on a NextSeq 500 system with a mean coverage for targeted regions of 263. Following the recommendation of the Broad Institute[187], the Best Practices workflow was adhered regarding variant calling and data processing. For variant calling, the following filtering standards were applied: (1) failed to pass UnifiedGenotype filter with GATK default criteria, (2) fraction of alternative reads ≤ 5%, (3) total read depth ≤5 or alternative read depth ≤3, (4) QUAL <30, (5) low impact according to dbNSFP[188], (6) common SNPs in the NCBI dbSNP version 147[189], (7) variants with allele frequency (AF), overall allele frequency in ESP (ESP_AF_GLOBAL), or allele frequencies (ESP6500 MAF_EA) >0.001 in the Exome Aggregation Consortium (ExAC, release 3.1)[190], (8) MAPQ score <40 for variants with ≥100 COSMIC cases or on breast cancer hot spot genes (*GATA3, KMT2C, MAP3K1, PIK3CA, TP53*)[117], (9) MAPQ score <55 for variants on other genes, (10) variants, which are present in minimum two samples including less than <100 COSMIC cases and (11) variants without a COSMIC case but being in the category of having ´moderate impact´ according to dbNSFP. Visual validation of all detected indels and SNVs was carried out using the Integrative Genomics Viewer (IGV) of the Broad Institute[191]. MutationMapper[192,193] was used to create lollipop plots (**Supplemental Figure S1**).

3.3.3 Exclusivity and co-occurrence analysis

In large cohorts of tumor patients, gene mutations frequently involved in the same cancer pathways do not often appear together in the same tumor[194]. Thus, in cancer genomic data, these genes involved in the same biological process create patterns of alterations that are mutually exclusive[194]. Ciriello et al. developed a method called Mutual Exclusivity Modules in cancer (MEMo) using statistical tests and correlation analyses to identify these sets of genes within oncogenic pathway modules systematically[195]. This method is based on the principles that member genes are known to engage in the same biological process or are predicted to do so. Therefore, they are often altered across a collection of tumor samples, and alteration events within these pathway modules occur mutually exclusive[195]. This MEMo algorithm from Ciriello et al. was used to perform a mutual exclusivity and co-occurrence analysis of CNAs (*CCND1, CDH1, COX2, DBC2, HER2, MYC, TP53, ZNF217*) and mutations (*PIK3CA, TP53*) for this cohort of 39 tumor samples along with PD Dr. med.

Daniela Hirsch (NCI, NIH, Bethesda, MD, USA)[195,196]. The visualization of the mutual exclusivity and co-occurrence analysis was carried out in Microsoft Excel 2019 (**Supplemental Figure S3**).

3.4 Statistics

Statistical analysis including comparisons between the different subgroups, for example, long versus short survival patients or diploid versus aneuploid tumors, was performed using Fisher exact tests, t-tests (two-sided), and Chi-Square tests as applicable to determine the corresponding *p*-values. All values underwent multiple testing corrections using the Benjamini-Hochberg method. The statistical analysis was based on a significance level of $p < 0.05$ after correction for multiple testing. The data obtained from targeted NGS were statistically analyzed by including all genes displaying a mutation in at least three samples (>7.5% of the cohort).

4 RESULTS

In previous studies, an association between the degree of tumor heterogeneity and tumor aggressiveness as well as between chromosomal aneuploidy and inferior prognosis in breast cancer patients could be shown[67,79,81,91]. This doctoral thesis was motivated by the desire to better understand the role of tumor heterogeneity as well as analyze chromosomal aneuploidy and genomic instability for improved prognostication focusing on older breast cancer patients, as they are underrepresented in cancer research. Therefore, a retrospective comprehensive genetic analysis of FFPE samples of 39 older breast cancer patients with profoundly different survival time and several clinical data available was conducted. As a result, a broad set of miFISH data using a breast cancer-specific gene panel, ploidy measurements using image cytometry and miFISH and phylogenetic trees for each tumor sample, as well as NGS data using a custom panel of 563 cancer-associated genes were generated. The data were analyzed comparing the groups of long versus short survival patients. Moreover, after finishing the ploidy measurements, the cohort was separated into diploid versus aneuploid tumors, and all generated data were statistically analyzed accordingly. In addition to this, the generated data were statistically analyzed for the subgroups formed by the different intrinsic subtypes as well as for tumors with a low versus a high instability index.

4.1 Clinicopathologic characteristics

39 breast cancer samples with a median patient age of 67 at the time of surgery and with a different time of survival after diagnoses (long survival, median 19 years, versus short survival, median 2.4 years) were matched for age, ER, PR, HER2 receptor and Ki67-status as well as the occurrence of metastasis. They were selected out of a cohort of 245 breast cancer patients. In the statistical analysis of the clinical parameters of long versus short survival patients, no significant difference for any of the matched parameters could be shown. Regarding the T1-2 stages and the absence of lymph node metastases in the statistical analyses, both occurred significantly more often in the long survival group.

The clinical and clinicopathological features, including survival time, age at diagnosis, TNM stage, ER-, PR-, HER2-status, Ki67- expression, as well as the corresponding p-values calculated in the statistical analysis are separately listed for the two groups of long and short survival patients in the supplement (**Supplemental Table 1**) and graphically presented in **Figure 7.**

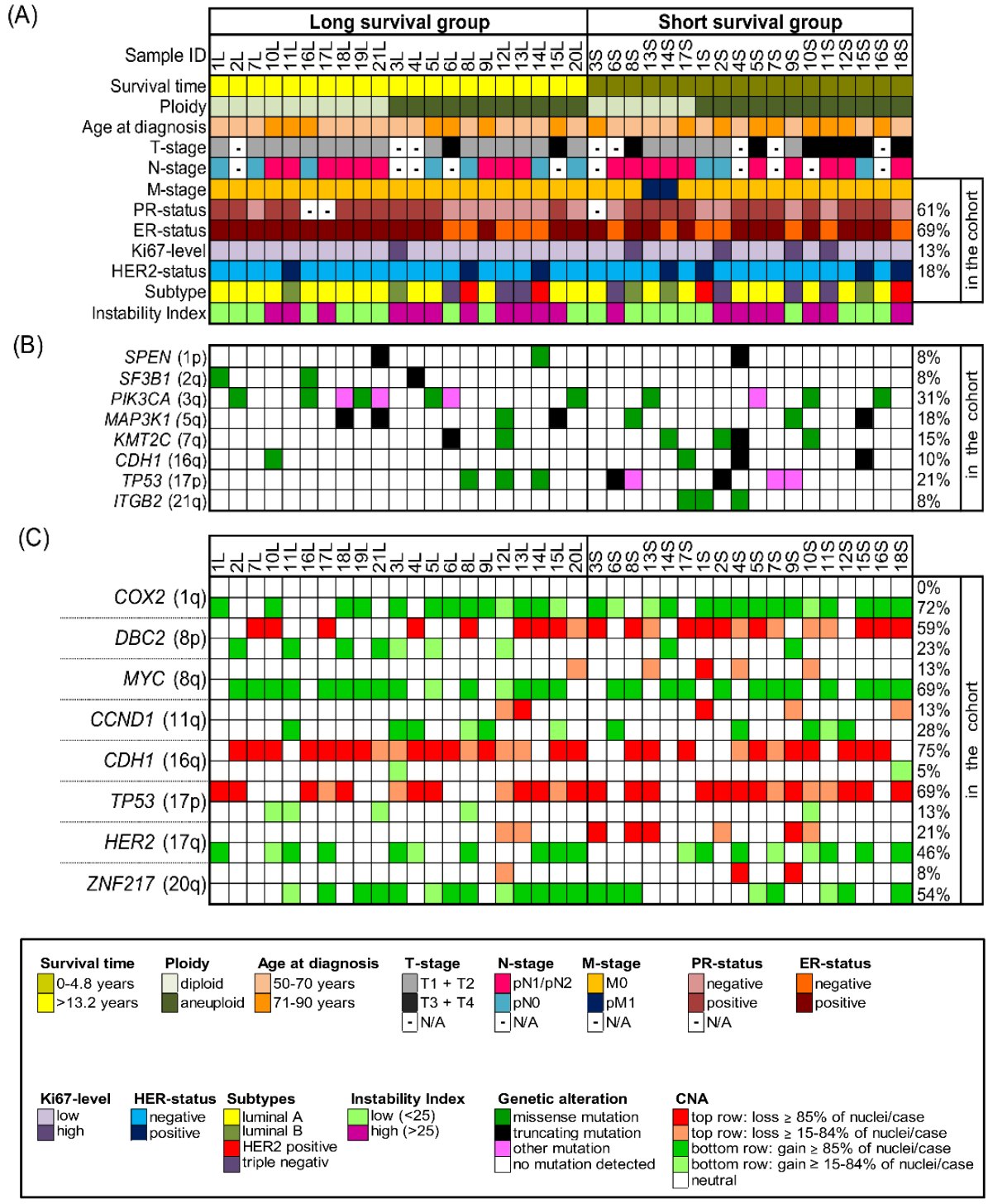

Figure 7 from Liegmann et al.[197]: Overview about the clinicopathological features, results of the 563-gene-mutation-analysis and miFISH-results for the entire cohort. (A) Summary of the clinicopathological features (rows) separately listed for the short and long survival group and plotted per individual sample (columns). **(B)** Extraction of the mutation analysis of 563-breast cancer-associated genes by NGS. Distribution of mutations that affected genes in at least three samples. The color code indicates the type of mutation. **(C)** CNAs of eight breast cancer-related genes were identified by miFISH and plotted vertically per individual sample (columns). Green color indicates a gain, red color a loss. Dark hues were chosen if the majority (≥85%) of all nuclei showed a gain/loss and light hues if 15–84% showed a gain/loss.

Furthermore, the 39 tumor samples were separated according to their ploidy, with 16 diploid cases, consisting of 10 long and six short survival cases, and 23 aneuploid cases, consisting of 11 long and 12 short survival cases. Regarding age, survival time after diagnosis, ER-, HER2- and Ki67-status, as well as the presence of lymph nodes and distant metastasis, no significant differences were determined in the statistical analysis. However, a significantly higher number of T1/2 stages and PR-positive tumors were observed in the diploid group.
The analysis of the intrinsic subtypes "triple-negative", "HER2 positive", and "luminal (A and B)" revealed that the triple-negative group had the shortest and the luminal group the most extended average survival after diagnosis; however, this difference did not reach statistical significance. No significant differences were determined in the other analyzed clinical and clinicopathological parameters (average age at diagnosis, T-, N- and M-status) between the intrinsic subtypes groups.

4.2 Targeted next-generation sequencing results

For the mutation analysis, targeted NGS with the OncoVar panel, consisting of 563 cancer-related genes (presented in **Supplemental Table 5**), was performed. In **Figure 7B**, mutated genes were visualized. The most frequently altered genes in the cohort´s tumor samples were *PIK3CA* (12/39, 31%) and *TP53* (8/39, 21%) followed by *MAP3K1* (7/39, 18%), *KMT2C* (6/39, 15%), *CDH1* (4/39, 10%), *ITGB2* (3/39, 8%), *SPEN* (3/39), and *SF3B1* (3/39). In summary, the spectrum of gene mutations determined in the tumor samples overlaps the significantly mutated genes of the breast cancer cohort reported in The Cancer Genome Atlas (TCGA) 2012[117]. In comparison to the TCGA cohort, differences were seen regarding the gene *MAP2K4*, in which no mutations were detected in the tumor samples of this thesis, and the genes *ITGB2* and *SPEN* not being reported as significantly mutated in the TCGA cohort.
The mutation type and its localization within the protein for the two most often mutated genes, *PIK3CA* and *TP53*, are shown in **Supplemental Figure S1.** Regarding *PIK3CA*, exclusively missense mutations including the known mutation hot spots in exon 9 (E542K in cases 2L, 5L, 19L and 13S; E545K in luminal A tumors 16L and 10S), helical domain, and exon 20 (H1047L in case 5S and H1047R in cases 6L, 18L and 21L) and kinase domain with corresponding high COSMIC ID were observed. ER-positivity co-occurred in 11 of the 12 cases with mutations in *PIK3CA*. For *TP53*, predominantly missense mutations also involving the known mutation hot spots in the DNA binding domain of the protein were detected.
Statistically analyzing the mutation frequencies of a) each of these genes and b) the overall mutation burden per sample in a comparison between the groups i) long versus short survival

patients, ii) diploid versus aneuploid tumors, and iii) tumors with a low versus a high instability index no significant differences were detected. However, the following trends were observed: mutations in *PIK3CA* occurred more frequently in tumors with a low instability index (45%) than in tumors with a high instability index (15.8%). In addition to this, in more tumors of long survival patients (8/21) compared to tumors of short survival patients (4/18) *PIK3CA* mutations were observed. Moreover, mutations in *SF3B1,* including one missense mutation with a high COSMIS ID number, were exclusively discovered in patients with long survival. The statistical analysis of the *TP53* mutation frequencies for all tumor samples separated by the intrinsic subtypes luminal A/B, HER2 positive, and triple-negative revealed a significantly different distribution (mutated in 7% of luminal A/B, in 50% of HER2 positive and 57% of triple-negative samples, $p = 0.038$).

4.3 Analysis of CNAs and ITH based on the miFISH results

For this thesis, a recently developed multiplex interphase FISH technique, which can visualize up to 20 loci in single cells simultaneously[104], was used to determine copy numbers of 10 loci as well as the ploidy of the tumor samples as described in MATERIALS AND METHODS. Additionally, DNA image cytometry was performed for 11 long- and nine short survival cases. The resulting DNA histograms are presented in **Figure 9**, **Figure 10 and Supplemental Figures S4 and S5**. Comparing the ploidy results of the DNA image cytometry and miFISH, the determined ploidy matched well.

Overall, at least two gene probes in each of the 39 tumor samples showed CNAs, with most cases revealing both losses and gains. **Figure 7C** displays a summary of all gains and losses for each gene probe and tumor sample. The most frequent alterations were gains of the oncogenes *COX2* in 72% (28/39) and *MYC* in 69% (27/39) of the tumor samples and losses of the tumor suppressor genes *CDH1* in 74% (29/39) and *TP53* in 69% (27/39). Genes that were often lost were rarely gained, and vice versa, as visualized in **Figure 7C**. Regarding the three targeted tumor suppressor genes, copy number losses were more frequently detected. Similarly, the five targeted oncogenes were more often subject to copy number gains. As an exception, copy number gains were revealed in nine of the 39 cases regarding the tumor suppressor gene *DBC2*. Noteworthy, in all these nine tumor samples, *MYC* also showed copy number gains. Co-occurring with the loss of chromosome 17, copy number losses of *HER2* were detected in eight tumor samples, in which *TP53* was lost as well. Equivalently, *TP53* was gained in five tumor samples co-occurring with a gain of chromosome 17. Unexpectedly, *CCND1* was subject to copy number losses in five of the 39 tumor samples. Remarkably, in 16 of the 39 cases (nine short survival and seven long

survival patients), a gain of *MYC* (located on 8q) co-occurred with a loss of *DBC2* (8p). Similarly, in 14 of the 39 tumors (equally distributed between short and long survival patients), a gain of *HER2* (17q) was accompanied by a loss of *TP53* (17p). Regarding copy number gains, genes with signal counts more than double the overall ploidy allocated were classified not only as gained but "amplified". The highest signal counts were observed for *HER2* amplified in seven tumor samples (in five long and two short survival cases), followed by *CCND1* with amplifications in six ER-positive tumor samples (three long and three short survival cases) as well as *MYC* amplified in 10 tumor samples (five long and five short survival cases).

The miFISH results of each of the 39 tumor samples are visualized as color charts and presented in **Figures 8-10** and in **Supplemental Figures S4 and S5.** In **Figure 8** examples of cases with special features are displayed (cases 9S, 10S, 13S and 14S). Going more into detail, case 13 was the only tumor raising the question of being hypodiploid since it was dominated by a clone with only one copy of the genes *DBC2*, *MYC*, *CDH1*, *TP53,* and *HER2.* Moreover, for the centromere probes for chromosomes 4 and 10, which are included in the probe panel as described in MATERIALS AND METHODS, only one copy each for most nuclei of case 13S were observed. To answer the question of hypodiploidy, further hybridizations with additional centromere and locus-specific probes as described in MATERIALS AND METHODS were carried out. As a result, losses for 10 of the 22 analyzed chromosomes were detected, as displayed in **Supplemental Figure S2**, supporting the hypothesis of case 13 being hypodiploid. In contrast, more than 90 % of analyzed tumor cells in case S14 (**Figure 8B**) showed no copy number losses; only copy number gains in *COX2, DBC2,* and *MYC* were revealed. Unlike cases 13S and 14S, case 10S was extremely unstable, with an instability index of 68.8, as evident from **Figure 8C**. Despite this high instability, a loss of *CDH1* accompanied by a gain of *CCND1* was maintained in essentially all tumor cells. Additionally, the combination of a loss of *CDH1* with a gain of *CCND1* was present in three more cases of the cohort (12S, 4L and 9L).

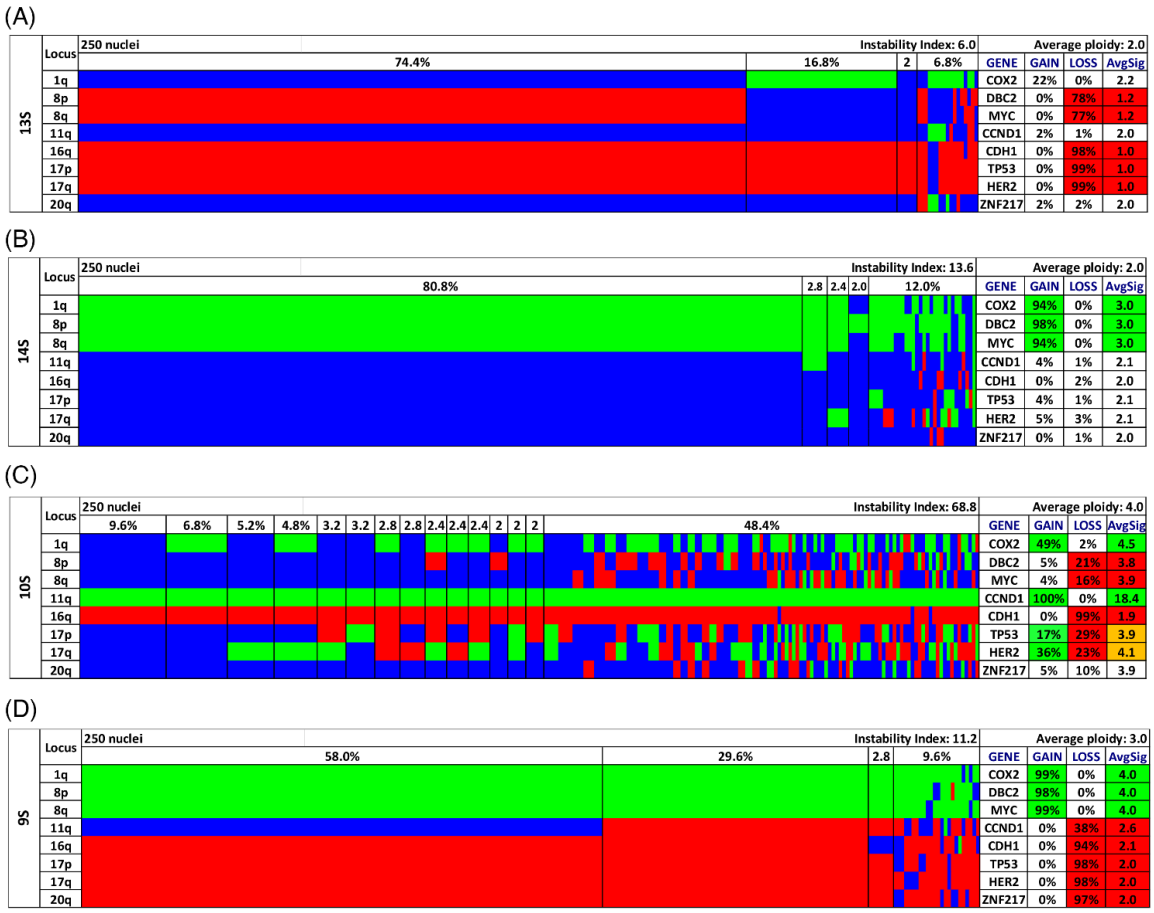

Figure 8 from Liegmann et al.[197]: MiFISH results of four notable short survival cases graphically presented as color charts. For every nucleus, copy number changes are visualized as gains (green), losses (red) and neutral (blue). Gene-specific miFISH markers are displayed vertically with each probe's unique chromosomal arm shown in the "Locus" column on the left of the plot, and the corresponding gene name on the right. Nuclei are arranged horizontally by the frequency of signal patterns from left to right. Different gain-and-loss patterns are separated by each vertical line stating the prevalence of the cell clone in the tumor population. Copy number gains and losses are depicted as percentages of the total cell population in the "Gain" and "Loss" column of the table on the right. Color-labeled percentages indicate a threshold of 15%. The column "AvgSig" refers to the average of all signal numbers specified for each of the 8 analyzed gene probes.

(A) Case 13S. The case 13S is dominated by several losses of the 8 gene probes for most nuclei.

(B) Case 14S. The case 14S reveals mostly gains for the majority of nuclei, also a gain of the tumor suppressor gene *DBC2*.

(C) Case 10S. The case 10S is extremely instable yet maintains a gain of *CCND1* accompanied by a loss of *CDH1* in essentially all nuclei.

(D) Case 9S. The case 9S shows in 30% of the analyzed nuclei in all 8 gene probes copy number changes and in 58% of the nuclei in 7 of the gene probes.

Unique about case 9S was that in 30% of all cells, copy number changes were detected in all gene probes. The major clone (58% of all cells) showed copy number changes in all but one gene probe (**Figure 8D**). In contrast, case 16L revealed the fewest copy number alterations of the cohort – a loss of *TP53* and *CDH1* were the only changes (**Supplemental Figure S4**). Taking a closer look at the overall tumor cell population based on the miFISH results, a large variability of ITH across the cohort was detected. Instability indices, which measure the frequency of altered clone patterns as a reflection of ITH (as described in MATERIALS AND METHODS), ranged from 2 to 86.6 (median 24.8) within the cohort, providing an idea of the genetic variety of breast cancer in women aged 50 years and above. Giving four examples of cases with a different ITH, two short survival cases (4S and 8S, **Figure 9**) and two long survival cases (5L and 7L, **Figure 10**) are displayed as color charts and histograms completed with an image of a representative H&E stain of each case. Interestingly, cases with a low as well as with a high instability index were found among the group of short and long survival patients. As an example of a short survival case with a low ITH, case 8S (**Figure 9E-H**) is presented. This tumor reveals a stable aberration pattern of gains of *MYC* and *ZNF217* and losses of *DBC2*, *CDH1*, *TP53,* and *HER2* in 95% of all cells, forming the major clone, resulting in a low ITH with an instability index of 7.6. Furthermore, the proliferation activity was assessed as high based on a high Ki67 expression, and the case exhibited a diploid DNA histogram. In contrast, case 4S (**Figure 9A-D**) was determined as aneuploid by image cytometry and showed a high instability index of 54, revealing a markedly increased ITH. The major clone, comprised of 32% of the cells in this sample, revealed gains of *COX2* and *HER2* and high-level amplification of *CCND1* as well as losses of *TP53* and *ZNF217*. The pattern in the second largest clone, represented by 20% of the cells, was consistent with the loss of *DBC2*, *MYC*, *TP53,* and *ZNF217*. An example of a long survival case with a low ITH is case 7L (**Figure 10E-H**), with a major clone consisting of 98% of all cells and the lowest instability index of the cohort (instability index of 2). The major clone showed losses of *CDH1* and *DBC2* and a gain of *MYC*, possibly indicative of the formation of an isochromosome 8q[198]. Case 7L exhibited a diploid DNA histogram. Case 5L (**Figure 10A-D**), on the other hand, demonstrated that high ITH and aneuploidy were also found in the long survival group. Losses of *TP53* and *CDH1* and gains of *COX2* and *ZNF217* were observed in the major clone, formed by 37% of the cells, and in several minor clones of case 5L.

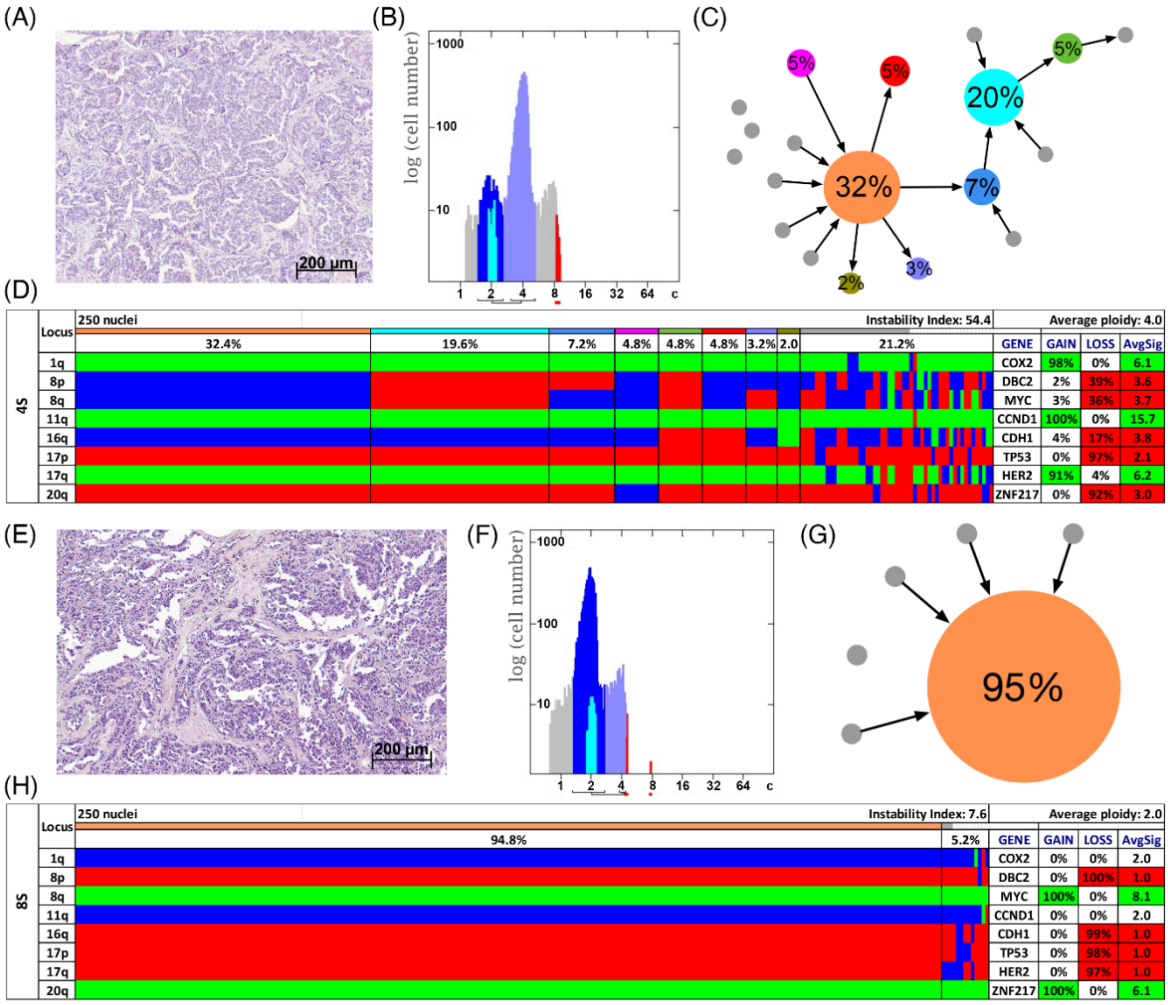

Figure 9 from Liegmann et al.[197]: Patients with short survival after diagnosis. Histology (A,E), image cytometry (B,F), imbalance clone plots (C,G) and miFISH results (D,H) for the cases 4S (A–D) and 8S (E–H).

(A,E) H&E-stained sections of the respective breast cancer samples showing the histomorphology. **(B,F)** DNA histograms presenting the quantitative analysis of the nuclear DNA content assessed by image cytometry using Feulgen-stained cytospins. For quantitative measurement of the DNA content the sample was screened for several diploid nuclei (granulocytes, lymphocytes) to set the 2c value indicating a diploid DNA content. The quantitative measurements of the nuclear DNA content (x axis) of the tumor cells given in "c" units were then calculated accordingly. The y axis represents the logarithm of the total cell count. In case 4S 5,810 and in case 8S 6,721 nuclei were analyzed.

(C,G) Imbalance clone plots visualizing the clonal composition of the analyzed breast cancer sample and their putative evolutionary trajectory. The area of the circles correlates with the occurrence of a cell-clone with a specific gain-and-loss pattern within the tumor cell population. Clones derived by a single gain or loss change are connected by arrows. The arrows indicate the clonal evolution according to gain-and-loss patterns in the color charts (D,H) starting from the clone with the fewest gains and losses. Thus, unconnected clones must differ in more than one gain or loss in their gain-and-loss pattern. Color coding allows assignment of the individual clones to the corresponding clones in the color charts in D and H.

(D,H) For every nucleus, copy number changes are visualized as gains (green), losses (red) and neutral (blue). Gene-specific miFISH markers are displayed vertically with each probe's unique chromosomal arm shown in the "Locus" column on the left of the plot, and the corresponding gene name on the right. Nuclei are plotted horizontally by pattern frequency. Different gain-and-loss patterns are separated by each vertical line stating the prevalence of the cell clone in the tumor population. Copy number gains and losses are depicted as percentages of the total cell population in the "Gain" and "Loss" column of the table on the right. The column "AvgSig" refers to the average of all signal numbers specified for each of the eight analyzed gene probes.

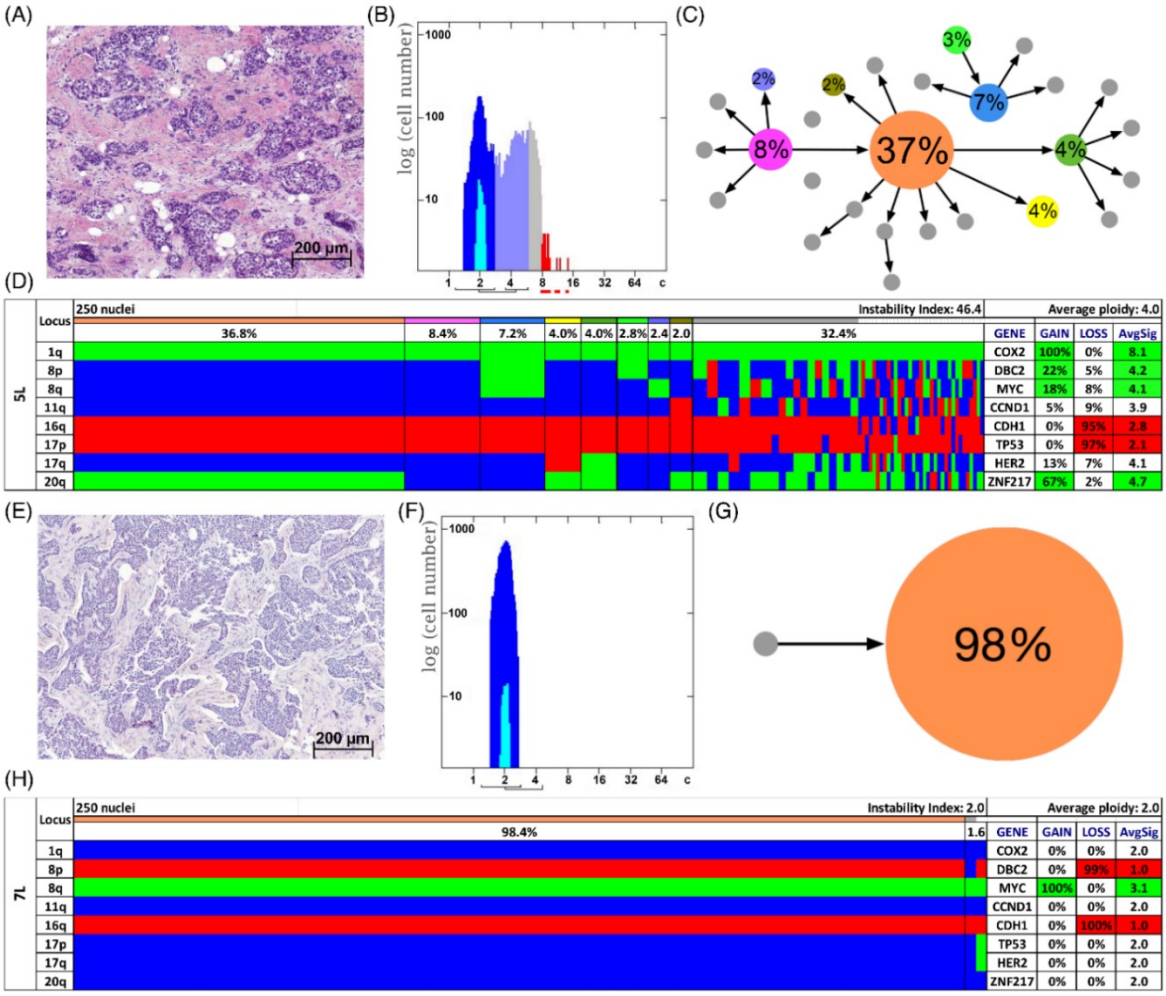

Figure 10 from Liegmann et al.[197]: Patients with long survival after diagnosis. Histology (A,E), image cytometry (B,F), imbalance clone plots (C,G) and miFISH results (D,H) for the cases 5L (A–D) and 7L (E–H). (B,F) In case 5L 4,759 and in case 7L 11,792 nuclei were analyzed. The DNA measurements revealed aneuploidy in case 5L and diploidy in case 7L. Detailed figure caption see **Figure 9**.

Additionally, imbalance plots visualizing the likely trajectory of clonal evolution and frequency of clones based on the miFISH data were created for the representative cases 5L, 7L, 4S, and 8S (**Figure 9C,G** and **Figure 10C,G**). The imbalance plots of the diploid cases 8S and 7L with a low instability index reflecting low ITH are depicted as an elementary trajectory. In contrast, the imbalance plots of the aneuploid cases 4S and 5L with high ITH show a complex trajectory with multiple circles illustrative of various clones within the tumor cell population.

4.4 Analysis of subgroups distinct by survival time, ploidy, and instability index

The selection of patients in the cohort took place based on their profoundly different survival time after diagnosis (median of 2.4 years in the short survival group versus median of 19 years in the long survival group). One aim in this thesis was to analyze if the genetic parameters obtained in the miFISH- and NGS-analysis could explain the severely different prognosis of the two groups. In **Figure 11** a selection of the statistical analysis results for the different subgroups are visualized as boxplots. Unexpectedly, after multiple testing corrections, the observed CNAs (both the overall number of CNAs per sample as well as separately analyzed for each gene probe) and average signal numbers were not significantly different between the groups of long and short survival (**Figure 11C**). Moreover, the instability indices as a reference point of ITH did not differ significantly between the groups of short and long survival ($p = 0.7$, **Figure 11A**).

To further examine the 39 patients´ miFISH data, we divided them according to their ploidy. In this way, we gained a group of 16 diploid cases (10 long- and 6 short survival cases) and 23 aneuploid cases (11 long- and 12 short-survival cases). Both the average signal numbers of each gene probe as well as the overall number of CNAs per sample showed significant differences between the groups. As visualized in **Figure 11D**, in diploid tumors an average of 4.5 CNAs per sample in comparison to 6.5 in aneuploid tumors was detected ($p = 0.0012$). Furthermore, 50% of diploid tumors showed a gain of *COX2* and a loss of *TP53* compared to 87% and 83% of aneuploid tumors; however, after multiple testing corrections, this comparison did not reach statistical significance. Remarkably, *TP53* was both lost and mutated in 6% (1/16) of diploid and 22% (5/23) of aneuploid cases, translating into an entire functional elimination of this tumor suppressor. Moreover, significant differences were revealed when comparing the instability indices of the two groups ($p = 0.0006$, **Figure 11B**), with lower instability indices (representing a lower ITH) in the diploid group. Giving some examples, these profound differences become apparent by comparing the color charts and

circle plots of the diploid tumor samples 7L and 8S with low ITH with the aneuploid tumor samples 5L and 4S with high ITH as presented in **Figure 9** and **Figure 10**).

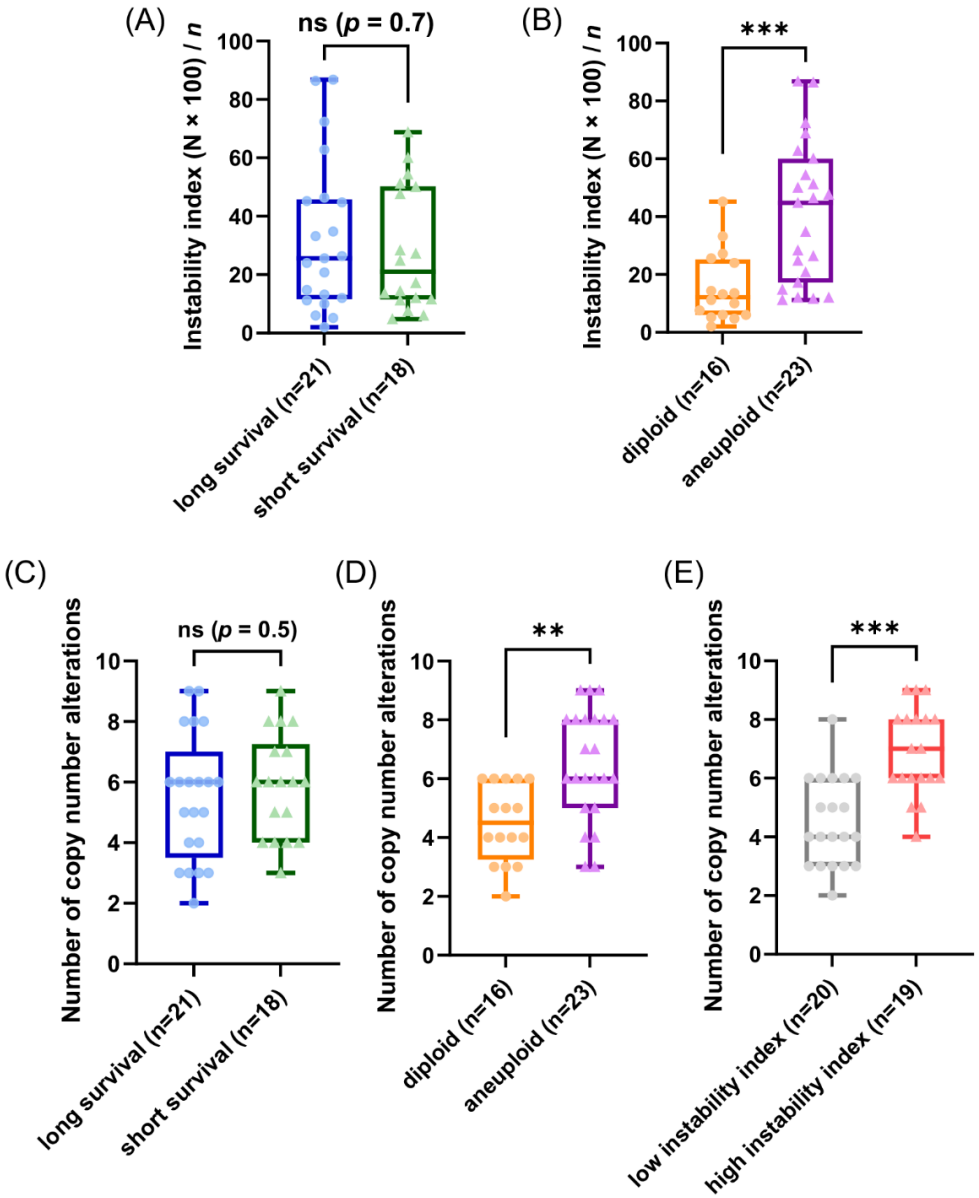

Figure 11 from Liegmann et al.[197]: Boxplots of instability indices and frequencies of CNAs per tumor sample for different subgroups (miFISH results).
(A,B) Instability indices including minimum, maximum, median and outliers are presented as boxplot for each subgroup: **(A)** long and short survival patients, **(B)** diploid versus aneuploid tumors.
(C–E) Frequency of CNAs per tumor sample including minimum, maximum, median and outliers are presented as a boxplot for each subgroup:
(C) long and short survival**, (D)** diploid versus aneuploid tumors and **(E)** tumors with low versus tumors with high instability index. ** **p ≤ 0.01**; *** **p ≤ 0.001**.

In addition to this, we divided the 39 tumors into two equal-sized groups based on their instability indices and examined their clinical data, miFISH, and NGS results. Patients in the first group had tumors with an instability index of 2 to 24.8 (average of 12), while the instability index of the second group ranged from 25.6 to 86.8 (average of 50.1). No significant differences were detected in the statistical analysis regarding the clinical parameters of these two groups. A significantly higher number of CNAs (4.5 versus 6.9, $p \leq 0.0001$) was observed in the group with the higher instability index as presented in **Figure 11E**. Another evident difference occurred regarding the mutation frequency of *PIK3CA,* with 16% in the group with a low instability index versus 45% in the group with a high instability index, not reaching statistical significance, though.

4.5 Clonal evolution analysis by phylogenetic tree modeling

To gain more information about the clonal tumor evolution, phylogenetic trees generated from the results of the miFISH analysis using the software FISHtrees 3.2 were generated for each of the 39 tumor samples. Starting with a diploid root cell that indicates a physiological status (2, 2, 2, 2, 2, 2, 2), the software creates a phylogenetic tree by heuristically selecting the signal pattern with the fewest CNAs and displaying the signal pattern of each cell.

Comparing the phylogenetic trees of the tumors of the long versus the short survival group, both simple FISHtrees with only a few nodes, reflecting only a few different signal patterns (measured by the total number of distinct mutational events), and with only a few different tree levels (measured in tree depth) as well as complex FISHtrees with multiple edges and a high tree depth could be observed in both groups. In contrast, when comparing the FISHtrees of the diploid and aneuploid tumors, the total number of mutational events ($p = 0.0008$) and the tree depth ($p = 0.0008$) were significantly different in the statistical analyses. In general, as anticipated, the FISHtrees of the aneuploid samlpes, in comparison to the diploid tumors, were more complex, reflecting the increased number of CNAs, higher genomic instability, and ITH. Boxplots of the statistical FISHtree group comparison of long survival versus short survival patients and diploid versus aneuploid tumors are presented in **Figure 12**.

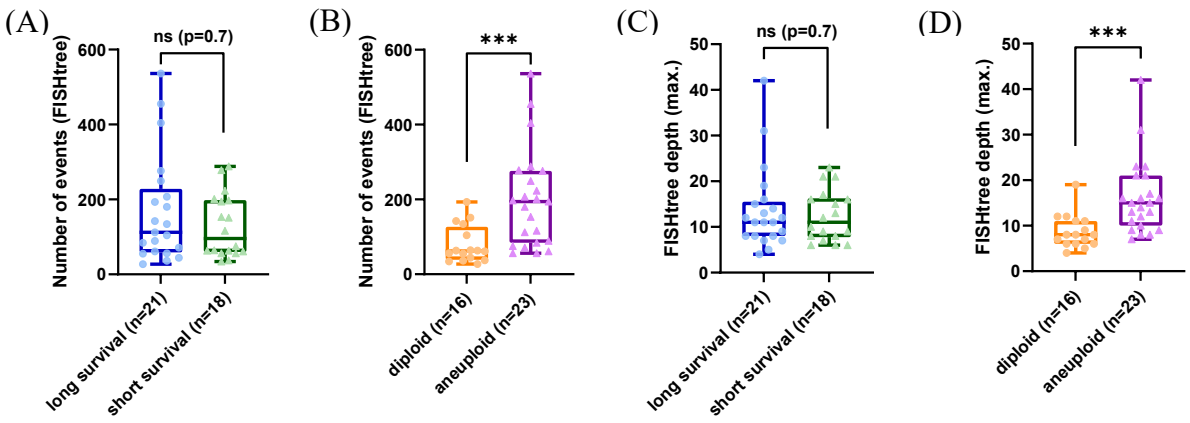

Figure 12: Boxplots of the FISHtree analysis presenting the total number of events in the tree and the maximum FISHtree depth for the different subgroups.
(A,B) Total number of events in the FISHtree including minimum, maximum, median and outliers are presented as a boxplot for each subgroup: **(A)** long versus short survival and **(B)** diploid versus aneuploid samples. In the statistical analysis a significant difference between diploid versus aneuploid tumors was calculated (**p=0.0008**).
(C,D) FISHtree depth including minimum, maximum, median and outliers are displayed as a boxplot for each subgroup: **(C)** long and short survival, **(D)** diploid versus aneuploid cases. In the statistical analysis a significant difference between diploid versus aneuploid samples was calculated (**p=0.0008**).

A typical FISHtree of a diploid case (simple structure) and an aneuploid case (complex structure) of long survival cases, 5L (aneuploid) and 7L (diploid) are presented in **Figure 13**. The diploid case 7L consisted of five clones, all displaying a loss of *CDH1* and a gain of *MYC.* Two of the five clones were major clones, both showing an additional loss of *DBC2*; the remaining three were minor clones. In the aneuploid case 5L, a high number of distinct mutational events (207) resulting in a high tree depth (15) was determined, reflecting an enormous degree of ITH. This case showed a multitude of minor clones and one major clone (pattern: 8,4,4,4,3,2,4,5). All clones of case 5L displayed a gain of *COX2,* and the majority (95%) of clones revealed a loss of *CDH1* and *TP53*. Whole genome duplication (WGD) was revealed to have presumably occurred as an initiating event in tumor development of case 5L starting from the diploid root node (labeled as node 1 in **Figure 13A**), leading to tetraploidization of the signal pattern in node 2. Later in tumor development, WGD presumably occurred in four following nodes (labeled as node 12, 15, 19, and 22, colored in pink), transforming from tetraploidy to octoploidy. Regarding the whole cohort, WGD frequently occurred in a minor fraction of cell clones, with most clones in these cases being diploid. Only in a few cases could the presumable occurrence of WGD as an initiating event (tetraploidization from node 1 to node 2) be observed.

(A)

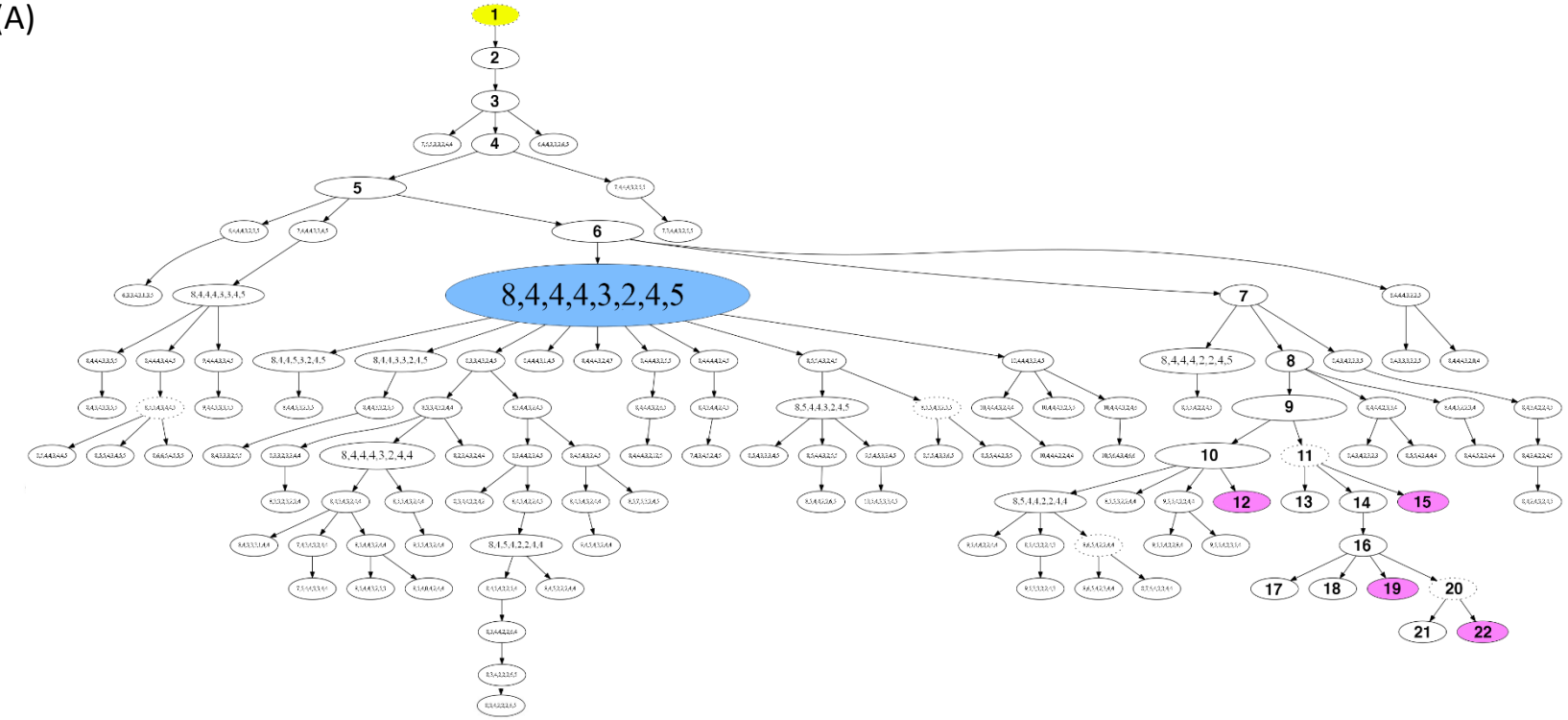

1: 2,2,2,2,2,2,2,2; **2:** 6,4,4,3,4,2,4,5; **3:** 7,4,4,3,3,2,4,5; **4:** 7,4,4,4,3,2,4,5; **5:** 7,4,4,4,3,2,3,5; **6:** 8,4,4,4,3,2,3,5; **7:** 8,4,4,4,2,2,3,5; **8:** 8,4,4,4,2,2,3,4; **9:** 8,4,4,4,2,2,4,4; **10:** 8,5,5,4,2,2,4,4; **11:** 8,4,4,3,2,2,4,4; **12:** 16,10,10,8,4,4,8,8; **13:** 8,4,4,3,2,1,4,4; **14:** 6,4,4,3,2,2,4,4; **15:** 16,6,5,6,4,4,8,8; **16:** 6,3,3,3,2,2,4,4; **17:** 6,3,3,3,2,2,2,5; **18:** 6,3,3,3,3,2,4,3; **19:** 12,6,6,6,4,4,8,8; **20:** 6,3,4,3,2,2,4,4; **21:** 6,3,4,4,1,2,4,4; **22:** 12,4,6,5,4,4,8,8;

(B)

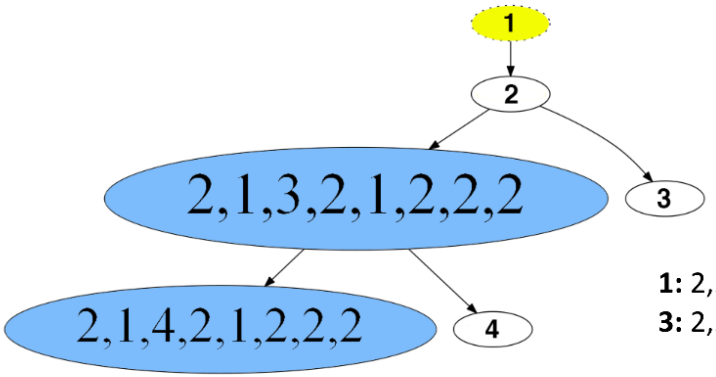

1: 2,2,2,2,2,2,2,2; **2:** 2,2,3,2,1,2,2,2;
3: 2,2,4,2,1,2,2,2; **4:** 2,1,3,2,1,3,3,2;

Figure 13 from Liegmann et al.[197]: Phylogenetic trees of exemplary long survival cases (A) 5L and **(B)** 7L. FISHtrees were designed using phylogenetic algorithms (software FISHtrees 3.2). The following gene order was used for displaying the FISH patterns: *COX2*, *DBC2*, *MYC*, *CCND1*, *CDH1*, *TP53*, *HER2* and *ZNF217*. Starting with a root node labeled in yellow color that indicates a physiological status (2, 2, 2, 2, 2, 2, 2), the software creates a phylogenetic tree by heuristically aiming to minimize the overall number of CNAs throughout the tree. In this way, clonal evolution is depicted. The patterns' frequency within the cell population is expressed in the node size, however, not being proportional to it. Nodes encircled by a solid line marks miFISH-signal-patterns observed in the tumor tissue. Whenever an upstream node cannot be linked to a downstream node, as the linking signal pattern was not observed in the tumor samples, the software algorithm predicts a transit signal pattern connecting these two nodes. The nodes containing such a predicted transit signal pattern are marked with a dashed circle line.
(A) The node of the major clone (here: tetraploid) is displayed in blue (pattern 8-4-4-4-3-2-4-5; consisting of 71 out of 250 analyzed nuclei). In the legend signal patterns for selected clones (1–22) are shown in detail. Whole genome duplication events occur in the pink labeled nodes 12, 15, 19 and 22 (patterns: 16-10-10-8-4-4-8-8; 16-6-5-6-4-4-8-8; 12-6-6-6-4-4-8-8; 12-4-6-5-4-4-8-8).
(B) The nodes indicating the presence of the major clone with the most prevalent pattern (2-1-3-2-1-2-2-2; consisting of 217 out of 250 analyzed nuclei) and the clone with the second most prevalent pattern (2-1-4-2-1-2-2-2; consisting of 29 out of 250 analyzed nuclei) are colored in blue. In the legend signal patterns for selected clones (1-4) are shown in detail.

4.6 Mutual exclusivity and co-occurrence analysis

The MeMo algorithm from Ciriello et al. was used for the mutual exclusivity and co-occurrence analysis of mutations (*PIK3CA, TP53*) and CNAs (*CCND1, CDH1, COX2, DBC2, HER2, MYC, TP53* and *ZNF217*)[196]. A significant mutual exclusivity of *PIK3CA* mutations and CNAs of *HER2,* as well as of *PIK3CA* mutations and CNAs of *CCND1,* was detected and visualized in **Figure 14**. Moreover, a significant co-occurrence of CNAs of *DBC2/MYC* ($p = 0.023$), *TP53/HER2* ($p = 0.042$) and *DBC2/HER2* ($p = 0.042$) could be determined. These results are presented in **Supplemental Figure S3**.

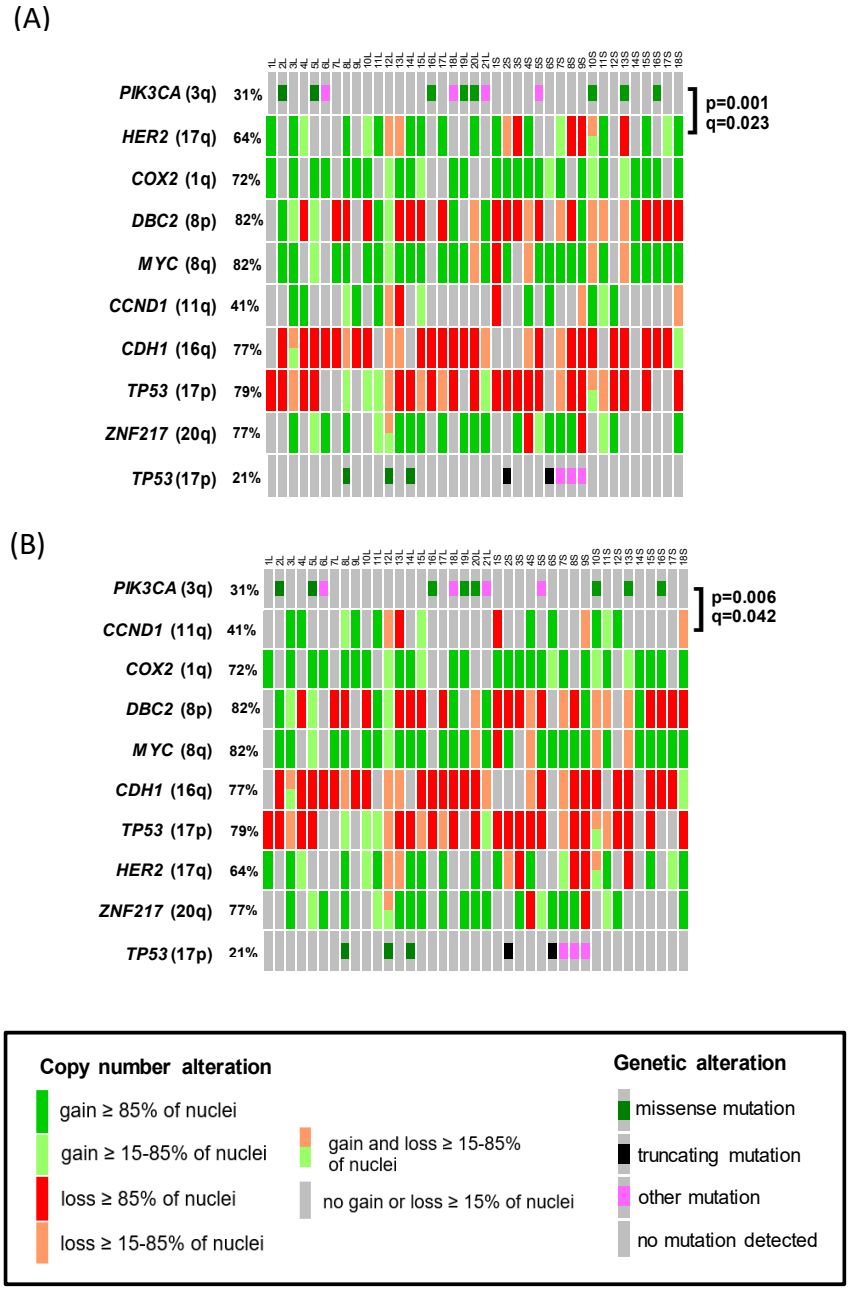

Figure 14: Mutual exclusivity analysis results of mutations in *PIK3CA* and *TP53* (OncoVar results) and CNA (miFISH data) implementing the MEMo algorithm as described in MATERIALS AND METHODS. Results are plotted vertically for each sample (columns) for the whole cohort (n=39). Note the marked, significant correlations (**A**: *PIK3C*A and *HER2*, **B**: *PIK3CA* and *CCND1*).

5 DISCUSSION

5.1 Overview and discussion of experimental miFISH results

Based on the miFISH results, the most frequent alterations of the 39 analyzed tumor samples were gains of the oncogenes *COX2*, *MYC*, and *HER2* and losses of the tumor suppressor genes *CDH1*, *TP53,* and *DBC2*. These most frequent alterations, as well as the distribution of gains and losses overall, are consistent with results documented in the TCGA database[117]. Furthermore, they are also consistent with prior findings of comparative genomic hybridization, precisely, the relative gains of chromosome arms or fractions of chromosomes 1q, 8q, 11q, 17q, and 20q, along with losses of chromosome arms 8p, 16q, and 17p[124–126].

5.1.1 Isochromosome formation, co-occurrence, and mutual exclusivity

In seven long and nine short survival patients (16/39), a loss of *DBC2* (8p) accompanied by a gain of *MYC* (8q) occurred as presented in **Figure 7**, leading to the hypothesis that an isochromosome 8q has been formed. Similarly, a hint of an isochromosome 17q is given with the concurrent loss of *TP53* (17p) and gain of *HER2* (17q) in seven short and seven long survival patients (14/39). An isochromosome is an unbalanced structural abnormality in which one of the arms is lost, and the remaining arm is duplicated. Thus, a loss of *DBC2* (8p) accompanied by a duplication of the oncogene *MYC* (8q) would be a typical constellation of an isochromosome 8q leading to the miFISH signal pattern in interphase nuclei of one copy of the *DBC2* probe and three copies of the *MYC* probe. When further analyzing the spatial arrangement of miFISH signals for chromosomes 8 and 17 in the cohort, the signal patterns strongly indicated the appearance of an isochromosome in around half of the samples. However, in the other half of the tumors, the signals were too complex to confirm or rule out the hypothesis of an isochromosome formation. Supporting the hypothesis of an isochromosome formation, in the mutual exclusivity and co-occurrence analysis of the eight analyzed genes (miFISH results) and the most often mutated genes, *PIK3CA* and *TP53* (NGS results), a significantly higher co-occurrence of *DBC2* and *MYC* ($q = 0.023$) as well as of *TP53* and *HER2* ($q = 0.042$) was discovered, as visualized in **Supplemental Figure S3**. In general, isochromosomes 8q and 17q are the most frequently isochromosomes detected in cancer[199]. According to cytogenic studies, isochromosome 8q and consistent 8p deletions are present in several human carcinomas, including breast cancer[198,200,201]. This suggests a substantial pathogenetic role in carcinogenesis.

5.1.2 Loss of an oncogene/ gain of a tumor suppressor gene

In some cases, the atypical loss of an oncogene and/ or the gain of a tumor suppressor gene were detected. To exemplify this statement, the loss of the prominent oncogene *HER2* was observed in 8/39 cases. A possible explanation for the loss of the oncogene *HER2*, which resides on 17q, could be the loss of the entire chromosome 17 driven by the benefit of losing a copy of the tumor suppressor gene *TP53*, located on 17p. Supporting this hypothesis, all eight cases with a *HER2* loss showed a concomitant loss of *TP53* as visualized in **Figure 7C** and, in more detail for the cases 8S, 9S and 13S, in **Figure 8** and **Figure 9**. Similarly, in 9/39 tumor samples, a gain of the prominent tumor suppressor gene *DBC2*, which resides on 8p, was observed. Remarkably, in all these nine tumor samples, a gain of the oncogene *MYC*, located on 8q, co-occurred (see **Figure 7C** and, in more detail regarding the cases 9S and 14S, in **Figure 8**). This leads to the hypothesis that the gain of the tumor suppressor gene *DBC2* occurs due to the gain of the whole chromosome 8 by profiting from an additional copy of the critical oncogene *MYC*.

5.1.3 Signal amplifications of miFISH probes

Comparing the average copy number, *HER2* showed the highest among the eight analyzed genes and was amplified in 18% (7/39) of the tumor samples. This aligns with research by Riou et al., describing that *HER2* gene amplifications were present in 18% of breast tumors[202]. In contrast to literature[202–206], *HER2* was predominantly amplified in long survival patients (five versus two), in which no one received targeted anti-*HER2* therapy. For instance, *HER2* amplification and the probability of mortality and multifocal distant metastases are significantly correlated, according to Riou et al.[202]. Moreover, in three long and three short survival cases (6/39), the oncogene *CCND1* was amplified, occurring exclusively in ER-positive breast carcinomas. This is in line with a study by Roy et al., in which ER positivity and *CCND1* amplification and protein expression were significantly correlated[207]. High *CCND1* amplification has been linked to a poor prognosis in ER-positive cancer in the literature[207,208]. However, this correlation could not be confirmed for the 39 tumor samples.

5.1.4 Inter- and intratumor heterogeneity based on miFISH results

Overall, the miFISH results displayed an enormous degree of inter- and intratumor heterogeneity within the cohort. On one side of the spectrum, in some tumor samples, the majority of the tumor cell population consists of only one single clone (see f.e. cases 7L and 8S in **Figure 9** and **Figure 10**). On the other side of the spectrum were cases in which less

than 10% of the tumor cell population revealed the same signal pattern (major clone), for example, case 10S with an instability index of 68.8 and high ITH (**Figure 8C**). Moreover, in some tumor samples, a copy number loss of only two tumor suppressor genes was sufficient for carcinogenesis, for example, in case 16L with an instability index of 5 and low ITH (**Supplemental Figure S4**). In contrast, other cases showed copy number changes in almost all analyzed genes (see f. e., case 9S in **Figure 8D**).

Remarkably, in some tumor samples, despite most of the eight analyzed genes showing CNAs, the number of clones within the tumor population, the instability index, and thus ITH were low, and/or the tumor was diploid. For example, in the signal pattern of case 8S, six of the analyzed eight genes presented CNAs. Nevertheless, a low ITH with a major clone comprising 95% of the tumor cell population, an instability index of 7.6, and diploidy were revealed (see **Figure 9**). This combination of a diploid tumor cell population with low ITH paired with a high number of copy number altered loci indicates tumor cells with a highly aberrant yet stable karyotype.

5.1.5 Statistical subgroup comparison of the miFISH and ploidy results

Surprisingly, the statistical analysis of the group comparison of long versus short survival patients did not reveal a significant difference regarding the number of CNAs, the ploidy (diploid versus aneuploid), or instability indices as visualized in **Figure 11A,C**. Thus, neither the number of CNAs, ploidy, nor the degree of ITH in breast cancer patients aged 50 years and above seem to predict the survival time after diagnosis -at least not for this cohort. To give two examples for this observation, cases 5L and 4S presented a high instability index, and cases 7L and 8S had a low instability index. However, 5L and 7L showed a long survival and 4S and 8S a short survival after diagnosis, as visualized in **Figure 9** and **Figure 10**. In contrast, previous studies mainly based on image cytometry discovered that both the degree of instability and aneuploidy were generally associated with a worse prognosis[67,179,181]. These previous studies chose patients not selected by age, whereas this analyzed cohort comprised exclusively patients within the age range of 50-85 years. Therefore, the increased incidence of comorbidities among breast cancer patients aged 50 years and above may contribute to these discrepancies. Contrary to the finding in this work that ploidy is not significantly correlated with the survival time, Cornelisse et al. evaluated breast carcinomas of exclusively postmenopausal patients in 1987 with the result of ploidy being an additional, independent prognostic factor[83].

Regarding the finding of no association between the number of CNAs and the survival time, it should be considered that miFISH was carried out for “only” eight breast cancer-associated

genes, hence only providing a snapshot of CNAs throughout the genome. Therefore, even though it is improbable, it cannot be ruled out that by including additional genes, CNAs might have been found that would have been able to distinguish the group of long versus short survival.

In addition to comparing the subgroups long versus short survival patients, the statistical analysis was carried out by separating the entire cohort into the groups a) diploid versus aneuploid cases and b) tumor samples with a low versus a high instability index. In the analysis of diploid versus aneuploid tumor samples, significantly higher levels of CNAs were revealed in the aneuploid samples, as visualized in **Figure 11D** ($p = 0.0012$). Chromosomal segregation errors in mitosis occur more frequently in aneuploid tumors as mitosis is more complex and are the most frequent cause for chromosomal instability[209], which in turn increases the amount of CNAs. Moreover, in line with literature[84,128,209,210], the instability index of aneuploid tumors was significantly higher than that of diploid tumors ($p < 0.0001$), as illustrated in **Figure 11B**. The link between aneuploidy and chromosomal instability is described by Potapova and Zhu et al. as a "vicious cycle," in which aneuploidy potentiates chromosomal instability and thus causes an increased karyotype diversity[210].

Within the cohort, notable characteristics in several cases were revealed, such as those presented in **Figure 8**. Remarkably, short survival case 13S displayed only one instead of two signals for five of the eight gene probes in the miFISH analysis. Thus, this case was dominated by exclusive losses of genes. Additional hybridizations revealed losses for 10 of the 22 chromosomes analyzed as visualized in **Supplemental Figure S1**, resulting in the statement of case 13S being hypodiploid. 1-2% of breast carcinomas have been reported to be hypodiploid, which is associated with a poor prognosis[211]. One year after being diagnosed, breast cancer patient 13S deceased. In case 13S, the *CCND1* probe presented two copies in the miFISH analysis for most cells. This contrasts with a study by Tanner et al. describing a significant correlation between a *CCND1*-gain and hypodiploidy in breast cancer[211]. Another notable case was case 10S (**Figure 8C**). Despite an extremely high level of chromosomal instability that produced several minor clones and a high instability score (68.8), a loss of *CDH1* and a gain of *CCND1* were evident in 99% of the tumor cells. This leads to the hypothesis of these two copy number changes being the driver of this malignancy. Otherwise, one would have anticipated that further advantageous gains and losses for tumorigenesis would have become significant major clones under selection pressure. Supporting this hypothesis, cancer genomes are reported as primarily dynamic and altering under selection pressure during carcinogenesis in the literature[87,209,212].

Consequently, for the tumorigenesis of breast cancer, deregulating essential pathways seems to be sufficient and does not necessarily need CNAs of multiple cancer genes.

5.1.6 Clonal evolution via phylogenetic analysis of CNAs

Additionally, based on the miFISH results, phylogenetic trees were created for each case to reconstruct carcinogenesis computationally and better understand the principles behind tumor evolution. The FISHtrees for the cohort revealed an enormous degree of ITH as well, as some were highly complex with several branches and nodes, whereas others consisted of a simple structure with only a low number of distinct mutational events and tree depth. As an example for a FISHtree with a simple structure, the FISHtree of the diploid long survival case 7L with an instability index of 2.0 resulting in an extremely low ITH is presented in **Figure 13B** (the corresponding color chart and imbalance plot for case 7L are displayed in **Figure 10G,H**). In contrast, the aneuploid case 5L with a high instability index of 46.4 serves as an example of a complex FISHtree with an increased number of distinct mutational events and tree depth and is displayed in **Figure 13A** (the corresponding color chart and imbalance plot for case 5L are shown in **Figure 10C,D**). Noteworthy, the change of the signal pattern from node 1 to node 2 in the FISHtree of case 5L is consistent with the duplication of the whole genome, a tetraploidization, being the initiating event of the development of this tumor. According to a study by Bielski et al. WGD frequently occurs in cancer and is associated with poor prognosis[213]. In addition to the initiating event in node 1, WGDs are likely to have also taken place in the four nodes 12, 15, 19, and 22 (shown in pink). Being positioned downstream of node 1 by the FISHtree algorithm, the WGDs of these four nodes probably happened later during tumor progression. The fact that the WGDs of these four nodes did not result in the proliferation of these clones suggests that WGD may not always provide a selective advantage. This is consistent with a study by Koçak et al. of younger breast cancer patients, in which WGD was detected but seemed to be not essential for tumorigenesis[128]. Additionally, this observation aligns with a publication by Lei et al. claiming that WGD is not necessarily required for carcinogenesis and frequently occurs more than once in cancer evolution[214].

5.2 Overview and discussion of sequencing results

Comparing the somatic mutation status of the 563 cancer-related gene panel (OncoVar) of the 39 breast cancer patients 50 years and above with the most frequently described mutations in the TCGA database[117], which contains a cohort of age-unbiased patients, a very similar picture emerged. Furthermore, no significant differences between the different

subgroups (long versus short survival patients, diploid versus aneuploid samples, tumors with a low versus high instability index) could be found when comparing the overall mutation burden per case or mutation frequencies for each of the eight evaluated genes. Going more into detail regarding the OncoVar results, *PIK3CA* was the most commonly mutated gene, in line with literature[117]. In 10 of 13 cases in the present cohort, the mutations in *PIK3CA* were observed in the three mutation hot spots of exon 9 and 20[215], for which oncogenic effects have been demonstrated[216,217]. Consistent with literature[117], the hot spot mutation E545K was only found in luminal A breast cancer (case 16L and 10S). Moreover, the mutations in *PIK3CA* were more prevalent in the long survival group and in ER-positive breast carcinomas, in line with literature[30,117]. In addition, in 21% (eight of 39) of the tumor samples, a mutation in *TP53* was detected, including mutation hot spots matching the 23% displayed in the Catalog of Somatic Mutation in Cancer (COSMIC) database[218]. A significant correlation between *TP53* mutations and intrinsic subtypes was revealed, with triple-negative tumors presenting the highest amount and luminal A/B tumors having the lowest amount of *TP53* mutations, aligned with literature[150,219,220].

5.3 Conclusion and outlook

ITH is a common phenomenon in breast cancer and a key challenge for treatment selection: tumors with a high degree of ITH consist of different cell clones, resulting in a higher likelihood of resistant ones, leading to treatment failure. Due to the significant relevance of this topic, this thesis aimed to gain further knowledge about ITH in breast cancer. A high degree of ITH within the analyzed cohort was revealed. On one side of the spectrum, cases in which most of the tumor cell population consists of only one single clone leading to a low ITH to cases on the other side of the spectrum presenting multiple different cell clones with less than 10% of the tumor cell population displaying the same signal pattern leading to a high ITH were detected. Thus, these results give an insight into the enormous extent of inter- and intratumor heterogeneity, causing huge challenges for the management of breast cancer. A new approach described in literature to improve breast cancer treatment is to gain more information about clonal evolution, resulting in the development of therapies that evolve over time, possibly leading to better survival outcomes[221]. Tumor evolution models such as phylogenetic trees visualize changes in tumor heterogeneity along the temporal axis. In this study, the clonal evolution of each of the 39 samples was reconstructed computationally, displaying the enormous degree of ITH ranging from cases with highly complex phylogenetic trees to cases with trees consisting of only a low number of nodes and branches, resulting in a simple structure.

Furthermore, an improved prognostication can lead to a more accurate and thus better treatment selection. Previous studies discovered that both the degree of genomic instability and aneuploidy were generally associated with a higher malignancy of the tumor and poorer prognosis[67,83,179,181], leading to the possibility of an improved disease prognostication. Next to ITH, genomic instability often occurs in cancer[118] and can lead to an accumulation of structural abnormalities of chromosomes or parts thereof, including CNAs[119]. Tumor progression can be promoted by CNAs[119,120,122] when occurring in oncogenes or tumor suppressor genes. Regarding the amount of CNAs among the cohort, significant differences were observed -with tumor samples ranging from losses in only two genes to cases with CNAs in almost all analyzed genes. Overall, at least two CNAs of the analyzed eight breast cancer-associated genes could be detected in each of the 39 tumors, indicating that CNAs in at least two genes were sufficient for carcinogenesis. To summarize, the most frequent alterations, as well as the distribution of gains and losses overall in patients with the age range from 50 to 85 years in this thesis, are consistent with results documented in the TCGA database[117] and with prior findings of comparative genomic hybridization[124–126], being analyzed for age-unbiased cohorts (and in a minority of analysis on breast cancer cell lines). However, due to the complex experimental design, “only” eight genes -although breast cancer-specific- were examined on a single cell level by miFISH. As a result, only a tiny section of possibly occurred CNAs were analyzed. Consequently, additional studies are necessary, including a higher number of genes being investigated on a single-cell level. Within these additional studies, the most recent findings regarding gene aberrations in breast cancer in the Cancer Genome Atlas Network (TCGA) should be considered, for example, the genes *PIK3CA* (chromosome 3)*, MAP3K1* (5)*, KMT2C* (7)*, CDKN2A* (9)*, PTEN* (10) and *RB1* (13).

In the statistical analysis of aneuploid versus diploid tumors, significantly higher CNAs and instability indices, reflecting the degree of genomic instability, were revealed in the aneuploid tumors. These correlations were previously described in a study by Koçak et al. for a collective of premenopausal breast cancer patients[128] as well as in a publication of Oltmann et al. for an age-unbiased cohort consisting of pre- and postmenopausal patients[84]. These previously described correlations could also be confirmed through this thesis for a cohort comprised of patients exclusively within the age range of 50 to 85 years.

Moreover, this work assessed the mutation status of 563 breast cancer-associated genes for each of the 39 tumor samples. This mutation status revealed a comparable distribution of gene mutations detected in tumors of patients 50 years and above and of the age-unbiased TCGA cohort (2012)[117].

Notably, among the breast cancer patients of this cohort, neither the number of CNAs nor the tumor ploidy nor the degree of ITH revealed an association with prognosis (distribution to the groups with short or long survival). Thus, these criteria do not appear to be relevant for the time of survival and therefore for disease prognosis among breast cancer patients aged 50 years and above, possibly because age at diagnosis and comorbidities play a major role on each patient's prognosis. However, these results contrast with a study by Koçak et al. focusing on exclusively younger breast cancer patients (premenopausal), which revealed a significant association between the degree of ITH and poorer prognosis as well as between the number of CNAs and poorer prognosis[128]. These contrasting results regarding younger breast cancer patients in the study by Koçak et al.[128] and patients aged 50 to 85 years in this work are supported by a publication of Lischka et al.[180]. Lischka et al. statistically analyzed premenopausal versus postmenopausal patients with different genome instability profiles. The result was that the genome instability profiles predicted disease outcomes independent of clinicopathological parameters playing a major role in disease prognostication in premenopausal patients. In contrast, in postmenopausal patients, genomic instability did not have a significant impact on each patient´s prognosis[180].

As a conclusion, the importance of increasing the focus on older patients being underrepresented in cancer research could be underlined through this work as some conditions, for example, the association between the degree of ITH and prognosis or between the number of CNAs and prognosis applying to breast cancer in younger patients might be insignificant for older patients.

Due to the project's relatively small cohort (n = 39), more research is required to confirm the findings on larger cohorts and further analyze the role of tumor heterogeneity, chromosomal aneuploidy, and genomic instability in breast cancer. As the status of menopause was not recorded in the present cohort, future studies should be carried out ideally on a data set including these data, thus being able to analyze pre- versus postmenopausal patients statistically. Overall, in cancer research future studies focusing on an older patient cohort are needed. These will play a vital part in ascertaining whether data from research studies on younger patients are applicable to both age groups.

6 SUMMARY

Despite the majority (70%) of female breast cancer cases being diagnosed in women aged 55 years and older and an increasing population of older breast cancer patients due to demographic change, older patients lack adequate representation in cancer research. Thus, this doctoral thesis focused on breast cancer patients aged 50 years and older, aiming to elucidate the role of intratumor heterogeneity, ploidy, and genomic instability and their influences on disease outcome. Therefore, a breast cancer collective of 39 patients with short (median 2.4 years) and long survival (median 19 years) were selected. Multiplex interphase fluorescence *in situ* hybridization (miFISH) was carried out to analyze copy number alterations (CNAs) of eight breast cancer-associated genes for their potential as biomarkers, as well as assessing genomic instability and tumor heterogeneity. Furthermore, image cytometry was performed to detect ploidy and phylogenetic tree modeling to gain more information about tumor development. Supplementary, targeted next-generation sequencing of 563 breast cancer-associated genes was carried out externally, and the obtained mutation status was statistically analyzed, compared to the miFISH results, and interpreted as part of this thesis.

The experimental part of this work revealed several CNAs of breast cancer-specific genes, as well as gene mutations frequently reported in breast carcinomas. The copy number gain of *COX2* occurred most frequently (in 72% of the cases), followed by *MYC* (69%), whereas losses were more common for *CDH1* (74%) and *TP53* (69%). Comparing aneuploid with diploid tumor samples, significantly higher average signal numbers, CNAs, and instability indices, reflecting the degree of genomic instability, were revealed in the aneuploid tumors. In 16 cases, the signal pattern indicated the formation of an isochromosome 8q and in 14 cases of an isochromosome 17q. Supporting the hypothesis of an isochromosome formation, CNAs of *DBC2/MYC* and *HER2/TP53* significantly co-occurred. Moreover, significant co-occurrence of CNA of *HER2/DBC2* was detected, and CNAs for *HER2* and *PIK3CA* mutations and CNAs for *CCND1* and *PIK3CA* mutations were significantly mutually exclusive. Overall, the distribution of gene mutations of the 563-breast cancer-associated genes, as well as the pattern of CNAs in the eight breast cancer-related genes (miFISH) detected in the 39 patients aged 50 years and older, were comparable to results of the age-unbiased TCGA-cohort. Notably, neither the quantity of CNAs, the tumor ploidy, nor the degree of intratumor heterogeneity revealed an association with the survival time, indicating that for patients above the age of 50, these criteria do not seem to have a substantial effect on disease prognosis.

7 ZUSAMMENFASSUNG

Brustkrebs ist die häufigste invasive Krebserkrankung bei Frauen mit einem durchschnittlichen Alter zum Todeszeitpunkt von 74 Jahren. Hierbei beeinflussen mehrere Faktoren das Risiko für Brustkrebs, wobei Alter eine große Rolle spielt: Die Inzidenz von Brustkrebs steigt mit dem Alter deutlich an. Dennoch sind ältere Frauen in der Krebsforschung unterrepräsentiert. Die Diagnose und Prognose basiert derzeit auf klinischen und histologischen Parametern sowie molekularen Merkmalen und ist für eine optimierte Behandlungsentscheidung von Brustkrebspatientinnen unerlässlich. Eine Herausforderung für die Stellung einer möglichst präzisen Diagnose und Prognose sowie für die Wahl einer erfolgreichen Therapie ist die Heterogenität innerhalb eines Tumors (intratumorale Heterogenität) sowie zwischen Brustkrebs verschiedener Individuen (intertumorale Heterogenität). Tumorheterogenität kommt häufig in Brustkrebs vor und führt zu einer großen Variabilität der klinischen und histologischen Parameter, der Tumoraggressivität und damit des Ansprechens auf eine Behandlung. Neben den allgemeinen klinischen Prognosefaktoren wie beispielsweise der TNM-Klassifikation sind spezifische Biomarker und Genexpressionssignaturen für eine möglichst genaue Charakterisierung etabliert worden, wie beispielsweise MammaPrint. Es hat sich gezeigt, dass die quantitative Bestimmung des nukleären DNA-Gehalts in Brustkrebszellen zu einer präziseren Prognose-Stellung führt, da ein Zusammenhang zwischen dem Grad der Aneuploidie und dem Krankheitsverlauf besteht. Zusammengefasst zeigen sich diploide Tumoren im Vergleich zu aneuploiden weniger aggressiv. Auch ist der Grad der genomischen Instabilität mit der Prognose assoziiert, wobei Patientinnen mit genomisch stabilen Tumoren eine signifikant bessere Prognose haben. Hierbei spiegelt sich der Grad der genomischen Instabilität in der Variabilität des DNA-Gehalts innerhalb der Tumorzellpopulation wider: weisen beispielsweise alle Zellen den gleichen DNA-Gehalt auf, so liegt ein genomisch stabiler Tumor vor. Genomische Instabilität kann zu einer Häufung struktureller Anomalien von Chromosomen einschließlich sogenannter Kopienzahlvariationen von Genen führen, welches die Tumorentstehung sowie das Tumorwachstum fördern kann.

Das Ziel dieser Doktorarbeit war es, die Rolle der inter- und intratumoralen Heterogenität, chromosomalen Aneuploidie, genomischen Instabilität sowie Kopienzahlvariationen von Genen bei Brustkrebs weiter zu erforschen. Ein verbessertes Verständnis dieser Tumor-Eigenschaften kann helfen, die Diagnose, Prognose und somit die Wahl der Behandlung zu verbessern. Darüber hinaus legt diese Doktorarbeit den Fokus auf ältere Brustkrebs-Patientinnen, da sie in der Krebsforschung unterrepräsentiert sind.

Die vorliegende Studie wurde an zwischen 1989 und 1992 am Universitätsklinikum Schleswig-Holstein in Lübeck gewonnenen Mammakarzinom-Proben durchgeführt und von der Ethikkommission der Universität zu Lübeck genehmigt (Aktenzeichen 08-012 und 20-507). Hierbei wurden 39 von 245 Brustkrebspatientinnen mit einem Durchschnittsalter von 67 Jahren und einem Follow-up von 22 Jahren ausgewählt, um eine umfassende genetische Analyse an Formalin-fixierten, Paraffin-eingebetteten Mamma-Biopsieproben durchzuführen. Diese 39 Patienten wurden in zwei Gruppen mit deutlich unterschiedlichem Überleben nach Diagnosestellung eingeteilt: Langüberlebende (n=21, Median 19 Jahre) versus Kurzüberlebende (n=18, Median 2,4 Jahren). In dieser Arbeit wurden mittels Multiplex-Interphase-Fluoreszenz-in-situ-Hybridisierung (miFISH) Kopienzahlvariationen von acht Brustkrebs-assoziierten Genen in mindestens 250 Einzelzellen für jede der 39 Tumorproben analysiert und die intratumorale Heterogenität detailliert abgebildet. Der Grad an genomischer Stabilität und intratumoralen Heterogenität innerhalb einer Tumorprobe wurde durch den Instabilitätsindex als Diversitätsmaß dargestellt, der Werte von 0 bis 100 annehmen kann. Je höher der Instabilitätsindex, desto ausgeprägter die intratumorale Heterogenität. Auf Grundlage der miFISH-Ergebnisse wurde zudem für jeden der 39 Tumore ein phylogenetischer Stammbaum erstellt, um die mögliche Evolution der verschiedenen Zellklone grafisch darzustellen. Darüber hinaus erfolgte eine Ploidiebestimmung der 39 Proben durch Bildzytometrie und miFISH mit anschließender Eingruppierung in diploide und aneuploide Tumoren. Bei der Bildzytometrie wurde eine quantitative Messung des DNA-Gehaltes an mindestens 1200 Kernen pro Tumorprobe an Feulgen-gefärbten Cytospins durchgeführt. Weiterhin erfolgte die Sequenzierung eines 563-Gen-Panel mittels Next-Generation Sequencing (NGS) an diesen 39 Tumorproben vom Frederick National Laboratory for Cancer Research in den USA. In dieser Arbeit wurden diese Sequenzier-Daten zusammengestellt, statistisch analysiert, mit den miFISH-Ergebnissen verglichen und interpretiert. Abschließend wurden Koexistenz- und Exklusivitätsanalysen von Mutationen in *PIK3CA* und *TP53* and Kopienzahlvariationen der Gene *CCND1, CDH1, COX2, DBC2, HER2, MYC, TP53, ZNF217* nach Algorithmen von Ciriello et al.[195,196] durchgeführt.

Die miFISH-Ergebnisse zeigten eine große Variabilität der intratumoralen Heterogenität innerhalb des Kollektivs. Insgesamt zeigten sich Kopienzahlvariationen für mindestens zwei der acht Brustkrebs-assoziierten Gene in jeder Tumorprobe. Die häufigsten Kopienzahlveränderungen waren Zugewinne in den Onkogenen *COX2* in 72% (28/39) und *MYC* in 69% (27/39) und Verluste in den Tumorsuppressorgenen *CDH1* in 74% (29/39) und *TP53* in 69% (27/39). In 16 von 39 Fällen trat ein Kopienzahlzugewinn von *MYC* (Chromosom 8q) zusammen mit einem *DBC2*-Kopienzahlverlust (8p) und in 14 Fällen ein

HER2-Zugewinn (17q) zusammen mit einem *TP53*-Verlust (17p) auf. In dem Kollektiv zeigten sich mehrere Fälle mit erwähnenswerten Besonderheiten, so beispielsweise der Fall 13S, bei dem Kopienzahlverluste auf 10 von 22 untersuchten Chromosomen auftraten. Die ausgeprägte Variabilität der intratumoralen Heterogenität innerhalb des Kollektivs spiegelt sich in den Werten der 39 berechneten Instabilitätsindices wider, die sich zwischen 2 und 86,6 befanden.

Die statistische Auswertung ergab, dass sich weder die Instabilitätsindices als Maß der genomischen Instabilität noch die Anzahl an Kopienzahlveränderungen der acht analysierten Gene noch die Anzahl an Genmutationen der 563 sequenzierten Gene zwischen den Gruppen der Langüberlebenden versus der Kurzüberlebenden signifikant voneinander unterschieden. Hingegen zeigte sich in dem statistischen Gruppenvergleich der aneuploiden versus diploide Tumore ein signifikant höherer Durchschnitt der gezählten Probensignale, der Kopienzahlvariationen sowie der Instabilitätsindices in der Gruppe der aneuploiden Tumoren. Dieses spiegelte sich auch in den für die 39 Tumoren erstellten phylogenetischen Stammbäume wider, wobei die Bäume der aneuploiden Tumoren im Vergleich zu den diploiden eine signifikant größere Baumtiefe (durchschnittliche Entfernung eines Knotenpunktes von der Baumwurzel) aufwiesen und deutlich komplexer waren.

Bei der Sequenzierung des 563-Gen-Panels zeigten sich am häufigsten Mutationen in den Genen *PIK3CA* (12/39, 31%), *TP53* (8/39, 21%), *MAP3K1* (7/39, 18%), *KMT2C* (6/39, 15%), *CDH1* (4/39, 10%), *ITGB2* (3/39, 8%), *SPEN* (3/39), und *SF3B1* (3/39). Mutationen in *PIKC3A* wurden fast ausschließlich in Luminal A Tumoren detektiert. Die Koexistenz- und Exklusivitätsanalysen ergaben eine signifikante Häufung des gemeinsamen Auftretens von Kopienzahlveränderungen von *DBC2/MYC* ($p = 0{,}023$), *TP53/HER2* ($p = 0{,}042$) und *DBC2/HER2* ($p = 0{,}042$) sowie eine signifikante Häufung einer gegenseitigen Exklusivität von *PIK3CA*-Mutationen und Kopienzahlvariationen von *HER2* sowie von *PIK3CA*-Mutationen und Kopienzahlvariationen von *CCND1*.

Zusammenfassend stimmten die in den 39 Tumorproben häufig gefundenen Kopienzahlveränderungen (Zugewinne in *COX2* (1q), *MYC* (8q) und *HER2* (17q) sowie Verluste in *CDH1* (16q), *TP53* (17p) und *DBC2* (8p)) und die Gesamtverteilung der Kopienzahlveränderungen mit den Ergebnissen aus der TCGA Brustkrebskohorte (2012)[117] sowie mit vorangegangenen Studien überein, in denen insbesondere die relativen Gewinne der Chromosomenarme oder Teile der Chromosomen 1q, 8q, 11q, 17q zusammen mit Verlusten der Chromosomenarme 8p, 16q und 17p gezeigt wurden[124–126]. Das Ko-Auftreten eines Verlustes von *DBC2* (8p) und Gewinns von *MYC* (8q) in 16 Fällen sowie eines Verlustes von *TP53* (17p) und Gewinns von *HER2* (17q) in 14 Fällen lässt die Bildung eines

Isochromosoms 8q beziehungsweise 17q vermuten. Zusätzlich zu dieser Beobachtung bestätigten die Koexistenz- und Exklusivitätsanalysen ein signifikant gehäuftes Ko-Auftreten von Kopienzahlveränderungen von *DBC2*/*MYC* sowie von *TP53*/*HER2*. In zytogenetischen Studien wurde gezeigt, dass die Isochromosomen 8q und 17q die am häufigsten vorkommenden Isochromosomen in Krebs einschließlich Brustkrebs sind[198–201]. Dies lässt auf eine substanzielle pathogenetische Rolle in der Karzinogenese schließen. Weiterhin konnten durch die miFISH-Einzelzellanalyse verschiedene Besonderheiten einzelner Tumorproben beobachtet werden. Beispielsweise wies der Fall 13S aus der Gruppe der Kurzüberlebenden Kopienzahlverluste in 10 von 22 untersuchten Chromosomen auf, die zu der Annahme eines stark hypodiploiden Tumors führten. Hypodiploidie wird in 1-2% aller Brustkrebsproben entdeckt und ist mit einer schlechten Prognose assoziiert[211].

Die Auswertung der Sequenzierdaten der 563-Krebs-assoziierten Gene ergab, dass das Mutationsspektrum der vorliegenden Kohorte mit Patientinnen im Alter von 50-85 Jahren dem aus der TCGA-Datenbank (2012)[117] und damit dem einer Kohorte ohne Alterseinschränkungen glich. Hierbei zeigten sich keine signifikanten Unterschiede zwischen den prognostischen Gruppen (Kurzüberlebende versus Langüberlebende). Darüber hinaus ergab die statistische Analyse der Kurzüberlebenden versus Langüberlebenden, dass weder die Anzahl der Kopienzahlveränderungen noch die Ploidie als Einteilung in diploid oder aneuploid noch der Grad an intratumoraler Heterogenität signifikant unterschiedlich war. Daraus lässt sich schlussfolgern, dass diese Parameter bei Patientinnen über 50 Jahren (Altersspanne der vorliegenden Kohorte: 50-85 Jahre) keinen wesentlichen Einfluss auf die Überlebensdauer nach Diagnosestellung haben. Möglicherweise spielen bei Patientinnen über 50 Jahren Komorbiditäten und das Alter bei Diagnosestellung eine übergeordnete Rolle bei der individuellen Prognosestellung.

Insgesamt konnte durch die vorliegende Arbeit ein umfassendes Bild der 39 Tumorproben mit einem hohen Grad an genomischer Instabilität und intratumoraler Heterogenität dargestellt werden. Im Gruppenvergleich von diploiden versus aneuploiden Tumorproben zeigten sich in der statistischen Analyse signifikante Unterschiede: so traten signifikant häufiger Kopienzahlveränderungen und ein höherer Grad an intratumoraler Heterogenität (gemessen durch den Instabilitätsindex) in der Gruppe der aneuploiden Tumoren auf, welches Ergebnisse vorheriger Studien bestätigt[84,128,209,210].

8 REFERENCE LIST

(1) Azamjah, N.; Soltan-Zadeh, Y.; Zayeri, F. Global Trend of Breast Cancer Mortality Rate: A 25-Year Study. *Asian Pac. J. Cancer Prev. APJCP* **2019**, *20* (7), 2015–2020.

(2) Zentrum für Krebsregisterdaten, Robert Koch Institut. *Krebs in Deutschland| 2015/2016| Brustdrüse C50, korrigierte Fassung vom 17.8.20202*. www.krebsdaten.de.

(3) Sung, H.; Ferlay, J.; Siegel, R. L.; Laversanne, M.; Soerjomataram, I.; Jemal, A.; Bray, F. Global Cancer Statistics 2020: GLOBOCAN Estimates of Incidence and Mortality Worldwide for 36 Cancers in 185 Countries. *CA. Cancer J. Clin.* **2021**, *71* (3), 209–249.

(4) Youlden, D. R.; Cramb, S. M.; Dunn, N. A. M.; Muller, J. M.; Pyke, C. M.; Baade, P. D. The Descriptive Epidemiology of Female Breast Cancer: An International Comparison of Screening, Incidence, Survival and Mortality. *Cancer Epidemiol.* **2012**, *36* (3), 237–248.

(5) White, J.; Kearins, O.; Dodwell, D.; Horgan, K.; Hanby, A. M.; Speirs, V. Male Breast Carcinoma: Increased Awareness Needed. *Breast Cancer Res. BCR* **2011**, *13* (5), 219.

(6) Ärzteblatt, D. Ä. G., Redaktion Deutsches. *Brustkrebs beim Mann*. Deutsches Ärzteblatt. https://www.aerzteblatt.de/archiv/31359/Brustkrebs-beim-Mann.

(7) Giordano, S. H.; Buzdar, A. U.; Hortobagyi, G. N. Breast Cancer in Men. *Ann. Intern. Med.* **2002**, *137* (8), 678–687.

(8) Majeed, W.; Aslam, B.; Javed, I.; Khaliq, T.; Muhammad, F.; Ali, A.; Raza, A. Breast Cancer: Major Risk Factors and Recent Developments in Treatment. *Asian Pac. J. Cancer Prev. APJCP* **2014**, *15* (8), 3353–3358.

(9) Sun, Y.-S.; Zhao, Z.; Yang, Z.-N.; Xu, F.; Lu, H.-J.; Zhu, Z.-Y.; Shi, W.; Jiang, J.; Yao, P.-P.; Zhu, H.-P. Risk Factors and Preventions of Breast Cancer. *Int. J. Biol. Sci.* **2017**, *13* (11), 1387–1397.

(10) Miki, Y.; Swensen, J.; Shattuck-Eidens, D.; Futreal, P. A.; Harshman, K.; Tavtigian, S.; Liu, Q.; Cochran, C.; Bennett, L. M.; Ding, W. A Strong Candidate for the Breast and Ovarian Cancer Susceptibility Gene BRCA1. *Science* **1994**, *266* (5182), 66–71.

(11) Wooster, R.; Bignell, G.; Lancaster, J.; Swift, S.; Seal, S.; Mangion, J.; Collins, N.; Gregory, S.; Gumbs, C.; Micklem, G. Identification of the Breast Cancer Susceptibility Gene BRCA2. *Nature* **1995**, *378* (6559), 789–792.

(12) Barnes, B.; Kraywinkel, K.; Nowossadeck, E.; Schönfeld, I.; Starker, A.; Wienecke, A.; Wolf, U. Bericht Zum Krebsgeschehen in Deutschland 2016, 2016.

(13) Wang, L. Early Diagnosis of Breast Cancer. *Sensors* **2017**, *17* (7). https://doi.org/10.3390/s17071572.

(14) Heinze, F.; Czwikla, J.; Heinig, M.; Langner, I.; Haug, U. German Mammography Screening Program: Program Sensitivity between 2010 and 2016 Estimated Based on German Health Claims Data. *BMC Cancer* **2023**, *23* (1), 852.

(15) Information, N. C. for B.; Pike, U. S. N. L. of M. 8600 R.; MD, B.; Usa, 20894. *The Breast Cancer Screening Program in Germany*; Institute for Quality and Efficiency in Health Care (IQWiG), 2018.

(16) Katalinic, A.; Eisemann, N.; Kraywinkel, K.; Noftz, M. R.; Hübner, J. Breast Cancer Incidence and Mortality before and after Implementation of the German Mammography Screening Program. *Int. J. Cancer* **2020**, *147* (3), 709–718.

(17) Statistisches Bundesamt. *Bevölkerung Deutschlands bis 2060, Ergebnisse der 14. koordinierten Bevölkerungsvorausberechnung*. bpb.de. https://www.bpb.de/nachschlagen/zahlen-und-fakten/soziale-situation-in-deutschland/61541/altersstruktur (accessed 10/13/2023).

(18) U.S. Department of Health and Human Services. *2017OlderAmericansProfile.pdf*. Administration for Community Living. https://acl.gov/sites/default/files/Aging%20and%20Disability%20in%20America/2017OlderAmericansProfile.pdf (accessed 10/13/2023).

(19) Smith, B. D.; Smith, G. L.; Hurria, A.; Hortobagyi, G. N.; Buchholz, T. A. Future of Cancer Incidence in the United States: Burdens Upon an Aging, Changing Nation. *J. Clin. Oncol.* **2009**, *27* (17), 2758–2765.

(20) Committee on Improving the Quality of Cancer Care: Addressing the Challenges of an Aging Population; Board on Health Care Services; Institute of Medicine. *Delivering High-Quality Cancer Care: Charting a New Course for a System in Crisis*; Levit, L., Balogh, E., Nass, S., Ganz, P. A., Eds.; National Academies Press: Washington, D.C., 2013; p 18359.

(21) Hurria, A.; Levit, L. A.; Dale, W.; Mohile, S. G.; Muss, H. B.; Fehrenbacher, L.; Magnuson, A.; Lichtman, S. M.; Bruinooge, S. S.; Soto-Perez-de-Celis, E.; Tew, W. P.; Postow, M. A.; Cohen, H. J. Improving the Evidence Base for Treating Older Adults With Cancer: American Society of Clinical Oncology Statement. *J. Clin. Oncol.* **2015**, *33* (32), 3826–3833.

(22) *AJCC Cancer Staging Handbook: From the AJCC Cancer Staging Manual*, 7th ed.; Edge, S., Byrd, D. R., Compton, C. C., Fritz, A. G., Greene, F., Trotti, A., Eds.; Springer-Verlag: New York, 2010.

(23) Brierley, J.; Gospodarowicz, M.; O'Sullivan, B. The Principles of Cancer Staging. *ecancermedicalscience* **2016**, *10*. https://doi.org/10.3332/ecancer.2016.ed61.

(24) Bertero, L.; Massa, F.; Metovic, J.; Zanetti, R.; Castellano, I.; Ricardi, U.; Papotti, M.; Cassoni, P. Eighth Edition of the UICC Classification of Malignant Tumours: An Overview of the Changes in the Pathological TNM Classification Criteria-What Has Changed and Why? *Virchows Arch. Int. J. Pathol.* **2018**, *472* (4), 519–531.

(25) Makki, J. Diversity of Breast Carcinoma: Histological Subtypes and Clinical Relevance. *Clin. Med. Insights Pathol.* **2015**, *8*, 23–31.

(26) Elston, C. W.; Ellis, I. O. Pathological Prognostic Factors in Breast Cancer. I. The Value of Histological Grade in Breast Cancer: Experience from a Large Study with Long-Term Follow-Up. *Histopathology* **1991**, *19* (5), 403–410.

(27) Bloom, H. J.; Richardson, W. W. Histological Grading and Prognosis in Breast Cancer; a Study of 1409 Cases of Which 359 Have Been Followed for 15 Years. *Br. J. Cancer* **1957**, *11* (3), 359–377.

(28) Lakhani, S.; Ellis, I.; Schnitt, S.; Tan, P.; van de Vijver, M. *WHO Classification of Tumours of the Breast 4th Edition*;

(29) Merkle, E.; Seidl, I.; Bähr, I.; Tulusan, A.; Maillot, K.; Sauerbrei, K.; Wirtz, P. Langzeituntersuchung Zur Bedeutung von Hormonrezeptoren Als Prognosefaktoren Beim Mammakarzinom. *Geburtshilfe Frauenheilkd.* **1990**, *50*, 528–532.

(30) Yang, S. X.; Polley, E.; Lipkowitz, S. New Insights on PI3K/AKT Pathway Alterations and Clinical Outcomes in Breast Cancer. *Cancer Treat. Rev.* **2016**, *45*, 87–96.

(31) *Tumorbiologie bei Brustkrebs | DKG*. https://www.krebsgesellschaft.de/onko-internetportal/basis-informationen-krebs/krebsarten/brustkrebs/tumorbiologie.html (accessed 10/13/2023).

(32) Olayioye, M. A. Update on HER-2 as a Target for Cancer Therapy: Intracellular Signaling Pathways of ErbB2/HER-2 and Family Members. *Breast Cancer Res.* **2001**, *3* (6), 385–389.

(33) Pichon, M.-F.; Hacene, K.; Guepratte, S.; Neumann, R. Serum HER-2 Extracellular Domain (ECD) before the First Metastasis in 128 Breast Cancer Patients. *Clin. Lab.* **2004**, *50* (3–4), 163–170.

(34) Ménard, S.; Fortis, S.; Castiglioni, F.; Agresti, R.; Balsari, A. HER2 as a Prognostic Factor in Breast Cancer. *Oncology* **2001**, *61 Suppl 2*, 67–72.

(35) Wolff, A. C.; Hammond, M. E. H.; Hicks, D. G.; Dowsett, M.; McShane, L. M.; Allison, K. H.; Allred, D. C.; Bartlett, J. M. S.; Bilous, M.; Fitzgibbons, P.; Hanna, W.; Jenkins, R. B.; Mangu, P. B.; Paik, S.; Perez, E. A.; Press, M. F.; Spears, P. A.; Vance, G. H.; Viale, G.; Hayes, D. F.; American Society of Clinical Oncology; College of American Pathologists. Recommendations for Human Epidermal Growth Factor Receptor 2 Testing in Breast Cancer: American Society of Clinical Oncology/College of American Pathologists Clinical Practice Guideline Update. *J. Clin. Oncol. Off. J. Am. Soc. Clin. Oncol.* **2013**, *31* (31), 3997–4013.

(36) Slamon, D.; Eiermann, W.; Robert, N.; Pienkowski, T.; Martin, M.; Press, M.; Mackey, J.; Glaspy, J.; Chan, A.; Pawlicki, M.; Pinter, T.; Valero, V.; Liu, M.-C.; Sauter, G.; von Minckwitz, G.; Visco, F.; Bee, V.; Buyse, M.; Bendahmane, B.; Tabah-Fisch, I.; Lindsay, M.-A.; Riva, A.; Crown, J. Adjuvant Trastuzumab in HER2-Positive Breast Cancer. *N. Engl. J. Med.* **2011**, *365* (14), 1273–1283.

(37) Ménard, S.; Pupa, S. M.; Campiglio, M.; Tagliabue, E. Biologic and Therapeutic Role of HER2 in Cancer. *Oncogene* **2003**, *22* (42), 6570–6578.

(38) *Prognostische und prädiktive Faktoren invasiver Mammakarzinome*. springermedizin.de. https://www.springermedizin.de/prognostische-und-praediktive-faktoren-invasiver-mammakarzinome/8299678 (accessed 10/13/2023).

(39) Scholzen, T.; Gerdes, J. The Ki-67 Protein: From the Known and the Unknown. *J. Cell. Physiol.* **2000**, *182* (3), 311–322.

(40) Soliman, N. A.; Yussif, S. M. Ki-67 as a Prognostic Marker According to Breast Cancer Molecular Subtype. *Cancer Biol. Med.* **2016**, *13* (4), 496–504.

(41) Schnitt, S. J. Classification and Prognosis of Invasive Breast Cancer: From Morphology to Molecular Taxonomy. *Mod. Pathol. Off. J. U. S. Can. Acad. Pathol. Inc* **2010**, *23 Suppl 2*, S60-64.

(42) Sørlie, T.; Tibshirani, R.; Parker, J.; Hastie, T.; Marron, J. S.; Nobel, A.; Deng, S.; Johnsen, H.; Pesich, R.; Geisler, S.; Demeter, J.; Perou, C. M.; Lønning, P. E.; Brown, P. O.; Børresen-Dale, A.-L.; Botstein, D. Repeated Observation of Breast Tumor Subtypes in Independent Gene Expression Data Sets. *Proc. Natl. Acad. Sci. U. S. A.* **2003**, *100* (14), 8418–8423.

(43) Cheang, M. C. U.; Chia, S. K.; Voduc, D.; Gao, D.; Leung, S.; Snider, J.; Watson, M.; Davies, S.; Bernard, P. S.; Parker, J. S.; Perou, C. M.; Ellis, M. J.; Nielsen, T. O. Ki67 Index, HER2 Status, and Prognosis of Patients With Luminal B Breast Cancer. *JNCI J. Natl. Cancer Inst.* **2009**, *101* (10), 736–750.

(44) Tong, L.; Yu, X.; Wang, S.; Chen, L.; Wu, Y. Research Progress on Molecular Subtyping and Modern Treatment of Triple-Negative Breast Cancer. *Breast Cancer Dove Med. Press* **2023**, *15*, 647–658.

(45) Rouzier, R.; Perou, C. M.; Symmans, W. F.; Ibrahim, N.; Cristofanilli, M.; Anderson, K.; Hess, K. R.; Stec, J.; Ayers, M.; Wagner, P.; Morandi, P.; Fan, C.; Rabiul, I.; Ross, J. S.; Hortobagyi, G. N.; Pusztai, L. Breast Cancer Molecular Subtypes Respond Differently to Preoperative Chemotherapy. *Clin. Cancer Res. Off. J. Am. Assoc. Cancer Res.* **2005**, *11* (16), 5678–5685.

(46) Onitilo, A. A.; Engel, J. M.; Greenlee, R. T.; Mukesh, B. N. Breast Cancer Subtypes Based on ER/PR and Her2 Expression: Comparison of Clinicopathologic Features and Survival. *Clin. Med. Res.* **2009**, *7* (1–2), 4–13.

(47) Carey, L. A.; Perou, C. M.; Livasy, C. A.; Dressler, L. G.; Cowan, D.; Conway, K.; Karaca, G.; Troester, M. A.; Tse, C. K.; Edmiston, S.; Deming, S. L.; Geradts, J.; Cheang, M. C. U.; Nielsen, T. O.; Moorman, P. G.; Earp, H. S.; Millikan, R. C. Race, Breast Cancer Subtypes, and Survival in the Carolina Breast Cancer Study. *JAMA* **2006**, *295* (21), 2492–2502.

(48) McDonald, E. S.; Clark, A. S.; Tchou, J.; Zhang, P.; Freedman, G. M. Clinical Diagnosis and Management of Breast Cancer. *J. Nucl. Med. Off. Publ. Soc. Nucl. Med.* **2016**, *57 Suppl 1*, 9S-16S.

(49) Cardoso, F.; Kyriakides, S.; Ohno, S.; Penault-Llorca, F.; Poortmans, P.; Rubio, I. T.; Zackrisson, S.; Senkus, E.; ESMO Guidelines Committee. Electronic address: clinicalguidelines@esmo.org. Early Breast Cancer: ESMO Clinical Practice Guidelines for Diagnosis, Treatment and Follow-Up†. *Ann. Oncol. Off. J. Eur. Soc. Med. Oncol.* **2019**, *30* (8), 1194–1220.

(50) Cardoso, F.; Cataliotti, L.; Costa, A.; Knox, S.; Marotti, L.; Rutgers, E.; Beishon, M. European Breast Cancer Conference Manifesto on Breast Centres/Units. *Eur. J. Cancer Oxf. Engl. 1990* **2017**, *72*, 244–250.

(51) Bhattacharyya, G. S.; Doval, D. C.; Desai, C. J.; Chaturvedi, H.; Sharma, S.; Somashekhar, S. p. Overview of Breast Cancer and Implications of Overtreatment of

Early-Stage Breast Cancer: An Indian Perspective. *JCO Glob. Oncol.* **2020**, No. 6, 789–798.

(52) Rapoport, B. L. Delayed Chemotherapy-Induced Nausea and Vomiting: Pathogenesis, Incidence, and Current Management. *Front. Pharmacol.* **2017**, *8*, 19.

(53) Cinausero, M.; Aprile, G.; Ermacora, P.; Basile, D.; Vitale, M. G.; Fanotto, V.; Parisi, G.; Calvetti, L.; Sonis, S. T. New Frontiers in the Pathobiology and Treatment of Cancer Regimen-Related Mucosal Injury. *Front. Pharmacol.* **2017**, *8*, 354.

(54) Kerckhove, N.; Collin, A.; Condé, S.; Chaleteix, C.; Pezet, D.; Balayssac, D. Long-Term Effects, Pathophysiological Mechanisms, and Risk Factors of Chemotherapy-Induced Peripheral Neuropathies: A Comprehensive Literature Review. *Front. Pharmacol.* **2017**, *8*, 86.

(55) Bernardi, D.; Errante, D.; Gallligioni, E.; Crivellari, D.; Bianco, A.; Salvagno, L.; Fentiman, I. S. Treatment of Breast Cancer in Older Women. *Acta Oncol. Stockh. Swed.* **2008**, *47* (2), 187–198.

(56) Varghese, F.; Wong, J. Breast Cancer in the Elderly. *Surg. Clin. North Am.* **2018**, *98* (4), 819–833.

(57) Salvo, N.; Barnes, E.; van Draanen, J.; Stacey, E.; Mitera, G.; Breen, D.; Giotis, A.; Czarnota, G.; Pang, J.; De Angelis, C. Prophylaxis and Management of Acute Radiation-Induced Skin Reactions: A Systematic Review of the Literature. *Curr. Oncol.* **2010**, *17* (4), 94–112.

(58) Lai, X.; Han, W.; Zhang, H.; Hou, J.; Wang, G.; Luo, X.; Li, X.; Wang, Q.; Zhang, Y.; Wang, H.; Li, Y. Prognostic Role of Radiotherapy in Low-Risk Elderly Breast Cancer Patients after Breast-Conserving Surgery: A Cohort Study. *Gland Surg.* **2022**, *11* (5), 847–859.

(59) *Cancer of the Breast (Female) - Cancer Stat Facts*. SEER. https://seer.cancer.gov/statfacts/html/breast.html (accessed 10/13/2023).

(60) Weigel, M. T.; Dowsett, M. Current and Emerging Biomarkers in Breast Cancer: Prognosis and Prediction. *Endocr. Relat. Cancer* **2010**, *17* (4), R245–R262.

(61) Beca, F.; Polyak, K. Intratumor Heterogeneity in Breast Cancer. In *Novel Biomarkers in the Continuum of Breast Cancer*; Stearns, V., Ed.; Advances in Experimental Medicine and Biology; Springer International Publishing: Cham, 2016; pp 169–189.

(62) *Breast cancer prognostic markers: an overview of a changing menu*. Medical Laboratory Observer. https://www.mlo-online.com/continuing-education/article/13008457/breast-cancer-prognostic-markers-an-overview-of-a-changing-menu (accessed 10/13/2023).

(63) Ellsworth, R. E.; Decewicz, D. J.; Shriver, C. D.; Ellsworth, D. L. Breast Cancer in the Personal Genomics Era. *Curr. Genomics* **2010**, *11* (3), 146–161.

(64) Filipits, M.; Rudas, M.; Jakesz, R.; Dubsky, P.; Fitzal, F.; Singer, C. F.; Dietze, O.; Greil, R.; Jelen, A.; Sevelda, P.; Freibauer, C.; Müller, V.; Jänicke, F.; Schmidt, M.; Kölbl, H.; Rody, A.; Kaufmann, M.; Schroth, W.; Brauch, H.; Schwab, M.; Fritz, P.; Weber, K. E.; Feder, I. S.; Hennig, G.; Kronenwett, R.; Gehrmann, M.; Gnant, M.; EP Investigators. A New Molecular Predictor of Distant Recurrence in ER-Positive,

HER2-Negative Breast Cancer Adds Independent Information to Conventional Clinical Risk Factors. *Clin. Cancer Res. Off. J. Am. Assoc. Cancer Res.* **2011**, *17* (18), 6012–6020.

(65) van 't Veer, L. J.; Dai, H.; van de Vijver, M. J.; He, Y. D.; Hart, A. A. M.; Mao, M.; Peterse, H. L.; van der Kooy, K.; Marton, M. J.; Witteveen, A. T.; Schreiber, G. J.; Kerkhoven, R. M.; Roberts, C.; Linsley, P. S.; Bernards, R.; Friend, S. H. Gene Expression Profiling Predicts Clinical Outcome of Breast Cancer. *Nature* **2002**, *415* (6871), 530–536.

(66) Paik, S.; Tang, G.; Shak, S.; Kim, C.; Baker, J.; Kim, W.; Cronin, M.; Baehner, F. L.; Watson, D.; Bryant, J.; Costantino, J. P.; Geyer, C. E.; Wickerham, D. L.; Wolmark, N. Gene Expression and Benefit of Chemotherapy in Women with Node-Negative, Estrogen Receptor-Positive Breast Cancer. *J. Clin. Oncol. Off. J. Am. Soc. Clin. Oncol.* **2006**, *24* (23), 3726–3734.

(67) Habermann, J. K.; Doering, J.; Hautaniemi, S.; Roblick, U. J.; Bündgen, N. K.; Nicorici, D.; Kronenwett, U.; Rathnagiriswaran, S.; Mettu, R. K. R.; Ma, Y.; Krüger, S.; Bruch, H.-P.; Auer, G.; Guo, N. L.; Ried, T. The Gene Expression Signature of Genomic Instability in Breast Cancer Is an Independent Predictor of Clinical Outcome. *Int. J. Cancer* **2009**, *124* (7), 1552–1564.

(68) Murakami, F.; Tsuboi, Y.; Takahashi, Y.; Horimoto, Y.; Mogushi, K.; Ito, T.; Emi, M.; Matsubara, D.; Shibata, T.; Saito, M.; Murakami, Y. Short Somatic Alterations at the Site of Copy Number Variation in Breast Cancer. *Cancer Sci.* **2021**, *112* (1), 444–453.

(69) Hannouf, M. B.; Zaric, G. S.; Blanchette, P.; Brezden-Masley, C.; Paulden, M.; McCabe, C.; Raphael, J.; Brackstone, M. Cost-Effectiveness Analysis of Multigene Expression Profiling Assays to Guide Adjuvant Therapy Decisions in Women with Invasive Early-Stage Breast Cancer. *Pharmacogenomics J.* **2020**, *20* (1), 27–46.

(70) Harris, L.; Fritsche, H.; Mennel, R.; Norton, L.; Ravdin, P.; Taube, S.; Somerfield, M. R.; Hayes, D. F.; Bast, R. C. American Society of Clinical Oncology 2007 Update of Recommendations for the Use of Tumor Markers in Breast Cancer. *J. Clin. Oncol.* **2007**, *25* (33), 5287–5312.

(71) S3-Leitlinie Mammakarzinom. **2020**, 469.

(72) *Breast Cancer*. ASCO. https://www.asco.org/research-guidelines/quality-guidelines/guidelines/breast-cancer (accessed 10/13/2023).

(73) *Circulating Tumor Cells, Disease Progression, and Survival in Metastatic Breast Cancer | NEJM*. https://www.nejm.org/doi/full/10.1056/nejmoa040766 (accessed 10/13/2023).

(74) Griffiths, A. J.; Miller, J. H.; Suzuki, D. T.; Lewontin, R. C.; Gelbart, W. M. Aberrant Euploidy. *Introd. Genet. Anal. 7th Ed.* **2000**.

(75) Weaver, B. A. A.; Cleveland, D. W. Does Aneuploidy Cause Cancer? *Curr. Opin. Cell Biol.* **2006**, *18* (6), 658–667.

(76) Sen, S. Aneuploidy and Cancer. *Curr. Opin. Oncol.* **2000**, *12* (1), 82–88.

(77) Boveri, T. *Zur Frage der Entstehung maligner Tumoren.*; Gustav Fischer: Jena, 1914.

(78) Davoli, T.; Xu, A. W.; Mengwasser, K. E.; Sack, L. M.; Yoon, J. C.; Park, P. J.; Elledge, S. J. Cumulative Haploinsufficiency and Triplosensitivity Drive Aneuploidy Patterns and Shape the Cancer Genome. *Cell* **2013**, *155* (4), 948–962.

(79) Hedley, D. W.; Rugg, C. A.; Ng, A. B.; Taylor, I. W. Influence of Cellular DNA Content on Disease-Free Survival of Stage II Breast Cancer Patients. *Cancer Res.* **1984**, *44* (11), 5395–5398.

(80) Li, L.; Mu, K.; Zhou, G.; Lan, L.; Auer, G.; Zetterberg, A. Genomic Instability and Proliferative Activity as Risk Factors for Distant Metastases in Breast Cancer. *Br. J. Cancer* **2008**, *99* (3), 513–519.

(81) Cornelisse, C. J.; van de Velde, C. J.; Caspers, R. J.; Moolenaar, A. J.; Hermans, J. DNA Ploidy and Survival in Breast Cancer Patients. *Cytometry* **1987**, *8* (2), 225–234.

(82) Holland, A. J.; Cleveland, D. W. Boveri Revisited: Chromosomal Instability, Aneuploidy and Tumorigenesis. *Nat. Rev. Mol. Cell Biol.* **2009**, *10* (7), 478–487.

(83) Cornelisse, C. J.; Velde, C. J. H. van de; Caspers, R. J. C.; Moolenaar, A. J.; Hermans, J. DNA Ploidy and Survival in Breast Cancer Patients. *Cytometry* **1987**, *8* (2), 225–234.

(84) Oltmann, J.; Heselmeyer-Haddad, K.; Hernandez, L. S.; Meyer, R.; Torres, I.; Hu, Y.; Doberstein, N.; Killian, J. K.; Petersen, D.; Zhu, Y. J.; Edelman, D. C.; Meltzer, P. S.; Schwartz, R.; Gertz, E. M.; Schäffer, A. A.; Auer, G.; Habermann, J. K.; Ried, T. Aneuploidy, TP53 Mutation, and Amplification of MYC Correlate with Increased Intratumor Heterogeneity and Poor Prognosis of Breast Cancer Patients. *Genes. Chromosomes Cancer* **2018**, *57* (4), 165–175.

(85) Pfister, K.; Pipka, J. L.; Chiang, C.; Liu, Y.; Clark, R. A.; Keller, R.; Skoglund, P.; Guertin, M. J.; Hall, I. M.; Stukenberg, P. T. Identification of Drivers of Aneuploidy in Breast Tumors. *Cell Rep.* **2018**, *23* (9), 2758–2769.

(86) Yao, Y.; Dai, W. Genomic Instability and Cancer. *J. Carcinog. Mutagen.* **2014**, *5*.

(87) Lengauer, C.; Kinzler, K. W.; Vogelstein, B. Genetic Instabilities in Human Cancers. *Nature* **1998**, *396* (6712), 643–649.

(88) Heim, S.; Mitelman, F. *Cancer Cytogenetics: Chromosomal and Molecular Genetic Aberrations of Tumor Cells*; John Wiley & Sons, 2015.

(89) Rajagopalan, H.; Nowak, M. A.; Vogelstein, B.; Lengauer, C. The Significance of Unstable Chromosomes in Colorectal Cancer. *Nat. Rev. Cancer* **2003**, *3* (9), 695–701.

(90) Wei, W.; Cheng, Y.; Wang, B. Chapter 27 - Cancer and Genomic Instability. In *Genome Stability*; Kovalchuk, I., Kovalchuk, O., Eds.; Academic Press: Boston, 2016; pp 463–486.

(91) McGranahan, N.; Burrell, R. A.; Endesfelder, D.; Novelli, M. R.; Swanton, C. Cancer Chromosomal Instability: Therapeutic and Diagnostic Challenges. *EMBO Rep.* **2012**, *13* (6), 528–538.

(92) Carter, S. L.; Eklund, A. C.; Kohane, I. S.; Harris, L. N.; Szallasi, Z. A Signature of Chromosomal Instability Inferred from Gene Expression Profiles Predicts Clinical Outcome in Multiple Human Cancers. *Nat. Genet.* **2006**, *38* (9), 1043–1048.

(93) Bakhoum, S. F.; Compton, D. A. Chromosomal Instability and Cancer: A Complex Relationship with Therapeutic Potential. *J. Clin. Invest.* **2012**, *122* (4), 1138–1143.

(94) Duesberg, P.; Fabarius, A.; Hehlmann, R. Aneuploidy, the Primary Cause of the Multilateral Genomic Instability of Neoplastic and Preneoplastic Cells. *IUBMB Life* **2004**, *56* (2), 65–81.

(95) Passerini, V.; Ozeri-Galai, E.; de Pagter, M. S.; Donnelly, N.; Schmalbrock, S.; Kloosterman, W. P.; Kerem, B.; Storchová, Z. The Presence of Extra Chromosomes Leads to Genomic Instability. *Nat. Commun.* **2016**, *7* (1), 10754.

(96) Nicholson, J. M.; Macedo, J. C.; Mattingly, A. J.; Wangsa, D.; Camps, J.; Lima, V.; Gomes, A. M.; Dória, S.; Ried, T.; Logarinho, E.; Cimini, D. Chromosome Mis-Segregation and Cytokinesis Failure in Trisomic Human Cells. *eLife* **2015**, *4*, e05068.

(97) Sansregret, L.; Swanton, C. The Role of Aneuploidy in Cancer Evolution. *Cold Spring Harb. Perspect. Med.* **2017**, *7* (1).

(98) Thompson, S. L.; Compton, D. A. Examining the Link between Chromosomal Instability and Aneuploidy in Human Cells. *J. Cell Biol.* **2008**, *180* (4), 665–672.

(99) Marusyk, A.; Almendro, V.; Polyak, K. Intra-Tumour Heterogeneity: A Looking Glass for Cancer? *Nat. Rev. Cancer* **2012**, *12* (5), 323–334.

(100) *Encyclopedia of Cancer | ScienceDirect*. https://www.sciencedirect.com/referencework/9780128124857/encyclopedia-of-cancer (accessed 10/13/2023).

(101) Nowell, P. C. The Clonal Evolution of Tumor Cell Populations. *Science* **1976**, *194* (4260), 23–28.

(102) McGranahan, N.; Swanton, C. Clonal Heterogeneity and Tumor Evolution: Past, Present, and the Future. *Cell* **2017**, *168* (4), 613–628.

(103) *BioRender*. BioRender. https://biorender.com/ (accessed 10/13/2023).

(104) Heselmeyer-Haddad, K.; Berroa Garcia, L. Y.; Bradley, A.; Ortiz-Melendez, C.; Lee, W.-J.; Christensen, R.; Prindiville, S. A.; Calzone, K. A.; Soballe, P. W.; Hu, Y.; Chowdhury, S. A.; Schwartz, R.; Schäffer, A. A.; Ried, T. Single-Cell Genetic Analysis of Ductal Carcinoma in Situ and Invasive Breast Cancer Reveals Enormous Tumor Heterogeneity yet Conserved Genomic Imbalances and Gain of MYC during Progression. *Am. J. Pathol.* **2012**, *181* (5), 1807–1822.

(105) Martelotto, L. G.; Baslan, T.; Kendall, J.; Geyer, F. C.; Burke, K. A.; Spraggon, L.; Piscuoglio, S.; Chadalavada, K.; Nanjangud, G.; Ng, C. K. Y.; Moody, P.; D'Italia, S.; Rodgers, L.; Cox, H.; da Cruz Paula, A.; Stepansky, A.; Schizas, M.; Wen, H. Y.; King, T. A.; Norton, L.; Weigelt, B.; Hicks, J. B.; Reis-Filho, J. S. Whole-Genome Single-Cell Copy Number Profiling from Formalin-Fixed Paraffin-Embedded Samples. *Nat. Med.* **2017**, *23* (3), 376–385.

(106) Kim, C.; Gao, R.; Sei, E.; Brandt, R.; Hartman, J.; Hatschek, T.; Crosetto, N.; Foukakis, T.; Navin, N. E. Chemoresistance Evolution in Triple-Negative Breast Cancer Delineated by Single-Cell Sequencing. *Cell* **2018**, *173* (4), 879-893.e13.

(107) Janiszewska, M.; Liu, L.; Almendro, V.; Kuang, Y.; Paweletz, C.; Sakr, R. A.; Weigelt, B.; Hanker, A. B.; Chandarlapaty, S.; King, T. A.; Reis-Filho, J. S.; Arteaga,

C. L.; Park, S. Y.; Michor, F.; Polyak, K. In Situ Single-Cell Analysis Identifies Heterogeneity for PIK3CA Mutation and HER2 Amplification in HER2-Positive Breast Cancer. *Nat. Genet.* **2015**, *47* (10), 1212–1219.

(108) Raynaud, F.; Mina, M.; Ciriello, G. Dynamic Emergence of Observed and Hidden Intra-Tumor Heterogeneity. *iScience* **2019**, *21*, 157–167.

(109) Greaves, M. Evolutionary Determinants of Cancer. *Cancer Discov.* **2015**, *5* (8), 806–820. https://doi.org/10.1158/2159-8290.CD-15-0439.

(110) Park, S. Y.; Gönen, M.; Kim, H. J.; Michor, F.; Polyak, K. Cellular and Genetic Diversity in the Progression of in Situ Human Breast Carcinomas to an Invasive Phenotype. *J. Clin. Invest.* **2010**, *120* (2), 636–644.

(111) Almendro, V.; Kim, H. J.; Cheng, Y.-K.; Gönen, M.; Itzkovitz, S.; Argani, P.; van Oudenaarden, A.; Sukumar, S.; Michor, F.; Polyak, K. Genetic and Phenotypic Diversity in Breast Tumor Metastases. *Cancer Res.* **2014**, *74* (5), 1338–1348.

(112) Haynes, B.; Sarma, A.; Nangia-Makker, P.; Shekhar, M. P. Breast Cancer Complexity: Implications of Intratumoral Heterogeneity in Clinical Management. *Cancer Metastasis Rev.* **2017**, *36* (3), 547–555.

(113) Baliu-Piqué, M.; Pandiella, A.; Ocana, A. Breast Cancer Heterogeneity and Response to Novel Therapeutics. *Cancers* **2020**, *12* (11), 3271.

(114) Foote, F. W.; Stewart, F. W. A Histologic Classification of Carcinoma of the Breast. *Surgery* **1946**, *19*, 74–99.

(115) Sørlie, T.; Perou, C. M.; Tibshirani, R.; Aas, T.; Geisler, S.; Johnsen, H.; Hastie, T.; Eisen, M. B.; van de Rijn, M.; Jeffrey, S. S.; Thorsen, T.; Quist, H.; Matese, J. C.; Brown, P. O.; Botstein, D.; Lønning, P. E.; Børresen-Dale, A. L. Gene Expression Patterns of Breast Carcinomas Distinguish Tumor Subclasses with Clinical Implications. *Proc. Natl. Acad. Sci. U. S. A.* **2001**, *98* (19), 10869–10874.

(116) Prat, A.; Pineda, E.; Adamo, B.; Galván, P.; Fernández, A.; Gaba, L.; Díez, M.; Viladot, M.; Arance, A.; Muñoz, M. Clinical Implications of the Intrinsic Molecular Subtypes of Breast Cancer. *Breast Edinb. Scotl.* **2015**, *24 Suppl 2*, S26-35.

(117) Cancer Genome Atlas Network. Comprehensive Molecular Portraits of Human Breast Tumours. *Nature* **2012**, *490* (7418), 61–70.

(118) Negrini, S.; Gorgoulis, V. G.; Halazonetis, T. D. Genomic Instability — an Evolving Hallmark of Cancer. *Nat. Rev. Mol. Cell Biol.* **2010**, *11* (3), 220–228.

(119) Bhattacharya, A.; Bense, R. D.; Urzúa-Traslaviña, C. G.; de Vries, E. G. E.; van Vugt, M. A. T. M.; Fehrmann, R. S. N. Transcriptional Effects of Copy Number Alterations in a Large Set of Human Cancers. *Nat. Commun.* **2020**, *11* (1), 715.

(120) Ried, T.; Meijer, G. A.; Harrison, D. J.; Grech, G.; Franch-Expósito, S.; Briffa, R.; Carvalho, B.; Camps, J. The Landscape of Genomic Copy Number Alterations in Colorectal Cancer and Their Consequences on Gene Expression Levels and Disease Outcome. *Mol. Aspects Med.* **2019**, *69*, 48–61.

(121) Veitia, R. A.; Bottani, S.; Birchler, J. A. Gene Dosage Effects: Nonlinearities, Genetic Interactions, and Dosage Compensation. *Trends Genet.* **2013**, *29* (7), 385–393.

(122) Lee, S. H. T.; Kim, J. Y.; Kim, P.; Dong, Z.; Su, C.-Y.; Ahn, E. H. Changes of Mutations and Copy-Number and Enhanced Cell Migration during Breast Tumorigenesis. *Adv. Biol.* **2023**, *7* (2), e2200072.

(123) Taylor, B. S.; Barretina, J.; Socci, N. D.; DeCarolis, P.; Ladanyi, M.; Meyerson, M.; Singer, S.; Sander, C. Functional Copy-Number Alterations in Cancer. *PLOS ONE* **2008**, *3* (9), e3179.

(124) Ried, T.; Just, K. E.; Holtgreve-Grez, H.; du Manoir, S.; Speicher, M. R.; Schröck, E.; Latham, C.; Blegen, H.; Zetterberg, A.; Cremer, T. Comparative Genomic Hybridization of Formalin-Fixed, Paraffin-Embedded Breast Tumors Reveals Different Patterns of Chromosomal Gains and Losses in Fibroadenomas and Diploid and Aneuploid Carcinomas. *Cancer Res.* **1995**, *55* (22), 5415–5423.

(125) Kallioniemi, A.; Kallioniemi, O. P.; Piper, J.; Tanner, M.; Stokke, T.; Chen, L.; Smith, H. S.; Pinkel, D.; Gray, J. W.; Waldman, F. M. Detection and Mapping of Amplified DNA Sequences in Breast Cancer by Comparative Genomic Hybridization. *Proc. Natl. Acad. Sci. U. S. A.* **1994**, *91* (6), 2156–2160.

(126) Tirkkonen, M.; Tanner, M.; Karhu, R.; Kallioniemi, A.; Isola, J.; Kallioniemi, O. P. Molecular Cytogenetics of Primary Breast Cancer by CGH. *Genes. Chromosomes Cancer* **1998**, *21* (3), 177–184.

(127) Mitelman, F. Catalogue of Chromosome Aberrations in Cancer. *Cytogenet. Cell Genet.* **1983**, *36* (1–2), 1–515.

(128) Koçak, A.; Heselmeyer-Haddad, K.; Lischka, A.; Hirsch, D.; Fiedler, D.; Hu, Y.; Doberstein, N.; Torres, I.; Chen, W.-D.; Gertz, E. M.; Schäffer, A. A.; Freitag-Wolf, S.; Kirfel, J.; Auer, G.; Habermann, J. K.; Ried, T. High Levels of Chromosomal Copy Number Alterations and TP53 Mutations Correlate with Poor Outcome in Younger Breast Cancer Patients. *Am. J. Pathol.* **2020**, *190* (8), 1643–1656.

(129) *Ptgs2 prostaglandin-endoperoxide synthase 2 [Rattus norvegicus (Norway rat)] - Gene - NCBI*. https://www.ncbi.nlm.nih.gov/gene/29527 (accessed 10/13/2023).

(130) Jana, D.; Sarkar, D. K.; Ganguly, S.; Saha, S.; Sa, G.; Manna, A. K.; Banerjee, A.; Mandal, S. Role of Cyclooxygenase 2 (COX-2) in Prognosis of Breast Cancer. *Indian J. Surg. Oncol.* **2014**, *5* (1), 59–65.

(131) Kim, H. S.; Moon, H.-G.; Han, W.; Yom, C. K.; Kim, W. H.; Kim, J. H.; Noh, D.-Y. COX2 Overexpression Is a Prognostic Marker for Stage III Breast Cancer. *Breast Cancer Res. Treat.* **2012**, *132* (1), 51–59.

(132) Sivula, A.; Talvensaari-Mattila, A.; Lundin, J.; Joensuu, H.; Haglund, C.; Ristimäki, A.; Turpeenniemi-Hujanen, T. Association of Cyclooxygenase-2 and Matrix Metalloproteinase-2 Expression in Human Breast Cancer. *Breast Cancer Res. Treat.* **2005**, *89* (3), 215–220.

(133) *MYC MYC proto-oncogene, bHLH transcription factor [Homo sapiens (human)] - Gene - NCBI*. https://www.ncbi.nlm.nih.gov/gene/4609 (accessed 10/13/2023).

(134) Wolfer, A.; Ramaswamy, S. MYC and Metastasis. *Cancer Res.* **2011**, *71* (6), 2034–2037. https://doi.org/10.1158/0008-5472.CAN-10-3776.

(135) Fallah, Y.; Brundage, J.; Allegakoen, P.; Shajahan-Haq, A. N. MYC-Driven Pathways in Breast Cancer Subtypes. *Biomolecules* **2017**, *7* (3).

(136) Fu, M.; Wang, C.; Li, Z.; Sakamaki, T.; Pestell, R. G. Minireview: Cyclin D1: Normal and Abnormal Functions. *Endocrinology* **2004**, *145* (12), 5439–5447.

(137) *ERBB2 erb-b2 receptor tyrosine kinase 2 [Homo sapiens (human)] - Gene - NCBI*. https://www.ncbi.nlm.nih.gov/gene/2064 (accessed 10/13/2023).

(138) Banck, M. S.; Li, S.; Nishio, H.; Wang, C.; Beutler, A. S.; Walsh, M. J. The ZNF217 Oncogene Is a Candidate Organizer of Repressive Histone Modifiers. *Epigenetics Off. J. DNA Methylation Soc.* **2009**, *4* (2), 100–106.

(139) Cowger, J. J. M.; Zhao, Q.; Isovic, M.; Torchia, J. Biochemical Characterization of the Zinc-Finger Protein 217 Transcriptional Repressor Complex: Identification of a ZNF217 Consensus Recognition Sequence. *Oncogene* **2007**, *26* (23), 3378–3386.

(140) Sun, Y.; Wong, N.; Guan, Y.; Salamanca, C. M.; Cheng, J. C.; Lee, J. M.; Gray, J. W.; Auersperg, N. The Eukaryotic Translation Elongation Factor eEF1A2 Induces Neoplastic Properties and Mediates Tumorigenic Effects of ZNF217 in Precursor Cells of Human Ovarian Carcinomas. *Int. J. Cancer* **2008**, *123* (8), 1761–1769.

(141) Quinlan, K. G. R.; Verger, A.; Yaswen, P.; Crossley, M. Amplification of Zinc Finger Gene 217 (ZNF217) and Cancer: When Good Fingers Go Bad. *Biochim. Biophys. Acta* **2007**, *1775* (2), 333–340.

(142) Ginestier, C.; Cervera, N.; Finetti, P.; Esteyries, S.; Esterni, B.; Adélaïde, J.; Xerri, L.; Viens, P.; Jacquemier, J.; Charafe-Jauffret, E.; Chaffanet, M.; Birnbaum, D.; Bertucci, F. Prognosis and Gene Expression Profiling of 20q13-Amplified Breast Cancers. *Clin. Cancer Res. Off. J. Am. Assoc. Cancer Res.* **2006**, *12* (15), 4533–4544.

(143) *RHOBTB2 Rho related BTB domain containing 2 [Homo sapiens (human)] - Gene - NCBI*. https://www.ncbi.nlm.nih.gov/gene/23221 (accessed 10/13/2023).

(144) Mao, H.; Qu, X.; Yang, Y.; Zuo, W.; Bi, Y.; Zhou, C.; Yin, H.; Deng, B.; Sun, J.; Zhang, L. A Novel Tumor Suppressor Gene RhoBTB2 (DBC2): Frequent Loss of Expression in Sporadic Breast Cancer. *Mol. Carcinog.* **2010**, *49* (3), 283–289.

(145) *CDH1 cadherin 1 [Homo sapiens (human)] - Gene - NCBI*. https://www.ncbi.nlm.nih.gov/gene/999 (accessed 10/13/2023).

(146) Lecuit, T.; Yap, A. S. E-Cadherin Junctions as Active Mechanical Integrators in Tissue Dynamics. *Nat. Cell Biol.* **2015**, *17* (5), 533–539.

(147) Bruner, H. C.; Derksen, P. W. B. Loss of E-Cadherin-Dependent Cell–Cell Adhesion and the Development and Progression of Cancer. *Cold Spring Harb. Perspect. Biol.* **2018**, *10* (3).

(148) Berx, G.; Cleton-Jansen, A. M.; Nollet, F.; de Leeuw, W. J.; van de Vijver, M.; Cornelisse, C.; van Roy, F. E-Cadherin Is a Tumour/Invasion Suppressor Gene Mutated in Human Lobular Breast Cancers. *EMBO J.* **1995**, *14* (24), 6107–6115.

(149) Riley, T.; Sontag, E.; Chen, P.; Levine, A. Transcriptional Control of Human P53-Regulated Genes. *Nat. Rev. Mol. Cell Biol.* **2008**, *9* (5), 402–412.

(150) Bertheau, P.; Lehmann-Che, J.; Varna, M.; Dumay, A.; Poirot, B.; Porcher, R.; Turpin, E.; Plassa, L.-F.; de Roquancourt, A.; Bourstyn, E.; de Cremoux, P.; Janin, A.; Giacchetti, S.; Espié, M.; de Thé, H. P53 in Breast Cancer Subtypes and New Insights into Response to Chemotherapy. *Breast Edinb. Scotl.* **2013**, *22 Suppl 2*, S27-29.

(151) Singh, B.; Berry, J. A.; Shoher, A.; Ramakrishnan, V.; Lucci, A. COX-2 Overexpression Increases Motility and Invasion of Breast Cancer Cells. *Int. J. Oncol.* **2005**, *26* (5), 1393–1399.

(152) Howe, L. R.; Subbaramaiah, K.; Brown, A. M.; Dannenberg, A. J. Cyclooxygenase-2: A Target for the Prevention and Treatment of Breast Cancer. *Endocr. Relat. Cancer* **2001**, *8* (2), 97–114.

(153) Liu, C. H.; Chang, S. H.; Narko, K.; Trifan, O. C.; Wu, M. T.; Smith, E.; Haudenschild, C.; Lane, T. F.; Hla, T. Overexpression of Cyclooxygenase-2 Is Sufficient to Induce Tumorigenesis in Transgenic Mice. *J. Biol. Chem.* **2001**, *276* (21), 18563–18569.

(154) Boland, G. P.; Butt, I. S.; Prasad, R.; Knox, W. F.; Bundred, N. J. COX-2 Expression Is Associated with an Aggressive Phenotype in Ductal Carcinoma in Situ. *Br. J. Cancer* **2004**, *90* (2), 423–429.

(155) Sahu, A.; Raza, K.; Pradhan, D.; Jain, A. K.; Verma, S. Cyclooxygenase-2 as a Therapeutic Target against Human Breast Cancer: A Comprehensive Review. *WIREs Mech. Dis.* **2023**, *15* (3), e1596.

(156) Yoshihara, T.; Collado, D.; Hamaguchi, M. Cyclin D1 Down-Regulation Is Essential for DBC2's Tumor Suppressor Function. *Biochem. Biophys. Res. Commun.* **2007**, *358* (4), 1076–1079.

(157) Siripurapu, V.; Meth, J.; Kobayashi, N.; Hamaguchi, M. DBC2 Significantly Influences Cell-Cycle, Apoptosis, Cytoskeleton and Membrane-Trafficking Pathways. *J. Mol. Biol.* **2005**, *346* (1), 83–89.

(158) Blancato, J.; Singh, B.; Liu, A.; Liao, D. J.; Dickson, R. B. Correlation of Amplification and Overexpression of the C-Myc Oncogene in High-Grade Breast Cancer: FISH, in Situ Hybridisation and Immunohistochemical Analyses. *Br. J. Cancer* **2004**, *90* (8), 1612–1619.

(159) Umekita, Y.; Yoshida, H. Cyclin D1 Expression in Ductal Carcinoma in Situ, Atypical Ductal Hyperplasia and Usual Ductal Hyperplasia: An Immunohistochemical Study. *Pathol. Int.* **2000**, *50* (7), 527–530.

(160) Moradi Binabaj, M.; Bahrami, A.; Khazaei, M.; Ryzhikov, M.; Ferns, G. A.; Avan, A.; Mahdi Hassanian, S. The Prognostic Value of Cyclin D1 Expression in the Survival of Cancer Patients: A Meta-Analysis. *Gene* **2020**, *728*, 144283.

(161) Beroukhim, R.; Mermel, C. H.; Porter, D.; Wei, G.; Raychaudhuri, S.; Donovan, J.; Barretina, J.; Boehm, J. S.; Dobson, J.; Urashima, M.; Mc Henry, K. T.; Pinchback, R. M.; Ligon, A. H.; Cho, Y.-J.; Haery, L.; Greulich, H.; Reich, M.; Winckler, W.; Lawrence, M. S.; Weir, B. A.; Tanaka, K. E.; Chiang, D. Y.; Bass, A. J.; Loo, A.; Hoffman, C.; Prensner, J.; Liefeld, T.; Gao, Q.; Yecies, D.; Signoretti, S.; Maher, E.; Kaye, F. J.; Sasaki, H.; Tepper, J. E.; Fletcher, J. A.; Tabernero, J.; Baselga, J.; Tsao, M.-S.; Demichelis, F.; Rubin, M. A.; Janne, P. A.; Daly, M. J.; Nucera, C.; Levine, R.

L.; Ebert, B. L.; Gabriel, S.; Rustgi, A. K.; Antonescu, C. R.; Ladanyi, M.; Letai, A.; Garraway, L. A.; Loda, M.; Beer, D. G.; True, L. D.; Okamoto, A.; Pomeroy, S. L.; Singer, S.; Golub, T. R.; Lander, E. S.; Getz, G.; Sellers, W. R.; Meyerson, M. The Landscape of Somatic Copy-Number Alteration across Human Cancers. *Nature* **2010**, *463* (7283), 899–905.

(162) Shi, Q.; Li, Y.; Li, S.; Jin, L.; Lai, H.; Wu, Y.; Cai, Z.; Zhu, M.; Li, Q.; Li, Y.; Wang, J.; Liu, Y.; Wu, Z.; Song, E.; Liu, Q. LncRNA DILA1 Inhibits Cyclin D1 Degradation and Contributes to Tamoxifen Resistance in Breast Cancer. *Nat. Commun.* **2020**, *11* (1), 5513.

(163) Gillett, C.; Fantl, V.; Smith, R.; Fisher, C.; Bartek, J.; Dickson, C.; Barnes, D.; Peters, G. Amplification and Overexpression of Cyclin D1 in Breast Cancer Detected by Immunohistochemical Staining. *Cancer Res.* **1994**, *54* (7), 1812–1817.

(164) Barnes, D. M.; Gillett, C. E. Cyclin D1 in Breast Cancer. *Breast Cancer Res. Treat.* **1998**, *52* (1–3), 1–15.

(165) Hwang, T. S.; Han, H. S.; Hong, Y. C.; Lee, H. J.; Paik, N.-S. Prognostic Value of Combined Analysis of Cyclin D1 and Estrogen Receptor Status in Breast Cancer Patients. *Pathol. Int.* **2003**, *53* (2), 74–80.

(166) Mylona, E.; Tzelepis, K.; Theohari, I.; Giannopoulou, I.; Papadimitriou, C.; Nakopoulou, L. Cyclin D1 in Invasive Breast Carcinoma: Favourable Prognostic Significance in Unselected Patients and within Subgroups with an Aggressive Phenotype. *Histopathology* **2013**, *62* (3), 472–480.

(167) McIntosh, G. G.; Anderson, J. J.; Milton, I.; Steward, M.; Parr, A. H.; Thomas, M. D.; Henry, J. A.; Angus, B.; Lennard, T. W.; Horne, C. H. Determination of the Prognostic Value of Cyclin D1 Overexpression in Breast Cancer. *Oncogene* **1995**, *11* (5), 885–891.

(168) Kenny, F. S.; Hui, R.; Musgrove, E. A.; Gee, J. M.; Blamey, R. W.; Nicholson, R. I.; Sutherland, R. L.; Robertson, J. F. Overexpression of Cyclin D1 Messenger RNA Predicts for Poor Prognosis in Estrogen Receptor-Positive Breast Cancer. *Clin. Cancer Res. Off. J. Am. Assoc. Cancer Res.* **1999**, *5* (8), 2069–2076.

(169) Birchmeier, W.; Behrens, J. Cadherin Expression in Carcinomas: Role in the Formation of Cell Junctions and the Prevention of Invasiveness. *Biochim. Biophys. Acta* **1994**, *1198* (1), 11–26.

(170) Yoshida, R.; Kimura, N.; Harada, Y.; Ohuchi, N. The Loss of E-Cadherin, Alpha- and Beta-Catenin Expression Is Associated with Metastasis and Poor Prognosis in Invasive Breast Cancer. *Int. J. Oncol.* **2001**, *18* (3), 513–520.

(171) Slamon, D. J.; Clark, G. M.; Wong, S. G.; Levin, W. J.; Ullrich, A.; McGuire, W. L. Human Breast Cancer: Correlation of Relapse and Survival with Amplification of the HER-2/Neu Oncogene. *Science* **1987**, *235* (4785), 177–182.

(172) Tiwari, R. K.; Borgen, P. I.; Wong, G. Y.; Cordon-Cardo, C.; Osborne, M. P. HER-2/Neu Amplification and Overexpression in Primary Human Breast Cancer Is Associated with Early Metastasis. *Anticancer Res.* **1992**, *12* (2), 419–425.

(173) Carr, J. A.; Havstad, S.; Zarbo, R. J.; Divine, G.; Mackowiak, P.; Velanovich, V. The Association of HER-2/Neu Amplification with Breast Cancer Recurrence. *Arch. Surg. Chic. Ill 1960* **2000**, *135* (12), 1469–1474.

(174) Gonzalez-Angulo, A. M.; Hortobágyi, G. N.; Esteva, F. J. Adjuvant Therapy with Trastuzumab for HER-2/Neu-Positive Breast Cancer. *The Oncologist* **2006**, *11* (8), 857–867. https://doi.org/10.1634/theoncologist.11-8-857.

(175) Strachan, Tom; Read, Andrew. *Human Molecular Genetics 2 - NLM Catalog - NCBI*; 2nd ed.; New York : Wiley-Liss, 1999.

(176) Thollet, A.; Vendrell, J. A.; Payen, L.; Ghayad, S. E.; Ben Larbi, S.; Grisard, E.; Collins, C.; Villedieu, M.; Cohen, P. A. ZNF217 Confers Resistance to the Pro-Apoptotic Signals of Paclitaxel and Aberrant Expression of Aurora-A in Breast Cancer Cells. *Mol. Cancer* **2010**, *9*, 291.

(177) Sharma, T.; Zhang, Y.; Zigrossi, A.; Cravatt, B. F.; Kastrati, I. Dimethyl Fumarate Inhibits ZNF217 and Can Be Beneficial in a Subset of Estrogen Receptor Positive Breast Cancers. *Breast Cancer Res. Treat.* **2023**, *201* (3), 561–570.

(178) Duffy, M. J.; O'Donovan, N.; McDermott, E.; Crown, J. Validated Biomarkers: The Key to Precision Treatment in Patients with Breast Cancer. *Breast Edinb. Scotl.* **2016**, *29*, 192–201.

(179) Auer, G.; Eriksson, E.; Azavedo, E.; Caspersson, T.; Wallgren, A. Prognostic Significance of Nuclear DNA Content in Mammary Adenocarcinomas in Humans. *Cancer Res.* **1984**, *44* (1), 394–396.

(180) Lischka, A.; Doberstein, N.; Freitag-Wolf, S.; Koçak, A.; Gemoll, T.; Heselmeyer-Haddad, K.; Ried, T.; Auer, G.; Habermann, J. K. Genome Instability Profiles Predict Disease Outcome in a Cohort of 4,003 Patients with Breast Cancer. *Clin. Cancer Res. Off. J. Am. Assoc. Cancer Res.* **2020**, *26* (17), 4606–4615.

(181) Kronenwett, U.; Ploner, A.; Zetterberg, A.; Bergh, J.; Hall, P.; Auer, G.; Pawitan, Y. Genomic Instability and Prognosis in Breast Carcinomas. *Cancer Epidemiol. Biomark. Prev. Publ. Am. Assoc. Cancer Res. Cosponsored Am. Soc. Prev. Oncol.* **2006**, *15* (9), 1630–1635.

(182) Hammond, M. E. H.; Hayes, D. F.; Wolff, A. C.; Mangu, P. B.; Temin, S. American Society of Clinical Oncology/College of American Pathologists Guideline Recommendations for Immunohistochemical Testing of Estrogen and Progesterone Receptors in Breast Cancer. *J. Oncol. Pract.* **2010**, *6* (4), 195–197.

(183) Dowsett, M.; Nielsen, T. O.; A'Hern, R.; Bartlett, J.; Coombes, R. C.; Cuzick, J.; Ellis, M.; Henry, N. L.; Hugh, J. C.; Lively, T.; McShane, L.; Paik, S.; Penault-Llorca, F.; Prudkin, L.; Regan, M.; Salter, J.; Sotiriou, C.; Smith, I. E.; Viale, G.; Zujewski, J. A.; Hayes, D. F. Assessment of Ki67 in Breast Cancer: Recommendations from the International Ki67 in Breast Cancer Working Group. *JNCI J. Natl. Cancer Inst.* **2011**, *103* (22), 1656–1664.

(184) Goldhirsch, A.; Winer, E. P.; Coates, A. S.; Gelber, R. D.; Piccart-Gebhart, M.; Thürlimann, B.; Senn, H.-J.; Albain, K. S.; André, F.; Bergh, J.; Bonnefoi, H.; Bretel-Morales, D.; Burstein, H.; Cardoso, F.; Castiglione-Gertsch, M.; Coates, A. S.; Colleoni, M.; Costa, A.; Curigliano, G.; Davidson, N. E.; Di Leo, A.; Ejlertsen, B.; Forbes, J. F.; Gelber, R. D.; Gnant, M.; Goldhirsch, A.; Goodwin, P.; Goss, P. E.;

Harris, J. R.; Hayes, D. F.; Hudis, C. A.; Ingle, J. N.; Jassem, J.; Jiang, Z.; Karlsson, P.; Loibl, S.; Morrow, M.; Namer, M.; Kent Osborne, C.; Partridge, A. H.; Penault-Llorca, F.; Perou, C. M.; Piccart-Gebhart, M. J.; Pritchard, K. I.; Rutgers, E. J. T.; Sedlmayer, F.; Semiglazov, V.; Shao, Z.-M.; Smith, I.; Thürlimann, B.; Toi, M.; Tutt, A.; Untch, M.; Viale, G.; Watanabe, T.; Wilcken, N.; Winer, E. P.; Wood, W. C. Personalizing the Treatment of Women with Early Breast Cancer: Highlights of the St Gallen International Expert Consensus on the Primary Therapy of Early Breast Cancer 2013. *Ann. Oncol.* **2013**, *24* (9), 2206–2223.

(185) Shakoori, A. R. Fluorescence In Situ Hybridization (FISH) and Its Applications. *Chromosome Struct. Aberrations* **2017**, 343–367.

(186) Gertz, E. M.; Chowdhury, S. A.; Lee, W.-J.; Wangsa, D.; Heselmeyer-Haddad, K.; Ried, T.; Schwartz, R.; Schäffer, A. A. FISHtrees 3.0: Tumor Phylogenetics Using a Ploidy Probe. *PloS One* **2016**, *11* (6), e0158569.

(187) McKenna, A.; Hanna, M.; Banks, E.; Sivachenko, A.; Cibulskis, K.; Kernytsky, A.; Garimella, K.; Altshuler, D.; Gabriel, S.; Daly, M.; DePristo, M. A. The Genome Analysis Toolkit: A MapReduce Framework for Analyzing next-Generation DNA Sequencing Data. *Genome Res.* **2010**, *20* (9), 1297–1303.

(188) Liu, X.; Wu, C.; Li, C.; Boerwinkle, E. dbNSFP v3.0: A One-Stop Database of Functional Predictions and Annotations for Human Non-Synonymous and Splice Site SNVs. *Hum. Mutat.* **2016**, *37* (3), 235–241.

(189) Sherry, S. T.; Ward, M.-H.; Kholodov, M.; Baker, J.; Phan, L.; Smigielski, E. M.; Sirotkin, K. dbSNP: The NCBI Database of Genetic Variation. *Nucleic Acids Res.* **2001**, *29* (1), 308–311.

(190) Karczewski, K. J.; Weisburd, B.; Thomas, B.; Solomonson, M.; Ruderfer, D. M.; Kavanagh, D.; Hamamsy, T.; Lek, M.; Samocha, K. E.; Cummings, B. B.; Birnbaum, D.; Daly, M. J.; MacArthur, D. G. The ExAC Browser: Displaying Reference Data Information from over 60 000 Exomes. *Nucleic Acids Res.* **2017**, *45* (Database issue), D840–D845.

(191) Robinson, J. T.; Thorvaldsdóttir, H.; Winckler, W.; Guttman, M.; Lander, E. S.; Getz, G.; Mesirov, J. P. Integrative Genomics Viewer. *Nat. Biotechnol.* **2011**, *29* (1), 24–26.

(192) Cerami, E.; Gao, J.; Dogrusoz, U.; Gross, B. E.; Sumer, S. O.; Aksoy, B. A.; Jacobsen, A.; Byrne, C. J.; Heuer, M. L.; Larsson, E.; Antipin, Y.; Reva, B.; Goldberg, A. P.; Sander, C.; Schultz, N. The cBio Cancer Genomics Portal: An Open Platform for Exploring Multidimensional Cancer Genomics Data. *Cancer Discov.* **2012**, *2* (5), 401–404.

(193) Gao, J.; Aksoy, B. A.; Dogrusoz, U.; Dresdner, G.; Gross, B.; Sumer, S. O.; Sun, Y.; Jacobsen, A.; Sinha, R.; Larsson, E.; Cerami, E.; Sander, C.; Schultz, N. Integrative Analysis of Complex Cancer Genomics and Clinical Profiles Using the cBioPortal. *Sci. Signal.* **2013**, *6* (269), pl1.

(194) Szczurek, E.; Beerenwinkel, N. Modeling Mutual Exclusivity of Cancer Mutations. *PLoS Comput. Biol.* **2014**, *10* (3), e1003503.

(195) Ciriello, G.; Cerami, E.; Sander, C.; Schultz, N. Mutual Exclusivity Analysis Identifies Oncogenic Network Modules. *Genome Res.* **2012**, *22* (2), 398–406.

(196) Ciriello, G.; Cerami, E.; Aksoy, B. A.; Sander, C.; Schultz, N. Using MEMo to Discover Mutual Exclusivity Modules in Cancer. *Curr. Protoc. Bioinforma.* **2013**, *Chapter 8*, Unit 8.17. https://doi.org/10.1002/0471250953.bi0817s41.

(197) Liegmann, A.-S.; Heselmeyer-Haddad, K.; Lischka, A.; Hirsch, D.; Chen, W.-D.; Torres, I.; Gemoll, T.; Rody, A.; Thorns, C.; Gertz, E. M.; Alkemade, H.; Hu, Y.; Habermann, J. K.; Ried, T. Single Cell Genetic Profiling of Tumors of Breast Cancer Patients Aged 50 Years and Older Reveals Enormous Intratumor Heterogeneity Independent of Individual Prognosis. *Cancers* **2021**, *13* (13), 3366.

(198) Rummukainen, J.; Kytölä, S.; Karhu, R.; Farnebo, F.; Larsson, C.; Isola, J. J. Aberrations of Chromosome 8 in 16 Breast Cancer Cell Lines by Comparative Genomic Hybridization, Fluorescence in Situ Hybridization, and Spectral Karyotyping. *Cancer Genet. Cytogenet.* **2001**, *126* (1), 1–7.

(199) Mertens, F.; Johansson, B.; Mitelman, F. Isochromosomes in Neoplasia. *Genes. Chromosomes Cancer* **1994**, *10* (4), 221–230.

(200) Anbazhagan, R.; Fujii, H.; Gabrielson, E. Allelic Loss of Chromosomal Arm 8p in Breast Cancer Progression. *Am. J. Pathol.* **1998**, *152* (3), 815–819.

(201) Yaremko, M. L.; Recant, W. M.; Westbrook, C. A. Loss of Heterozygosity from the Short Arm of Chromosome 8 Is an Early Event in Breast Cancers. *Genes. Chromosomes Cancer* **1995**, *13* (3), 186–191.

(202) Riou, G.; Mathieu, M. C.; Barrois, M.; Le Bihan, M. L.; Ahomadegbe, J. C.; Bénard, J.; Lê, M. G. C-erbB-2 (HER-2/Neu) Gene Amplification Is a Better Indicator of Poor Prognosis than Protein over-Expression in Operable Breast-Cancer Patients. *Int. J. Cancer* **2001**, *95* (4), 266–270.

(203) Gilcrease, M. Z.; Woodward, W. A.; Nicolas, M. M.; Corley, L. J.; Fuller, G. N.; Esteva, F. J.; Tucker, S. L.; Buchholz, T. A. Even Low-Level HER2 Expression May Be Associated with Worse Outcome in Node-Positive Breast Cancer. *Am. J. Surg. Pathol.* **2009**, *33* (5), 759–767.

(204) Parikh, M.; Galkin, M.; Brunson, A.; Keegan, T.; Chew, H. K. Breast Cancer-Specific Survival in Patients with HER2-Positive, Node-Negative T1a and T1b Breast Cancer. *Cancer Treat. Res. Commun.* **2018**, *16*, 38–44.

(205) Krishnamurti, U.; Silverman, J. F. HER2 in Breast Cancer: A Review and Update. *Adv. Anat. Pathol.* **2014**, *21* (2), 100–107.

(206) Asif, H. M.; Sultana, S.; Ahmed, S.; Akhtar, N.; Tariq, M. HER-2 Positive Breast Cancer - a Mini-Review. *Asian Pac. J. Cancer Prev. APJCP* **2016**, *17* (4), 1609–1615.

(207) Roy, P. G.; Pratt, N.; Purdie, C. A.; Baker, L.; Ashfield, A.; Quinlan, P.; Thompson, A. M. High CCND1 Amplification Identifies a Group of Poor Prognosis Women with Estrogen Receptor Positive Breast Cancer. *Int. J. Cancer* **2010**, *127* (2), 355–360.

(208) Aaltonen, K.; Amini, R.-M.; Landberg, G.; Eerola, H.; Aittomäki, K.; Heikkilä, P.; Nevanlinna, H.; Blomqvist, C. Cyclin D1 Expression Is Associated with Poor Prognostic Features in Estrogen Receptor Positive Breast Cancer. *Breast Cancer Res. Treat.* **2009**, *113* (1), 75–82.

(209) van Jaarsveld, R. H.; Kops, G. J. P. L. Difference Makers: Chromosomal Instability versus Aneuploidy in Cancer. *Trends Cancer* **2016**, *2* (10), 561–571.

(210) Potapova, T. A.; Zhu, J.; Li, R. Aneuploidy and Chromosomal Instability: A Vicious Cycle Driving Cellular Evolution and Cancer Genome Chaos. *Cancer Metastasis Rev.* **2013**, *32* (0).

(211) Tanner, M. M.; Karhu, R. A.; Nupponen, N. N.; Borg, A.; Baldetorp, B.; Pejovic, T.; Fernö, M.; Killander, D.; Isola, J. J. Genetic Aberrations in Hypodiploid Breast Cancer: Frequent Loss of Chromosome 4 and Amplification of Cyclin D1 Oncogene. *Am. J. Pathol.* **1998**, *153* (1), 191–199.

(212) Vogelstein, B.; Papadopoulos, N.; Velculescu, V. E.; Zhou, S.; Diaz, L. A.; Kinzler, K. W. Cancer Genome Landscapes. *Science* **2013**, *339* (6127), 1546–1558.

(213) Bielski, C. M.; Zehir, A.; Penson, A. V.; Donoghue, M. T. A.; Chatila, W.; Armenia, J.; Chang, M. T.; Schram, A. M.; Jonsson, P.; Bandlamudi, C.; Razavi, P.; Iyer, G.; Robson, M. E.; Stadler, Z. K.; Schultz, N.; Baselga, J.; Solit, D. B.; Hyman, D. M.; Berger, M. F.; Taylor, B. S. Genome Doubling Shapes the Evolution and Prognosis of Advanced Cancers. *Nat. Genet.* **2018**, *50* (8), 1189–1195.

(214) Lei, H.; Gertz, E. M.; Schäffer, A. A.; Fu, X.; Tao, Y.; Heselmeyer-Haddad, K.; Torres, I.; Shi, X.; Wu, K.; Li, G.; Xu, L.; Hou, Y.; Dean, M.; Ried, T.; Schwartz, R. Tumor Heterogeneity Assessed by Sequencing and Fluorescence in Situ Hybridization (FISH) Data. *bioRxiv* **2020**, 2020.02.29.970392.

(215) Vorkas, P. A.; Poumpouridou, N.; Agelaki, S.; Kroupis, C.; Georgoulias, V.; Lianidou, E. S. PIK3CA Hotspot Mutation Scanning by a Novel and Highly Sensitive High-Resolution Small Amplicon Melting Analysis Method. *J. Mol. Diagn. JMD* **2010**, *12* (5), 697–704.

(216) Samuels, Y.; Wang, Z.; Bardelli, A.; Silliman, N.; Ptak, J.; Szabo, S.; Yan, H.; Gazdar, A.; Powell, S. M.; Riggins, G. J.; Willson, J. K. V.; Markowitz, S.; Kinzler, K. W.; Vogelstein, B.; Velculescu, V. E. High Frequency of Mutations of the PIK3CA Gene in Human Cancers. *Science* **2004**, *304* (5670), 554.

(217) Kang, S.; Bader, A. G.; Vogt, P. K. Phosphatidylinositol 3-Kinase Mutations Identified in Human Cancer Are Oncogenic. *Proc. Natl. Acad. Sci. U. S. A.* **2005**, *102* (3), 802–807.

(218) Forbes, S. A.; Bindal, N.; Bamford, S.; Cole, C.; Kok, C. Y.; Beare, D.; Jia, M.; Shepherd, R.; Leung, K.; Menzies, A.; Teague, J. W.; Campbell, P. J.; Stratton, M. R.; Futreal, P. A. COSMIC: Mining Complete Cancer Genomes in the Catalogue of Somatic Mutations in Cancer. *Nucleic Acids Res.* **2011**, *39* (Database issue), D945–D950.

(219) Liu, Z.; Jiang, Z.; Gao, Y.; Wang, L.; Chen, C.; Wang, X. TP53 Mutations Promote Immunogenic Activity in Breast Cancer. *J. Oncol.* **2019**, *2019*.

(220) Sadzeviciene, I.; Snipaitiene, K.; Scesnaite-Jerdiakova, A.; Daniunaite, K.; Sabaliauskaite, R.; Laurinaviciene, A.; Drobniene, M.; Ostapenko, V.; Jarmalaite, S. Analysis of Intrinsic Breast Cancer Subtypes: The Clinical Utility of Epigenetic Biomarkers and TP53 Mutation Status in Triple-Negative Cases. *Int. J. Mol. Sci.* **2022**, *23* (23), 15429.

(221) Amirouchene-Angelozzi, N.; Swanton, C.; Bardelli, A. Tumor Evolution as a Therapeutic Target. *Cancer Discov.* **2017**, *7* (8), 805–817.

9 SUPPLEMENT

9.1 Table of figures

Main part

Supplement

9.2 List of tables

Main part

Supplement

9.3 Supplemental Figures

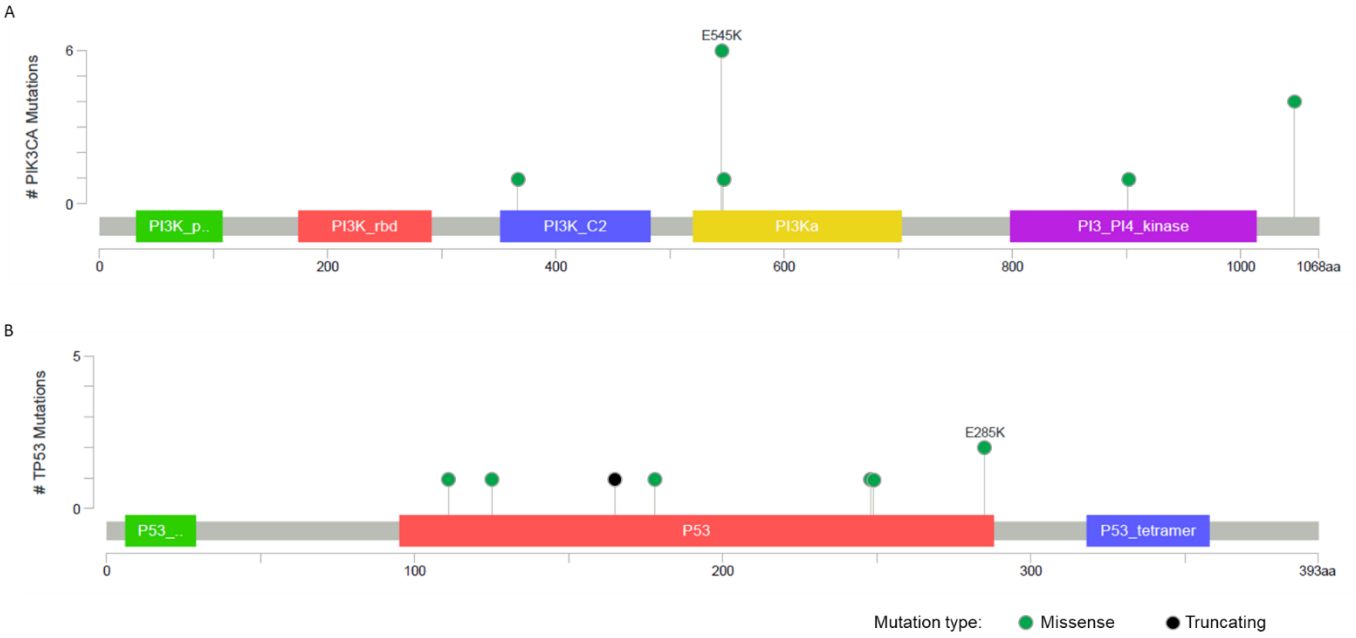

9.3.1 Supplemental Figure S1. Lollipop chart displaying the mutation localizations in PIK3CA (A) and TP53 (B).

(A) The linear PIK3CA protein and its domains are visualized to map mutations using Pfam (Protein family database from Wellcome Trust Sanger Institute). The various PIK3CA domains are color-coded as follows: PI3-kinase family, p85-binding domain (32–108) in green, PI3-kinase family, ras-binding domain (174–291) in red, Phosphoinositide 3-kinase C2 (351–483) in blue, Phosphoinositide 3-kinase family, accessory domain (PIK domain) (520–703) in yellow, and Phosphatidylinositol 3- and 4-kinase (798–1014) in purple.

(B) Mutations are mapped on the linear TP53 protein and its domains from Pfam. The color markings of TP53 indicate its distinct domains: TP53 transactivation motif (5–29) in green, TP53 DNA binding domain (95–289) in red, and TP53 tetramerization motif (319–358) in blue.

(A+B): The height of the "lollipops" (y-axis) represents the number of cases showing a mutation at the same site. “Lollipops”: green, missense mutation; black, truncating mutation. Figure created by PD Dr. med. Daniela Hirsch.

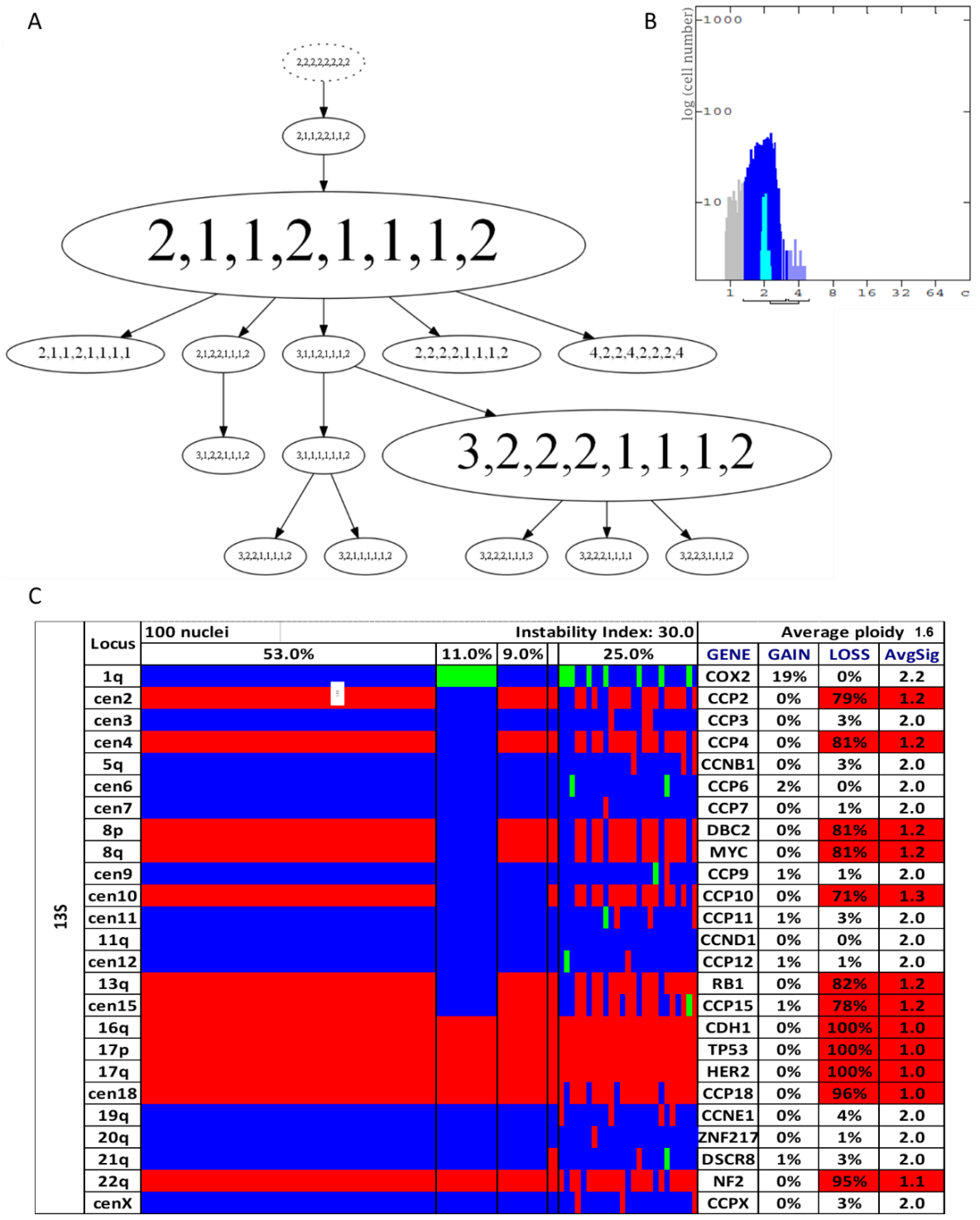

9.3.2 Supplemental Figure S2. Phylogenetic tree (A), DNA histogram (B) and color chart (C) of miFISH results for hypodiploid case 13S.

(A) Consensus phylogenetic tree of miFISH results with the eight described gene probes using phylogenetic algorithms (software FISHtrees 3.2).

(B) DNA histogram showing the quantitative measurements of the nuclear DNA content assessed by image cytometry using Feulgen-stained cytospins.

(C) Color chart of miFISH analysis with 25 gene probes: centromere probes CCP2, 3, 4, 6, 7, 9, 10, 11, 12, 15, 18, X and locus-specific probes *COX2, CCNB1, DBC2, MYC, CCND1, RB1, CDH1, TP53, HER2, CCNE1, ZNF217, DSCR8, NF2*, as described in Materials and Methods. For every nucleus, copy number changes are visualized as gains (green), losses (red) and neutral (blue).

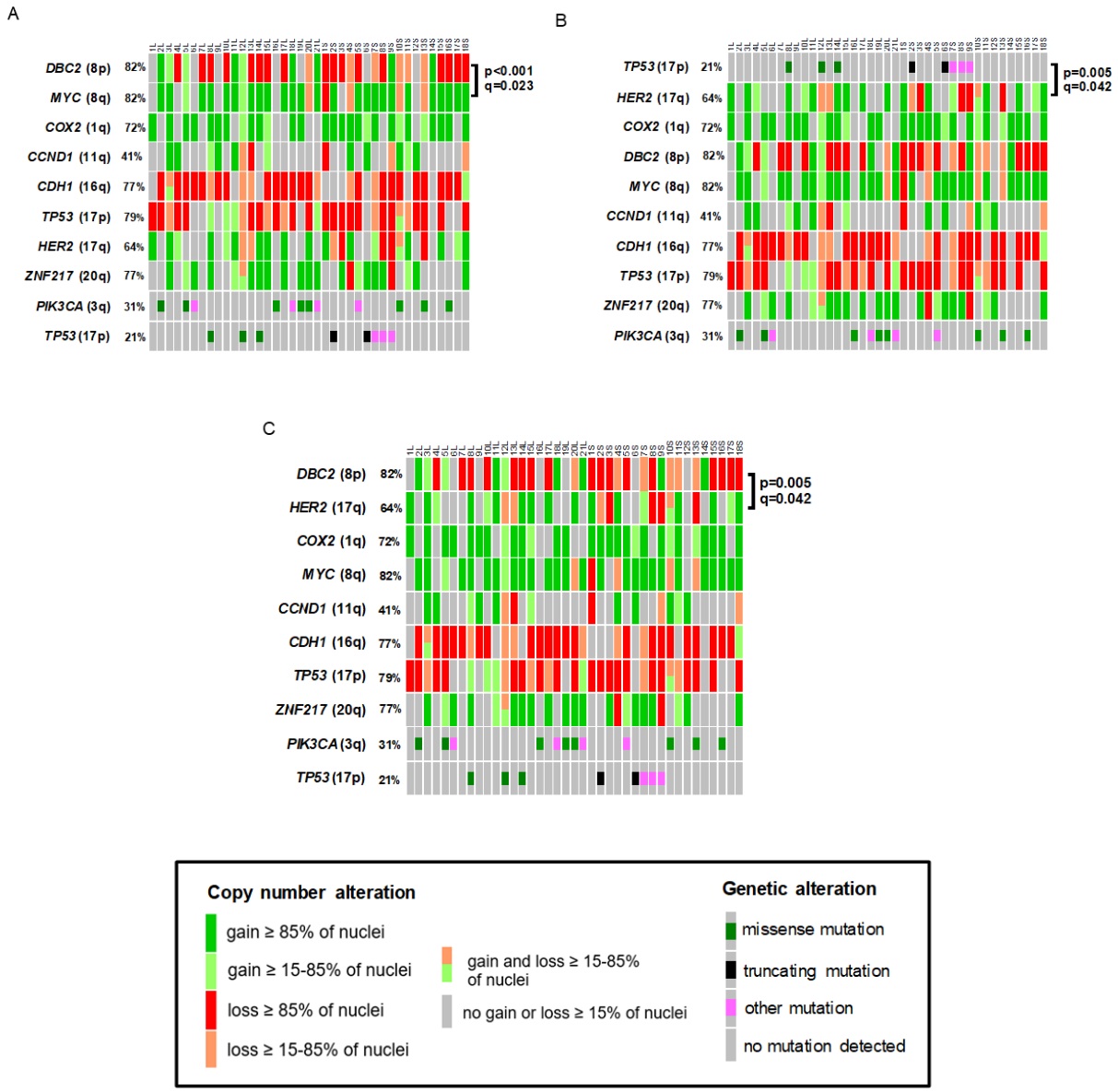

9.3.3 Supplemental Figure S3. Visualization of the significant co-occurrence analysis results of mutations in *TP53* and *PIK3CA* (NGS results) and CNAs (miFISH results). Results are plotted vertically per individual sample (columns) for the entire cohort (n=39) differently sorted by their significant correlations (upper two genes). **(A)** co-occurrence of *DBC2* and *MYC*, **(B)** co-occurrence of *TP53* and *HER2* and **(C)** co-occurrence of *DBC2* and *HER2*.

9.3.4 Supplemental Figure S4: Long survival cases.

Case 1L:

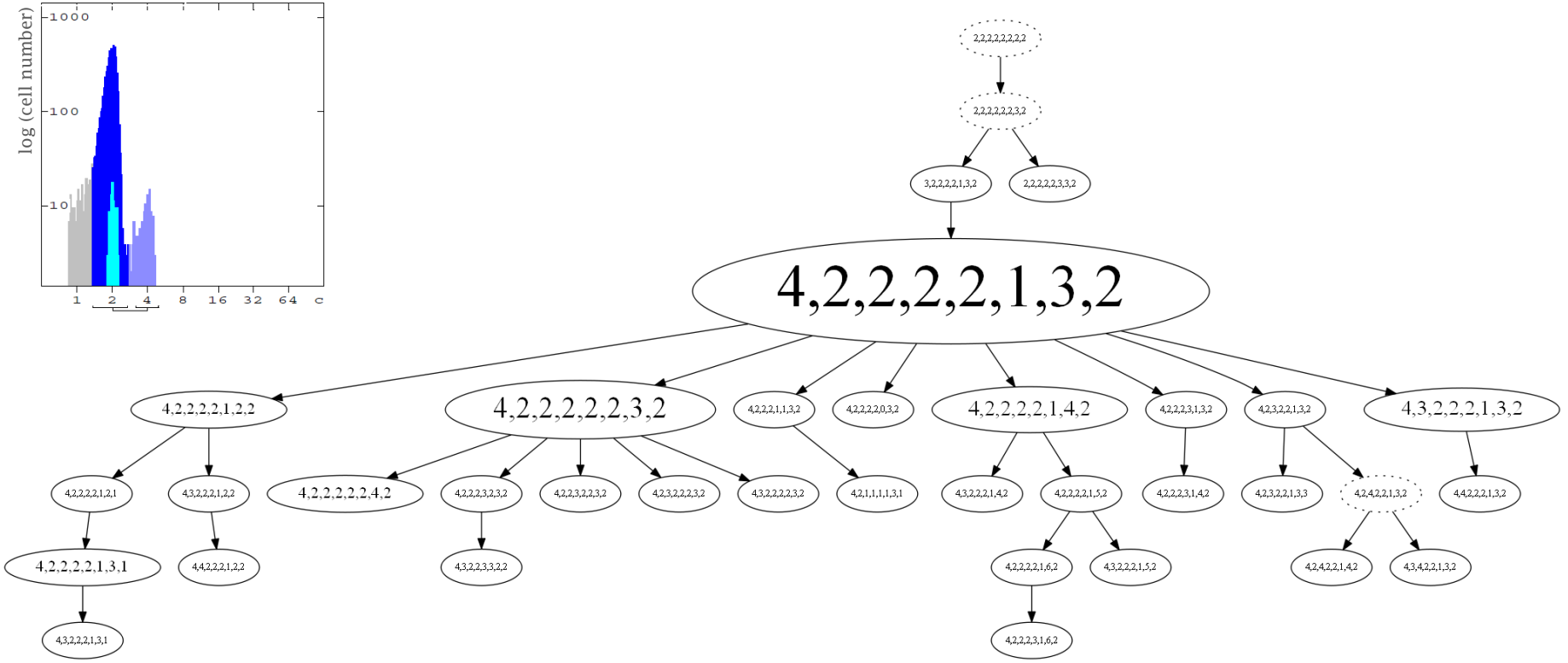

	Locus	250 nuclei					Instability Index: 13.2	Average ploidy: 2.0			
		74,4%	8,4%	4,8%	2	2	8,4%	GENE	GAIN	LOSS	AvgSig
1L	1q							COX2	100%	0%	4,0
	8p							DBC2	7%	0%	2,1
	8q							MYC	2%	0%	2,0
	11q							CCND1	0%	0%	2,0
	16q							CDH1	2%	1%	2,0
	17p							TP53	1%	89%	1,1
	17q							HER2	96%	0%	3,1
	20q							ZNF217	0%	3%	2,0

Case 2L:

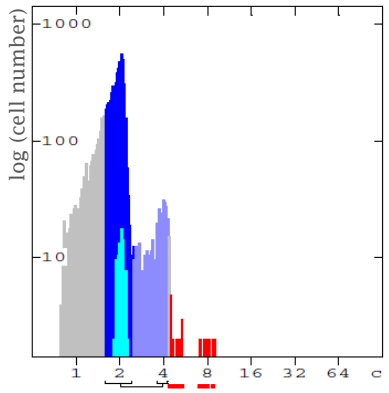

2L	Locus	250 nuclei					Instability Index: 11.2	Average ploidy: 2.1			
		67,6%	8,4%	7,6%	5,6%	10,8%	GENE	GAIN	LOSS	AvgSig
	1q						COX2	0%	1%	2,1
	8p						DBC2	97%	0%	3,1
	8q						MYC	97%	0%	3,1
	11q						CCND1	1%	0%	2,1
	16q						CDH1	0%	98%	1,1
	17p						TP53	0%	89%	1,2
	17q						HER2	11%	2%	2,2
	20q						ZNF217	8%	0%	2,2

Case 3L:

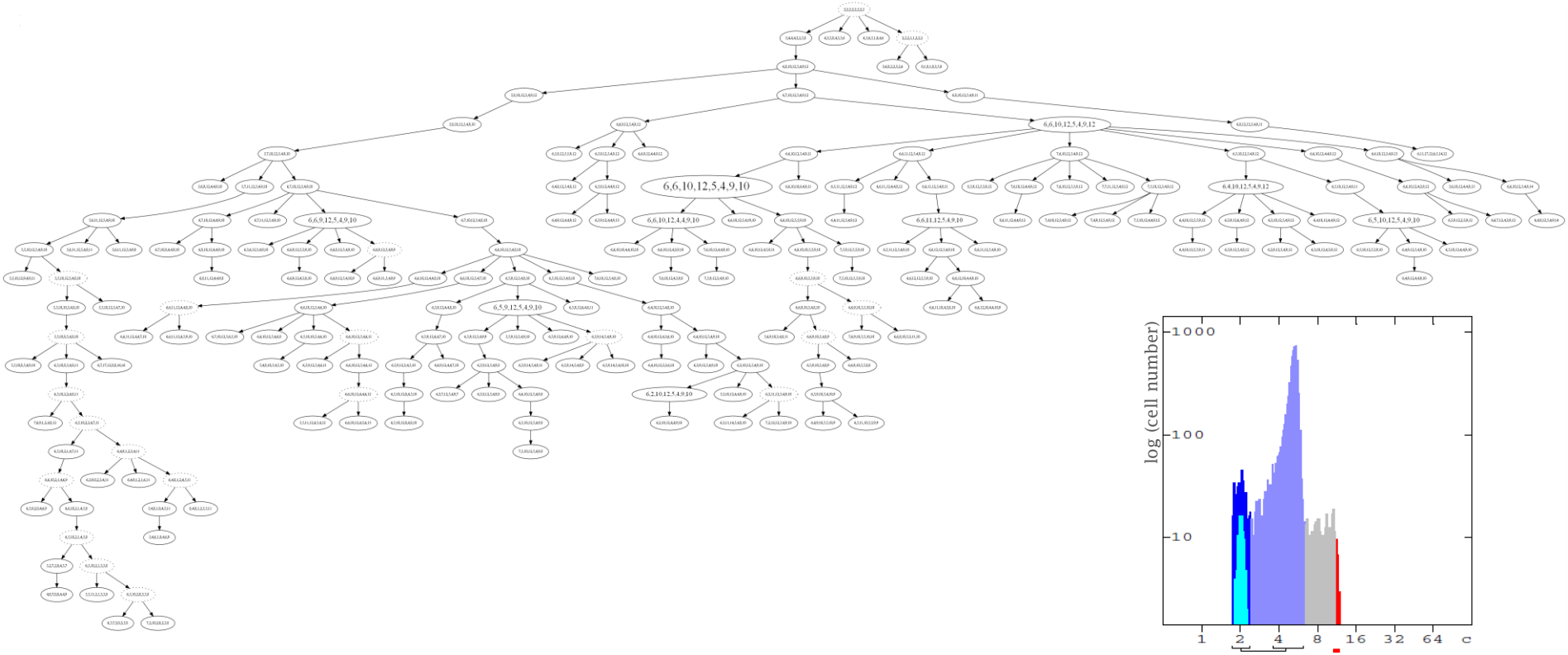

3L	Locus	250 nuclei											Instability Index: 72.4	Average ploidy: 4.6			
		23,6%	14,0%	9,6%	8,8%	8,0%	4,0%	3,6%	3,6%	2,8%	2,4	2,4	17,2%	GENE	GAIN	LOSS	AvgSig
	1q													COX2	92%	1%	6,0
	8p													DBC2	62%	11%	5,3
	8q													MYC	99%	0%	9,7
	11q													CCND1	93%	6%	11,1
	16q													CDH1	20%	22%	4,5
	17p													TP53	3%	62%	4,0
	17q													HER2	97%	0%	8,5
	20q													ZNF217	99%	1%	10,3

Case 4L:

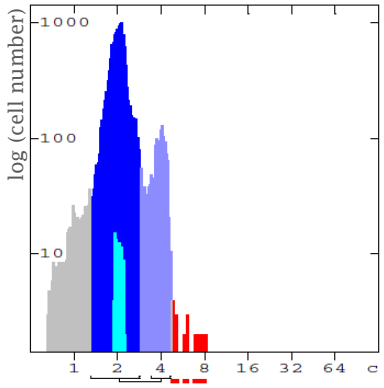

4L	Locus	250 nuclei							Instability Index: 34.8	Average ploidy: 2.6			
		55,2%	10,8%	6,4%	2,8%	2,4	2,4	2,4	17,6%	GENE	GAIN	LOSS	AvgSig
	1q									COX2	1%	5%	2,6
	8p									DBC2	0%	98%	1,3
	8q									MYC	12%	7%	2,7
	11q									CCND1	100%	0%	10,1
	16q									CDH1	0%	95%	1,4
	17p									TP53	0%	98%	1,3
	17q									HER2	81%	5%	3,6
	20q									ZNF217	4%	8%	2,6

Case 6L:

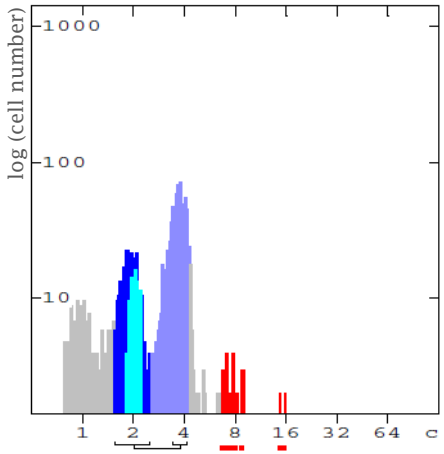

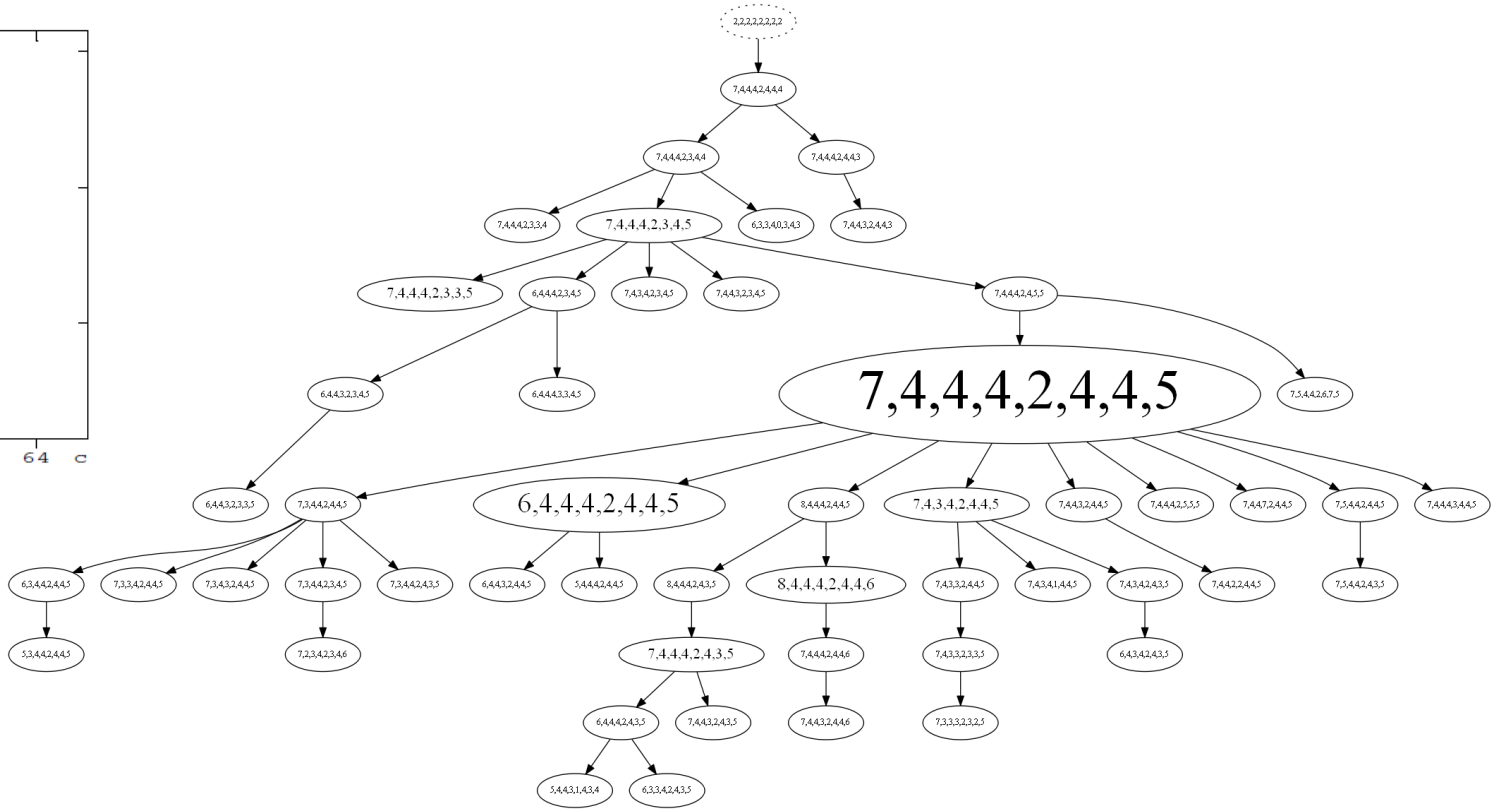

6L	Locus	250 nuclei					Instability Index: 20.8	GENE	GAIN	LOSS	AvgSig
		76,8%	2,4	2,4	2,0	2,0	14,4%				Average ploidy: 4,0
	1q							COX2	100%	0%	6,9
	8p							DBC2	1%	4%	4,0
	8q							MYC	0%	6%	3,9
	11q							CCND1	1%	6%	3,9
	16q							CDH1	0%	100%	2,0
	17p							TP53	1%	7%	3,9
	17q							HER2	2%	7%	3,9
	20q							ZNF217	97%	1%	5,0

Case 8L:

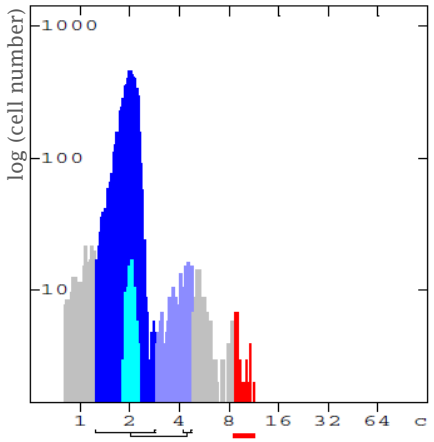

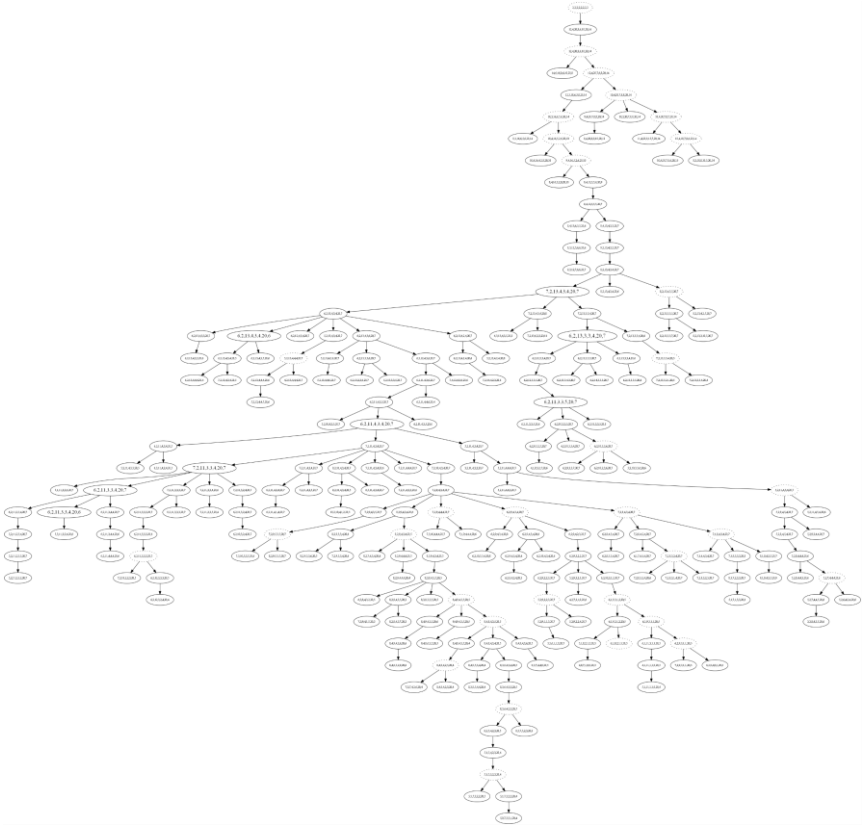

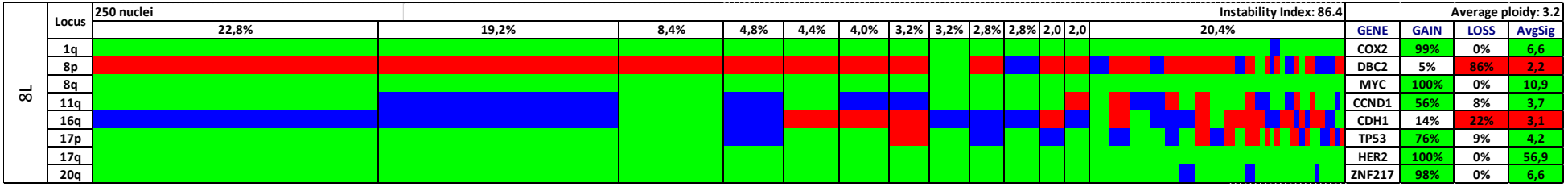

GENE	GAIN	LOSS	AvgSig
COX2	99%	0%	6,6
DBC2	5%	86%	2,2
MYC	100%	0%	10,9
CCND1	56%	8%	3,7
CDH1	14%	22%	3,1
TP53	76%	9%	4,2
HER2	100%	0%	56,9
ZNF217	98%	0%	6,6

Case 9L:

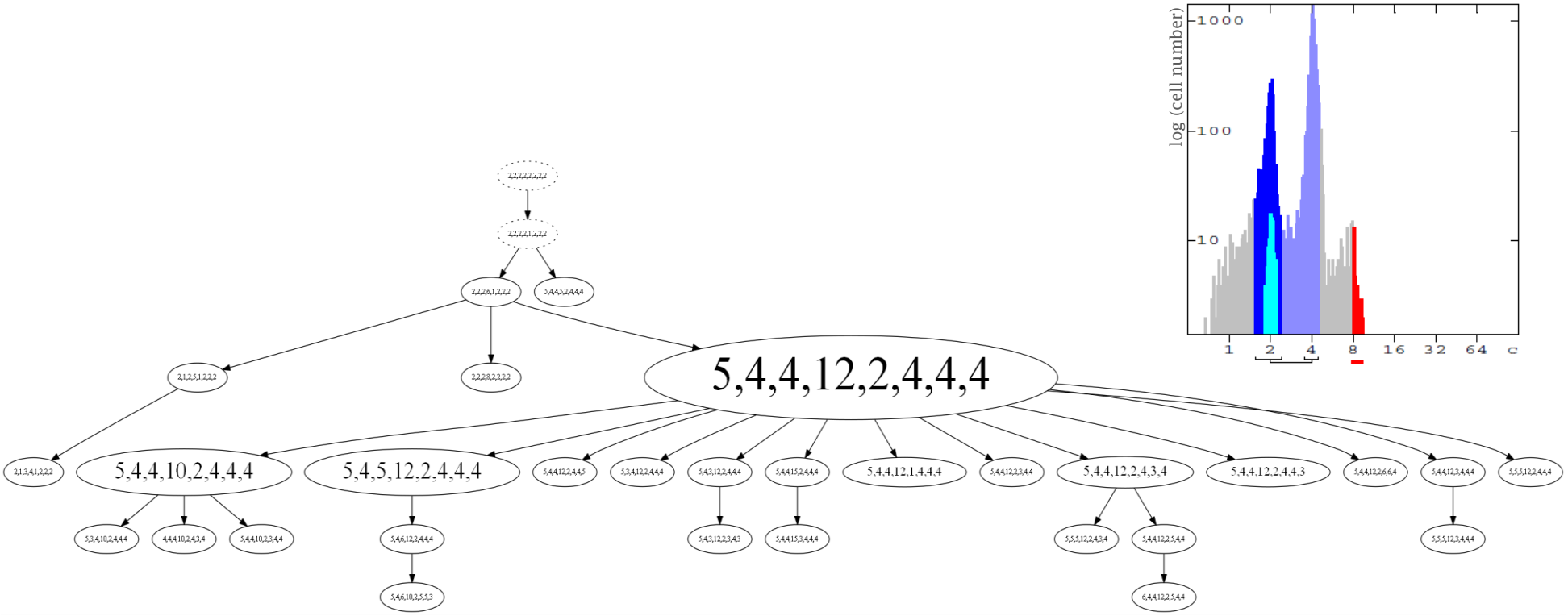

9L	Locus	250 nuclei				Instability Index: 12.0	Average ploidy: 4,0			
		81,6%	6,0%	2,8%	9,6%		GENE	GAIN	LOSS	AvgSig
	1q						COX2	98%	0%	5,0
	8p						DBC2	2%	2%	4,0
	8q						MYC	8%	1%	4,1
	11q						CCND1	100%	0%	11,8
	16q						CDH1	0%	100%	2,0
	17p						TP53	2%	1%	4,0
	17q						HER2	1%	4%	3,9
	20q						ZNF217	0%	2%	4,0

Case 10L:

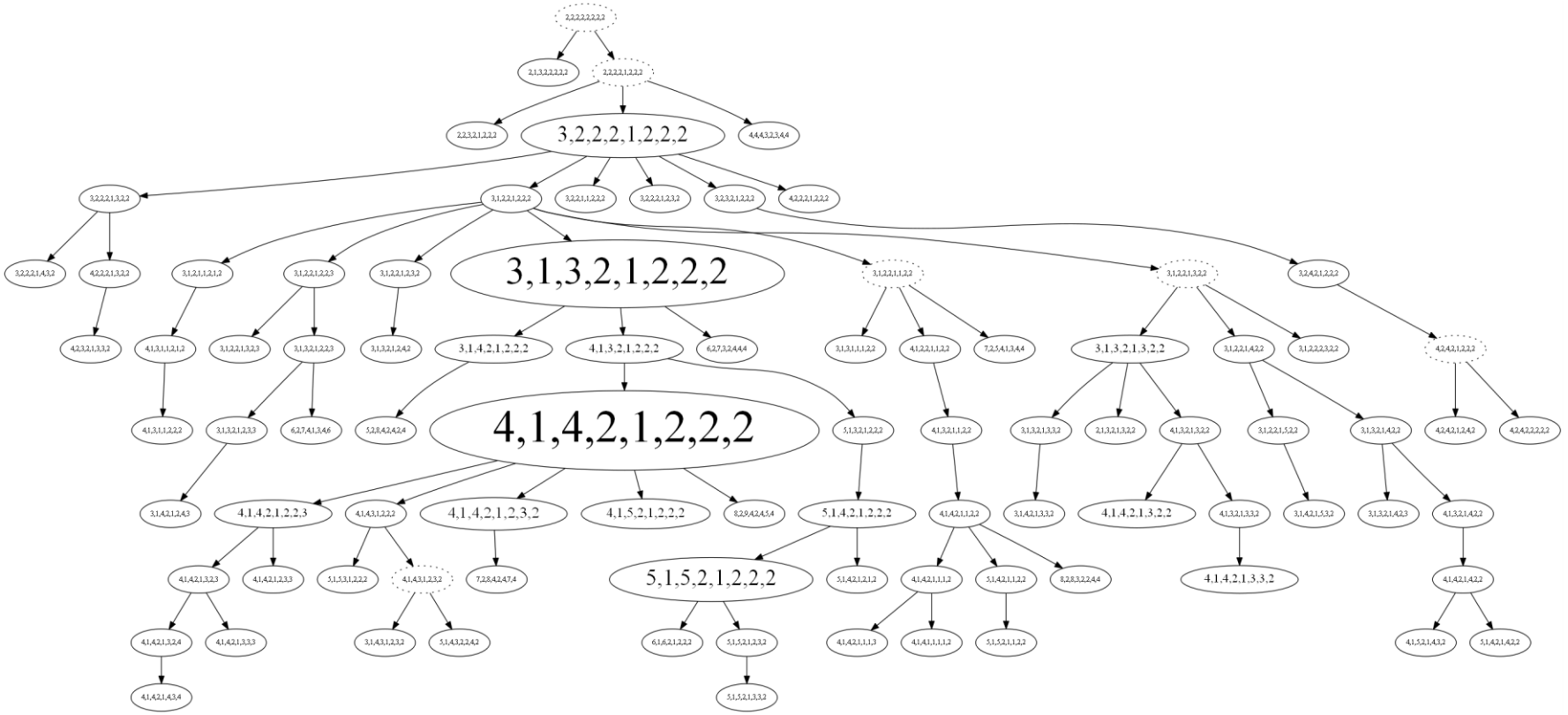

10L	Locus	250 nuclei							Instability Index: 33.2	GENE	GAIN	LOSS	AvgSig
		53,2%	6,4%	5,6%	5,6%	4,0%	2,4	2,0	20,8%				Average ploidy: 2.1
	1q									COX2	99%	0%	3,8
	8p									DBC2	0%	88%	1,2
	8q									MYC	88%	0%	3,7
	11q									CCND1	2%	3%	2,0
	16q									CDH1	0%	98%	1,0
	17p									TP53	16%	5%	2,2
	17q									HER2	16%	3%	2,2
	20q									ZNF217	8%	0%	2,2

Case 11L:

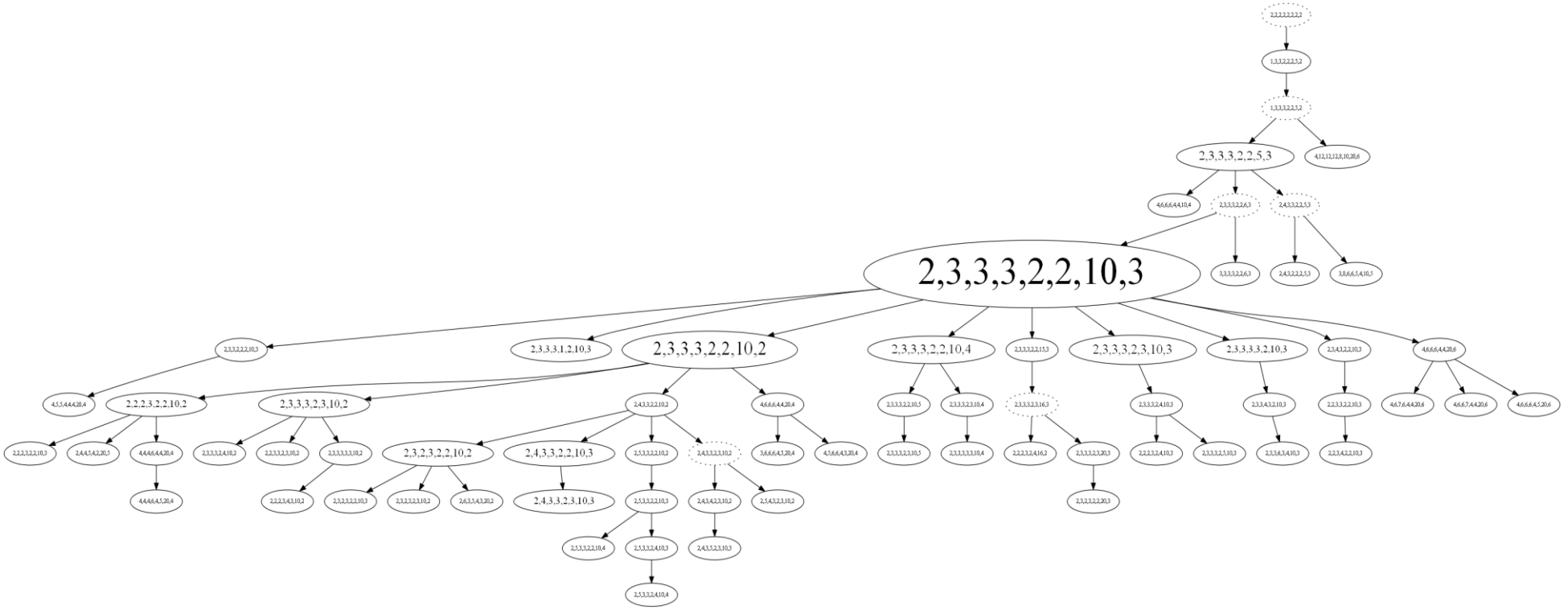

11L	Locus	250 nuclei							Instability Index: 25.6	GENE	GAIN	LOSS	AvgSig
		59,6%	10,0%	8,8%	3,6%	2,4	2,0	2,0	11,6%				Average ploidy: 2.1
	1q									COX2	0%	2%	2,1
	8p									DBC2	94%	0%	3,3
	8q									MYC	92%	0%	3,1
	11q									CCND1	98%	0%	3,2
	16q									CDH1	5%	1%	2,2
	17p									TP53	19%	0%	2,4
	17q									HER2	100%	0%	10,6
	20q									ZNF217	78%	0%	3,0

Case 12L:

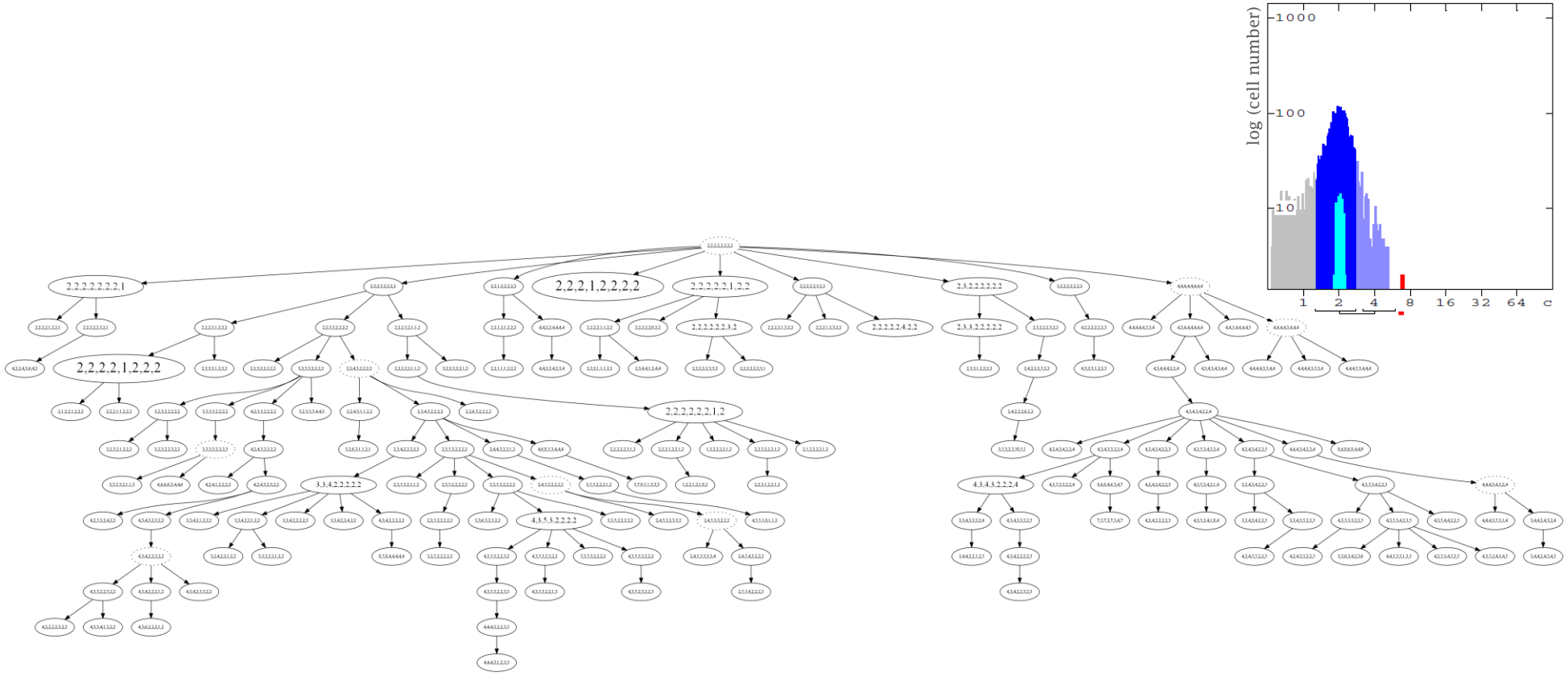

12L	Locus	250 nuclei											Instability Index: 62.8	Average ploidy: 2.512			
		7.6%	5.2%	4.4%	4.4%	3.6%	2.4	2.0	2.0	2.0	2.0	2.0	62.4%	GENE	GAIN	LOSS	AvgSig
	1q													COX2	32%	4%	2.9
	8p													DBC2	22%	10%	2.7
	8q													MYC	48%	3%	3.3
	11q													CCND1	11%	21%	2.4
	16q													CDH1	8%	33%	2.2
	17p													TP53	10%	36%	2.3
	17q													HER2	5%	40%	2.1
	20q													ZNF217	18%	17%	2.6

Case 13L:

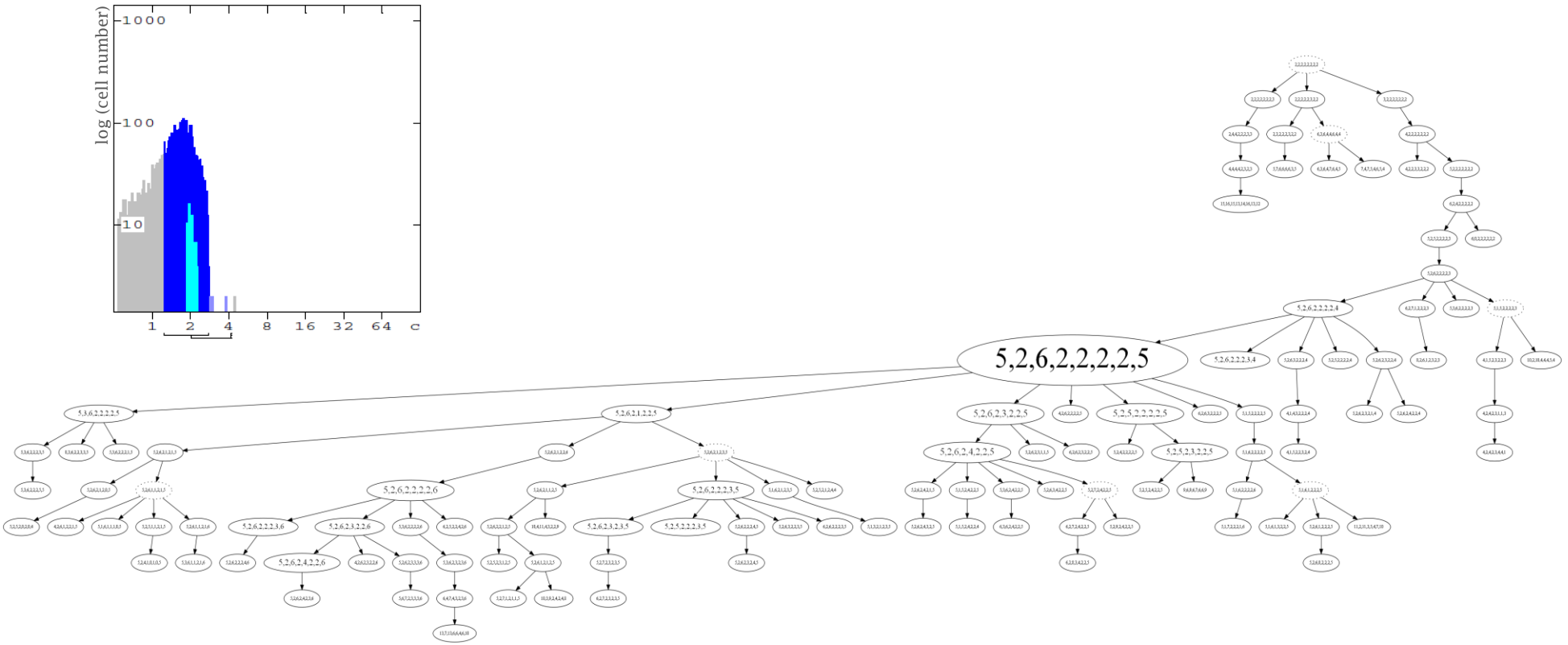

	Locus	250 nuclei							Instability Index: 44.8	Average ploidy: 3.084			
		42,8%	12,8%	9,2%	7,6%	2,8%	2,4	2,0	20,4%	GENE	GAIN	LOSS	AvgSig
13L	1q									COX2	98%	1%	5,1
	8p									DBC2	3%	88%	2,2
	8q									MYC	95%	0%	5,8
	11q									CCND1	2%	91%	2,1
	16q									CDH1	14%	64%	2,5
	17p									TP53	2%	90%	2,2
	17q									HER2	4%	78%	2,3
	20q									ZNF217	90%	2%	5,0

Case 14L:

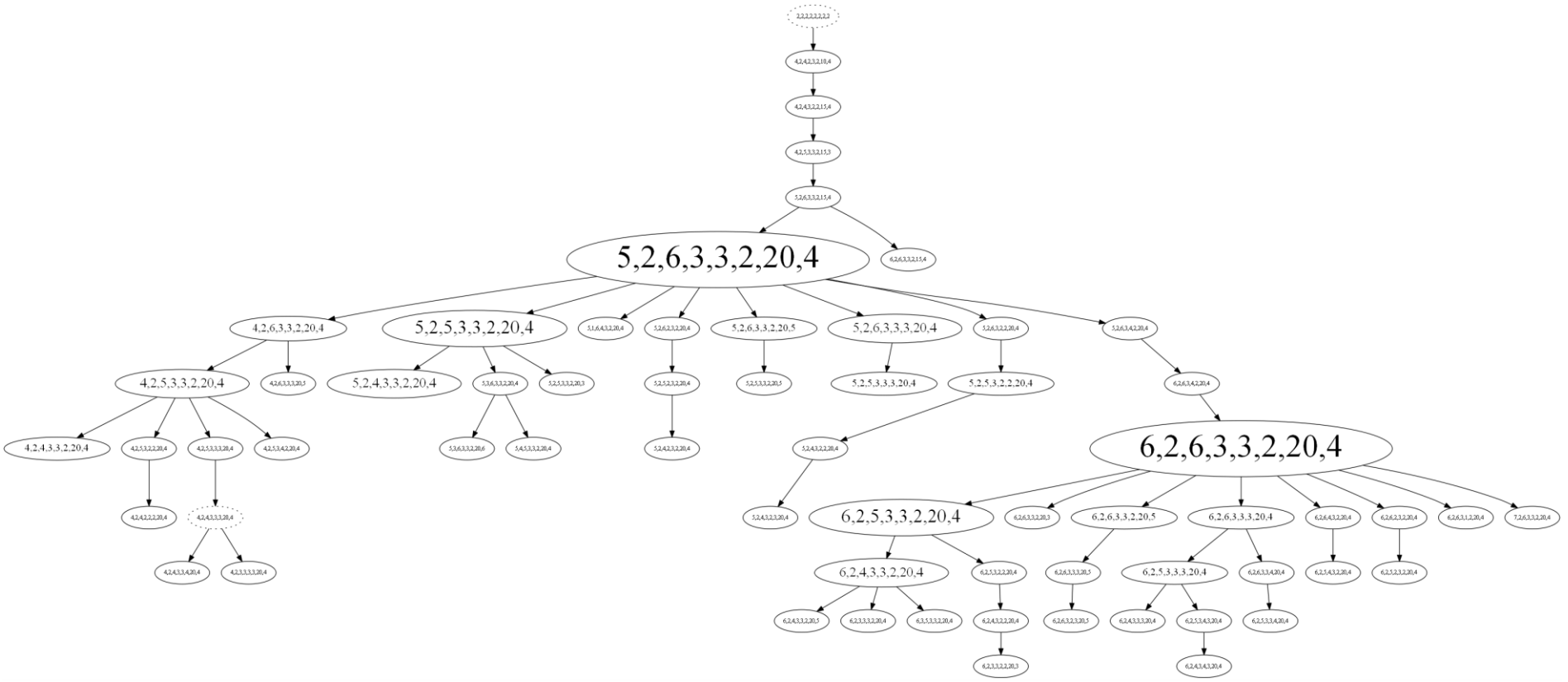

14L	Locus	250 nuclei					Instability Index: 26.4	Average ploidy: 3.0			
		71,6%	10,8%	4,0%	2,8%	10,8%		GENE	GAIN	LOSS	AvgSig
	1q							COX2	100%	0%	5,3
	8p							DBC2	0%	98%	2,0
	8q							MYC	99%	0%	5,3
	11q							CCND1	1%	3%	3,0
	16q							CDH1	2%	6%	3,0
	17p							TP53	2%	85%	2,2
	17q							HER2	100%	0%	30,2
	20q							ZNF217	98%	0%	4,0

Case 15L:

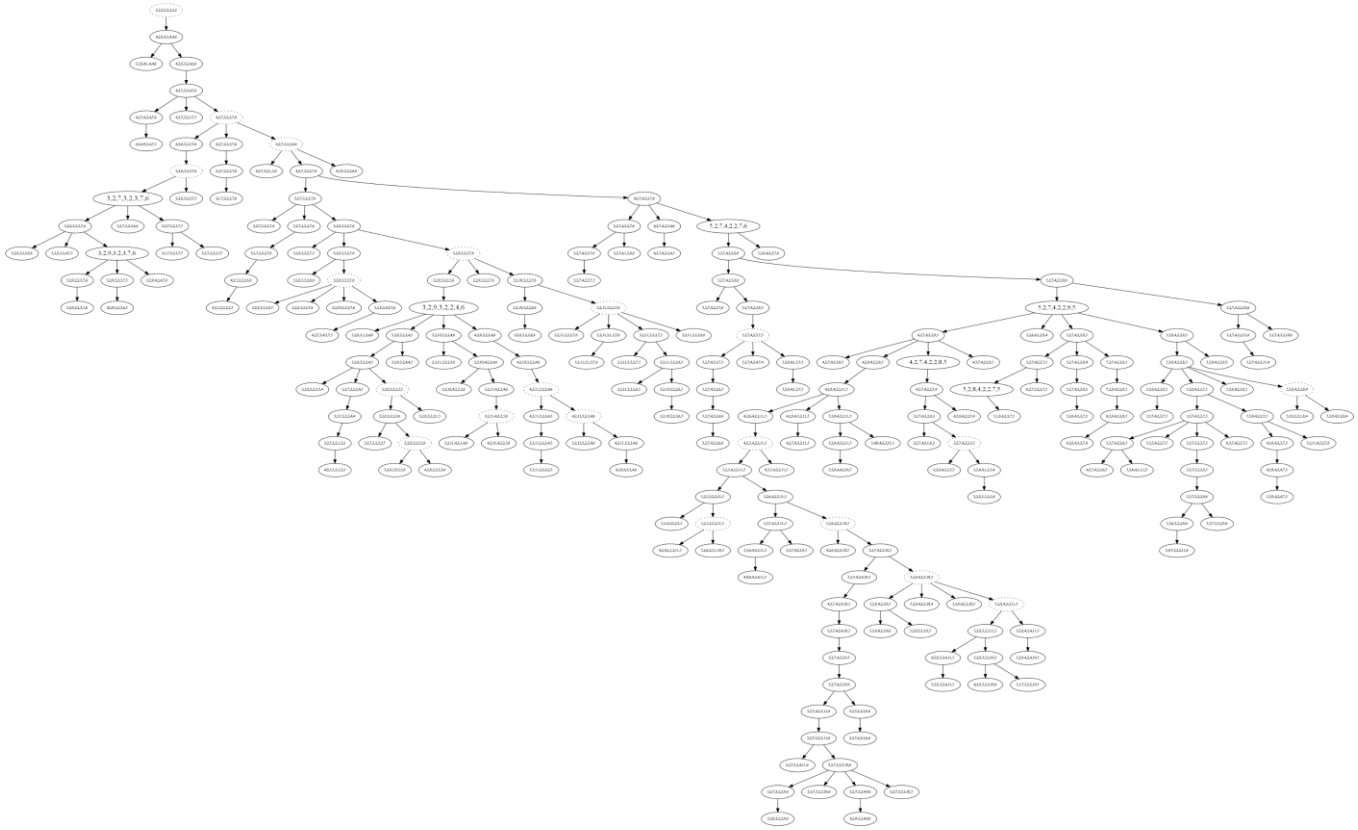

	Locus	250 nuclei													Instability Index: 86.8	GENE	GAIN	LOSS	AvgSig
		15,2%	10,8%	10,8%	5,2%	4,4%	4,0%	3,2%	3,2%	2,8%	2,8%	2,8%	2,4	2,0	30,4%				
15L	1q															COX2	54%	5%	3,9
	8p															DBC2	1%	82%	2,2
	8q															MYC	100%	0%	7,8
	11q															CCND1	50%	8%	3,5
	16q															CDH1	1%	89%	2,1
	17p															TP53	9%	60%	2,5
	17q															HER2	96%	1%	7,3
	20q															ZNF217	96%	1%	5,4

Average ploidy: 3.0

Case 16L:

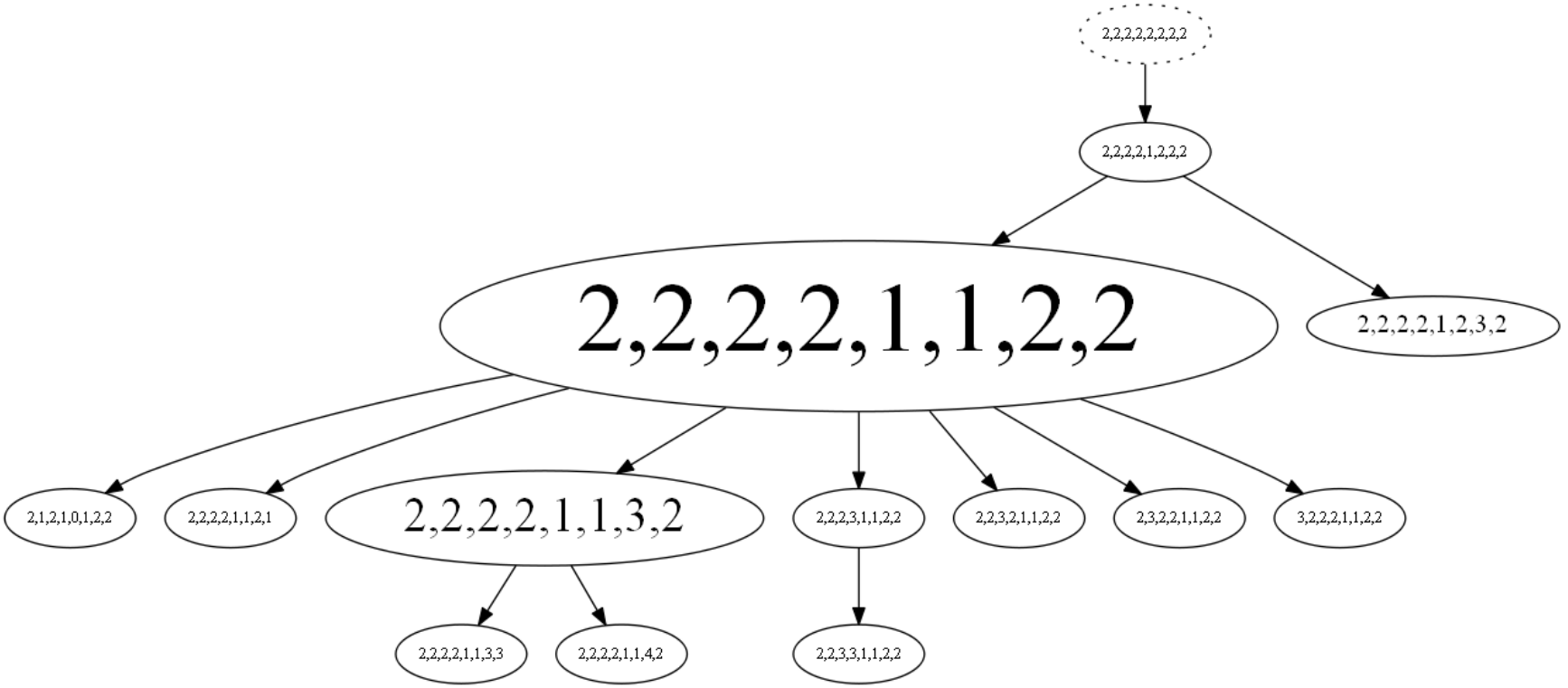

16L

Locus	250 nuclei			Instability Index: 5.2		Average ploidy: 2.0			
	88,0%			5,6%	6,4%	GENE	GAIN	LOSS	AvgSig
1q						COX2	0%	0%	2,0
8p						DBC2	1%	0%	2,0
8q						MYC	1%	0%	2,0
11q						CCND1	1%	0%	2,0
16q						CDH1	0%	100%	1,0
17p						TP53	0%	98%	1,0
17q						HER2	7%	0%	2,1
20q						ZNF217	0%	1%	2,0

Case 17L:

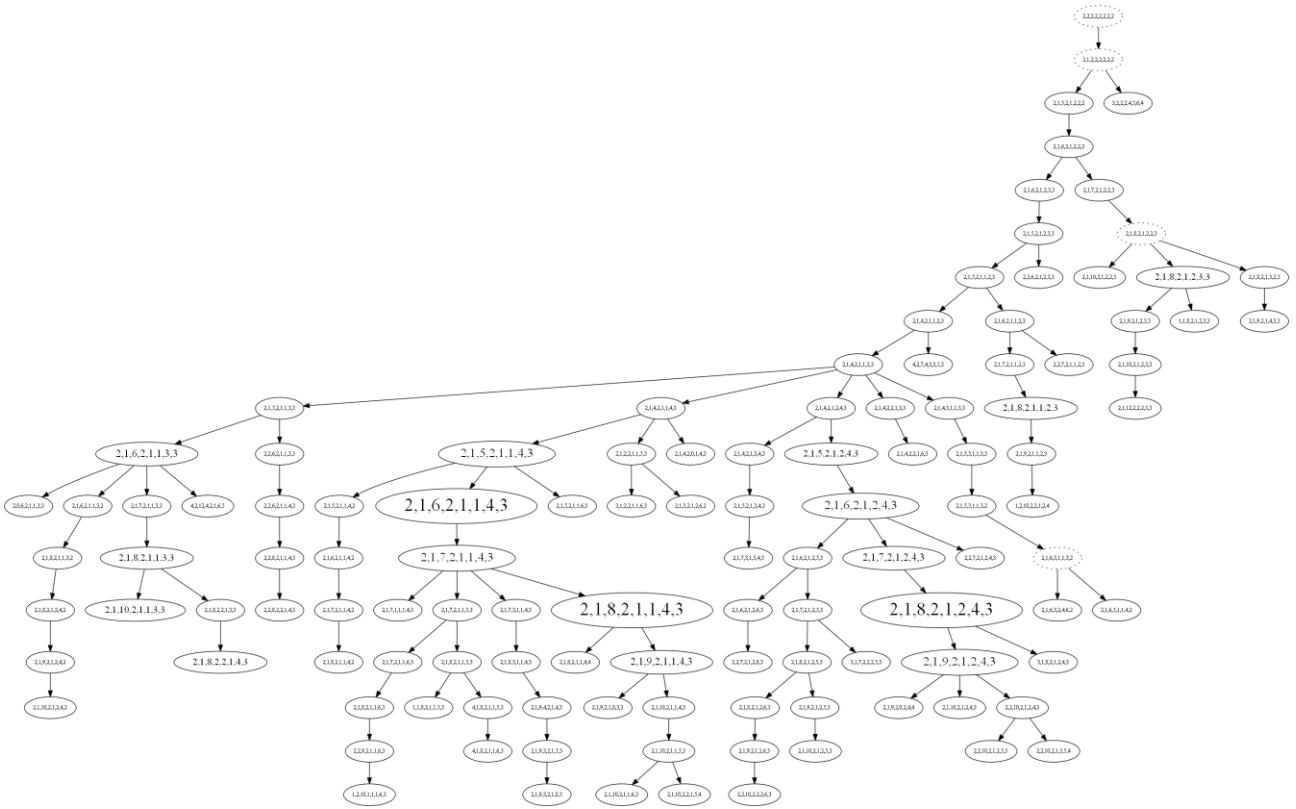

17L	Locus	250 nuclei									Instability Index: 45.2	Average ploidy: 2.1			
		38,4%	21,6%	6,4%	5,2%	3,6%	3,2%	2,4	2,0	2,0	15,2%	GENE	GAIN	LOSS	AvgSig
	1q											COX2	2%	8%	2,0
	8p											DBC2	0%	93%	1,1
	8q											MYC	99%	0%	7,2
	11q											CCND1	4%	7%	2,1
	16q											CDH1	0%	92%	1,1
	17p											TP53	3%	67%	1,4
	17q											HER2	92%	0%	3,9
	20q											ZNF217	86%	0%	3,0

Case 18L:

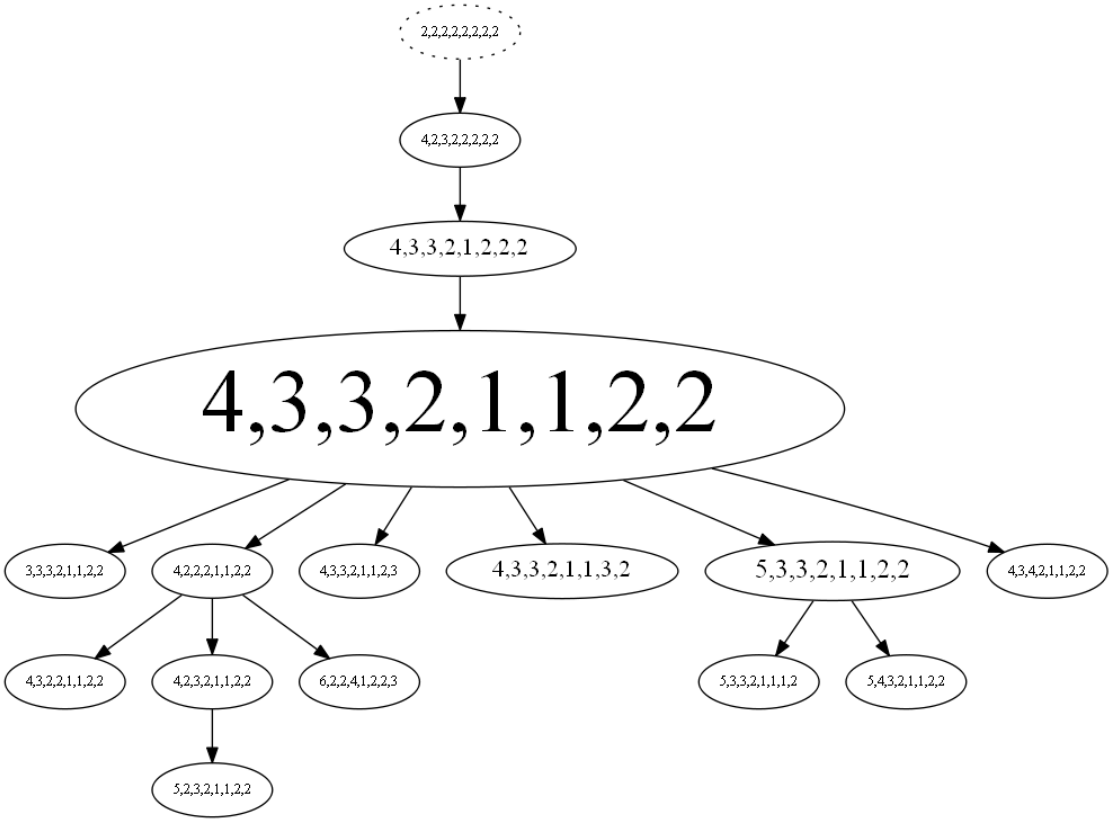

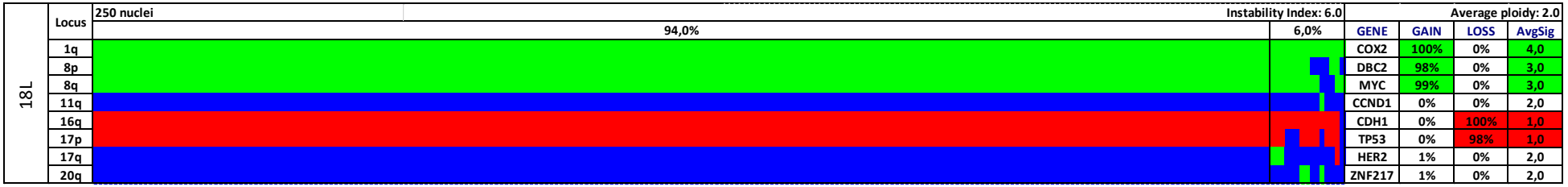

GENE	GAIN	LOSS	AvgSig
COX2	100%	0%	4,0
DBC2	98%	0%	3,0
MYC	99%	0%	3,0
CCND1	0%	0%	2,0
CDH1	0%	100%	1,0
TP53	0%	98%	1,0
HER2	1%	0%	2,0
ZNF217	1%	0%	2,0

Case 19L:

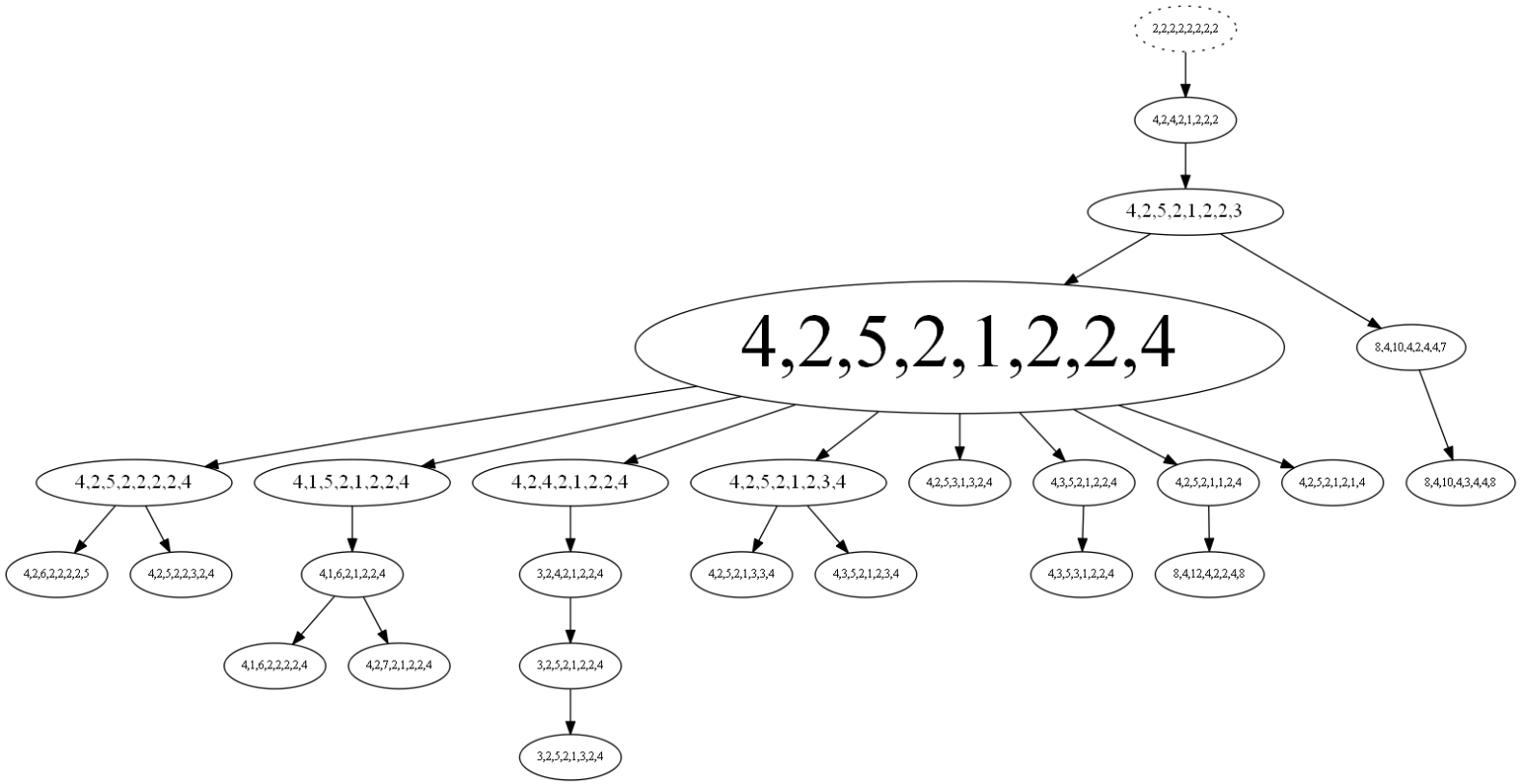
2,2,2,2,2,2,2,2
4,2,4,2,1,2,2,2
4,2,5,2,1,2,2,3
4,2,5,2,1,2,2,4
8,4,10,4,2,4,4,7
4,2,5,2,2,2,2,2,4
4,1,5,2,1,2,2,4
4,2,4,2,1,2,2,4
4,2,5,2,1,2,3,4
4,2,5,3,1,3,2,4
4,3,5,2,1,2,2,4
4,2,5,2,1,1,2,4
4,2,5,2,1,2,1,4
8,4,10,4,3,4,4,8
4,2,6,2,2,2,2,5
4,2,5,2,2,3,2,4
4,1,6,2,1,2,2,4
3,2,4,2,1,2,2,4
4,2,5,2,1,3,3,4
4,3,5,2,1,2,3,4
4,3,5,3,1,2,2,4
8,4,12,4,2,2,4,8
4,1,6,2,2,2,2,4
4,2,7,2,1,2,2,4
3,2,5,2,1,2,2,4
3,2,5,2,1,3,2,4

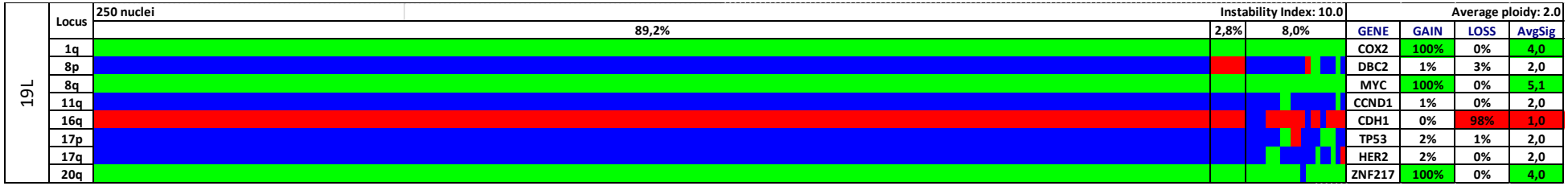
19L
Locus
250 nuclei
Instability Index: 10.0
Average ploidy: 2.0
89,2%
2,8%
8,0%
1q
8p
8q
11q
16q
17p
17q
20q
GENE GAIN LOSS AvgSig
COX2 100% 0% 4,0
DBC2 1% 3% 2,0
MYC 100% 0% 5,1
CCND1 1% 0% 2,0
CDH1 0% 98% 1,0
TP53 2% 1% 2,0
HER2 2% 0% 2,0
ZNF217 100% 0% 4,0

Case 20L:

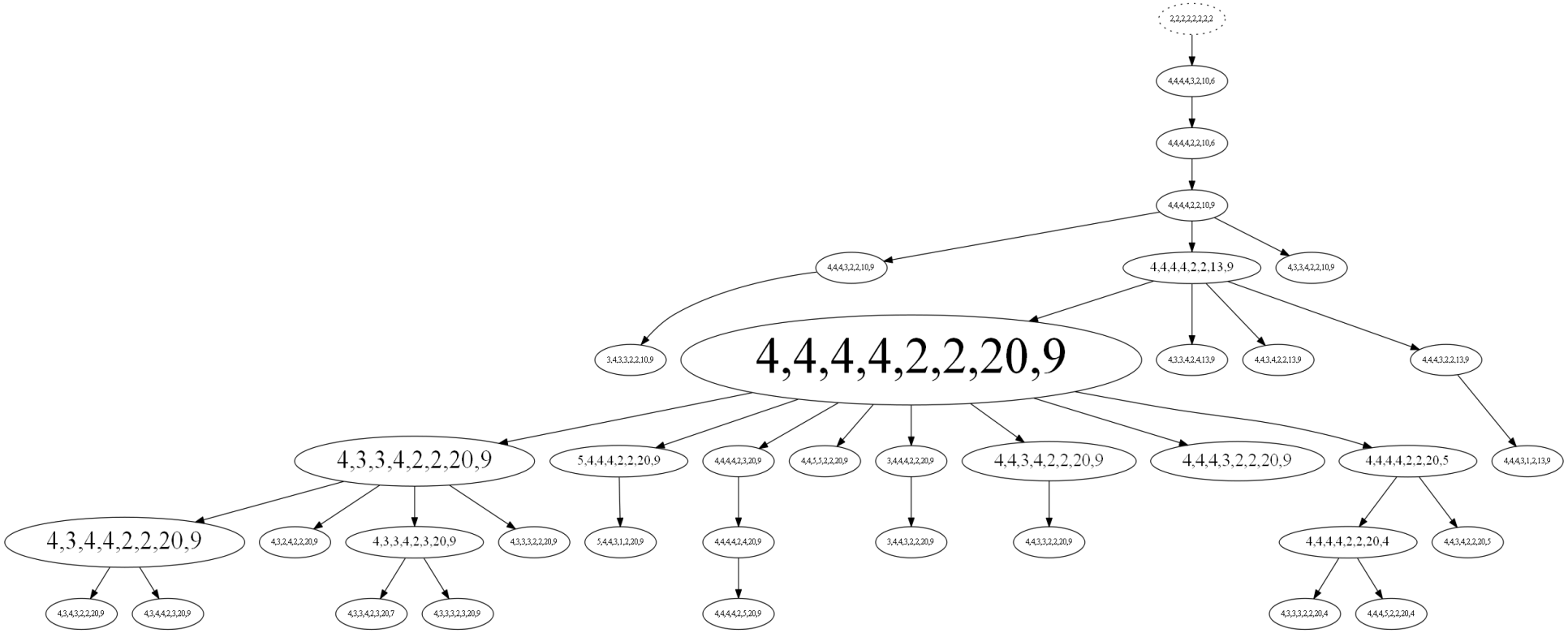

20L

Locus	250 nuclei						Instability Index: 14.8	Average ploidy: 4.0			
	61,2%	12,0%	6,8%	5,6%	5,6%	8,8%	GENE	GAIN	LOSS	AvgSig
1q							COX2	2%	1%	4,0
8p							DBC2	0%	21%	3,8
8q							MYC	0%	20%	3,8
11q							CCND1	1%	9%	3,9
16q							CDH1	0%	100%	2,0
17p							TP53	0%	99%	2,1
17q							HER2	100%	0%	19,5
20q							ZNF217	98%	0%	8,8

Case 21L:

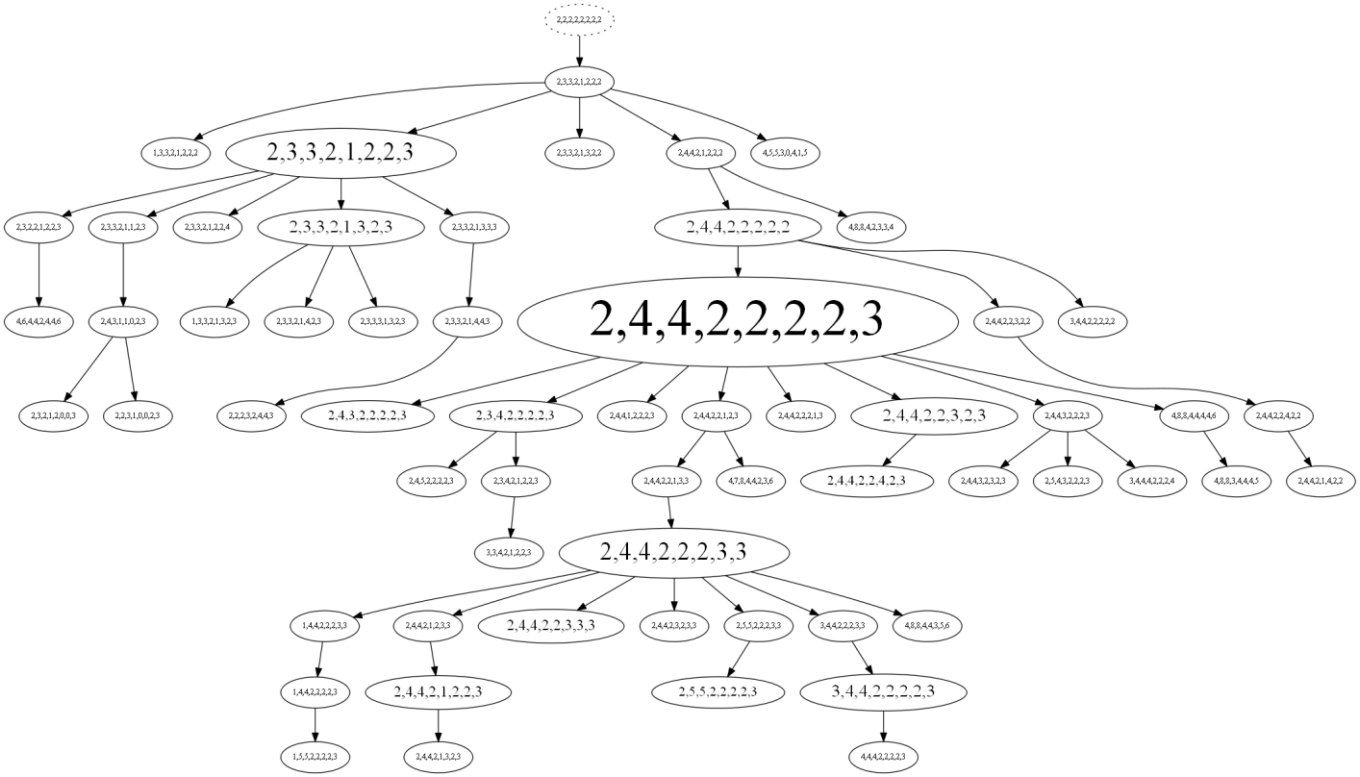

21L

Locus	250 nuclei								Instability Index: 24.0	Average ploidy: 2.1			
	44,0%	10,4%	6,0%	5,2%	4,8%	4,8%	3,2%	2,8%	18,8%	GENE	GAIN	LOSS	AvgSig
1q										COX2	6%	2%	2,1
8p										DBC2	99%	0%	3,9
8q										MYC	98%	0%	3,9
11q										CCND1	3%	3%	2,1
16q										CDH1	0%	24%	1,8
17p										TP53	17%	4%	2,2
17q										HER2	13%	2%	2,2
20q										ZNF217	92%	0%	3,0

9.3.5 Supplemental Figure S5: Short survival cases.

Case 1S:

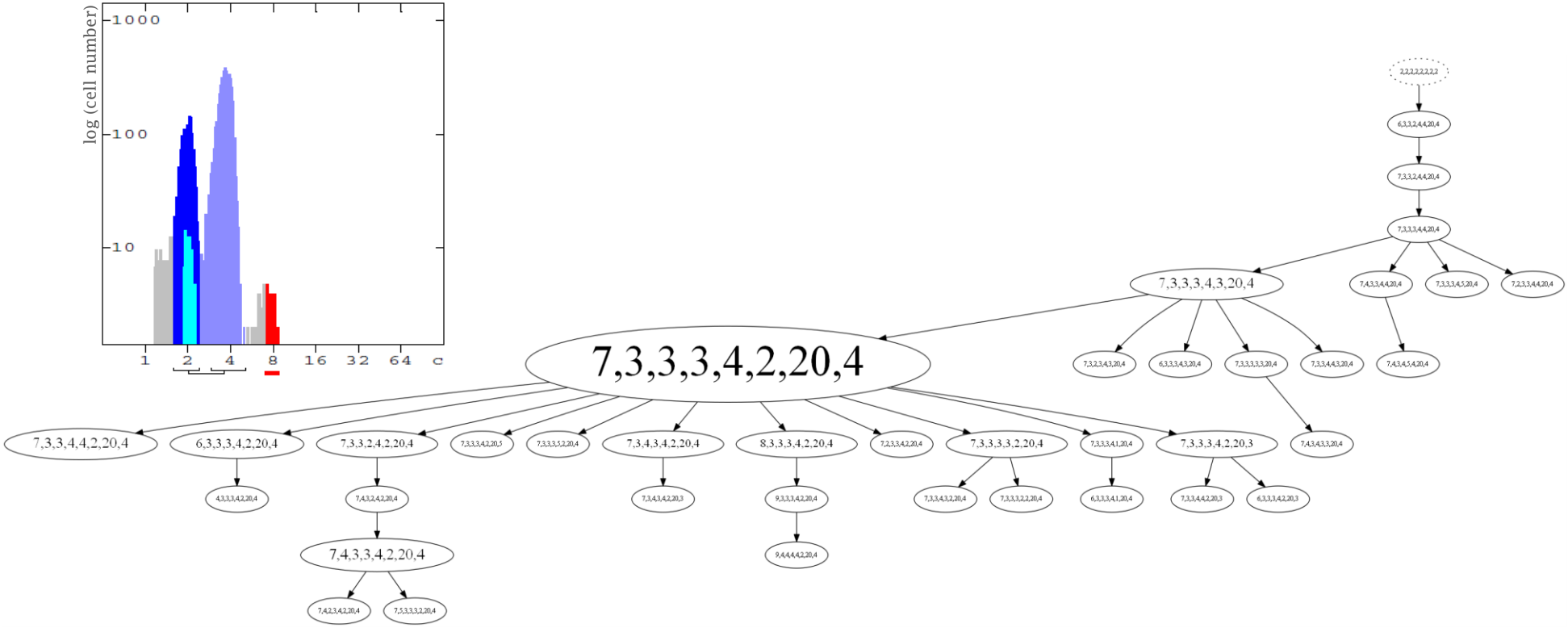

1S	Locus	250 nuclei							Instability Index: 17.2				Average ploidy: 4.0			
		77,2%						5,6%	3,6%	3,2%	2,0	2,0	6,4%	GENE	GAIN	LOSS	AvgSig
	1q													COX2	100%	0%	7,0
	8p													DBC2	0%	92%	3,1
	8q													MYC	0%	98%	3,0
	11q													CCND1	0%	94%	3,0
	16q													CDH1	1%	4%	4,0
	17p													TP53	0%	97%	2,1
	17q													HER2	100%	0%	29,7
	20q													ZNF217	1%	3%	4,0

Case 2S:

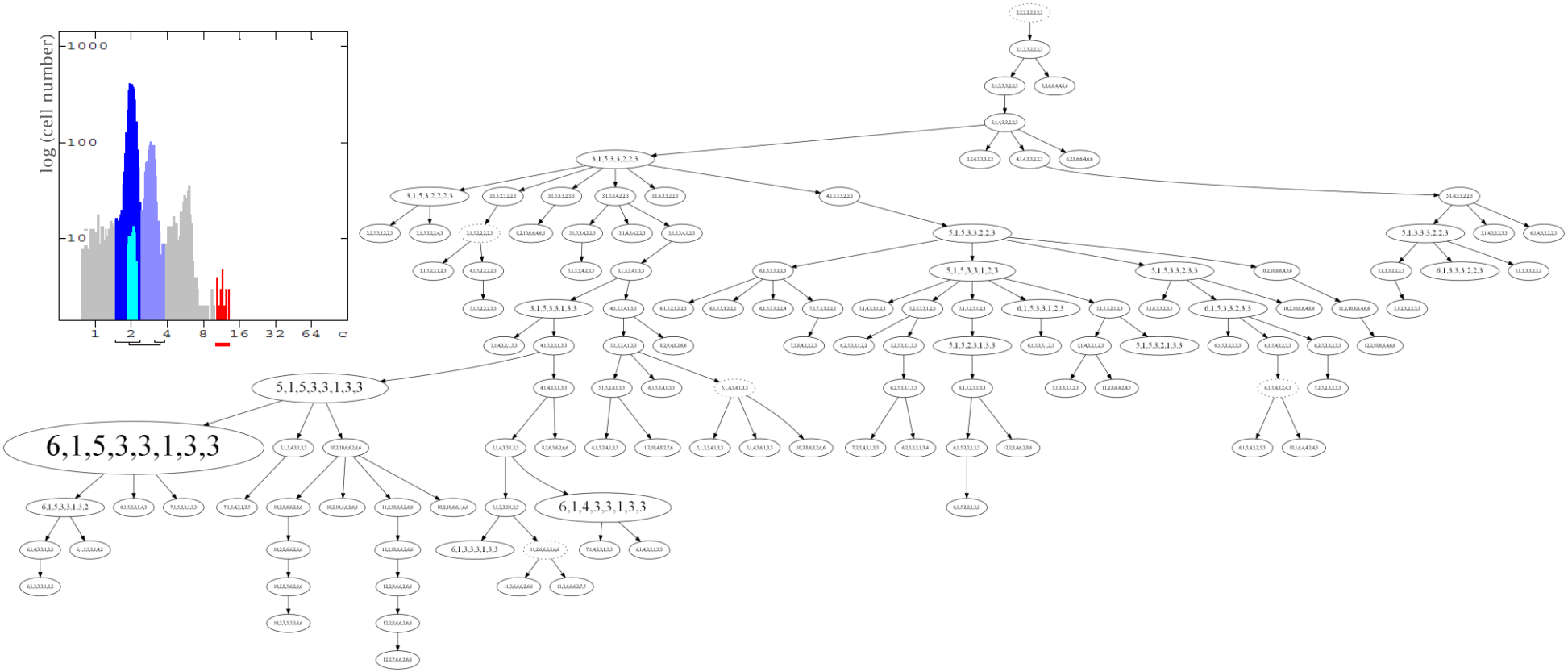

	Locus	250 nuclei										Instability Index: 47.6	Average ploidy: 3.3			
		45,2%	10,8%	3,6%	3,2%	3,2%	2,4	2,4	2,4	2,0	2,0	22,8%	GENE	GAIN	LOSS	AvgSig
2S	1q												COX2	89%	0%	5,9
	8p												DBC2	0%	99%	1,2
	8q												MYC	91%	0%	5,2
	11q												CCND1	3%	10%	3,3
	16q												CDH1	8%	10%	3,3
	17p												TP53	0%	99%	1,4
	17q												HER2	4%	27%	3,1
	20q												ZNF217	2%	6%	3,3

Case 3S:

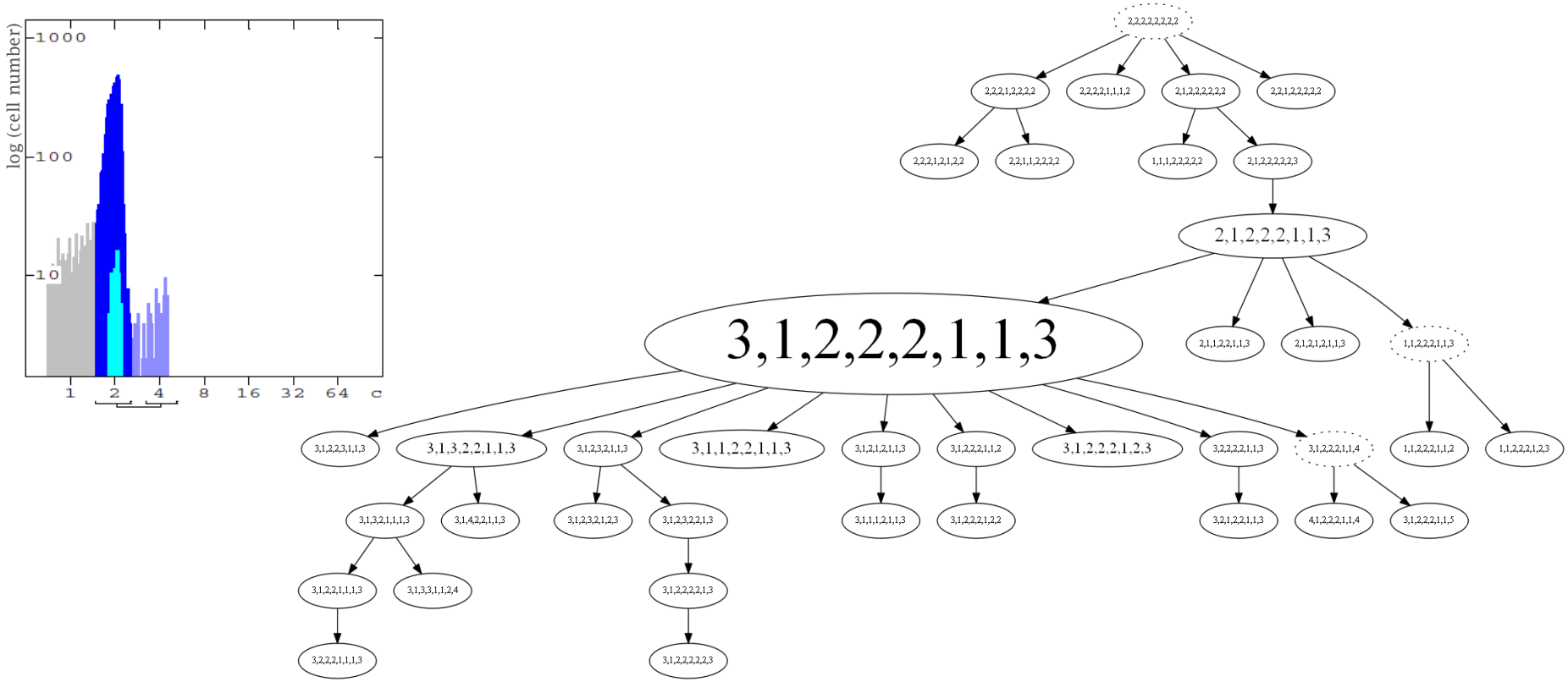

3S	Locus	250 nuclei					Instability Index: 14.4	GENE	GAIN	LOSS	AvgSig
		76,0%	4,4%	2,4	2,0	15,2%					Average ploidy: 2.0
	1q							COX2	90%	1%	2,9
	8p							DBC2	0%	97%	1,0
	8q							MYC	2%	5%	2,0
	11q							CCND1	2%	3%	2,0
	16q							CDH1	1%	2%	2,0
	17p							TP53	0%	96%	1,0
	17q							HER2	0%	93%	1,1
	20q							ZNF217	96%	0%	3,0

Case 4S:

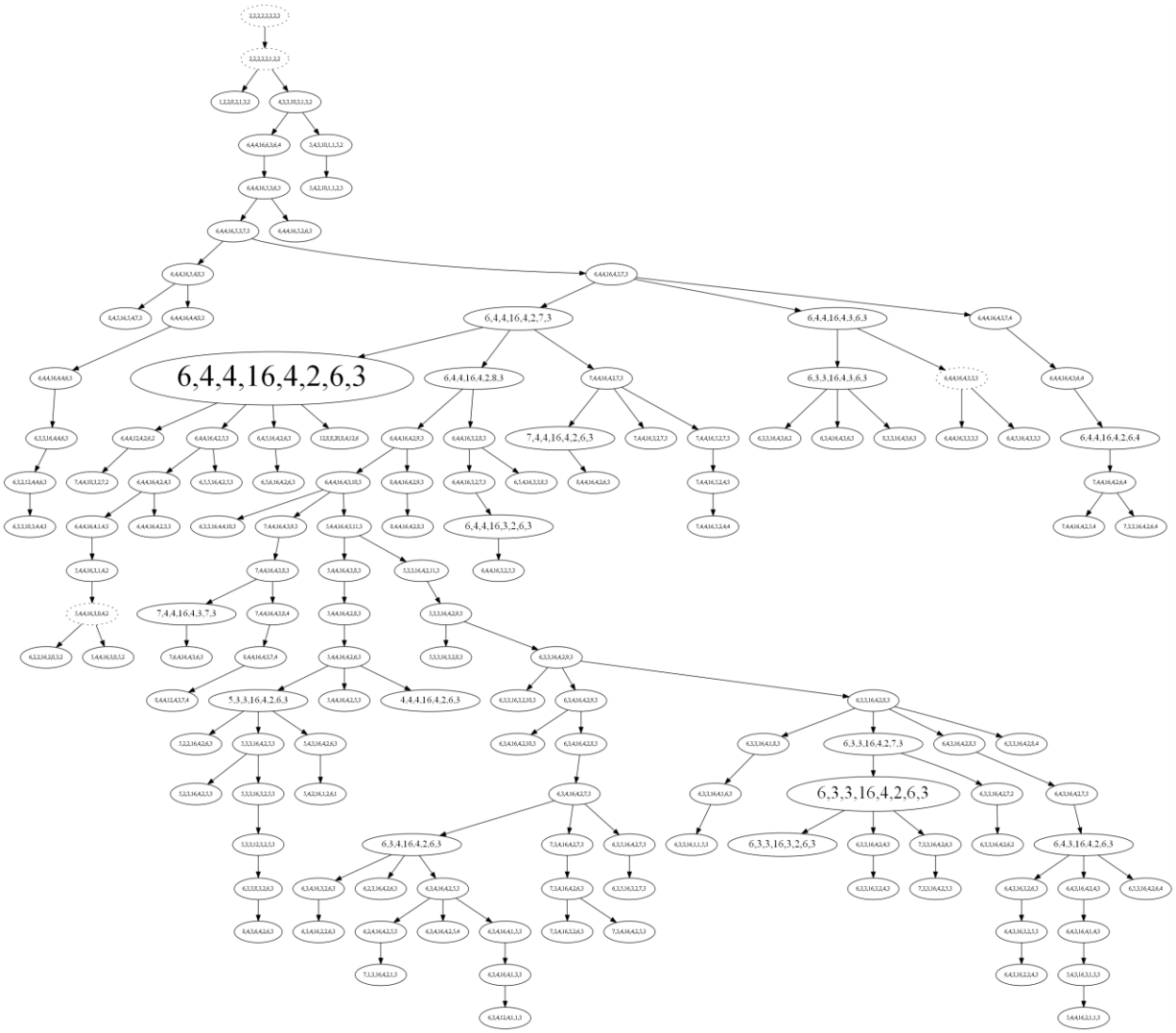
6,4,4,16,4,2,6,3
6,4,4,16,4,2,7,3
6,4,4,16,4,3,6,3
6,4,4,16,4,2,8,3
7,4,4,16,4,2,6,3
6,3,3,16,4,3,6,3
6,4,4,16,4,2,6,4
6,4,4,16,3,2,6,3
7,4,4,16,4,2,7,3
5,3,3,16,4,2,6,3
4,4,4,16,4,2,6,3
6,3,3,16,4,2,7,3
6,3,3,16,4,2,6,3
6,3,4,16,4,2,6,3

Case 5S:

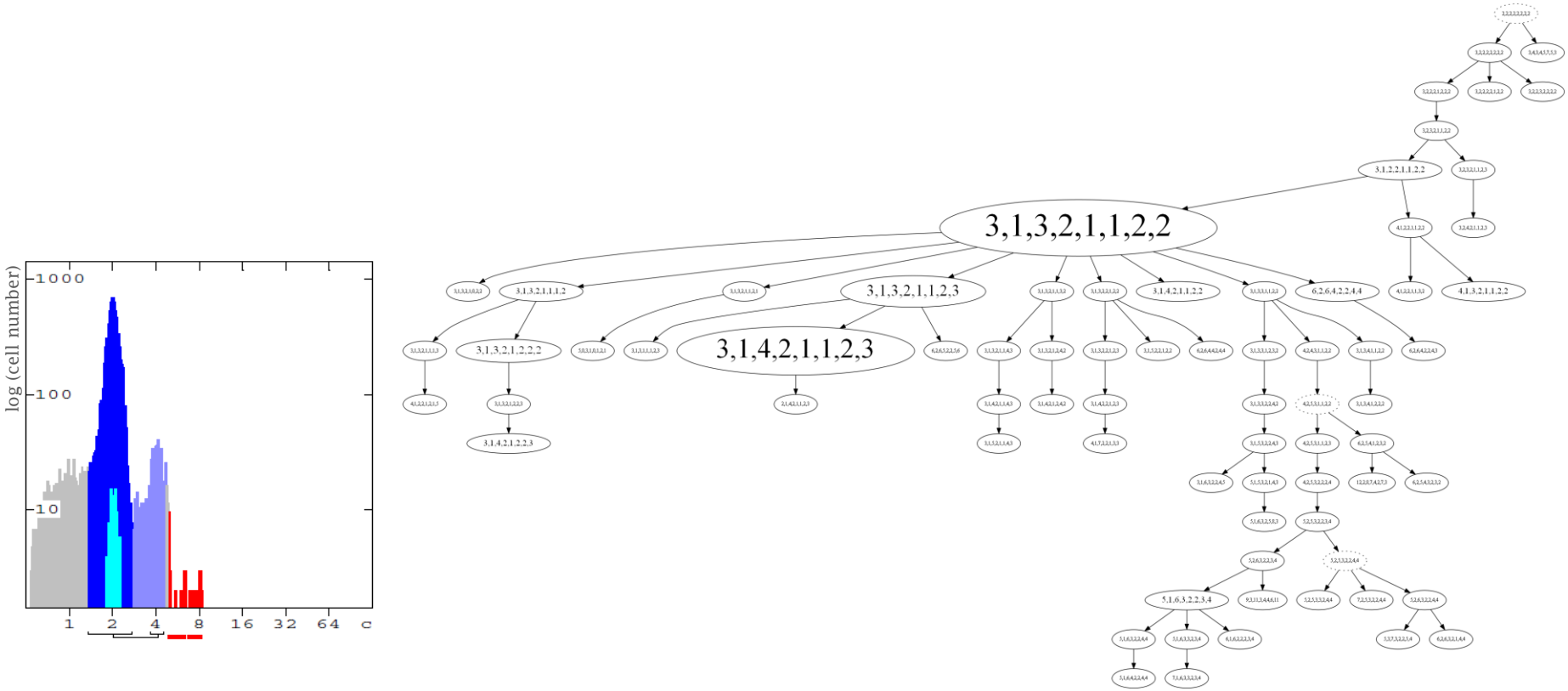

	Locus	250 nuclei							Instability Index: 28.4	Average ploidy: 2.3			
		36,0%	29,6%	3,6%	3,2%	2,4	2,0	23,2%		GENE	GAIN	LOSS	AvgSig
5S	1q									COX2	98%	0%	3,4
	8p									DBC2	0%	96%	1,1
	8q									MYC	95%	0%	3,6
	11q									CCND1	5%	8%	2,2
	16q									CDH1	0%	95%	1,2
	17p									TP53	1%	89%	1,2
	17q									HER2	7%	7%	2,3
	20q									ZNF217	39%	4%	2,6

Case 6S:

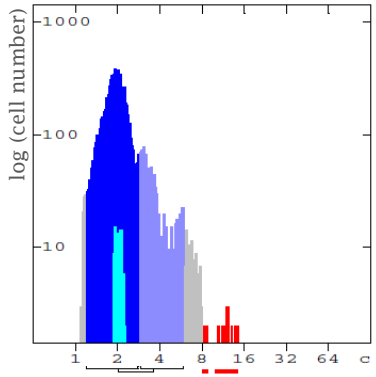

	Locus	250 nuclei							Instability Index: 27.2	Average ploidy: 2.1			
		48,4%	27,2%	2,8%	2,8%	2,4	2,0	14,4%	GENE	GAIN	LOSS	AvgSig
6S	1q								COX2	67%	0%	2,8
	8p								DBC2	4%	3%	2,1
	8q								MYC	100%	0%	6,2
	11q								CCND1	98%	1%	4,0
	16q								CDH1	1%	6%	2,0
	17p								TP53	4%	3%	2,1
	17q								HER2	5%	3%	2,1
	20q								ZNF217	96%	0%	3,1

Case 7S:

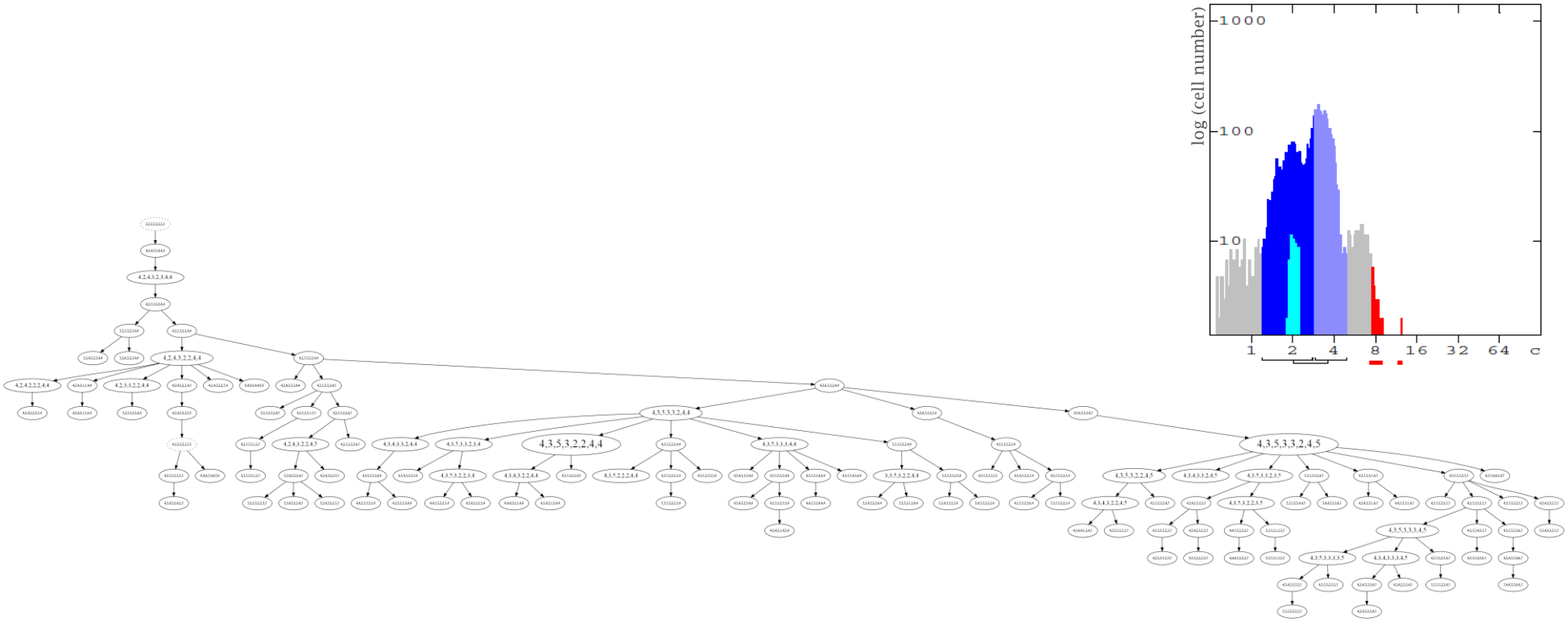

	Locus	250 nuclei										Instability Index: 51.2				Average ploidy: 3.0	
		18,4%	16,8%	7,2%	6,8%	4,0%	3,6%	2,4	2,4	2,4	2,0	34,0%	GENE	GAIN	LOSS	AvgSig
7S	1q												COX2	88%	0%	3,9
	8p												DBC2	5%	21%	2,8
	8q												MYC	94%	0%	4,6
	11q												CCND1	2%	9%	2,9
	16q												CDH1	2%	53%	2,5
	17p												TP53	4%	76%	2,2
	17q												HER2	80%	3%	3,9
	20q												ZNF217	97%	0%	4,5

Case 8S:

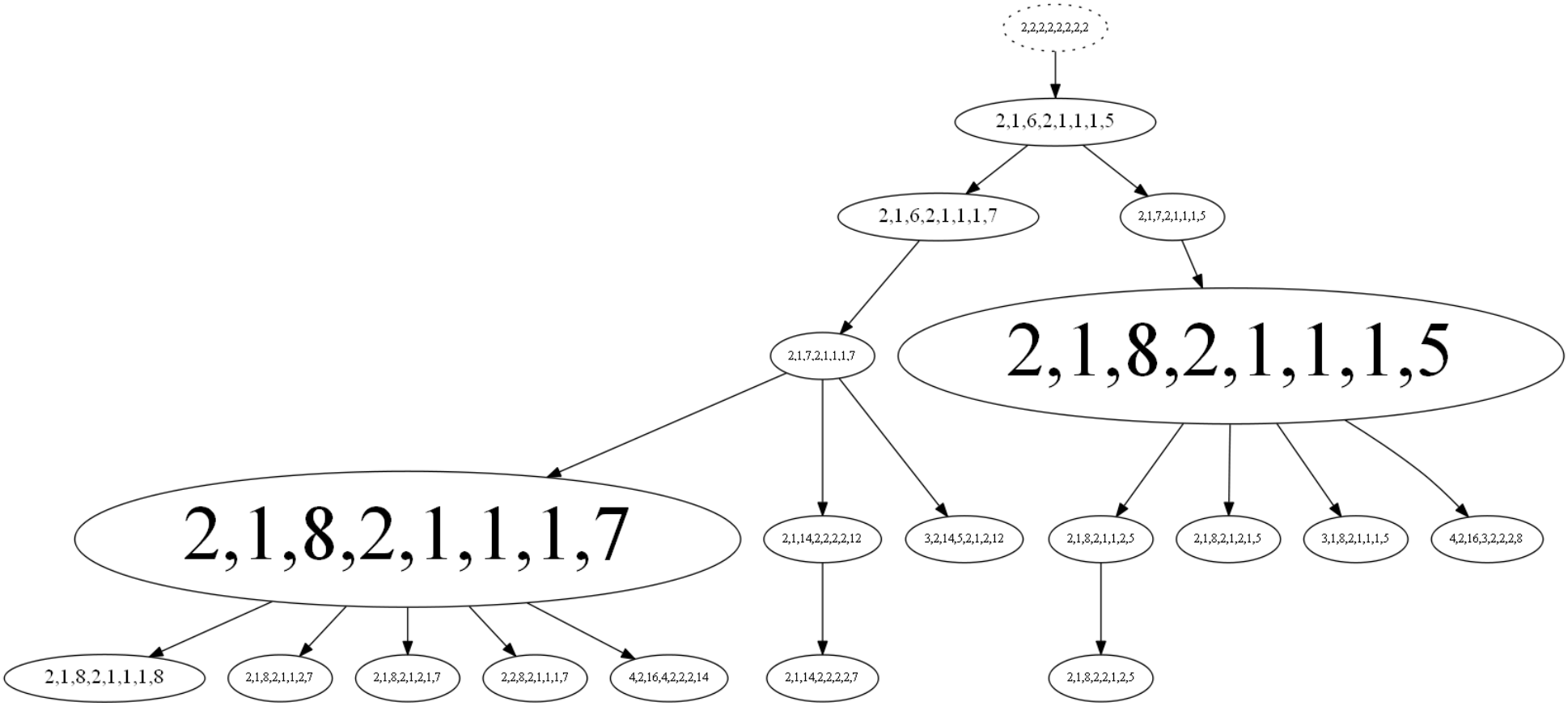
2,2,2,2,2,2,2
2,1,6,2,1,1,1,5
2,1,6,2,1,1,1,7
2,1,7,2,1,1,1,5
2,1,7,2,1,1,1,7
2,1,8,2,1,1,1,5
2,1,8,2,1,1,1,7
2,1,14,2,2,2,2,12
3,2,14,5,2,1,2,12
2,1,8,2,1,1,2,5
2,1,8,2,1,2,1,5
3,1,8,2,1,1,1,5
4,2,16,3,2,2,2,8
2,1,8,2,1,1,1,8
2,1,8,2,1,1,2,7
2,1,8,2,1,2,1,7
2,2,8,2,1,1,1,7
4,2,16,4,2,2,2,14
2,1,14,2,2,2,2,7
2,1,8,2,2,1,2,5

Case 9S:

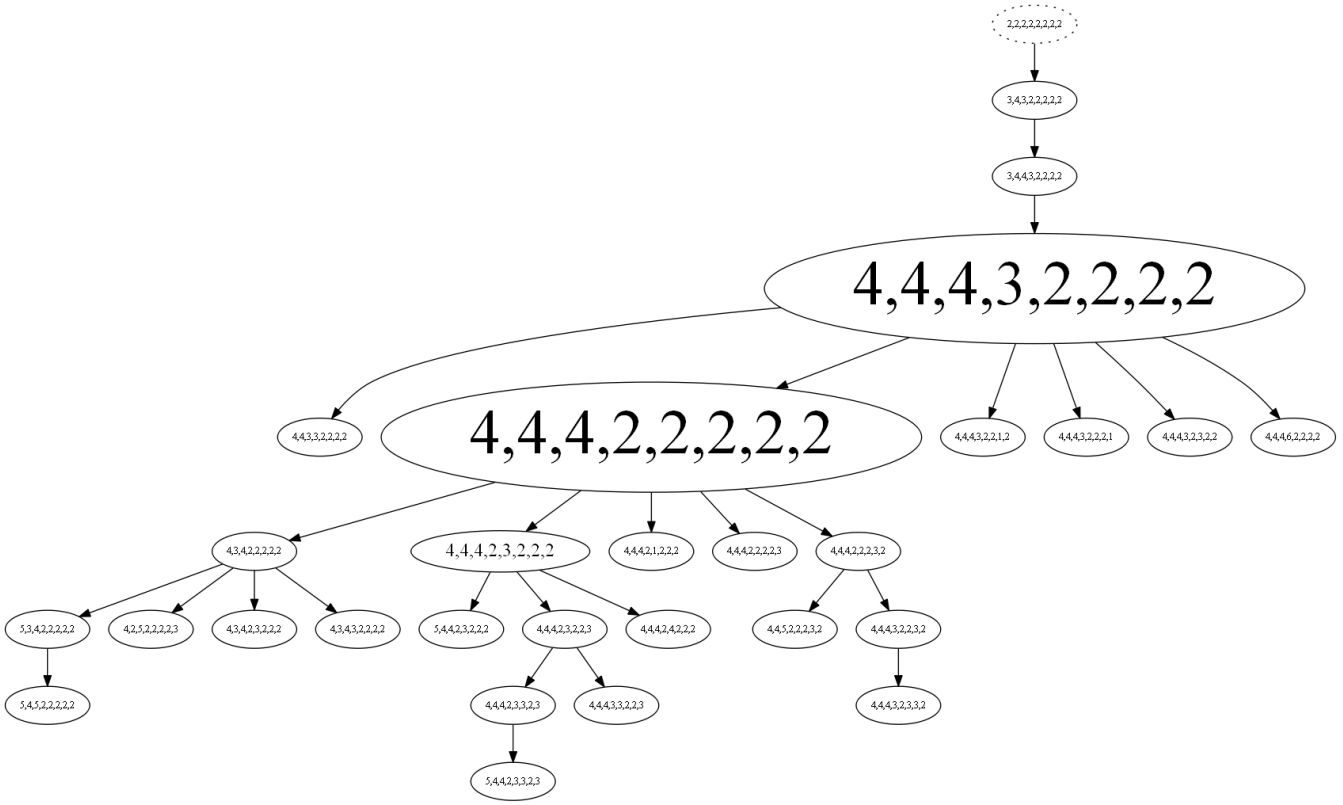

	Locus	250 nuclei				Instability Index: 11.2	Average ploidy: 3.0			
		58,0%	29,6%	2,8%	9,6%	GENE	GAIN	LOSS	AvgSig
9S	1q					COX2	99%	0%	4,0
	8p					DBC2	98%	0%	4,0
	8q					MYC	99%	0%	4,0
	11q					CCND1	0%	38%	2,6
	16q					CDH1	0%	94%	2,1
	17p					TP53	0%	98%	2,0
	17q					HER2	0%	98%	2,0
	20q					ZNF217	0%	97%	2,0

Case 10S:

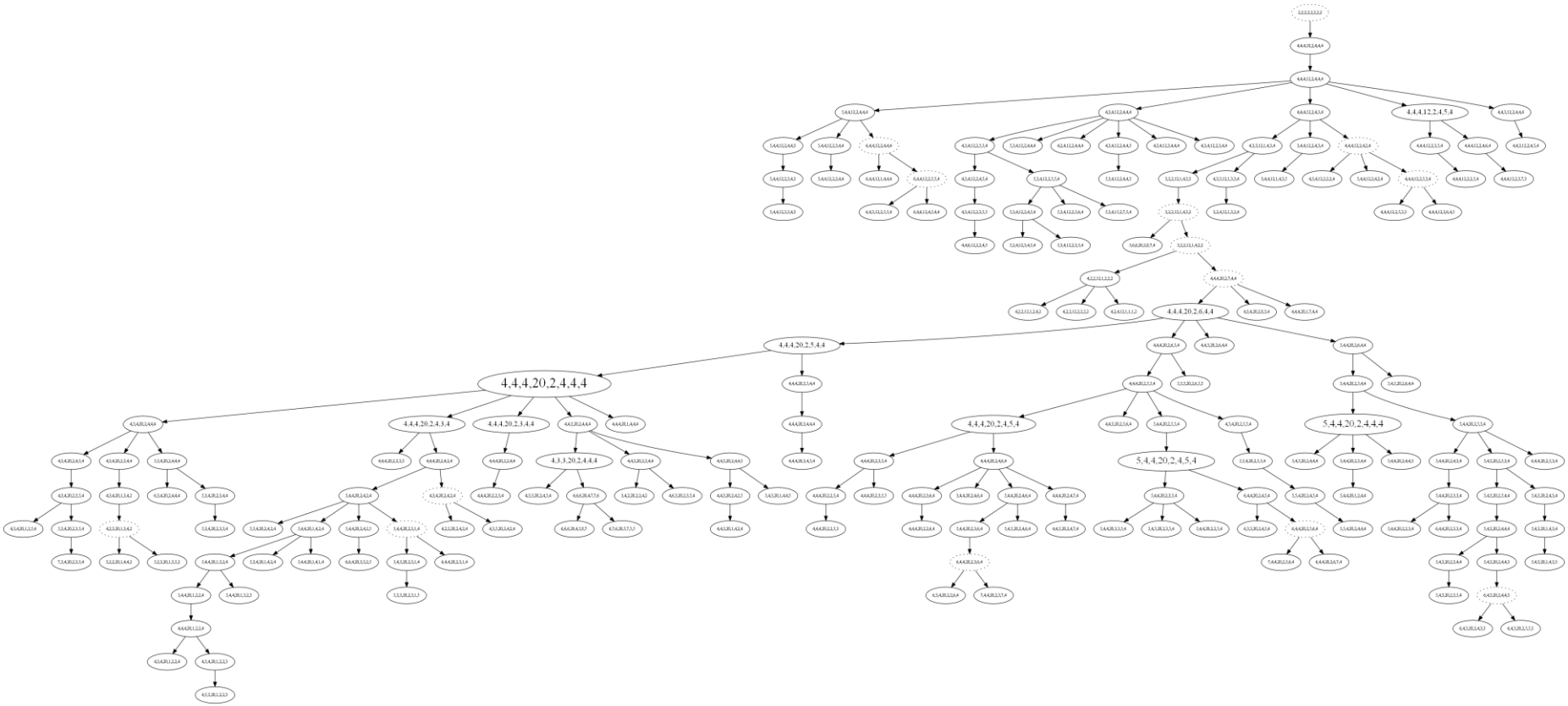

10S	Locus	250 nuclei													Instability Index: 68.8	Average ploidy: 4,0			
		9,6%	6,8%	5,2%	4,8%	3,2%	3,2%	2,8%	2,8%	2,4	2,4	2,4	2,0	2,0	2,0	48,4%	GENE	GAIN	LOSS	AvgSig
	1q																COX2	49%	2%	4,5
	8p																DBC2	5%	21%	3,8
	8q																MYC	4%	16%	3,9
	11q																CCND1	100%	0%	18,4
	16q																CDH1	0%	99%	1,9
	17p																TP53	17%	29%	3,9
	17q																HER2	36%	23%	4,1
	20q																ZNF217	5%	10%	3,9

Case 11S:

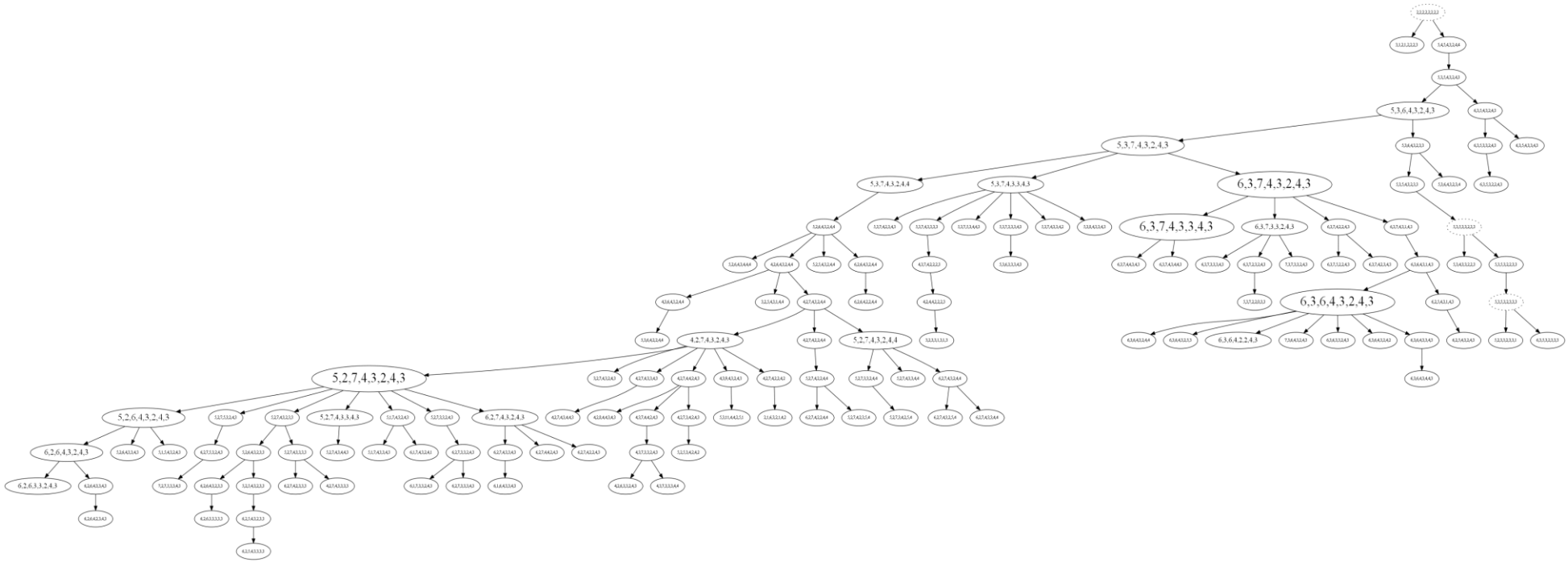

11S	Locus	250 nuclei										Instability Index: 50.0	GENE	GAIN	LOSS	AvgSig
		20,8%	17,2%	9,6%	6,4%	5,2%	4,0%	3,2%	3,2%	2,4	2,0	2,0	24,0%	Average ploidy: 3,0			
	1q													COX2	98%	0%	5,4
	8p													DBC2	0%	50%	2,5
	8q													MYC	99%	0%	6,5
	11q													CCND1	84%	1%	3,8
	16q													CDH1	4%	11%	2,9
	17p													TP53	2%	72%	2,3
	17q													HER2	90%	2%	3,9
	20q													ZNF217	17%	3%	3,1

Case 12S:

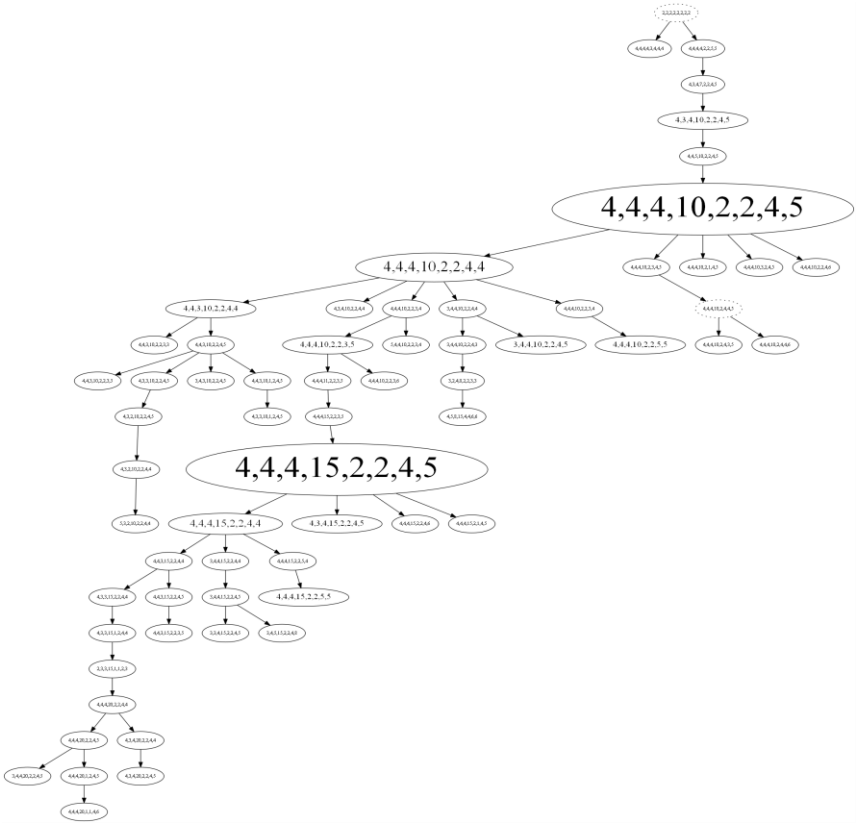

12S

Locus	250 nuclei								Instability Index: 24.8				Average ploidy: 4,0			
	60,0%	11,2%	3,6%	3,6%	3,2%	2,4	2,0	14,0%	GENE	GAIN	LOSS	AvgSig
1q									COX2	1%	5%	3,9
8p									DBC2	1%	8%	3,9
8q									MYC	2%	8%	3,9
11q									CCND1	99%	0%	12,1
16q									CDH1	0%	100%	2,0
17p									TP53	0%	98%	2,0
17q									HER2	5%	6%	4,0
20q									ZNF217	81%	1%	4,8

Case 14S:

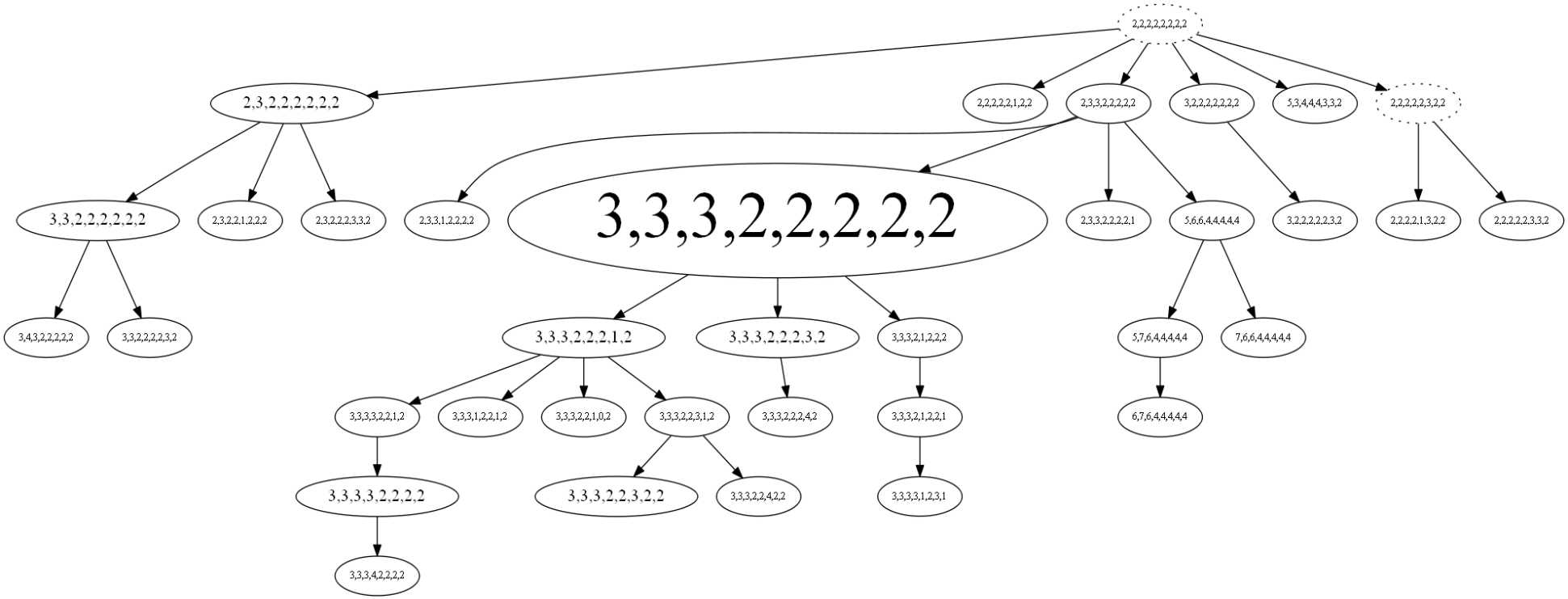

14S

Locus	250 nuclei				Instability Index: 13.6	Average ploidy: 2.0			
	80,8%	2,8%	2,4	2,0	12,0%	GENE	GAIN	LOSS	AvgSig
1q						COX2	94%	0%	3,0
8p						DBC2	98%	0%	3,0
8q						MYC	94%	0%	3,0
11q						CCND1	4%	1%	2,1
16q						CDH1	0%	2%	2,0
17p						TP53	4%	1%	2,1
17q						HER2	5%	3%	2,1
20q						ZNF217	0%	1%	2,0

Case 15S:

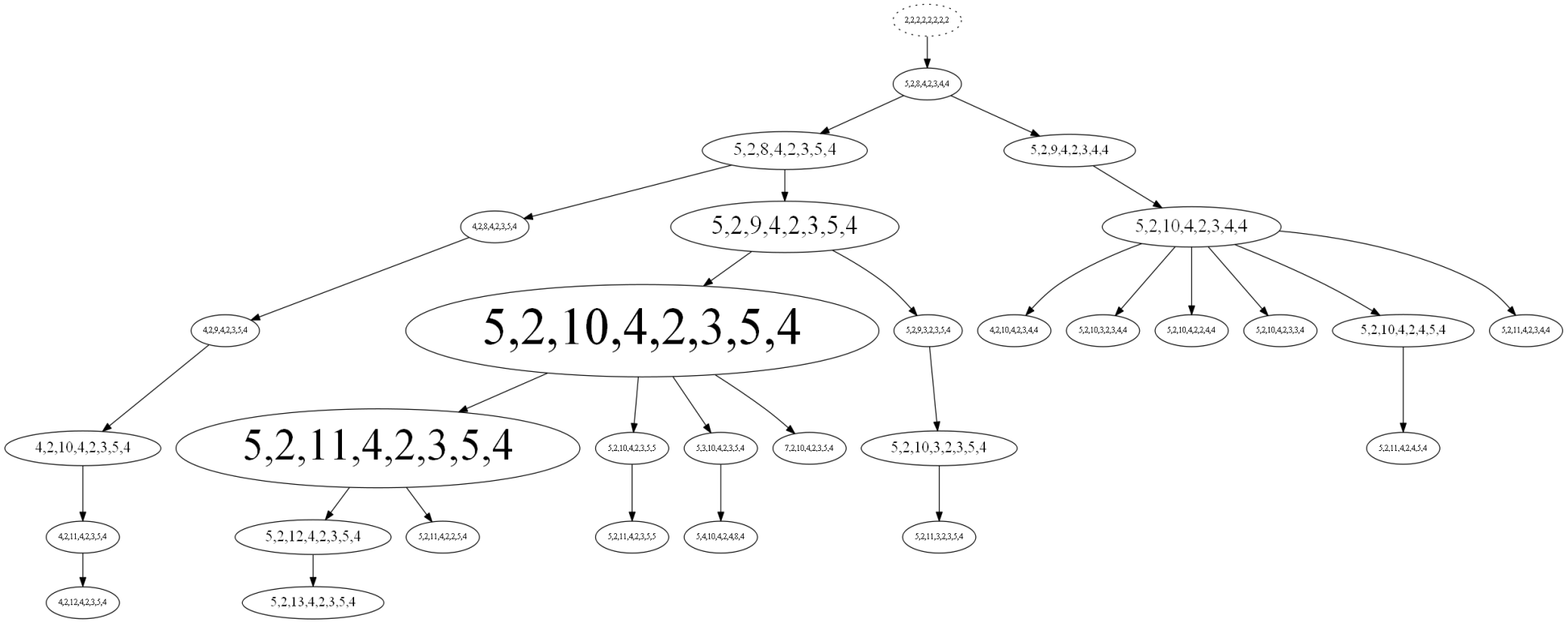

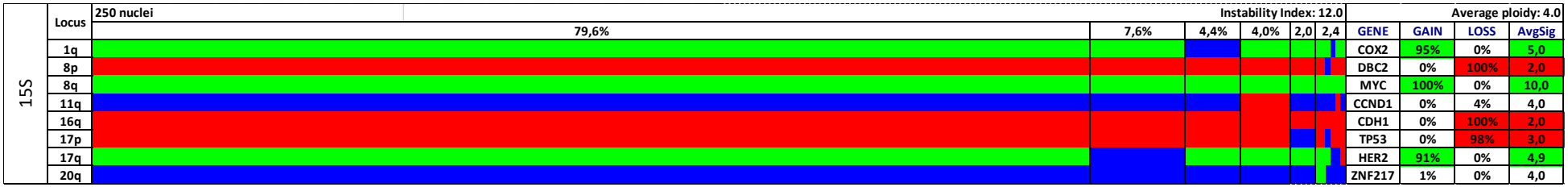

Average ploidy: 4.0

GENE	GAIN	LOSS	AvgSig
COX2	95%	0%	5,0
DBC2	0%	100%	2,0
MYC	100%	0%	10,0
CCND1	0%	4%	4,0
CDH1	0%	100%	2,0
TP53	0%	98%	3,0
HER2	91%	0%	4,9
ZNF217	1%	0%	4,0

Case 16S:

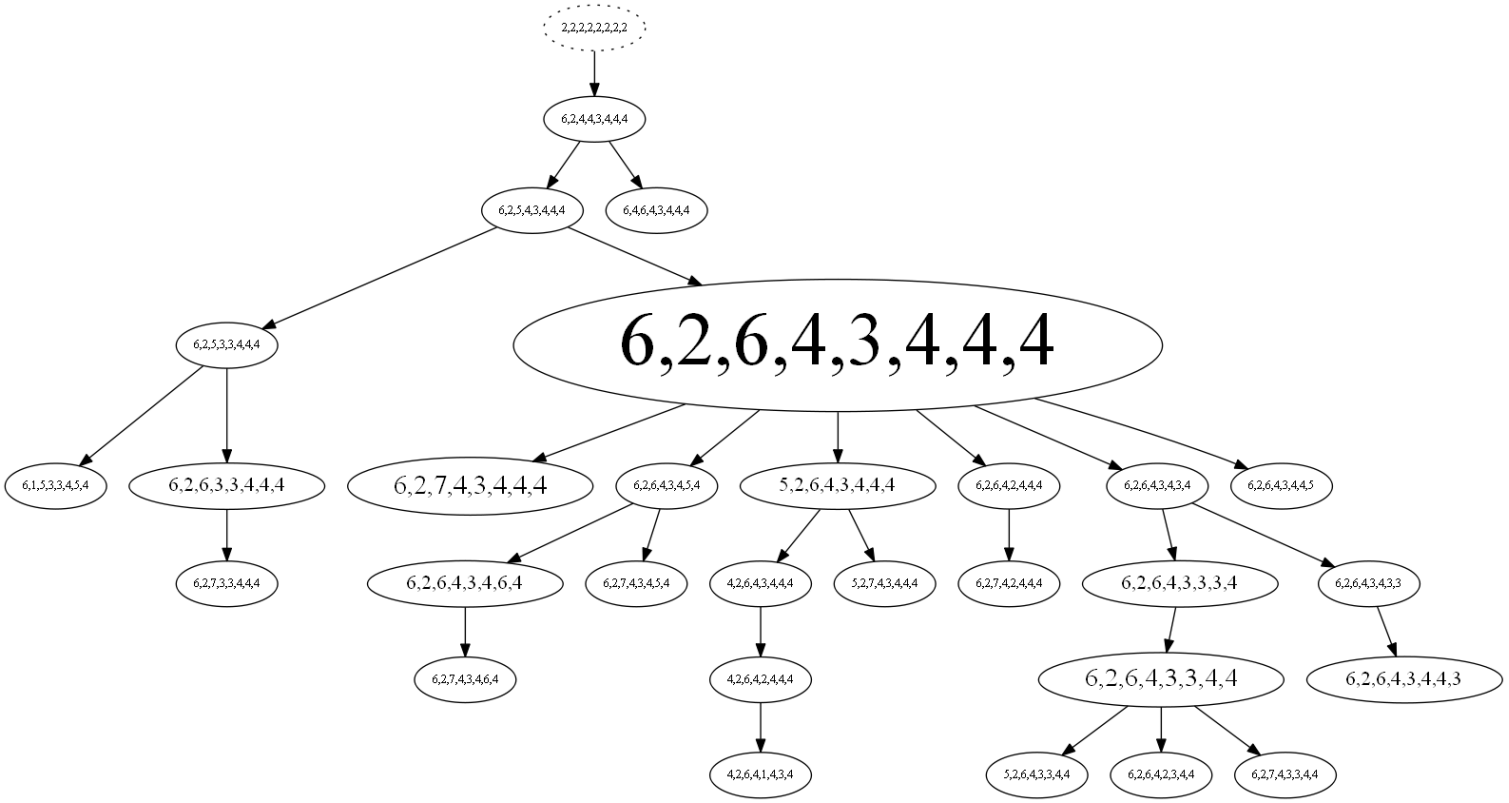

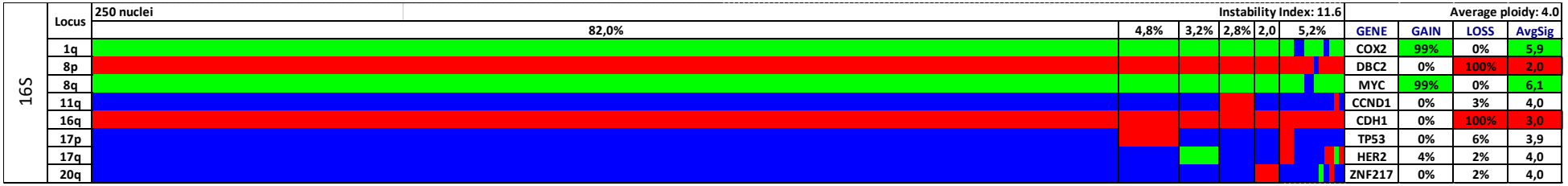

GENE	GAIN	LOSS	AvgSig
COX2	99%	0%	5,9
DBC2	0%	100%	2,0
MYC	99%	0%	6,1
CCND1	0%	3%	4,0
CDH1	0%	100%	3,0
TP53	0%	6%	3,9
HER2	4%	2%	4,0
ZNF217	0%	2%	4,0

Case 17S:

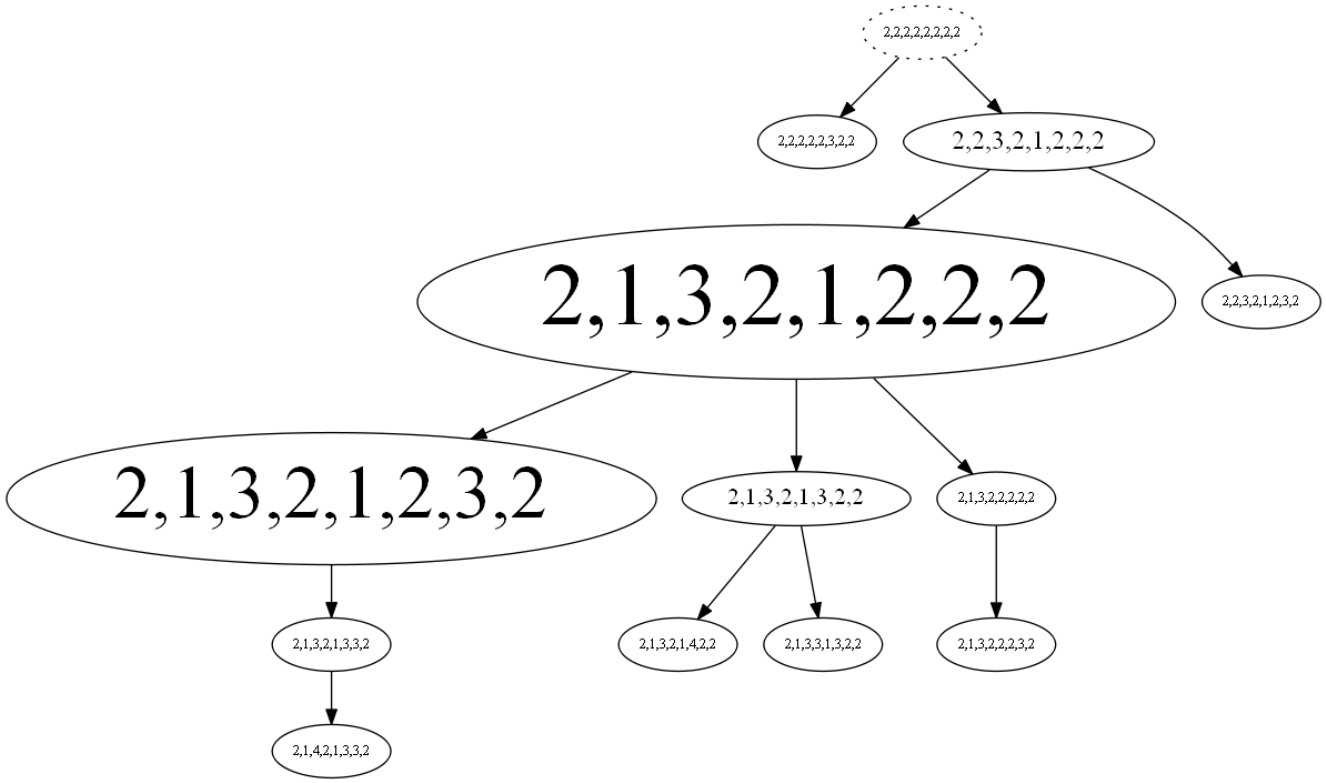

17S

Locus	250 nuclei				Instability Index: 4.8	Average ploidy: 2.0			
	78,8%		13,6%	2,4	5,2%	GENE	GAIN	LOSS	AvgSig
1q						COX2	0%	0%	2,0
8p						DBC2	0%	96%	1,0
8q						MYC	100%	0%	3,0
11q						CCND1	0%	0%	2,0
16q						CDH1	0%	99%	1,0
17p						TP53	4%	0%	2,0
17q						HER2	16%	0%	2,2
20q						ZNF217	0%	0%	2,0

Case 18S:

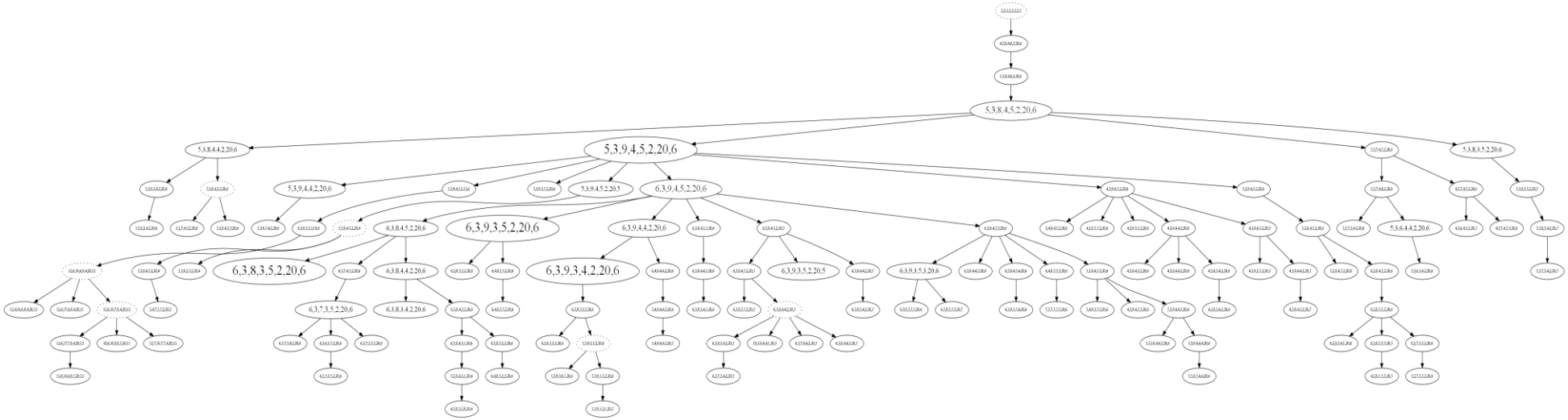

18S	Locus	250 nuclei						Instability Index: 60.0	Average ploidy: 4.1			
		30,4%	21,6%	14,8%	12,0%	3,2%	3,2%	14,8%	GENE	GAIN	LOSS	AvgSig
	1q								COX2	91%	0%	5,6
	8p								DBC2	0%	95%	3,0
	8q								MYC	100%	0%	8,6
	11q								CCND1	2%	50%	3,6
	16q								CDH1	61%	7%	4,6
	17p								TP53	0%	98%	2,1
	17q								HER2	100%	0%	36,5
	20q								ZNF217	98%	0%	6,0

9.4 Supplemental Tables

9.4.1 Supplemental Table 1: The Clinicopathological features of each breast cancer sample (n=39), separated into the groups "long survival patients versus short survival patients" sorted by sample ID with corresponding p-values.

		Clinical data											
Sample ID		Age at diagnosis (years)	Survival (years)	pT-status	pN-status	pM-status	ER-status	PR-status	Her2neu-status	Ki67 (% stained cells)	Intrinsic subtype	Ploidy (by FISH)	Av. Ploidy (by FISH)
Long Survival Samples	1L	55	19.1	pT2	pN0	pM0	pos	pos	neg	< 5	Luminal A	diploid	2
	2L	55	19.6	ND	ND	pM0	pos	pos	neg	< 5	Luminal A	diploid	2.1
	3L	56	20.5	ND	ND	pM0	pos	pos	neg	20	Luminal B, HER2 negative	aneuploid	4.6
	4L	68	19.5	ND	ND	pM0	pos	pos	neg	< 5	Luminal A	aneuploid	2.6
	5L	73	15.7	pT2	pN0	pM0	pos	pos	neg	< 5	Luminal A	aneuploid	4
	6L	78	17.0	pT4	ND	pM0	neg	neg	neg	< 5	Triple negative	aneuploid	4
	7L	66	19.3	pT1	pN0	pM0	pos	neg	neg	< 5	Luminal A	diploid	2
	8L	70	20.5	pT2	pN0	pM0	neg	neg	pos	< 5	HER2 positive	aneuploid	3.2
	9L	77	13.2	pT2	pN1	pM0	pos	neg	neg	< 5	Luminal A	aneuploid	4
	10L	85	13.9	pT1	pN1	pM0	pos	pos	neg	5	Luminal A	diploid	2.1
	11L	71	19.6	pT2	pN1	pM0	pos	pos	pos	5	Luminal B, HER2 positive	diploid	2.1
	12L	60	19.5	pT2	pN2	pM0	neg	neg	neg	< 5	Triple negative	aneuploid	2.5
	13L	55	20.5	pT1	pN1	pM0	neg	neg	neg	< 5	Triple negative	aneuploid	3.1
	14L	61	17.6	pT2	pN0	pM0	neg	neg	pos	< 5	HER2 positive	aneuploid	3
	15L	72	20.5	pT4	ND	pM0	pos	pos	neg	10	Luminal A	aneuploid	3
	16L	71	20.6	pT1	pN0	pM0	pos	ND	neg	< 5	Luminal A	diploid	2
	17L	56	20.7	pT2	pN1	pM0	pos	ND	neg	< 5	Luminal A	diploid	2.1
	18L	59	21.5	pT2	pN1	pM0	pos	pos	neg	< 5	Luminal A	diploid	2
	19L	51	20.5	pT2	pN1	pM0	pos	pos	neg	5	Luminal A	diploid	2
	20L	50	21.5	pT1	pN0	pM0	pos	neg	neg	< 5	Luminal A	aneuploid	4
	21L	51	19.5	pT2	pN1	pM0	pos	pos	neg	5	Luminal A	diploid	2.1
Short Survival Samples	1S	59	3.3	pT2	pN0	M0	neg	neg	pos	< 5	HER2 positive	aneuploid	4
	2S	81	1.6	pT2	pN0	M0	neg	neg	neg	60	Triple negative	aneuploid	3.3
	3S	74	2.1	ND	ND	M0	pos	ND	neg	5	Luminal A	diploid	2
	4S	67	0.8	ND	ND	M0	pos	pos	neg	< 5	Luminal A	aneuploid	4
	5S	82	3.0	pT4	pN1	pM0	pos	pos	neg	5	Luminal A	aneuploid	2.3
	6S	55	0.2	ND	pN1	pM0	neg	neg	neg	5	Triple negative	diploid	2.1
	7S	82	2.0	ND	ND	pM0	pos	pos	neg	5	Luminal A	aneuploid	3
	8S	53	2.9	pT3	pN1	pM0	pos	pos	neg	20	Luminal B, HER2 negative	diploid	2
	9S	62	0.5	pT2	pN1	pM0	neg	neg	neg	80	Triple negative	aneuploid	3
	10S	73	3.4	pT4	ND	pM0	pos	pos	neg	< 5	Luminal A	aneuploid	4
	11S	78	1.6	pT4	pN1	pM0	neg	neg	neg	40	Triple negative	aneuploid	3
	12S	77	1.8	pT4	pN1	pM0	pos	pos	neg	5	Luminal A	aneuploid	4
	13S	58	1	pT2	pN1	pM1	pos	pos	neg	< 5	Luminal A	diploid	2
	14S	58	1.2	pT2	pN1	pM1	neg	pos	pos	10	Luminal B, HER2 positive	diploid	2
	15S	69	4.8	pT4	pN0	pM0	pos	pos	pos	< 5	Luminal B, HER2 positive	aneuploid	4
	16S	84	3.7	ND	ND	pM0	pos	pos	neg	< 5	Luminal A	aneuploid	4
	17S	84	4.5	pT2	pN2	pM0	pos	pos	neg	< 5	Luminal A	diploid	2
	18S	50	4.1	pT3	pN1	pM0	neg	neg	pos	< 5	HER2 positive	aneuploid	4.1

	av. age at diagnosis (years)	av. Survival (years)	pT-status	pN-status	pM-status	ER-status	PR-status	Her2neu-status	Ki67	Intrinsic subtype
Overview Long Survival	63.8	19.0	16 T1/2, 2 T3/4, 3 ND	7 pN0, 9 pN1/2, 5 ND	21 pM0	16/21	11/19	3/21	20 low (0-20%), 1 high (>20%)	14 Luminal A, 2 Luminal B, 3 Triple negative, 2 Her2 positive
Overview Short Survival	69.2	2.4	6 T1/2, 7 T3/4, 5 ND	3 pN0, 10 pN1/2, 5 ND	16 pM0, 2 pM1	11/18	11/17	4/18	14 low (0-20%), 4 high (>20%)	9 Luminal A, 3 Luminal B, 4 Triple negative, 2 Her2 positive
p-value calculation	av. age vs av. age		T1/T2 vs T3/T4	N0 vs N1/N2	pM0 vs pM1	ER-status neg vs pos	PR-status neg vs pos	HER2/neu-status neg vs pos	Ki67 expression low vs high	Intrinsic subtype
p-values	0.135[2]		0.017[1]	0.0434[1]	0.207[1]	0.488[1]	0.742[1]	0.683[1]	0.162[1]	Luminal A 0.342[1] Luminal B 0.646[1] Triple neg 0.683[1] HER2 positive 1[1]

[1] Fisher exact test; [2] Student t test

ND, not determined; av., average; vs, versus.

9.4.2 Supplemental Table 2: List of laboratory equipment.

Equipment	Supplier
Centrifuge VWR Scientific Model V	VWR International, West Chester, PA, USA
Centrifuge Eppendorf 5415 D	Eppendorf AG, Hamburg, Germany
DUET scanning imaging workstation	BioView Ltd., Rehovot, Israel
Epredia™ Diamond Point Marker	Thermo Fisher Scientific, Waltham, MA
Fluorescence microscope BX63 with eight slide-stage	Olympus, Tokyo, Japan
Freezer (-86°C)	Sanyo Electric Co., Ltd., Japan
Fridge (4°C)	Sanyo Electric Co., Ltd., Japan
ICM imaging system	Ahrens ACAS, Hamburg, Germany
Incubator (37°C)	Fisher Scientific, Pittsburgh, PA, USA
Microscope „ECLIPSE Ci-S“ with a halogen lamp 6V 30W, type 5761	Nikon Europe BV, Amsterdam, Netherlands Philips, Amsterdam, Netherlands
Microwave	KitchenAid, Benton Harbor, MI, USA
NanoDrop 1000 Spectrophotometer	Thermo Fisher Scientific, Wilmington, DE, USA
NextSeq 500 system	Illumina, San Diego, CA, USA
Optical filters	Chroma, Bellow Falls, VT, USA
Pipetman® Classic Pipettes	Gilson, Inc., Middleton, WI, USA
Phase Contrast Microscope	Carl Zeiss, Oberkochen, Germany
Single cytological funnel with white filter card, Cat.no. 1207U81	Thomas Scientific, Swedesboro, NJ, USA
ThermoBrite StatSpin System	Abbott, Chicago, IL, USA
Thermo Shandon Cytospin ® 3	Thermo Fisher Scientific, Waltham, MA
Thermomixer Eppendorf 5436	Eppendorf AG, Hamburg, Germany
Thermomixer D Eppendorf	Eppendorf AG, Hamburg, Germany

Equipment	Supplier
Thermomixer R Eppendorf	Eppendorf AG, Hamburg, Germany
Vortex-Genie 2	Scientific Industries, Woburn, USA
Water baths (37°C, 48°C)	VWR International, West Chester, PA, USA

9.4.3 Supplemental Table 3: List of consumables.

Consumable	Supplier
Aluminum foil, Reynolds Wrap®	Reynolds Cons. Pro., Lake Forest, IL, USA
Coverslips, 22x22 mm2, Glass	VWR International, West Chester, PA, USA
Eppendorf Safe-Lock Tubes	Eppendorf AG, Hamburg, Germany
Rubber Cement	Marabu GmbH & Co. KG, Tamm, Germany
Pipette tips 10ul, 20ul, 100ul, 200ul, 1,000ul	Neptune Scientific, San Diego, CA, USA
Thermo Microscope Slides Superfrost®	Thermo Fisher Scientific, Waltham, MA, USA

9.4.4 Supplemental Table 4: List of reagents.

Reagent	Supplier
Absolute Ethyl Alcohol, 200 proof	The Warner Graham Co., Cockeysville, MD, USA
ATL lysis buffer	Qiagen, Germantown, MD, USA
Buffer AE (10 mM Tris-HCl, 0.5 mM EDTA, pH 9.0)	Qiagen, Germantown, MD, USA
Buffer PE (10 mM Tris-HCl, 80% ethanol, pH 7.5))	Qiagen, Germantown, MD, USA
Buffer PM (binding buffer)	Qiagen, Germantown, MD, USA
DAPI (4′,6-diamidino-2-phenylindole)	Sigma-Aldrich, St. Louis, MS, USA
Deionized Formamide	Thermo Fisher Scientific, Waltham, MA, USA
dsDNA High Sensitivity Assay Kit	Life Technologies, Carlsbad, CA, USA
Entellan	Merck KGaA, Darmstadt, Germany
FISH probes CCP4 (4p11.1-q11.1) CCP10 (10p11.1-q11.1) *COX2* (1q31.1) *DBC2* (8p21.3) *MYC* (8q24.21) *CCND1* (11q13.3) *CDH1* (16q22.1) *TP53* (17p13.1) *HER2/ERBB2* (17q12) *ZNF217* (20q13.2)	Cytotest, Rockville, MD, USA
Fluorochrome conjugates Fluorophore DY-415-dUTP, (# 415-34) Fluorophore DY-505-dUTP, (# 505-34) Fluorophore DY-547P1-dUTP, (# 547-34) Fluorophore DY-590-dUTP, (# 590-34) Fluorophore DY-594-dUTP, (594-34) Fluorophore DY-651-dUTP, (# 651-34)	Dyomics, Jena, Germany
4.5 % Formaldehyde	Carl Roth, Karlsruhe, Germany

Reagent	Supplier
HCl 1M HCl 5M	Thermo Fisher Scientific, Waltham, MA, USA Merck KGaA, Darmstadt, Germany
KAPA Hyper Prep Kits for Illumina	Illumina, San Diego, CA, USA
Mineral oil	Alfa Aesar, Tewksbury, MA, USA
MilliporeSigma™ Water (Sterile purified Water)	Thermo Fisher Scientific, Waltham, MA, USA
Natrium-Acetate 3M (pH=5.2)	Quality Biologicals, Gaithersburg, MD, USA
NP40 Detergent	Quality Biological, Gaithersburg, MD, USA
Phosphate Buffered Saline pH7.4 (PBS) 1X	KD Medical, Columbia, MD, USA
Protease Type XXIV, Bacterial	Sigma-Aldrich, St. Louis, MS, USA
Proteinase K	Qiagen, Qiagen, Germantown, MD, USA
Qiaquick spin columns	Qiagen, Germantown, MD, USA
Qubit	Life Technologies, Carlsbad, CA, USA
Rubber Cement (Fixogum)	Marabu, Tamm, Germany
Schiff´s reagent	Carl Roth, Karlsruhe, Germany
Sodium pyrosulfite	Sigma-Aldrich, St. Louis, MS, USA
20X SSC	Thermo Fisher Scientific, Massachusetts, USA
Sulforhodamine SR101	Sigma-Aldrich, St. Louis, MS, USA
Tris-HCl 1M (pH 8.0)	Quality Biologicals, Gaithersburg, MD, USA
UltraPure™ DNase/RNase-Free Distilled Water	Life Technologies, Carlsbad, CA, USA
Vectashield Antifade Mounting Medium w/o DAPI	Vector Laboratories, Burlingame, CA, USA
Xylene	Sigma-Aldrich, St. Louis, MS, USA
Xylol	J.T. Baker, Pennsylvania, USA

9.4.5 Supplemental Table 5: Genes included in the OncoVar assay (n=563).

OncoVar genes									
ABL1	*BLM*	*CTNNA1*	*FANCG*	*HIF1A*	*LCK*	*MYH11*	*PIK3CG*	*RUNX1T1*	*TET2*
ABL2	*BLNK*	*CTNNB1*	*FANCI*	*HIST1H3B*	*LDLR*	*MYH7*	*PIK3R1*	*RYR1*	*TFE3*
ACN9	*BMPR1A*	*CUL2*	*FANCL*	*HLF*	*LIFR*	*MYH9*	*PIK3R2*	*RYR2*	*TGFBR1*
ACTA2	*BRAF*	*CUL3*	*FANCM*	*HNF1A*	*LMNA*	*MYL2*	*PIM1*	*SAMD9*	*TGFBR2*
ACTC1	*BRCA1*	*CYLD*	*FAS*	*HOOK3*	*LPHN3*	*MYL3*	*PKHD1*	*SBDS*	*TGM7*
ACVR1	*BRCA2*	*CYP2C19*	*FBN1*	*HOXA3*	*LPP*	*MYLK*	*PKP2*	*SCN5A*	*THBS1*
ACVR1B	*BRD3*	*CYP2D6*	*FBXO11*	*HRAS*	*LRP1B*	*NBN*	*PLAG1*	*SDHA*	*TIAF1*
ACVR2A	*BRIP1*	*DAXX*	*FBXW7*	*HSP90AA1*	*LTF*	*NCOA1*	*PLCG1*	*SDHAF1*	*TIMP3*
ACVRL1	*BTK*	*DCC*	*FGF10*	*HSP90AB1*	*LTK*	*NCOA2*	*PLEKHG5*	*SDHAF2*	*TLR4*
ADAMTS20	*BUB1B*	*DDB2*	*FGF14*	*ICK*	*MAF*	*NCOA3*	*PML*	*SDHB*	*TLX1*
AFF1	*C11ORF30*	*DDIT3*	*FGF19*	*IDH1*	*MAFB*	*NCOA4*	*PMS1*	*SDHC*	*TMEM127*
AFF3	*CACNA1S*	*DDR2*	*FGF23*	*IDH2*	*MAGEA1*	*NF1*	*PMS2*	*SDHD*	*TMEM43*
AKAP9	*CALR*	*DEK*	*FGF3*	*IFITM1*	*MAGI1*	*NF2*	*PNP*	*SEPT9*	*TNFAIP3*
AKT1	*CARD11*	*DICER1*	*FGF4*	*IFITM3*	*MAGOH*	*NFE2L2*	*POLD1*	*SETD2*	*TNFRSF14*
AKT2	*CASC5*	*DNMT3A*	*FGF6*	*IGF1R*	*MALT1*	*NFKB1*	*POLE*	*SF3B1*	*TNK2*
AKT3	*CBFB*	*DOT1L*	*FGFR1*	*IGF2*	*MAML1*	*NFKB2*	*POLH*	*SGK1*	*TNNI3*
ALK	*CBL*	*DPYD*	*FGFR2*	*IGF2R*	*MAML2*	*NFKBIA*	*POT1*	*SH2B3*	*TNNT2*
AMER1	*CCND1*	*DSC2*	*FGFR3*	*IKBKB*	*MAP2K1*	*NIN*	*POU5F1*	*SH2D1A*	*TOP1*
APC	*CCND2*	*DSG2*	*FGFR4*	*IKBKE*	*MAP2K2*	*NKX2-1*	*PPARG*	*SIRT1*	*TP53*
APEX1	*CCND3*	*DSP*	*FH*	*IKZF1*	*MAP2K4*	*NLRP1*	*PPP2R1A*	*SMAD2*	*TPM1*
APOB	*CCNE1*	*DST*	*FLCN*	*IL2*	*MAP3K1*	*NOTCH1*	*PRDM1*	*SMAD3*	*TPR*
AR	*CD274*	*EGFR*	*FLI1*	*IL21R*	*MAP3K7*	*NOTCH2*	*PRKAG2*	*SMAD4*	*TRAF7*
ARAF	*CD44*	*EML4*	*FLT1*	*IL6*	*MAPK1*	*NOTCH3*	*PRKAR1A*	*SMARCA4*	*TRIM24*
ARFRP1	*CD79A*	*EP300*	*FLT3*	*IL6ST*	*MAPK8*	*NOTCH4*	*PRKDC*	*SMARCB1*	*TRIM33*
ARID1A	*CD79B*	*EP400*	*FLT4*	*IL7R*	*MARK1*	*NPM1*	*PRSS1*	*SMO*	*TRIP11*
ARID1B	*CDC73*	*EPHA3*	*FN1*	*ING4*	*MARK4*	*NRAS*	*PSIP1*	*SMUG1*	*TRRAP*
ARID2	*CDH1*	*EPHA5*	*FNIP1*	*INHBA*	*MAX*	*NSD1*	*PTCH1*	*SOCS1*	*TSC1*
ARNT	*CDH11*	*EPHA6*	*FNIP2*	*IRF4*	*MBD1*	*NTRK1*	*PTEN*	*SOX10*	*TSC2*
ASXL1	*CDH2*	*EPHA7*	*FOXL2*	*IRS2*	*MBIP*	*NTRK2*	*PTGS2*	*SOX11*	*TSHR*
ATF1	*CDH20*	*EPHB1*	*FOXO1*	*ITGA10*	*MCL1*	*NTRK3*	*PTPN11*	*SOX2*	*U2AF1*
ATM	*CDH5*	*EPHB4*	*FOXO3*	*ITGA9*	*MDM2*	*NUMA1*	*PTPRD*	*SPEN*	*UBA1*
ATR	*CDK12*	*EPHB6*	*FOXP1*	*ITGB2*	*MDM4*	*NUP214*	*PTPRT*	*SPOP*	*UBR5*
ATRX	*CDK4*	*ERBB2*	*FOXP4*	*ITGB3*	*MED12*	*NUP93*	*RAC1*	*SRC*	*UGT1A1*
AURKA	*CDK6*	*ERBB3*	*FZR1*	*JAK1*	*MEF2B*	*NUP98*	*RAD50*	*SRSF2*	*USP9X*
AURKB	*CDK8*	*ERBB4*	*G6PD*	*JAK2*	*MEN1*	*PAK3*	*RAD51*	*SSX1*	*VHL*
AURKC	*CDKN1B*	*ERCC1*	*GAS6*	*JAK3*	*MET*	*PALB2*	*RAD51C*	*STAG1*	*WAS*
AXIN1	*CDKN2A*	*ERCC2*	*GATA1*	*JUN*	*MGMT*	*PARP1*	*RAF1*	*STAG2*	*WHSC1*
AXIN2	*CDKN2B*	*ERCC3*	*GATA2*	*KAT6A*	*MITF*	*PAX3*	*RALGDS*	*STAT3*	*WISP3*
AXL	*CDKN2C*	*ERCC4*	*GATA3*	*KAT6B*	*MLH1*	*PAX5*	*RARA*	*STAT4*	*WRN*
BAI3	*CEBPA*	*ERCC5*	*GDNF*	*KCNH2*	*MLLT10*	*PAX7*	*RB1*	*STK11*	*WT1*
BAP1	*CHEK1*	*ERG*	*GID4*	*KCNJ5*	*MMP2*	*PAX8*	*RECQL4*	*STK36*	*XPA*
BARD1	*CHEK2*	*ESR1*	*GLA*	*KCNQ1*	*MN1*	*PBRM1*	*REL*	*SUFU*	*XPC*
BCL10	*CIC*	*ETS1*	*GNA11*	*KDM5A*	*MPL*	*PBX1*	*RET*	*SYK*	*XPO1*
BCL11A	*CKS1B*	*ETV1*	*GNA13*	*KDM5C*	*MRE11A*	*PCSK9*	*RHEB*	*SYNE1*	*XRCC1*
BCL11B	*CMPK1*	*ETV4*	*GNAQ*	*KDM6A*	*MSH2*	*PDE4DIP*	*RHOA*	*TAF1*	*XRCC2*
BCL2	*COL1A1*	*ETV5*	*GNAS*	*KDR*	*MSH6*	*PDGFB*	*RHOH*	*TAF1L*	*ZNF217*
BCL2L1	*COL3A1*	*EWSR1*	*GPC3*	*KEAP1*	*MTOR*	*PDGFRA*	*RICTOR*	*TAL1*	*ZNF384*
BCL2L2	*CRBN*	*EXT1*	*GPR124*	*KIF1B*	*MTR*	*PDGFRB*	*RNASEL*	*TBX22*	*ZNF521*
BCL3	*CREB1*	*EXT2*	*GRIN2A*	*KIT*	*MTRR*	*PDK1*	*RNF2*	*TCEB1*	*ZNF703*
BCL6	*CREBBP*	*EZH2*	*GRM8*	*KLF6*	*MUC1*	*PER1*	*RNF213*	*TCEB2*	*ZRSR2*
BCL9	*CRKL*	*FAM46C*	*GSK3B*	*KLHL6*	*MUTYH*	*PGAP3*	*RNF43*	*TCF12*	
BCOR	*CRLF2*	*FANCA*	*GTF2I*	*KMT2A*	*MYB*	*PGR*	*ROS1*	*TCF3*	
BCORL1	*CRTC1*	*FANCB*	*GUCY1A2*	*KMT2B*	*MYBPC3*	*PHOX2B*	*RPS6KA2*	*TCF7L1*	
BCR	*CSF1R*	*FANCC*	*H3F3A*	*KMT2C*	*MYC*	*PIK3C2B*	*RPS6KB1*	*TCF7L2*	
BIRC2	*CSMD3*	*FANCD2*	*H3F3B*	*KNSTRN*	*MYCL*	*PIK3CA*	*RPTOR*	*TCL1A*	
BIRC3	*CSNK2A1*	*FANCE*	*HCAR1*	*KRAS*	*MYCN*	*PIK3CB*	*RRM1*	*TERT*	
BIRC5	*CTCF*	*FANCF*	*HGF*	*LAMP1*	*MYD88*	*PIK3CD*	*RUNX1*	*TET1*	

9.5 Supplemental Protocols

9.5.1 Description of the Feulgen-staining

Under avoidance of light, Cytospin slides were incubated in 4.5 % formaldehyde for fixation at room temperature overnight in a fume hood. Afterwards, cytospins were washed under running tap water (until the smell of formaldehyde was entirely removed). Cytospin slides were then incubated with 5 M hydrochloric acid for 60 minutes at room temperature under avoidance of light, followed by three washing steps with sterile purified water. For staining, cytospin slides were incubated for 120 minutes with Schiff´s reagent covered with Alu foil for light protection. Afterwards, cytospin slides were washed under running tap water, followed by three washing steps for 10 minutes respectively in freshly prepared sodium pyrosulfite washing solution: In the first step, 2.4g of sodium pyrosulfite was solved in 125 ml sterile purified water. Then, 10 ml of this solved pyrosulfite was added to 10 ml of 1 M hydrochloric acid and 180 ml of sterile purified water. For dehydration, cytospin slides were incubated in an increasing ethanol series of 1 x 70%, 2 x 96%, and 2 x 100% for 3 minutes, respectively. Slides were quickly immersed two times in xylol, followed by a longer incubation step for 5-10 minutes. Finally, 1-2 drops of Entellan were added onto the slide, and a 24 x 60 mm coverslip was touched onto the cytospin slide under avoidance of bubble formation. In addition to the cytospins, a slide with tonsil tissue was Feulgen-stained as a control.

10 DANKSAGUNGEN

Ich danke allen beteiligten Personen, die mich bei meiner Promotion unterstützt und diese möglich gemacht haben. Herrn Professor Dr. Dr. Tobias Keck danke ich für die Möglichkeit, meine Doktorarbeit in der Klinik für Chirurgie des UKSH am Campus Lübeck durchführen zu können.

Besonders hervorheben möchte ich meine große Dankbarkeit gegenüber Herrn Professor Dr. Dr. Jens K. Habermann für seine langjährige Unterstützung und die Vergabe des Themas, die mir die Möglichkeit gab, in einem inspirierenden Umfeld eigenständig zu forschen. Lieber Jens, ich danke Dir für Deinen ganz besonderen Einsatz. Du hast meine Berufswahl entscheidend geprägt und mich in die Welt der wissenschaftlichen Forschung eingeführt. Insbesondere danke ich Dir für die Betreuung meiner Bachelorarbeit 2013, dem für meinen persönlichen Werdegang wegweisenden 4-wöchigen Praktikum im Institut für Humangenetik 2014, das nur durch Deinen außergewöhnlichen Einsatz ermöglicht wurde, und Deine fortlaufende Betreuung während dieser Doktorarbeit mit all den kompetenten, wissenschaftlichen und freundschaftlichen Gesprächen. Außerordentlich danke ich Dir für die Organisation des Austausches mit dem Labor von Professor Ried am NIH und Dein Vertrauen in meine Fähigkeiten.

Ich bedanke mich sehr herzlich bei allen Mitarbeitern der Arbeitsgruppe von Professor Habermann. Mein besonderer Dank gilt hierbei Dr. Annette Lischka für die kompetente Supervision bei der Probenauswahl und der guten Korrespondenz mit dem Lübecker Labor während meiner Forschungsaufenthalte in den USA. Außerdem möchte ich mich bei Katja Klempt-Giessen für das Anfertigen der Schnitte der FFPE-Blöcke bedanken. Prof. Timo Gemoll danke ich für die Unterstützung bei der Image Cytometry.

Ganz herzlich bedanke ich mich bei Prof. Dr. Thomas Ried für die herzliche Aufnahme in seinem Labor am NCI, NIH, Bethesda, USA, sowie für die exzellente Betreuung des Projektes. Darüber hinaus bedanke ich mich bei Prof. Ried sehr für die Möglichkeit, in seinem Labor mit einem internationalen Team forschen, an vielen Seminaren des NCI und NIH teilnehmen zu können sowie ein Poster über dieses Projekt auf dem NIH Research Festival im September 2018 vorstellen zu dürfen. Durch die Forschung, Seminare und vielen wissenschaftlichen Gespräche mit Prof. Dr. Ried, weiteren führenden Forschern seiner Arbeitsgruppe und aus dem NCI konnte ich meinen Wissensstand in der Tumor- und Zytogenetik entscheidend erweitern. Sehr bedanke ich mich bei der Arbeitsgruppe von Prof. Dr. Ried für die lehrreichen und schönen Monate in hilfsbereiter und freundschaftlicher Arbeitsatmosphäre. Hervorheben möchte ich das außergewöhnlich große Engagement mit dem ich von Dr. Kerstin Heselmeyer-Haddad in die Vielfarben-Fluoreszenz in situ

Hybridisierung eingearbeitet und während meiner Forschungsaufenthalte am NIH exzellent fachlich betreut worden bin, wofür ich mich sehr herzlich bei Dir, liebe Kerstin, bedanken möchte. Auch möchte ich mich bei Irianna Torres für die kompetente Einführung beim Herstellen der Cytospins und dem Umgang mit dem Fluoreszenzmikroskops bedanken. Des Weiteren gilt mein Dank Dr. Wei-Dong und dem Frederick National Laboratory for Cancer Research in Maryland, USA, für das Durchführen der DNA-Extraktion und des Next-Generation Sequencing. Bei dem bioinformatischen Spezialisten Herrn Dr. Yue Hu möchte ich mich für die Bearbeitung der Rohdaten der NGS-Ergebnisse und seine Unterstützung bei der statistischen Auswertung bedanken. Für viele fachlich-kompetente Ratschläge, Antworten und Erklärungen auf meine wissenschaftlichen Fragen und anregende Diskussionen über miFISH, NGS und Wissenschaft im Allgemeinen möchte ich mich ganz herzlich bei Prof. Dr. Daniela Hirsch bedanken.

Ich danke allen Co-Autoren der 2021 erschienenen Publikation (PMID: 34282768) für ihren Beitrag zum Gelingen dieses Projektes. Der Frauenklinik des UKSH danke ich für die Entnahme und Bereitstellung des Tumormaterials. Dem Institut für Pathologie der Universität zu Lübeck sowie des UKSH danke ich für die Bestimmung des HER2-, ER- und PR-Rezeptorstatus sowie des Ki67-Expressionslevels und besonders Herrn Professor Thorns für die histopathologische Begutachtung der Schnitte. Hendrik Alkmade danke ich für das Zusammentragen der klinischen Daten der 245 Brustkrebs-Patientinnen.

Für die großzügige finanzielle Unterstützung während des 7-monatigen Forschungsaufenthalts 2018 am NIH in den USA danke ich der Forschungskommission Medizin der Universität zu Lübeck für das Promotionsstipendium „Lübecker Exzellenzmedizin“. Besonderer Dank gilt meinen Eltern für die Ermöglichung der weiteren, darauffolgenden Forschungsaufenthalte am NIH.

Ich danke Dr. Heselmeyer-Haddad für das Lesen des Material- und Methodenteils sowie die guten Ratschläge zu diesem Teil der Dissertation. Herrn Prof. Dr. Dr. Jens Habermann danke ich für das Lesen und die hilfreichen, kompetenten Anmerkungen zu dieser Dissertation.

Ich bedanke mich bei dem Journal PNAS für die Erlaubnis, die Graphik von Kallioniemi et al. (1994) in dieser Arbeit zeigen zu dürfen (Figure 2). Herrn Prof. Dr. med. Karl-Friedrich Klotz danke ich für die Übernahme der amtlichen Kobetreuung und sein großes Engagement in der Promotionskommission. Dem Prüfungsausschuss danke ich für die Übernahme der Gutachten und dem damit verbundenen Zeitaufwand.

11 PUBLICATIONS

A. S. Liegmann, K. Heselmeyer-Haddad, A. Lischka1, D. Hirsch, W. D. Chen, I. Torres, T.Gemoll, A. Rody, C. Thorns, E. M. Gertz, H. Alkemade, Y. Hu, J. K. Habermann, T. Ried
"Single Cell Genetic Profiling of Tumors of Postmenopausal Breast Cancer Patients Reveals Enormous Intratumor Heterogeneity Independent of Prognosis"
Oral Presentation; 15.3.2022
32. Jahrestagung der GfH in Würzburg, Germany

Anna-Sophie Liegmann, Kerstin Heselmeyer-Haddad, Annette Lischka, Daniela Hirsch, Wei-Dong Chen, Irianna Torres, Timo Gemoll, Achim Rody, Christoph Thorns, Edward Michael Gertz, Hendrik Alkemade, Yue Hu, Jens K. Habermann and Thomas Ried
"Single Cell Genetic Profiling of Tumors of Breast Cancer Patients Aged 50 Years and Older Reveals Enormous Intratumor Heterogeneity Independent of Individual Prognosis"
Publication; Epub: 05.07.2021
Cancers, *13*(13), 3366, PMCID: PMC8267950

Anna-Sophie Liegmann, Annette Lischka, Kerstin Heselmeyer-Haddad, Thomas Ried, Jens K. Habermann
"The significance of ploidy and tumor-associated gene mutations for the prognosis of breast cancer in postmenopausal patients"
Oral presentation; 26.11.2018
Zentrales Doktorandenseminar, University of Lübeck, Lübeck, Germany

Anna-Sophie Liegmann, Annette Lischka, Jens K. Habermann, Thomas Ried, Kerstin Heselmeyer-Haddad
"The significance of ploidy and tumor-associated gene mutations for the prognosis of breast cancer in postmenopausal patients"
Poster Presentation; 14.09.2018
National Institutes of Health Research Festival, Bethesda, MD, USA

Natalie Doberstein, Martina Oberländer, Anna-Sophie Liegmann, Christoph Thorns, Timo Gemoll, Jens K. Habermann
„Instabilität des Genoms -Anzeichen für eine schlechte Prognose bei Brustkrebs?"
Poster Presentation; 10.06.2015
Doktorandentag, University of Lübeck, Lübeck, Germany